UTS UNIVERSITY OF TECHNOLOGY SYDNEY

Assessment of Residual Load Capacity of ASR Affected Reinforced Concrete Structures

by Jinsong Cao

Thesis submitted in fulfilment of the requirements for the degree of

DOCTOR OF PHILOSOPHY

under the supervision of

Principal Supervisor: Dr Nadarajah Gowripalan
Co-Supervisor: A/Prof. Shami Nejadi
Co-Supervisor: Prof. Vute Sirivivatnanon

University of Technology Sydney
Faculty of Engineering and Information Technology

April 2021

Certificate of Original Authorship

I, *Jinsong Cao*, declare that this thesis, is submitted in fulfilment of the requirements for the award of Doctor of Philosophy, in the School of Civil and Environmental Engineering, Faculty of Engineering and Information Technology at the University of Technology Sydney.

This thesis is wholly my own work unless otherwise referenced or acknowledged. In addition, I certify that all information sources and literature used are indicated in the thesis.

This document has not been submitted for qualification at any other academic institution.

This research is supported by the Australian Government Research Training Program.

Signature: Production Note:
Signature removed prior to publication.

Date: 12/04/2021

Acknowledgements

This PhD journey is like running a Marathon, it will not be possible without the support, training and patience provided by my supervisors, Dr Nadarajah Gowripalan, Dr. Shami Nejadi and Prof. Vute Sirivivatnanon. I feel so lucky to have all of you as my supervisors and I am grateful to you for providing me this precious opportunity to enrich the experience of my life, to broaden my horizon about my research, and more importantly, to see the big picture and overcome challenges during this journey. I am deeply grateful for your generosity, your invaluable guidance and continuous support.

I would also like to sincerely thank all staffs at UTS Tech Lab, especially Mr. Rami Haddad, Mr. Mulugheta Hailu, Ms Ann Yan and Mr. Peter Brown, Mr. Peter Winnacott, Mr. Scott Graham, the technical assistance, the facilities, equipment, and the team work you provided were really helpful for my experimental work.

Particularly, I would like to thank Dr Marie Joshua Tapas for generously providing support in performing SEM analysis and for confirming ASR products. Likewise, I would like to thank Ms Vu Tran Huyen and Mr. Thuc Nhu Nguyen for generously helping cast the three-meter long beams. I will never forget the scene when we were working together.

I am also thankful to all the friends I met. You are the ones that make my PhD journey full of laughter, happiness and beauty. I am the lucky one to see the spring, the summer, the autumn and the winter with you.

I am extremely grateful to my mother, for her love and encouragement.

I would like to thank the Australian Research Council Research Hub for Nanoscience Based Construction Materials Manufacturing (ARC NanoComm Hub) and Cement, Concrete & Aggregates Australia (CCAA) for providing financial support for the project.

List of Publications

- Cao, J., Gowripalan, N., Sirivivatnanon, V. & South, W. 2020, 'Accelerated test for assessing the potential risk of alkali-silica reaction in concrete using an autoclave', Construction and Building Materials, vol. 271, p. 121871.
- Gowripalan, N., Cao, J., Sirivivatnanon, V. & South, W., 2021, 'Comparison of the effect of ASR deterioration on the load carrying capacity of concrete structural elements in accelerated laboratory tests and in the field', Accepted for 16th International Conference on Alkali Aggregate Reaction in Concrete, June 2021, Lisbon, Portugal.
- Cao, J., Gowripalan, N., Sirivivatnanon, V. & South, W., 2019, 'Accelerated autoclave test for determining alkali silica reaction of concrete', Concrete in Australia, Vol. 45, No. 2, pp.37-40.
- Cao, J., Gowripalan, N., Sirivivatnanon, V. and South, W., 2019, 'Assessment of ASR expansions using an ultra-accelerated test', In 29th Biennial Conference of the Concrete Institute of Australia. Accepted for oral presentation in Concrete 2019 "Concrete in Practice-Progress Through Knowledge", September 8-11, 2019, Sydney, Australia.
- Gowripalan, N. and Cao, J., 2018, 'Effect of alkali silica reaction on bond strength and load capacity of reinforced concrete structures', Proceedings of the 5th International fib Congress, Melbourne, Australia, pp. 3088-3099.

Table of Contents

Certificate of Original Authorship i

Acknowledgements ii

List of Publications iii

List of Figures x

List of Tables xvii

Abstract xviii

Chapter 1

Introduction 1

1.1 Background 1

1.2 Research Scope of the Whole Project 3

1.3 Research Objectives of the Current Project 3

1.4 Research Contributions 4

1.5 Structure of the Thesis 4

Chapter 2

Literature Review 6

2.1 ASR Mechanism 6

2.2 Conditions for Deleterious ASR 9

2.3 ASR-Induced Concrete Expansion and Cracking 12

2.3.1 ASR Expansion 13

2.3.2 Cracking 19

2.4 Degradation of Mechanical Properties of ASR-Affected Concrete 22

2.5 Structural Effects of ASR 27

2.5.1 Bond Strength 27

2.5.2 Flexural Capacity 36

2.5.3 Shear Capacity 49

2.5.4 Long-term Behaviour 68
2.6 Secondary Effects of ASR - Corrosion of Reinforcement 71
2.7 Accelerated Test Methods for ASR 72
2.7.1 80 °C Accelerated Mortar Bar Test (AMBT) 72
2.7.2 38 °C Concrete Prism Test (CPT) 74
2.7.3 60 °C Accelerated Concrete Prism Test (ACPT) 75
2.7.4 Ultra-accelerated Autoclave Test Methods for ASR 77
2.8 Numerical modelling of ASR 87
Chapter 3
Accelerated Autoclave Test for Assessing Alkali-Silica Reaction of Concrete 90
3.1 Overview 90
3.2 130 °C Autoclave Test Program 92
3.2.1 Materials and Mix Proportions 92
3.2.2 Specimen Fabrication and Autoclave Test Procedure 94
3.2.3 Expansion of Concrete Prisms 95
3.2.4 Testing of Mechanical Properties 98
3.3 Results and Discussion 101
3.3.1 Expansion and cracking of specimens 101
3.3.2 Compressive Strength Testing Results 103
3.3.3 Flexural Strength Testing Results 105
3.3.4 Modulus of Elasticity Test on 90-day Non-reactive Cylinders 106
3.3.5 Compressive Strength Test on 90-day Non-reactive Cylinders 107
3.3.6 SEM Observation of 90-day Non-reactive Cylinders after Autoclaving 108
3.4 Summary 110
Chapter 4
Novel Accelerated Test Method for ASR by Using an Autoclave 111
4.1 Overview 111

4.2 Phase I Experimental Program – Mortar Specimens 113
4.2.1 Materials and Mix Proportions 113
4.2.2 Specimen Fabrication and Steam Warming Procedure 115
4.2.3 Expansion Measurements 117
4.3 Results and Discussion for Phase I Experiments 118
4.3.1 Expansion of Mortar Bars 118
4.3.2 Influence of Total Alkali Content (2.5%, 3.0%, 3.5%) 119
4.3.3 Influence of Temperature on Expansion (70 °C and 80 °C) 120
4.3.4 Microscopic Observation for Assessment of ASR 121
4.3.5 Summary of Phase I Experimental Program 125
4.4 Phase II Experimental Program – Concrete Specimens 126
4.4.1 Materials and Mix Proportions 126
4.4.2 Specimen Fabrication and Steam Warming Procedure 128
4.4.3 Expansion and Mass Change 131
4.4.4 Cracking of Specimens 134
4.4.5 Microscopic Observation 135
4.4.6 Mechanical Properties of Concrete under Accelerated ASR Test 138
4.5 Comparison of Expansion Results 141
4.5.1 Comparison of AMBT and 80 °C Autoclave Test Results 141
4.5.2 Comparison of CPT and 80 °C Autoclave Test Results 142
4.5.3 Summary 144
4.6 Concluding Remarks 144

Chapter 5

Flexural and Shear Behaviour of Small-scale Reinforced Concrete Beams Affected by ASR 146

5.1 Overview 146
5.2 Experimental Program 149

5.2.1 Materials and Mix Proportions 149
5.2.2 Specimen Fabrication 150
5.2.3 ASR Acceleration 153
5.2.4 Expansion and Mass Change Measurements 154
5.2.5 Testing of Mechanical Properties 155
5.2.6 Load Capacity Test under Four-Point Loading 157
5.3 Results and Discussion 160
5.3.1 Cracking of Specimens 160
5.3.2 Length Change of Concrete Prisms 162
5.3.3 Modulus of Elasticity 163
5.3.4 Compressive Strength 164
5.3.5 Splitting Tensile Strength 165
5.3.6 Load Capacity of Reinforced Concrete Beams 166
5.5 Summary 181

Chapter 6

Bond Behaviour Between Reinforcing Steel Bar and ASR Affected Concrete 183
6.1 Overview 183
6.1.1 Effect of ASR on Bond Characteristics 183
6.1.2 Pull-out Test 187
6.1.3 Bond-slip Model (CEB-FIP Model Code 1990) 190
6.2 Experimental Program 192
6.2.1 Materials and Mix Proportions 192
6.2.2 Specimen Fabrication 193
6.2.3 ASR Acceleration 197
6.2.4 Testing of Mechanical Properties 198
6.2.5 Pull-out Test 198
6.2.6 SEM Examination for Steel-Concrete Interface 200

6.3 Results and Discussion 200
6.3.1 Mechanical properties 200
6.3.2 Bond Strength 201
6.3.3 Bond Stress - Slip Relationship 202
6.3.4 Microstructural Investigation 207
6.4 Summary 208
Chapter 7
Fabrication and Monitoring of Large-scale ASR-affected Beams 209
7.1 Overview 209
7.2 Specimen Fabrication and Conditioning 210
7.2.1 Specimen Design and Reinforcement Detailing 210
7.2.2 Materials and Mix Proportions 211
7.2.3 Concrete Mixing and Placement 213
7.2.4 Curing and Demolding of Beams 215
7.2.5 38 °C Climate Chamber Conditioning 218
7.3 Experimental Program 220
7.3.1 Expansion Measurements 220
7.3.2 ASR Acceleration 224
7.3.3 Testing of Mechanical Properties for Companion Cylinders 228
7.4 Results and Discussion 229
7.4.1 Match-cured Specimens 229
7.4.2 Visual Observations 234
7.4.3 Convex Curvature of Reinforced Concrete Beam Caused by ASR 248
7.4.4 Expansions 250
7.5 Summary 254
Chapter 8
Conclusions and Recommendations 257

8.1 Overview 257

8.2 Conclusions 258

8.3 Recommendations for Future Work 260

References 262

Appendices 280

Appendix A. Morphology of ASR Products 280

Appendix B. Mechanical Property Test Results (2.5% Na_2O_{eq} boosting) 291

List of Figures

Figure 2. 1 Alkali-silica reaction process (adapted from Giannini (2012)) 6
Figure 2. 2 ASR expansion (Larive 1998) 16
Figure 2. 3 ASR induced expansion (Karthik, Mander & Hurlebaus 2016a) 18
Figure 2. 4 Macrocracking and microcracking due to ASR (Courtier 1990)..... 19
Figure 2. 5 Cracking pattern of ASR affected reinforced concrete beam 21
Figure 2. 6 Experiment results of mechanical property degradation from literature..... 24
Figure 2. 7 Schematic diagram of stresses between ribs of a deformed reinforcement (Park & Paulay 1975) 29
Figure 2. 8 Bond failure mechanism between ribs of deformed bar 30
Figure 2. 9 Schematic tensile stress ring in concrete (Tepfers 1979) 30
Figure 2. 10 Bond behaviour at different ASR damage levels 35
Figure 2. 11 Flexural load capacity of reactive and non-reactive beams tested by..... 38
Figure 2. 12 Flexural load capacity of reactive and non-reactive beams tested by..... 42
Figure 2. 13 Flexural load capacity of reactive and non-reactive beams tested by Monette, Gardner & Grattan-Bellew (2002) 45
Figure 2. 14 Moment capacity of reactive and non-reactive beams tested by 47
Figure 2. 15 Flexural capacity change with the expansion 48
Figure 2. 16 Reinforcement detail and shear span of tested beams 52
Figure 2. 17 Shear strength ratio (ASR damaged beam / control beam) 53
Figure 2. 18 Punching shear versus expansion of slabs (Clark & Ng, 1989)..... 56
Figure 2. 19 Shear strength ratio (ASR damaged beam / control beam) 58
Figure 2. 20 Size of the specimen and schematic test set-up 63
Figure 2. 21 Fluorescent impregnated beam observed under UV light 63
Figure 2. 22 Shear test results vs. Calculated shear capacity 64
Figure 2. 23 Shear resistance change with restrained and free expansion 66
Figure 2. 24 Shear capacity of ASR affected concrete structures 68
Figure 2. 25 FE model of an ASR affected gravity dam..... 69
Figure 2. 26 Long-term deterioration of ASR affected dam 70
Figure 2. 27 Relation between expansion and total alkali content, different types of cement 79
Figure 2. 28 Effect of the water-to-cement ratio on the expansion of mortar bars 80
Figure 2. 29 Impact of autoclaving temperature on mortar bar expansions..... 81

Figure 2. 30 Impact of autoclaving duration on mortar bar expansions 82
Figure 2. 31 Laval/CANMET autoclave mortar bar test procedure 83
Figure 2. 32 Expansions of different mixtures under various alkali contents and autoclaving durations at 133 °C (Giannini & Folliard 2013)..... 85
Figure 2. 33 Rheological model by Ulm et al. 2000..... 87

Figure 3. 1 Cracking of bridge beams due to ASR..... 90
Figure 3. 2 ASR affected bridge beams from a demolished bridge deck 91
Figure 3. 3 Test specimens in an autoclave..... 94
Figure 3. 4 Temperature-time and pressure-time relationships for one cycle of autoclaving 95
Figure 3. 5 Expansion of reactive aggregate B prisms with 3% Na_2O_{eq} boosting after autoclaving at ages of 3, 7, and 28 days..... 96
Figure 3. 6 Expansion of reactive aggregate B prisms with 5% Na_2O_{eq} boosting after autoclaving at ages of 3, 7, and 28 days..... 97
Figure 3. 7 Non-reactive concrete cylinders (90-day) in Zirbus LVSA 50/70 autoclave 101
Figure 3. 8 Average expansion (of 3 specimens made with aggregate B) at the ages of 3, 7 and 28 days 102
Figure 3. 9 Crack patterns of reactive aggregate B prisms with 3% Na_2O_{eq} boosting after 3 cycles of autoclaving at ages of 3, 7, and 28 days 103
Figure 3. 10 Compressive strength of 28-day value and..... 104
Figure 3. 11 Flexural strength of 28-day value and..... 105
Figure 3. 12 Residual modulus of elasticity compared to the 90-day value 107
Figure 3. 13 Compressive strength of non-reactive concrete cylinders tested at the age of 90 days and after 1, 2, 3 cycles of 130 °C autoclaving 107
Figure 3. 14 Microscopic observation on samples of autoclaved specimens by SEM . 109

Figure 4. 1 Grading curve of crushed aggregates 114
Figure 4. 2 Temperature and pressure in the autoclave chamber adopted for the multi-cycle accelerated test..... 117
Figure 4. 3 Expansion of specimens after steam warming in an autoclave 118
Figure 4. 4 Expansion – Alkali content relationship (80 °C autoclave steam warming) 119

Figure 4. 5 SEM-EDS map of ASR gel within an aggregate 122
Figure 4. 6 SEM-EDS map of ASR gel lining pore with sponge-like morphology 123
Figure 4. 7 SEM-EDS map of ASR gel at aggregate-cement paste interface 124
Figure 4. 8 Cumulated PSD of fine aggregates (Sydney sand) 126
Figure 4. 9 Cumulated PSD of coarse aggregates (dacite aggregate) 127
Figure 4. 10 70L Pan mixer 129
Figure 4. 11 Zirbus LSVA 50/70 autoclave used for the test 130
Figure 4. 12 Specimens as placed in the autoclave 130
Figure 4. 13 Time-temperature cycles adopted in the autoclave chamber 131
Figure 4. 14 Expansion of concrete prisms after 3 cycles in the autoclave 132
Figure 4. 15 Mass change of concrete prisms after 3 cycles in the autoclave 133
Figure 4. 16 External cracks on cylinder after 3 cycles in the autoclave 134
Figure 4. 17 External map cracking on prism after 3 cycles in the autoclave 134
Figure 4. 18 Internal cracks and ASR gel in aggregate from concrete prism after 3 cycles in the autoclave observed using laser confocal scanning microscope 135
Figure 4. 19 SEM-EDS map of ASR gel formed in an aggregate 136
Figure 4. 20 SEM images showing ASR products with rosette-like morphology 137
Figure 4. 21 SEM images showing ASR products with network and plate-like morphology 137
Figure 4. 22 SEM images showing ASR products with crystalline morphology 138
Figure 4. 23 Influence of alkali loading on compressive strength of concrete cylinders tested at age of 3, 7 and 28 days 139
Figure 4. 24 Change in compressive strength and modulus of elasticity of concrete cylinders with 2.5% alkali boosting after 3 cycles in the autoclave 140
Figure 4. 25 Comparison of expansion results between 80°C autoclave treatment with alkali boosting and AMBT for dacite aggregate mortar bar 142
Figure 4. 26 Comparison of expansion results between 80°C autoclave treatment with 2.5% alkali boosting and CPT for dacite aggregate prism 143

Figure 5. 1 Detail of reinforcement of small-scale reinforced concrete beam 151
Figure 5. 2 Reinforcing steel bars in steel moulds 152
Figure 5. 3 Specimens cast for flexural and shear test 152
Figure 5. 4 Specimens as placed in the Zirbus LVSA 50/70 autoclave 154
Figure 5. 5 Length measurement using a comparator 155

Figure 5. 6 Modulus of elasticity test on 100 mm diameter 200 mm height cylinder .. 156
Figure 5. 7 Splitting tensile strength test 157
Figure 5. 8 Schematic test set up for load capacity test (adapted from ASTM C78) ... 158
Figure 5. 9 2D-DIC imaging systems 158
Figure 5. 10 Testing of reinforced concrete beams under four-point loading with 2D-DIC system 160
Figure 5. 11 Crack pattern of cylinders after 3 cycles of autoclaving 161
Figure 5. 12 External cracks on reinforced beam after 3 cycles in the autoclave 161
Figure 5. 13 White exudation on surface of small-scale reinforced concrete beam after 2nd cycle of autoclaving 162
Figure 5. 14 Length change of concrete prisms after 3 cycles in the autoclave 163
Figure 5. 15 Change in modulus of elasticity of concrete cylinders 164
Figure 5. 16 Change in compressive strength of cylinders 165
Figure 5. 17 Change in splitting tensile strength 166
Figure 5. 18 Load capacity test results of small-scale reinforced concrete beam with two N5 deformed bars 167
Figure 5. 19 Beam D7-1: (a) Failure mode; (b) Load-displacement curve 169
Figure 5. 20 Beam D7-2: (a) Failure mode; (b) Load-displacement curve 170
Figure 5. 21 Beam D7-3: (a) Failure mode; (b) Load-displacement curve 171
Figure 5. 22 Beam D7-4: (a) Failure mode; (b) Load-displacement curve 172
Figure 5. 23 Beam D7-5: (a) Failure mode; (b) Load-displacement curve 173
Figure 5. 24 Load capacity test results of small-scale reinforced concrete beam with two N8 deformed bars 174
Figure 5. 25 Beam D4-1: (a) Failure mode; (b) Load-displacement curve 175
Figure 5. 26 Beam D4-2: (a) Failure mode; (b) Load-displacement curve 176
Figure 5. 27 Beam D4-3 after 1 cycle of autoclaving: (a) Failure mode; (b) Load-displacement curve 177
Figure 5. 28 Beam D4-4 after 2 cycles of autoclaving: (a) Failure mode; (b) Load-displacement curve 178
Figure 5. 29 Beam D4-5 after 3 cycles of autoclaving: (a) Failure mode; (b) Load-displacement curve 179

Figure 6. 1 Change in bond strength with expansion (Haddad & Nymayr 2007) 185
Figure 6. 2 Change in bond strength with restrained expansion (Li et al. 2020) 186

Figure 6. 3 ASR gel formation at steel-concrete interface and its effect on bond (Gardoni et al. 2013) 187
Figure 6. 4 Schematic pull-out test diagram (Castel & Foster 2015) 188
Figure 6. 5 Influence of embedment length on bond stress distribution 190
Figure 6. 6 Bond stress – slip model (CEB-FIP Model Code 1990) 190
Figure 6. 7 Rib pattern of 8 mm diameter deformed bar 193
Figure 6. 8 Pull-out test specimen design (50 mm bond length specimen) 194
Figure 6. 9 Reinforcing steel bars with 80 mm long tubes 195
Figure 6. 10 Rebars sitting in steel moulds ready for concrete casting 195
Figure 6. 11 Pull-out Specimens and cylinders + prisms 196
Figure 6. 12 Stress-strain curve of reinforcing steel bar 198
Figure 6. 13 Schematic diagram of pull-out test set up 199
Figure 6. 14 Instrumentation and test set-up for the pull-out tests 200
Figure 6. 15 Bond stress – slip relationship 203
Figure 6. 16 Bond stress – slip relationship and failure mode (specimens with 50 mm bond length, tested after 1st cycle of autoclaving at 80 °C) 204
Figure 6. 17 Bond stress – slip relationship and failure mode (specimens with 50 mm bond length, tested after 2nd cycle of autoclaving at 80 °C) 205
Figure 6. 18 Bond stress – slip relationship and failure mode (specimens with 50 mm bond length, tested after 3nd cycle of autoclaving at 80 °C) 206
Figure 6. 19 SEM image of ASR gel with cracked platy-crystal morphology 207

Figure 7. 1 Reinforcement details of full-scale 3 m long reinforced concrete beam 211
Figure 7. 2 Concrete mixing using a 70L pan mixer 213
Figure 7. 3 Slump test 214
Figure 7. 4 Concrete placement for plain concrete beam 214
Figure 7. 5 Concrete placement for reinforced concrete beam 215
Figure 7. 6 Moist curing of beams and companion specimens in the laboratory at a temperature of 23 ± 2 °C 216
Figure 7. 7 Demolding of R1 beam – reactive plain concrete beam 217
Figure 7. 8 Moving reinforced concrete beam into 38 °C climate chamber 219
Figure 7. 9 DEMEC points arrangement (R1 beam – reactive plain concrete beam) 221
Figure 7. 10 DEMEC points arrangement (R2 beam – reactive reinforced concrete beam) 222

Figure 7. 11 DEMEC points arrangement (R3 beam – reactive reinforced concrete beam) 222
Figure 7. 12 DEMEC points arrangement (R4 beam – reactive reinforced concrete beam) 223
Figure 7. 13 DEMEC points arrangement (NR1 beam, non-reactive reinforced concrete beam, flipped over) 223
Figure 7. 14 DEMEC points adhered on surface of cylinder and length measurement 224
Figure 7. 15 Water supplying conditions of plain concrete beam and reinforced concrete beams tested by Multon & Toutlemonde (2010) 225
Figure 7. 16 Schematic diagram of supplying water to the beams 226
Figure 7. 17 Water supply of R1 beam – plain concrete beam, simply supported 227
Figure 7. 18 Water supply of R3 beam – reinforced concrete beam 227
Figure 7. 19 Change in modulus of elasticity of cylinders with 1.25% alkali loading . 230
Figure 7. 20 Change in compressive strength of cylinders with 1.25% alkali loading 232
Figure 7. 21 External cracks on cylinders after 1 year of immersing in water 234
Figure 7. 22 External cracks on cylinders at the age of 500 days, immersed in water and stored in 38 °C climate chamber, without autoclaving specimens 235
Figure 7. 23 External cracks on cylinders after 1 year of immersing in water and stored in 38 °C climate chamber (with 130 °C autoclaving for 5 hours at the age of 180-day) 236
Figure 7. 24 Comparison of cylinders at the age of more than 5 years cured in: (a) fog-room with 100%RH at 23 °C and (b) field exposure conditions (Karthik, Mander & Hurlebaus 2016b) 237
Figure 7. 25 External cracks on prism (after 500 days of immersing in water 238
Figure 7. 26 R1 beam surface (photo taken on 03/05/2019 after the beam was moved into the 38 °C climate chamber) 239
Figure 7. 27 Cracking on R1 beam surface 240
Figure 7. 28 Cracking on R1 beam surface 240
Figure 7. 29 Map cracking on R1 beam surface 241
Figure 7. 30 Cracking on R1 beam surface 241
Figure 7. 31 Map cracking on R1 beam surface 242
Figure 7. 32 Cracking on R1 beam surface 242
Figure 7. 33 Longitudinal cracking on R2 beam surface 244

Figure 7. 34 Longitudinal cracking on R2 beam surface 245
Figure 7. 35 Longitudinal cracking on R3 beam surface 246
Figure 7. 36 Longitudinal cracking on R3 beam surface 247
Figure 7. 37 (a) Schematic set-up of laser displacement sensor; (b) Deployment of laser sensor for R2 beam to measure the displacement of the beam 249
Figure 7. 38 Upward displacement of R2 beam 250
Figure 7. 39 Average free expansion of prisms and cylinders stored in 38 °C climate chamber with the 3 m long beams 251
Figure 7. 40 Average longitudinal and lateral expansion of R1 plain concrete beam stored in 38 °C climate chamber 252
Figure 7. 41 Average longitudinal and lateral expansion of R2 reinforced concrete beam stored in 38 °C climate chamber 252
Figure 7. 42 Average longitudinal and lateral expansion of R3 reinforced concrete beam stored in 38 °C climate chamber 253

Figure A. 1 SEM images showing ASR products with rosette-type morphology 280
Figure A. 2 SEM images showing ASR products with rosette-type morphology 281
Figure A. 3 SEM images showing ASR products with crystalline morphology 282
Figure A. 4 SEM images showing ASR products with crystalline morphology 283
Figure A. 5 SEM images showing ASR products with rosette-type morphology 284
Figure A. 6 SEM images showing ASR products with rosette-type morphology 285
Figure A. 7 SEM images showing ASR products with crystalline morphology 286
Figure A. 8 SEM images showing ASR products with network and plate-like morphology (sample from 80 °C accelerated autoclave test) 287
Figure A. 9 SEM images showing ASR products with plate-like morphology 288
Figure A. 10 SEM images showing ASR products with plate-like morphology 289
Figure A. 11 SEM images showing ASR products with crystalline and rosette-type morphology (observed from 38 °C CPT test sample) 290

Figure B. 1 MOE test results (28-day) 292
Figure B. 2 MOE test results (after 1 cycle of 80 °C autoclaving) 292
Figure B. 3 MOE test results (after 2 cycles of 80 °C autoclaving) 293
Figure B. 4 MOE test results (after 3 cycles of 80 °C autoclaving) 293

List of Tables

Table 2. 1 Some potentially reactive aggregate types (Blight & Alexander 2011)..... 11
Table 2. 2 Retained mechanical property in percentage of 28-day values of unaffected concrete (ISE 1992) 23
Table 2. 3 Shear capacity of slabs tested by Bilodeau et al. (2016) 61
Table 2. 4 Summary of ultra-accelerated autoclave tests..... 78

Table 3. 1 Oxide composition of Portland cement used in the mixes 93
Table 3. 2 Concrete mix proportions 93
Table 3. 3 Comparison of mechanical properties between low-alkali..... 99
Table 3. 4 Modulus of elasticity of 90-day non-reactive cylinders 106

Table 4. 1 Chemical composition of general-purpose Portland cement (wt.%)..... 114
Table 4. 2 Chemical composition of the aggregates (wt. %) 115
Table 4. 3 Mix proportions per cubic metre of concrete..... 127
Table 4. 4 Aggregate reactivity classification (ASTM C1778-20) 141

Table 5. 1 Mix proportions per cubic metre of concrete..... 150
Table 5. 2 Load capacity test results of N5 rebar beams 167
Table 5. 3 Load capacity test results of N8 rebar beams 174

Table 6. 1 ASR acceleration for pull-out test specimens..... 197
Table 6. 2 Average compressive strength, modulus of elasticity and splitting tensile strength at 28-day and after 1, 2 and 3 cycles of autoclaving 201
Table 6. 3 Pull-out test results 202

Table 7. 1 Full-scale 3 m long beams 210
Table 7. 2 Concrete mix proportion for 3 m long full-scale beams..... 212
Table 7. 3 Companion cylinders and prisms of 3 m long full-scale beams 228
Table 7. 4 Modulus of elasticity of cylinders with 1.25% alkali loading 230
Table 7. 5 Compressive strength of cylinders with 1.25% alkali loading 233

Table B. 1 Modulus of elasticity test results 291
Table B. 2 Compressive strength test results 294
Table B. 3 Splitting tensile strength test results 295

Abstract

Alkali-silica reaction (ASR) in concrete is one of the most harmful long-term durability problems for concrete structures. Concerns about the potential risks of ASR to the affected structures led to considerable research in the past several decades. Conventionally, field load testing on actual structures, or large scale in-situ testing are employed to assess the residual load capacity of the ASR affected structures. Such methods, however, are labour intensive, time consuming and may cause unpredictable further damage to the structure. This study aims to investigate the residual load capacity and bond deterioration of ASR affected reinforced concrete structures through laboratory accelerated tests. Based on previous research on accelerated autoclave test for ASR, a novel multi-cycle accelerated test by adopting 80 °C steam warming, with 60-hour cycles and appropriate alkali loading is investigated. Results revealed that, for concrete with highly reactive dacite aggregate and 2.5% alkali boosting, an expansion of 0.18% was achieved after 3 cycles. The compressive strength showed an initial increase at low expansion levels followed by a reduction at higher expansion levels. Modulus of elasticity, however, systematically decreased with increasing expansion. Furthermore, the multi-cycle accelerated test was applied to study the flexural and shear behaviour of small-scale reinforced concrete beams. Results suggest that chemical prestressing induced by ASR expansion has beneficial effects on strength and stiffness of the affected structure at early stages. Effect of high ASR expansion levels on the long-term structural behaviour, however, needs further investigation.

Chapter 1

Introduction

1.1 Background

Reinforced concrete has been widely used in bridges, dams, and building structures due to its advantages, such as low maintenance requirements, economical, and its ability to be pre-cast or cast in-situ as required. Reinforced concrete, as a structural material, however, also has its disadvantages. The deterioration phenomenon of concrete material is one of them. Alkali-silica reaction (ASR) in concrete is a potential source of deterioration. Damage caused by ASR in concrete is one of the major durability problems for concrete structures and has been observed as such in many countries around the world (Rajabipour et al. 2015). Concerns about the residual load capacity of structures due to ASR damage in the concrete were raised and had led to the research in the past several decades.

Stanton (1940) investigated the premature failure of concrete pavements and partial failure of bridge structures in California. It was found that the excessive expansion due to a chemical reaction inside the concrete was the predominant factor that induced tensile stresses, which could in some circumstances exceed the tensile strength of the material, resulting in cracking of concrete. This was identified as alkali-silica reaction. Since then, numerous papers on this deleterious chemical reaction have been published, including researches on reaction mechanism, test methods, effective methods to mitigate potential ASR and impact of ASR on structural behaviour of the affected concrete structures. Various models including theoretical approaches, microscale, mesoscale or macroscale models, have been developed by different researchers to predict the ASR effects.

However, the mechanism of the chemical and physical reaction has hitherto not been clearly understood (Pan et al. 2012; Rajabipour et al. 2015).

From the early 1940s to 1958, a national research programme in Australia for exploring the nature of ASR was organised by the Commonwealth Scientific and Industrial Research Organisation (CSIRO). Vivian H. E. led the programme and conducted systematic research on chemistry and mechanism of ASR, using opal as the preferred reactive aggregate. A holistic concept of ASR was established through this research programme (Idorn 1989).

Based on the research conducted by Stanton, Vivian, and Hansen, Powers & Steinour (1955) interpreted the nature of the alkali-silica reaction and the mechanism of the expansion caused by ASR. Powers concluded that the most reactive minerals are amorphous or contain amorphous constituents. The mechanism of expansion was interpreted as the alkali-silica complex imbibes water, causing swelling pressure in the hardened concrete matrix and forming cracks in concrete. Powers further pointed out that cement with less than 0.6 percent alkali is usually safe based on mortar bar tests. However, “a safe reaction might be converted to an unsafe one if the specimen is dried and re-saturated before the reaction is complete” (Powers & Steinour 1955).

In the field of predicting and assessing the structural performance of ASR affected concrete structures, a considerable amount of research work has been conducted. Research on the load-carrying capacity of ASR affected reinforced concrete beams, however, shows some contradictory results. On one hand, reduction in material properties, such as compressive strength, tensile strength, and modulus of elasticity was reported due to ASR in concrete. On the other hand, experimental studies performed by different researchers showed that the residual load-carrying capacity of the ASR affected

beams was not significantly affected or even slightly increased indeed. However, when compared to the service life of a structure, these tests are only a snapshot in time. The long-term ASR effects on the load-carrying capacity of the structure are still unclear. A reliable analytical tool to assess capacity reduction due to ASR, especially the long-term effects of ASR is thus needed. The capacity reduction also needs to be verified by suitable accelerated testing in the laboratory.

1.2 Research Scope of the Whole Project

The research of this dissertation is under the context of a wider project funded through the Australian Research Council Research Hub for Nanoscience Based Construction Materials Manufacturing (ARC NanoComm Hub) with the support of the Cement, Concrete & Aggregates Australia (CCAA), which is currently being conducted at the University of Technology Sydney. The aims of the whole research project include:

- Aim 1: To develop an accurate analytical model to assess the residual load capacity of alkali-silica reaction (ASR) damaged reinforced concrete structures.
- Aim 2: To verify the analytical model by accelerated laboratory ASR tests.
- Aim 3: To identify the most affected parameter of a reinforced concrete element by ASR (whether it is shear capacity, moment capacity, bond deterioration, or serviceability related parameters such as deformation and cracking), and ultimately, to assess the overall capacity reduction of the whole super-structure.

1.3 Research Objectives of the Current Project

This study aims to investigate the residual load capacity and bond deterioration of ASR affected reinforced concrete structures through laboratory accelerated tests. Accelerated ASR experiments on the deterioration of concrete material properties, bond deterioration

between reinforcement and concrete, bending moment capacity, and shear capacity of ASR affected beams would lead to advanced models and provide verification to assess the residual load capacity of ASR affected reinforced concrete structures, accurately.

1.4 Research Contributions

The thesis investigated the ultra-accelerated autoclave test for screening potential reactivity of aggregates. The influence of ultra-accelerated autoclave tests on the mechanical properties of concrete is also investigated. A novel multi-cycle autoclave test method is developed to identify the potential reactivity of aggregates and to assess the potential risk of ASR.

By adopting the developed multi-cycle accelerated autoclave test method, experimental studies on bond behaviour of ASR affected reinforced concrete through performing pull-out tests, moment capacity and shear capacity of reinforced concrete beams under four-point loading are conducted. Results show that the multi-cycle accelerated autoclave test method is able to accelerate ASR expansion within a short period of time. This test is conducted to simulate ASR deterioration effect in the field.

Full-scale 3 m long plain and reinforced concrete beams are also cast and are currently being stored at 38 °C in a climate chamber for studying the long-term behaviour of ASR affected concrete members.

1.5 Structure of the Thesis

Structure of this dissertation consists of eight chapters. Chapter 1 is a brief introduction to ASR and the research scope. Chapter 2 provides a detailed literature review. Literature on the mechanism of ASR, effects of deleterious ASR on mechanical property, and structural behaviour are reviewed. Various laboratory accelerated test methods for

identifying the reactivity of aggregates and for assessing the potential risk of ASR are reviewed and summarised. Chapter 3 investigates the ultra-accelerated autoclave test for ASR and the mechanical property of concrete under ultra-accelerated autoclave test conditions. Chapter 4 presents the development of a new multi-cycle accelerated autoclave test method for determining the reactivity of aggregates and for assessing the potential risk of ASR. Experiments on both mortar and concrete specimens led to the novel multi-cycle accelerated autoclave test for ASR.

In Chapter 5, small-scale reinforced concrete beams with a low ratio of reinforcement are subjected to a multi-cycle accelerated autoclave test. The bending moment capacity of the small-scale beams under accelerated autoclave test condition is obtained through four-point loading. Similarly, shear capacity of small-scale beams with relatively high reinforcement ratio is also studied under accelerated autoclave test. Chapter 6 investigates the bond behaviour between reinforcement and ASR affected concrete. The specimens are subjected to the multi-cycle accelerated autoclave test and then pull-out test. Chapter 7 presents the fabrication and expansion monitoring of the full-scale 3 m long beams currently being stored in 38 °C climate chamber, which are prepared for further studying the long-term ASR effect on behaviour of the affected concrete members in the future.

Chapter 8 draws the conclusions of this research. Recommendations and future work are also presented in this chapter.

Chapter 2

Literature Review

2.1 ASR Mechanism

ASR is a potential long-term chemical reaction process in concrete. In this process, the alkali in the pore solution of hydrated cement paste react with certain types of siliceous minerals in the aggregates. The product of this chemical reaction is an ASR gel at the reactive particle sites and in the cement paste. This gel can swell by imbibing water or moisture, and cause expansion of the concrete. When excessive expansion happens, the stress induced by the expansive force exceeds the tensile strength of the concrete and leads to cracking of the hardened concrete (Giannini 2012; Pan et al. 2012; Rajabipour et al. 2015). The mechanism of ASR reaction is demonstrated in Figure 2.1.

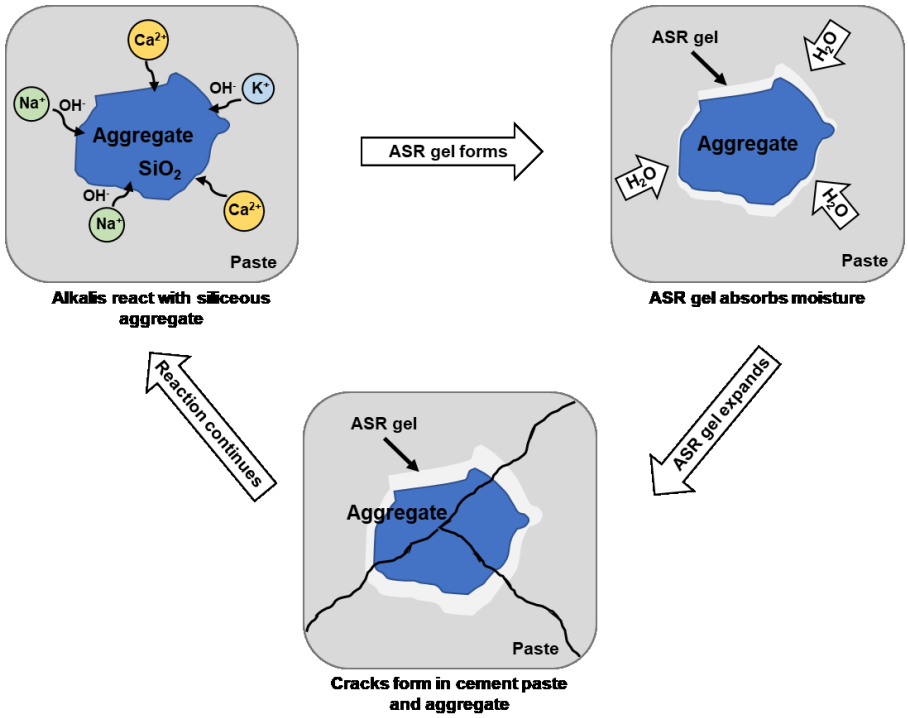

Figure 2. 1 Alkali-silica reaction process (adapted from Giannini (2012))

This deleterious long-term ASR process is very complicated, and the mechanism of chemical and physical reaction has hitherto not been clearly understood (Pan et al. 2012). As reported by Pan et al. (2012), ASR process can be depicted in two distinct stages as shown in Figure 2.1, following description proposed by Dent Glasser & Kataoka (1981). First, the silica in reactive aggregates reacts with the alkali ions in pore solution and produces the alkali-silica gel:

$$\equiv Si - O - Si \equiv \; + \; R^{+}OH^{-} \; \rightarrow \; \equiv Si - O - R \; + \; H - O - Si \equiv \qquad (2.1)$$

(Alkali-silica gel)

where R^+ represents an alkali ion (Na^+, K^+, etc.), which has considerable concentrations in the pore solution during concrete mixing. The produced weak silicic acid immediately reacts with alkali ions to continue to form alkali-silica gel:

$$\equiv Si - O - H \; + \; R^{+}OH^{-} \; \rightarrow \; \equiv Si - O - R \; + \; H_2O \qquad (2.2)$$

In the first stage, the hygroscopic alkali-silica gel is created following Equations (2.1) and (2.2). In the second stage, based on the description in Equation (2.3), the alkali-silica gel absorbs water and expands.

$$\equiv Si - O - R \; + \; n\,H_2O \; \rightarrow \; \equiv Si - O^{-} - (H_2O)_n \; + \; R^{+} \qquad (2.3)$$

where, n denotes the hydration number.

However, the swelling ability or the expansion capacity of the produced ASR gel can be significantly affected by the availability of Ca^{2+}. With reference to Thomas (1998), Leemann et al. (2011), and Mahanama et al. (2019), when calcium is available, the silica dissolved from the aggregates was first consumed by calcium to produce calcium silica hydrate (C-S-H) that has a lower Si saturation point than ASR gel. Afterwards, the dense C-S-H gel serves as a firm barrier on voids in aggregates and defects on the aggregate

surface to prevent the leaching out of silica and reaction products, permitting silica ion concentration in voids to reach saturation to form dense ASR gel with high swelling capacity. In terms of the role of sodium and potassium ions on the formation of ASR gel, they are allowed to penetrate into the voids and the defects that are isolated by the dense C-S-H gel, and thus contribute to the production of a viscous gel, resulting in high expansion pressure and consequent tensile stresses. Once the tensile strength of the concrete is exceeded, cracks form. In summary, main findings relating to the ASR mechanism from literature can be addressed as followings:

- In addition to the alkali ions from the cement, the aggregate will release alkali ions over time. Supplementary Cementitious Materials (SCMs) and external aggressive substances (e.g., seawater, de-icing salts) will also provide alkali ions for the reaction (Thomas 2011).
- Portland cement with limited value of alkalis (Na_2O + 0.658 K_2O), e.g., less than a threshold of 0.6% in terms of equivalent Na_2O by mass, is usually safe. However, a safe reaction might be converted to an unsafe one if the specimen is dried and re-saturated before the reaction is complete (Powers & Steinour 1955).
- Aggregate, as the main source of reactive silica, is essential to ASR. Aggregate composition and mineralogy, aggregate size, pessimum reactive contents are essential to deleterious ASR.
- The reaction product of alkali and reactive silica, ASR gel, varies widely in chemical composition and morphology. According to findings of Thaulow, Jakobsen & Clark (1996), ASR gel consists of 53 – 63% silica, 20 – 30% calcium and around 15% of sodium and potassium. The gel is hygroscopic, and it expands as it absorbs water, allowing the movement of ions (i.e., Na^+, K^+, Ca^{2+} and OH^-)

towards the aggregate and retarding outward transfer of silica ions from the reactive aggregate, which results in osmosis and expansion pressure.

- The expansion pressure produced by the expanding of hygroscopic ASR gel is unable to create damage in concrete. However, the presence of free calcium hydroxide from the cement paste can promote synthesizing a dense C-S-H barrier which restricts the removal of the reaction products from the reaction area but allows the access of Na^+ and OH^- ions to the reaction sites. This leads to the increasing pressure at the interface of cement paste and aggregate, resulting in microcracking and consequent degradation of concrete. Also, calcium partially exchanges with alkalis in the gel, changing its morphology and viscosity. The alkalis discharged from this process further react with the reactive siliceous constituents in the deeper layer of the aggregate grains, resulting in recycling of some of the alkalis and keeping the reaction to continue (Wang & Gillott 1991).

Overall, ASR is a slow, time-dependent complex process in concrete structures which involves the development of the high concentration of alkali metal hydroxides in the pore solution, dissolution of reactive siliceous constituents in certain types of aggregates, the formation of ASR gels, swelling of gel by imbibing water and subsequent cracking and deterioration of the concrete structures.

2.2 Conditions for Deleterious ASR

Based on the basic fundamentals of the reaction interpreted in Chapter 2.1, it is generally acknowledged that for ASR to occur in hardened concrete, three conditions need to be satisfied: a sufficient alkali content in pore solution of concrete; a critical amount of reactive siliceous minerals in aggregates; and adequate moisture. However, for

deleterious ASR which causes the damage of concrete, a fourth condition is required, that is, the availability of calcium (Thomas 2018).

As for the source of alkalis, the majority of alkalis are from Portland cement (Mather 1999). But alkalis may also be supplied by other sources. Studies by Bérubé et al. (2002) revealed that a considerable amount of alkalis can be released from the reactive aggregate to the concrete pore solution with time. Other sources, such as chemical admixtures, de-icing salts, seawater can also provide alkalis to concrete. In general, high total alkali content in concrete elevates the pH and hydroxide ion (OH^-) concentration in concrete pore solution, resulting in the accelerated dissolving of the reactive silica in aggregates and a consequent higher risk of ASR (Islam et al. 2016). On the other hand, Bérubé & Frenette (1994) demonstrated that specimens prepared with low alkali cement produced significantly lower expansion compared to the specimens prepared with high alkali content cement. Thus, in common practice, the alkali content in cement is limited to less than 0.6% Na_2O_{eq} to reduce the risk of ASR (Powers & Steinour 1955). Therefore, in the research concerning accelerated ASR in the laboratory, the alkali is externally supplied by immersing the specimens in alkali solutions such as the standard test method in AS1141.60.1 and ASTM 1260, or internally boosted by adding alkali in the mixing water to accelerate the reaction.

Different types of susceptible reactive aggregates reported in the literature are listed in Table 2.1 (Blight & Alexander 2011). The structure of the silica, crystalline or amorphous, and the quantity of reactive silica in the aggregates, have a significant influence on creating deleterious ASR. In addition, mineralogy and chemical composition of aggregates can vary the damage reaction (Strack et al. 2020). Furthermore, size and grading of the aggregates also affect the expansion caused by ASR (Dunant & Scrivener 2012; Gautam et al. 2017; Hobbs & Gutteridge 1979; Multon et al. 2010).

Table 2. 1 Some potentially reactive aggregate types (Blight & Alexander 2011)

Aggregate types		References
Igneous	Andesite	Bérubé & Fournier (1993); Islam & Ghafoori (2013); Swamy (1992); Bérubé et al. (2002); Korkanç & Tuğrul (2005); Çopuroğlu et al. (2009)
	Dacite	
	Rhyolite	
	Basalt	
Metamorphic	Hornfels	
	Phyllite	
	Argillite	
	Quartzite	
Sedimentary	Sandstone	
	Greywacke	
	Chert	
	Flint	
	Shale	

The availability of sufficient moisture is critical for ASR. The role of water in the process of reaction lies in two aspects. In the first place, the ASR gel absorbs water and swells, resulting in the expansion and cracking of the concrete matrix. Secondly, water also acts as a medium transporting alkali cations and hydroxyl ions. It participates directly in the dissolution, reaction, and formation of ASR gel (Swamy 1992). In hardened concrete, after completion of hydration, relative humidity around 80% to 90% is retained due to the residual water in the pores (Swamy 1992). At this level of internal humidity, the reaction tends to occur at limited locations, such as aggregate - cement paste interface, because the mobility of reactants and reaction products is limited due to insufficient moisture (Dent Glasser & Kataoka 1981). However, with increasing of the internal humidity, by supplying water or moving the specimen into high humidity storage conditions, the

expansion caused by ASR is significantly increased (Multon & Toutlemonde 2010; Poyet et al. 2006).

For damaging ASR to occur, the supply of calcium in concrete must be available (Thomas 2018). Although the role of calcium in ASR is equivocal, studies by many researchers (Hou et al. 2005; Hou, Struble & Kirkpatrick 2004; Leemann et al. 2011; Thomas 1998; Thomas 2001; Wang & Gillott 1991) have confirmed that the presence of calcium can aggravate ASR, increase expansion and subsequently cause damage to the concrete. Wang & Gillott (1991) proposed a mechanism relating the effect of calcium on the ASR expansion and concluded that, firstly, calcium promotes the generating of a dense gel-like C-S-H, which helps to preserve a high OH^- concentration and allow the concentration of the dissolved silica to increase. Secondly, Ca^{2+} exchanges for alkali ions in the ASR gel, leading to the recycling of some of the alkalis and further producing of ASR gel. Thomas (1998) studied the effect of calcium in ASR and revealed that, although evidence of ASR existed in specimens without free calcium, the specimens showed limited expansion. On the contrary, for systems with sufficient calcium, significant expansion was observed.

Generally, for ASR in ordinary Portland cement (OPC) concrete, only the first three conditions are addressed in most publications. Other conditions, such as temperature, wetting-drying cycles, constraints from reinforcement, and stress status of the structure can also have a great influence on the evolution of ASR, making this long-term deterioration process more complicated and difficult to predict.

2.3 ASR-Induced Concrete Expansion and Cracking

ASR-induced expansion and cracking in concrete, and the subsequent loss of strength of the concrete or deterioration in serviceability of structure, are features of ASR-related distress in concrete (ISE 1992; Thomas et al. 2013). The primary physical response to

ASR is the expansion of the concrete. This is ascribed to the characteristic of the ASR gel produced in the process of the chemical reaction. The gel absorbs water from the surrounding environment and swells when sufficient water or moisture exists. As the gel swells, it exerts pressure and builds up tensile stress in the surrounding concrete, resulting in microcracking in the concrete matrix, and volumetric expansion of the bulk concrete. With the help of petrographic analysis, microcracking, and microstructure of the reaction products can be examined (Ben Haha et al. 2007; Fernandes et al. 2015; Regourd & Hornain 1987). Many concrete, although with signs of ASR under petrographic examination, show non-deleterious characteristics (ISE 1992). However, with the development of ASR, excessive expansion occurs, and the tensile stress induced by the expansion can surpass the tensile strength of the concrete, consequently, macrocracking forms. Ultimately, the mechanical properties of the concrete deteriorate.

2.3.1 ASR Expansion

An overall expansion occurs accompanying with the development of ASR in the concrete. There are several factors affecting the expansion: the mix composition of the concrete, the environmental conditions, stress state due to the applied load, and restraint due to reinforcement or boundary conditions.

ASR expansion is highly dependent on the concrete mix design. Cement content and alkali level, quantity and crystalline nature of the reactive mineral, aggregate size, and gradation, water to cement ratio (w/c) result in different levels of ASR expansion (Swamy 1992). First, the high the alkali content, the more the silica are prone to be dissolved, and thus a larger ASR gel volume will be produced. Consequently, the ASR expansion will be higher (Multon et al. 2010). Secondly, ASR expansion is heavily influenced by the crystalline structure of the reactive silica in aggregates and the quantity of reactive

minerals. For different types of aggregate, ASR expansion behaviour is different (Islam & Ghafoori 2013). In addition, the water to cement ratio has crucial influence on the permeability and the free water content in the concrete. Higher water to cement ratio (w/c) is likely to retain sufficient amounts of water in concrete after the completion of hydration which can sustain and promote ASR (Fournier & Bérubé 2000; Swamy 1992). Moreover, ASR expansion is also influenced by aggregate size and aggregate grading. Hobbs & Gutteridge (1979) performed experimental tests on concrete specimens with quartz aggregates and found that for grains with sizes between 0.15 and 10 mm, expansion negatively co-related to aggregate size. Multon et al. (2010) observed that for reactive siliceous limestone aggregates, specimens with coarse particles 0.63 mm to 1.25 mm showed largest expansion while no expansion occurred for mortars with particle size less than 0.08 mm. Regarding the effects of coarse aggregate grading on concrete ASR expansion, Gautam et al. (2017) found that the expansions of finer-aggregate-dominated specimens were approximately 50% higher than that of the coarser-aggregate-dominated specimens.

ASR expansion is also influenced by temperature and water supply (Swamy 1992). Gautam & Panesar (2017) reported that when the conditioning temperature was elevated from 38 °C to 50 °C, the expansion rate was increased 2.22 times while the overall expansion trend and the ultimate expansion were similar. Laboratory tests conducted by different researchers (Larive 1998; Multon & Toutlemonde 2010; Poyet et al. 2006) also revealed that sufficient water supplying can significantly promote ASR expansion. Meanwhile, if there is no sufficient water, e.g., lower than 50% of relative humidity in the concrete, ASR expansion will be temporarily inhibited (Swamy 1992). However, if the specimen is re-exposed to sufficient level of moisture, the ASR gel produced

previously will swell rapidly and cause the concrete to continue to expand (Multon & Toutlemonde 2010).

The stress state of structure due to applied load and restraint due to reinforcement or boundary condition can also affect the evolution of ASR expansion. Structures are normally subjected to loads, e.g., dead loads or externally applied sustained loadings. Experimental studies have shown that ASR-induced expansion is reduced along the compressed direction with the increasing of the compressive stress (Larive 1998; Multon & Toutlemonde 2006). Nevertheless, the volumetric ASR expansion was unlikely to be altered by stress conditions (Multon & Toutlemonde 2006). When concrete is under load or restrained conditions, the expansions are pronounced in the less-restrained direction. Mohammed, Hamada & Yamaji (2003b) confirmed this anisotropic expansion behaviour by performing experiments on reinforced concrete specimens. The authors concluded that in the restraint direction, the expansion is significantly reduced due to the passive restraint produced by the steel reinforcement, while the lateral strain is significantly increased. Kagimoto, Yasuda & Kawamura (2014) studied the effects of uniaxial restraints provided by externally installed steel rods on ASR expansion, the expansion of concrete prisms in perpendicular to the restraint direction was found increased. Berra et al. (2010) compared the ASR-induced expansion behaviour under unrestrained and restrained conditions, suggested that the development of ASR-induced expansion may depend on the alkali content and the reactive aggregate type in the concrete mix. Morenon et al. (2017) analysed how restraint and stress state can influence the ASR expansion and proposed a model to take these effects and ASR mechanisms into consideration.

Based on a series of stress-free expansion tests, Larive (1998) proposed a kinetic model to characterize the ASR expansion. The kinetic model is expressed as:

$$\varepsilon(t) = \varepsilon^{\infty} \frac{1-e^{-\frac{t}{\tau_c}}}{1+e^{-\frac{(t-\tau_L)}{\tau_c}}} \tag{2.4}$$

where ε^{∞} is the maximum expansion, τ_c and τ_L represent the characteristic time and the latency time, respectively.

Figure 2.2 shows the ASR evolution curve characterized by Equation (2.4). During the period of latency time τ_L, the development of ASR is slow, then, the ASR expansion develops fast, within the period of characteristic time τ_c. Afterward, the expansion gradually reaches its maximum value.

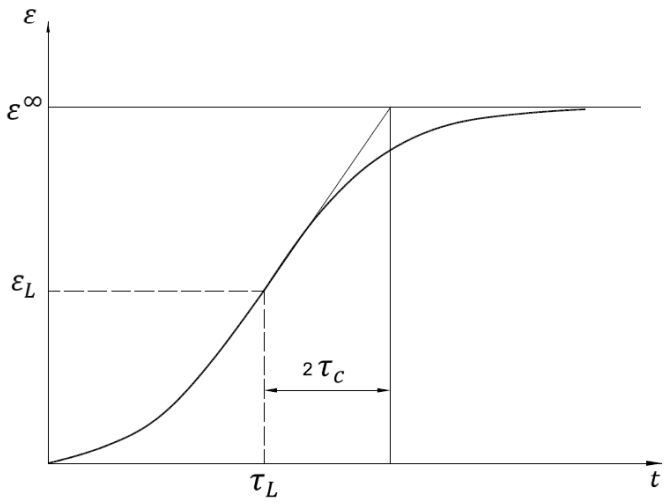

Figure 2. 2 ASR expansion (Larive 1998)

Johnston, Stokes & Surdahl (2000) introduced another kinetic-based model, namely, Kolmogorov–Avrami–Mehl–Johnson (K–A–M–J) model. The model was used by the authors to interpret ASTM C 1260 test results. The model has the following form to depict the reaction kinetics of the nucleation and growth or phase changing:

$$\alpha_t = 1 + \alpha_0 - e^{-k(t-t_0)^M} \tag{2.5}$$

where α_0 is the expansion at time t_0; α_t is the expansion at time t; k is the expansion rate

constant; M is the slope of the regression line.

Capra & Bournazel (1998) proposed a phenomenological model to predict the anisotropic expansion induced by ASR-induced in concrete, by taking into consideration of principal parameters relating to chemical reaction, environmental conditions (e.g., temperature and humidity), and stress status. The evolution of ASR-induced expansion is thus described as:

$$\varepsilon^{asr}(H,T,\sigma,t) = (H)^m \cdot \frac{\varepsilon_0}{A_0} \cdot \left(1 - A_0 - e^{-k_0 \cdot e^{-\frac{E_a}{RT}} \cdot t}\right) \cdot f(\sigma) \quad (2.6)$$

where: H is the relative humidity, m is suggested by the authors to be 8; A_0 and ε_0 are constant parameters relating to concrete material properties, e.g., porosity; k_0 is a kinetic constant to be experimentally determined, E_a is the activation energy, R is the perfect gas constant, and T is the temperature; σ represents the stress tensor and $f(\sigma)$ is the relation between stresses and strains.

For reinforced concrete structures, ASR expansion behaviour is influenced by reinforcement details, load conditions, and stress state of the structure. Based on experimental observations, Karthik, Mander & Hurlebaus (2016a) proposed a semi-empirical reinforced concrete expansion model to predict the swelling strains induced by ASR (see Figure 2.3). The model considered the effects of the applied load, reinforcement ratio, and the environmental variables including temperature and humidity. It takes a hyperbolic tangent function to represent the overall time-dependent expansion strain as shown in Equation (2.7).

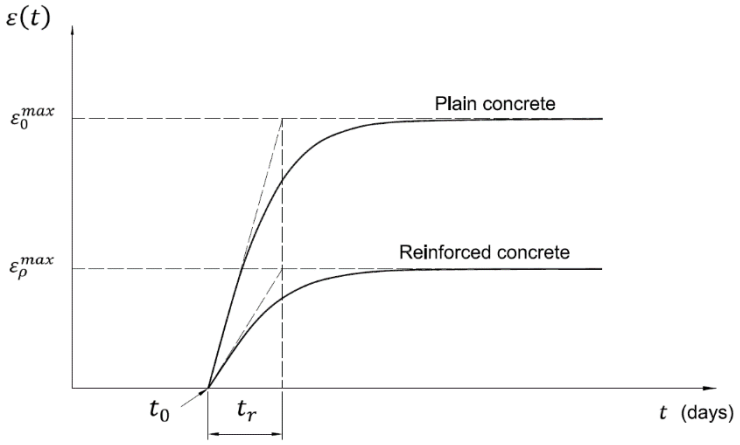

Figure 2. 3 ASR induced expansion (Karthik, Mander & Hurlebaus 2016a)

$$\varepsilon(t) = \varepsilon_\rho^{max} tanh\left(exp\left(\frac{T}{18} + S - 3.11\right)\left\langle\frac{t-t_0}{t_{r,T_0}}\right\rangle\right) \tag{2.7}$$

where:

$\varepsilon(t)$ is the ASR induced expansion strain in reinforced concrete at time t, taking into consideration the influence of temperature and moisture;

ε_ρ^{max} is the maximum expansion in concrete by taking into consideration the influence of reinforcement ratio;

T denotes temperature (° C);

S represents the degree of saturation (0 to 1);

t_0 stands for the initiation time when expansion commences;

t_r is the "rise time";

T_0 represents a constant temperature of 38 ° C.

Expansion results were validated by comparing with small-scale laboratory experimental data and the authors suggested that the model can be further expanded to predict expansion strains for the field reinforced concrete structures affected by ASR.

2.3.2 Cracking

As a result of the gel swelling, and some form of differential expansion effects, normally two types of cracking occurs in ASR affected concrete: macrocracking and microcracking (see Figure 2.4). Cracking is often one of the signs indicating that the concrete is affected by ASR. Cracking is also one of the sources that may cause deterioration of concrete. ASR-induced cracking raises concerns about the durability of the structure. It can cause concrete material property degradation, result in bond deterioration, and ultimately affect the serviceability and load capacity of the structure (Chana 1989; Fan & Hanson 1998; Swamy & Al-Asali 1989).

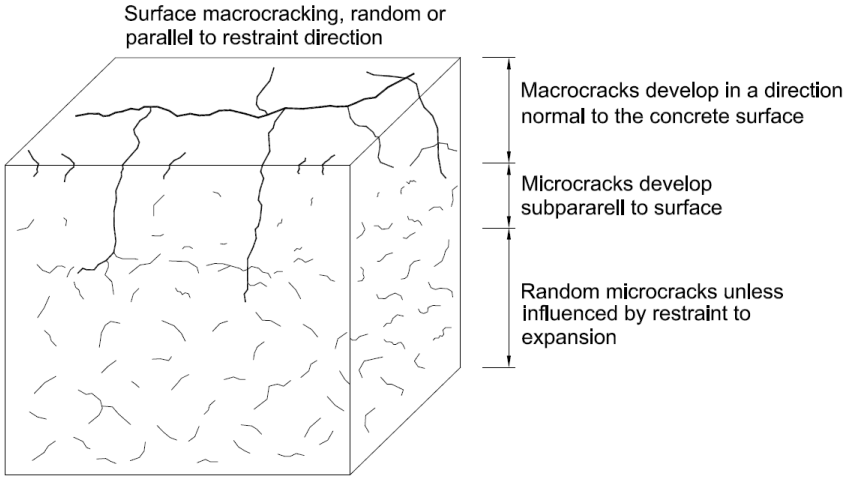

Figure 2. 4 Macrocracking and microcracking due to ASR (Courtier 1990)

According to Courtier (1990), ions penetrate into the microstructure of the reactive aggregate and the reaction products swell by absorbing water thus cause a volume increase. As a result, the reactive particle ruptures and random pattern microcracking occurs. Similarly, Ben Haha et al. (2007) and Sanchez et al. (2015) argued that as ASR develops, the microcracking initiates in the reactive aggregate grains and propagates into the adjacent paste matrix. Dunant & Scrivener (2010) suggested that for slowly reactive aggregates, due to “gel pockets” are formed inside the aggregate particles, microcracking

is first created in the aggregate particles then extends to the cement paste as expansion increases. For rapidly reactive aggregates, ASR happens mainly on the surface of the aggregate thus microcracking forms at the outer part of the aggregate particle and in the paste matrix close to the aggregate, even at the early stage of the reaction. As most cases of ASR distress in ordinary concrete are caused by slowly reactive aggregates, it is generally recognized that the microcracking originates from the aggregate particles, and then develops to the paste matrix (Multon & Sellier 2016).

The microcracking in concrete caused by ASR expansion, or the aggravation of the existing microcracking due to further ASR expansion, affects the mechanical properties of the concrete, e.g., a reduction of elastic modulus, a lesser gain of compressive strength than undamaged concrete, and ultimately, a reduced tensile and compressive strength with the development of ASR (Courtier 1990). The degradation of material properties caused by ASR is further addressed in Chapter 2.4.

Macrocracking is one of the visual features of ASR. Due to the ASR gel swelling, bulk volumetric expansion, and the differentials in the expansion, macrocracking can occur at the surface layer of concrete members (Courtier 1990). In unrestrained plain concrete, macrocracking tends to develop in a more random pattern which is commonly referred to as map cracking. In concrete restrained by loading, such as columns sustaining compression loading, the ASR-induced cracks often appear along the direction of restraint. In reinforced concrete, due to the restraint effect provided by reinforcement, the expansion is elastically restrained aligned with the reinforcement, and thus it produces tensile stresses in the reinforcing steel bars and compressive stress in the surrounding concrete. When the expansion is restrained in one direction, the ASR-induced expansion is transferred to the lesser confined direction. Consequently, the macrocracks tend to be developed along the direction parallel to the reinforcing bars, typically aligned with the

primary reinforcement as shown in Figure 2.5 (Barbosa, Hansen, Hansen, et al. 2018; Hobbs 1988; Thomas, Fournier & Folliard 2013).

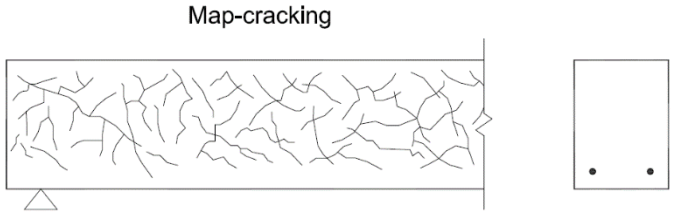

(a) Without top steel reinforcement

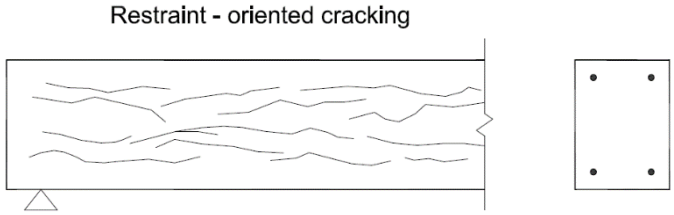

(b) With top and bottom steel reinforcement

Figure 2. 5 Cracking pattern of ASR affected reinforced concrete beam (adapted from the Institution of Structural Engineers, ISE 1992)

Macrocracking as a result of ASR raises concerns about the durability of the affected structure. Cracking opening makes the concrete vulnerable to water ingress and facilitates the ingress of aggressive chemicals such as Cl^-, Na^+ ions. While water and Na^+ can aggravate ASR, ingress of Cl^- can lead to corrosion of the reinforcing steel (ISE 1992; Page & Treadaway 1982). Cracking initiated by ASR also increases the permeability of the concrete and decreases the resistance to freezing – thawing. Combined effects of freezing – thawing and ASR can exacerbate the deterioration of the structure (Deschenes Jr et al. 2018). In addition, macrocracking induced by ASR may affect the bond strength between reinforcing steel bar and concrete, as cracks on cover concrete has a crucial impact on the bond strength (Desnerck, Lees & Morley 2015; Haddad & Numayr 2007). The service life of ASR-affected structures can thus be significantly influenced by these

combined factors relating to the macrocracking of the concrete, although macrocracking may also alleviate the expansion phenomenon in some degree, by absorbing the ASR gel as a "healing" process thus limit the amount of available gel that causing further expansion in concrete (Garcia-Diaz et al. 2006).

2.4 Degradation of Mechanical Properties of ASR-Affected Concrete

For reliably assessing the residual load capacity of the ASR-affected structure, it is essential to understand the ASR effect on the mechanical properties of the affected concrete. According to Courtier (1990), ASR-induced cracking in concrete including microcracking and macrocracking are the main causes of reduction in the stiffness and strength of the affected concrete. The size and the amounts of cracks, also the orientation of the cracks have crucial impacts on the stiffness and strength of the concrete material (Barbosa, Hansen, Hansen, et al. 2018; Sanchez et al. 2015). In other words, the degradation of the mechanical properties is more related to the cracking parameters, such as the density of the cracking, the orientation of cracks, and the proportions of cracks in aggregate and in the paste. However, to quantify these cracking parameters in ASR-affected concrete is not easy. In practice, the reduction in modulus of elasticity, tensile strength, and compressive strength is generally related to the amount of expansion in concrete, and is depicted as a function of free expansion in a combination of crack widths (ISE 1992). The ISE (1992) proposed lower bounds of the residual mechanical properties for unrestrained ASR-affected concrete with different free-expansion levels (see Table 2.2).

Table 2. 2 Retained mechanical property in percentage of 28-day values of unaffected concrete (ISE 1992)

Mechanical Property	Percentage retained related to free expansion*				
	0.5 mm/m	1.0 mm/m	2.5 mm/m	5.0 mm/m	10.0 mm/m
Cube compressive strength	100	85	80	75	70
Cylinder compressive strength	95	80	60	60	--
Tensile strength	85	75	55	40	--
Modulus of elasticity	100	70	50	35	30

(* The free expansion is given figures as mm/m in units, as the expansion incorporates strains and crack width as a combination.)

Table 2.2. assumes that the unaffected concrete does not have property degradation at the age of 28 days, as it is unlikely to experience any appreciable amount of expansion in that period (28 days). The values of the retained mechanical property between the provided expansion numbers can be obtained by linear interpolation. It can be seen from Table 2.2 that, with the increasing of free expansion, the material properties show a decreasing trend. The figures from Table 2.2 implies that the modulus of elasticity is more significantly influenced ASR expansion with respect to strength values. Among the strength values, tensile strength is more sensitive to ASR expansion than compressive strength and shows more reduction than the compressive strength. However, in actual structures, concrete is generally restrained by reinforcement and under biaxial or triaxial stress state condition. Expansion or damage of the concrete is thus different to the free expansion condition, hence, figures from Table 2.2 should be adjusted when it comes to the residual strengths and stiffnesses of actual structures under different conditions (ISE 1992).

Based on the experiment results from different researchers (Ahmed et al. 2003; Giaccio et al. 2008; Hobbs 1988; Sanchez et al. 2018; Sargolzahi et al. 2010; Smaoui et al. 2006; Swamy & Al-Asali 1988), the degradation of mechanical properties of ASR-affected concrete is plotted in Figure 2.6. Lower bounds of residual mechanical properties recommended by ISE (1992) are also plotted. More experimental data can be found in the literature; however, they are not included in Figure 2.6.

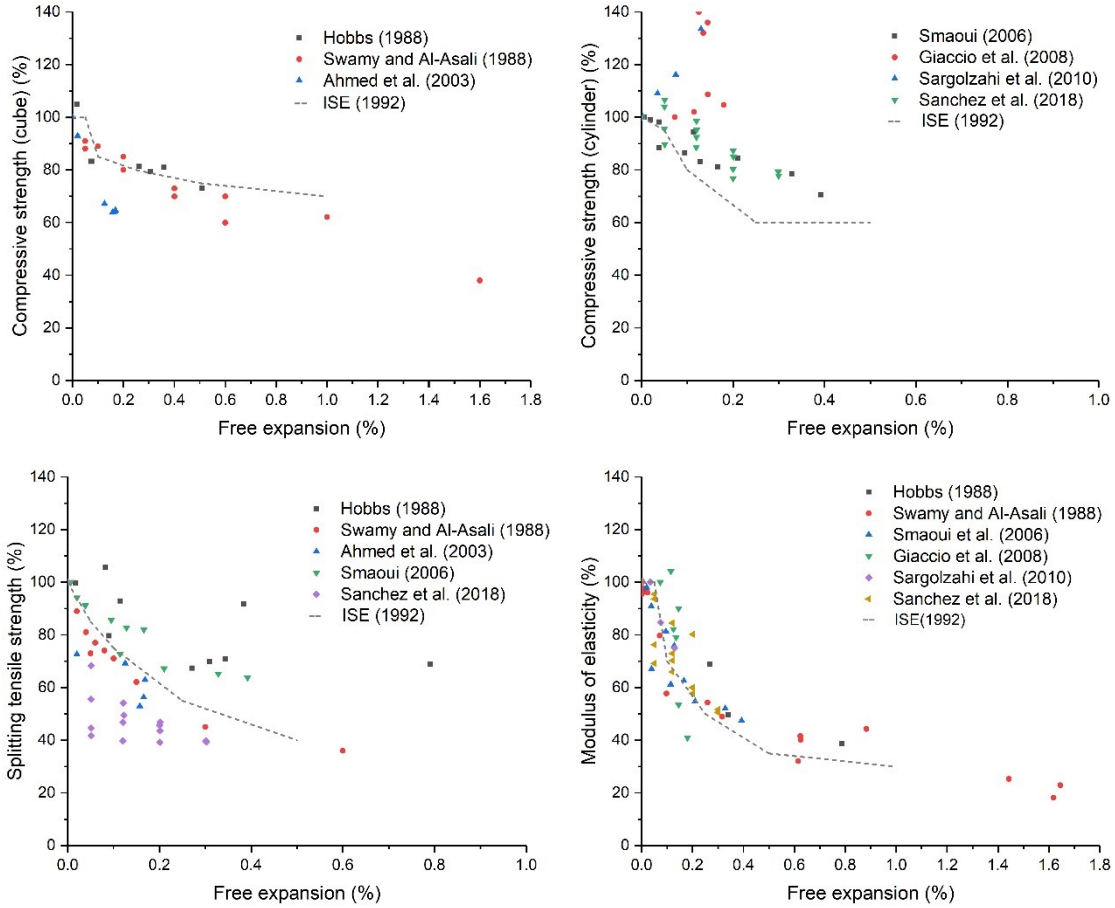

Figure 2. 6 Experiment results of mechanical property degradation from literature

For ASR affected concrete material, early studies showed that the elastic modulus is the most affected property. For example, Ahmed et al. (2003) reported that for specimens with an extreme expansion of 2.70%, a decrease of elastic modulus could reach up to 90%. Similarly, Marzouk & Langdon (2003) reported a decrease of 80% in the elastic modulus for concrete specimens with highly reactive aggregates. Even at 0.15%~0.2%

expansion levels, a reduction of 40% in elastic modulus can be seen from experimental data shown in Figure 2.6, due to the influence of microcracking induced by ASR in the affected concrete. Based on experimental findings, the elastic modulus is recognized as the most sensitive property for ASR affected concrete (Ahmed et al. 2003; Giaccio et al. 2008).

Another sensitive property is tensile strength. Marzouk & Langdon (2003) performed direct tensile strength tests on normal strength concrete specimens, reported a decreasing of 37% in tensile strength for specimens containing highly reactive aggregates, and a decreasing of 31% in tensile strength for specimens with moderate reactive aggregates. Ahmed et al. (2003) found that reduction of the direct tensile strength reached around 50% and 80% for concrete specimens containing reactive Thames Valley sand and mixes containing fused silica, respectively. The reduction in splitting tensile strengths for these two types of mixes was reported to be approximately 35% and 60%, respectively. Sanchez et al. (2018) reported that for expansion levels of 0.05%, reduction of tensile strength can reach 15% to 60%; to expansion levels of about 0.12%, 40% to 65% of tensile strength can be lost; at high-level expansion, 0.2%, significant drops in tensile strength ranging from 45% to 80% is observed. As explained by Sanchez et al. (2018), the tensile strength reduction is attributed to the ASR-induced cracking, because this parameter is highly related to the cracking status of the material (Sanchez et al. 2018).

According to Ahmed et al. (2003), the compressive strength value does not act as a good deterioration indicator for the ASR affected concrete. Marzouk & Langdon (2003) reported that for specimens with highly reactive aggregates, the compressive strength has a 28% decrease. For specimens with moderately reactive aggregates, however, it was not significantly influenced. Experiments performed by Ahmed et al. (2003) showed no significant loss of compressive strength for mixes with reactive Thames Valley sand.

Similarly, Giaccio et al. (2008) performed tests on ASR damaged concrete specimens containing rapid reactive aggregates and slow rate reactive coarse aggregates. While the compressive strength of the concrete samples with rapid reactive aggregates showed no gain, the compressive strength of specimens with slow rate reactive aggregates was found to increase indeed. Larive (1998) monitored the evolution of mechanical properties in the laboratory, found that at 0.20% to 0.3% expansion levels, the compressive strength was not influenced by ASR. However, Sanchez et al. (2018) argue that at expansion levels up to 0.05%, ASR showed a minor influence on the compressive strength, in average only 5% of reduction is reported; when the expansion increased to about 0.12%, the compressive strength is found slightly influenced, with a loss of 10% in average; at a higher level of expansion 0.2%, compressive strength starts dropping, with approximately 25% of reduction; at expansion level of 0.3%, compressive strength can have 35% to 40% of decrease. Barbosa, Hansen, Hansen, et al. (2018) performed tests on cores obtained from ASR-affected field structure to exam the role of crack orientation on compressive strength. The results confirmed that the compressive strength is significantly influenced by the crack pattern. The compressive strength of cores was reduced up to 56%, when the cracking is parallel to the loading direction. However, the compressive strength of cores was found decreased up to 67%, when the cracking is perpendicular to the loading direction. That implies it is important to consider the cracking orientation in assessing the ASR-damaged concrete structure, as the compressive strength is a fundamental parameter for the evaluation.

Overall, studies from the literature showed that modulus of elastic is the most affected property, followed by tensile strength, and then compressive strength, with respect to the expansion evolution. However, when it comes to evaluate the ASR effects on reinforced concrete structures, it is critical to take into account the restraint effects of reinforcement

and the stress state of the structure (Morenon et al. 2017).

2.5 Structural Effects of ASR

Effects of ASR on structural behaviour vary in terms of the geometry of the structure element, confinements due to reinforcement configuration and reinforcement ratio, boundary conditions, the applied load, and stress status of the structure member (Bilodeau et al. 2016; Clark 1989; Jones & Clark 1996; Mohammed, Hamada & Yamaji 2003a; Morenon et al. 2017; Multon & Toutlemonde 2006). In addition, size effects, chemical prestressing caused by ASR expansion, environmental effects such as temperature and moisture also influence the ASR effects on structural members (Allard et al. 2018; Fournier et al. 2009; Multon, Seignol & Toutlemonde 2005). Furthermore, secondary effects of ASR, e.g., corrosion, or ASR combined with other types of damage, such as wetting – drying cycles and freezing – thawing, will make the problem much more complicated (Carse 1996; Deschenes Jr et al. 2018; Sanchez et al. 2020). All these factors make the quantitative predictions of structural effects caused by ASR difficult. However, although the effects of ASR on structural behaviour are complicated and a general conclusion on structural consequences is difficult to make, the serviceability, and ultimately the load-carrying capacity of an affected structure might be influenced positively, negatively, or neutrally by ASR. To provide insight on the effects of ASR on structural behaviour, several aspects of structural implications of ASR are detailed in the following sections, including bond strength, flexural capacity, shear capacity, and long-term structural behaviour due to ASR.

2.5.1 Bond Strength

The bond between reinforcement and the surrounding concrete is crucial in assuring a reinforced element to work as a single element. It affects the load capacity and the

serviceability performance of a reinforced concrete structure. (Desnerck, Lees & Morley 2015; Lee & Mulheron 2015). ASR may lead to expansion and cracking in concrete, and degradation of mechanical properties. Furthermore, it may lead to easy penetration of water containing harmful chemicals, causing a potential risk of corrosion of the reinforcement. Over time, the bond between the ASR-affected concrete and embedded reinforcing steel bar can deteriorate, resulting in lower anchorage capacity or a changed bond behaviour (Chana 1989; Desnerck, Lees & Morley 2015; Haddad & Numayr 2007).

Lutz & Gergely (1967) studied the bond behaviour between concrete and the embedded reinforcing steel bar. Research performed by the authors revealed that, for plain reinforcing steel bars, bond forces mainly consisted of three components, namely, (1) chemical adhesion, (2) friction, and (3) mechanical interaction, between the concrete and the embedded reinforcing steel bar. Lutz & Gergely (1967) found that, for plain bars, the chemical adhesion is the dominant component when the load level is relatively low. When the load is increased, and the reinforcing steel bar starts slipping, the chemical adhesion lost quickly, then the bond force depends mainly on the friction between the reinforcing steel bar and the concrete. Lutz & Gergely (1967) also noticed that some mechanical interlocking existed due to the roughness of the plain bar surface. For deformed reinforcing steel bars, the researchers reported that the bond force is primarily due to the mechanical interaction, as the mechanical interlocking is enhanced by the ribs of the bar. Compared to the mechanical action, the chemical adhesion has a small effect on the bond force, and the friction only occurs after the reinforcing steel bar slips (Lutz & Gergely, 1967). The bond strength between the ribs of a deformed reinforcement basically consists of the following stresses as shown in Figure 2.7.

- Shear stresses Va, which is caused by adhesion between reinforcing steel and concrete;

- Shear stresses Vc between the ribs, which is exerted on the cylindrical concrete surface;
- Bearing stresses f_b, which is acting on the rib.

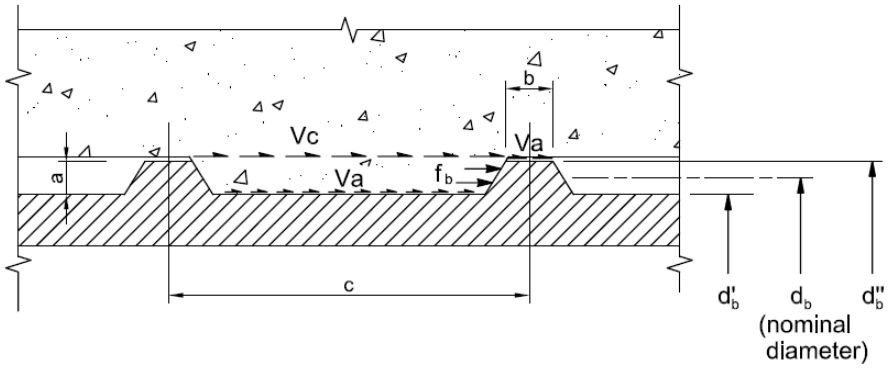

Figure 2. 7 Schematic diagram of stresses between ribs of a deformed reinforcement (Park & Paulay 1975)

Principally, there are three types of bond failure mechanism (Lutz & Gergely 1967): (1) crushing of the concrete when loading and shear failure (see Figure 2.8), (2) splitting of the concrete due to wedging action, and (3) yield and fracture of reinforcing steel bar. In the first failure mode, due to the surrounding concrete fails to bear the shear force, the reinforcing steel bar is directly pulled out from the concrete. It normally happens when the reinforcement is a plain steel bar, the concrete has a thick cover for the deformed bar, or when the embedment length is short. When the circumferential tensile stress (Figure 2.9) surpasses the tensile strength of the surrounding concrete, the second failure pattern occurs, that is, the splitting of the concrete cover. This failure mode normally happens when a deformed reinforcing steel bar with a small concrete cover is applied. The third failure mode occurs under conditions such as long reinforcement embedment length, thick concrete cover, or small reinforcing steel bar diameter.

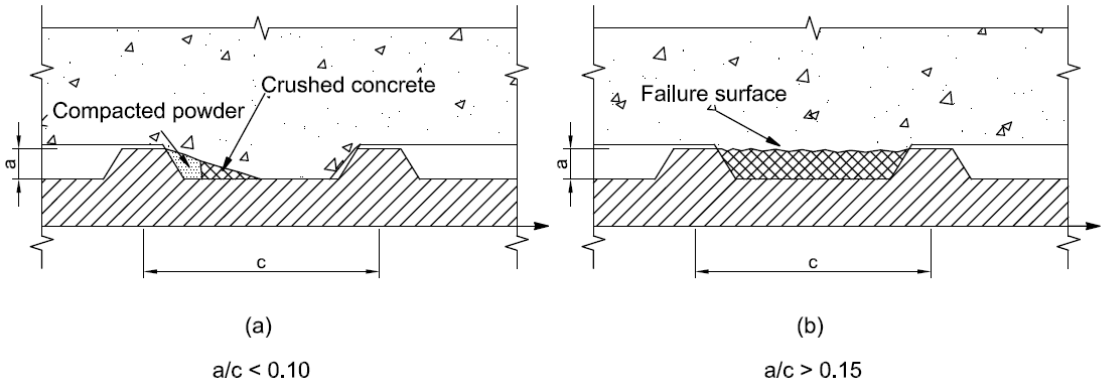

Figure 2. 8 Bond failure mechanism between ribs of deformed bar (Park & Paulay 1975)

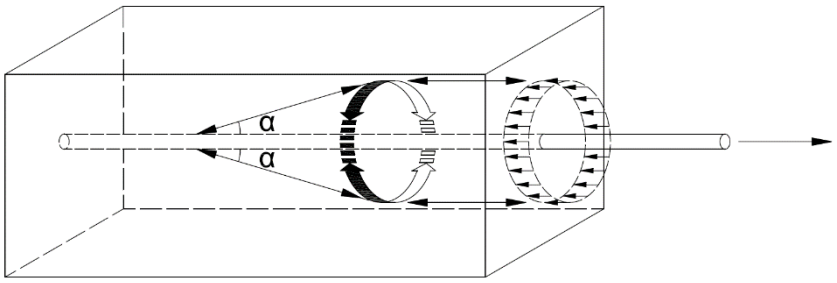

Figure 2. 9 Schematic tensile stress ring in concrete (Tepfers 1979)

Study on factors affecting the bond strength dated back to the 1930s. Menzel (1939) systematically studied the various factors influencing the bond strength from the results of pull-out tests. The author summarised a different kind of factors which influence the bond strength, including bar surface profile, type of lug and position of lug on deformed bars, length of bar embedment, bar position, the thickness of the concrete cover, consistency of concrete, and bleeding of concrete after casting. Ferguson & Thompson (1965) studied the factors that affect the bonding through experiments, proposed that the bond strength is proportionately related to the square of the concrete strength. Ferguson & Thompson (1965) also studied the effect of the spacing of the reinforcing steel bars on the bond strength. Tepfers (1979) analysed the influence of internal cracks along the

radial and longitudinal direction in a concrete ring model on the bond reduction. The findings were consistent with observations made by other researchers (Desnerck, Lees & Morley 2015). The influence of various factors on the bonding performance of reinforced concrete is summarised as follows.

- Concrete strength

  Concrete strength has a crucial influence on the bond strength of reinforced concrete. As the strength of concrete increases, the bond strength increases, and the bond strength is proportionately related to the concrete splitting strength. Meanwhile, the higher the concrete strength is, the lower the slip of the reinforcing bar will occur (Lundgren 2005; Yalciner, Eren & Sensoy 2012).

- Concrete composition

  The concrete composition can affect the bond behaviour between concrete and reinforcement remarkably. For example, the coarser the aggregate is used in the concrete, the higher the bond capacity will be. An excessive amount of cement in the concrete mix will lead to a considerable decrease in bond strength, and a large increase in the amount of steel slip. The presence of silica fume in the concrete mix will enhance the bond strength especially for concrete with high compressive strength, as it may affect the morphology and microstructure of the steel-reinforcement transition zone (Aslani & Nejadi 2012).

- Concrete cover

  The bond strength of plain bars is less affected by the depth of the concrete cover, but the deformed steel bars are more affected. For deformed bars, when the thickness of the concrete cover increases, the bond strength improves. Thus, in a pull-out test, higher bond capacity is expected when the concrete has a thicker cover. Also, the bond failure mode is significantly influenced by the concrete cover and reinforcement

spacing. Concrete splitting failure occurs when the concrete cover is small while a direct pull-out of the reinforcing steel bar occurs when the concrete has a thicker cover (Yalciner, Eren & Sensoy 2012).

- Type of bar

  Plain bars exhibit much lower bond strength with respect to the deformed bars. The bond strength of a deformed reinforcing steel bar is not sensitive to the bar profile change. However, the slip of the steel bar is significantly influenced by the bar profile change.

- Casting position

  The horizontally placed steel bars have markedly lower bond capacity with respect to the vertically placed steel bars. The reinforcement bar at the top of a structural member has lower bond resistance than the reinforcement bar at the bottom of the member.

- Presence of transverse reinforcement

  The presence of transverse reinforcement can enhance the bond strength between the reinforcing steel bar and the concrete, avoid splitting failure and improve the bonding behaviour (Lin & Zhao 2016).

- Corrosion of reinforcing steel bar

  There is an argument that at a low level of corrosion and when there are no corrosion-induced longitudinal cracks, the corrosion products may improve the bond behaviour between the reinforcement and concrete, thus may have a beneficial effect on bond. However, when corrosion develops, and the longitudinal crack appears, deterioration in the bond will happen, due to the weakening of the rib-concrete mechanical interlocking force and the breaking of the steel-concrete interface (Castel et al. 2016; Fu & Chung 1997; Tondolo 2015; Yalciner, Eren & Sensoy 2012).

- Cracking of concrete cover

  Tests performed by Desnerck, Lees & Morley (2015) revealed that the bond behaviour between concrete and ribbed reinforcing steel bars can be significantly influenced by the presence of longitudinal cracks in concrete cover. The bond strength can be significantly decreased even when minor cracks with widths of 0.03-0.04 mm are presented in the concrete matrix (Desnerck, Lees & Morley 2015).

As mentioned earlier, ASR may lead to degradation of the mechanical property of the affected concrete. Besides, based on the above-summarised influence factors, bond strength is significantly influenced by the concrete strength. Hence, ASR may cause a remarkable decrease in bond strength between the reinforcing steel bars and the affected concrete. Furthermore, excessive ASR expansion induces cracking in the concrete, and the presence of cracking in concrete cover can lead to decreasing in bond strength, thus ASR may further cause a detrimental effect on bond behaviour. In addition, ASR-induced cracking may facilitate the penetration of water and aggressive chemicals, causing corrosion of reinforcement, as a secondary effect of ASR. The bond strength between reinforcing steel bar and concrete can be remarkably compromised at such conditions. Moreover, bond stresses in anchorage regions can be remarkably increased due to the chemical prestressing effect. Increasing in bond stresses may cause anchorage failure, thus may also affect the ultimate load-carrying capacity of reinforced concrete structures. In literature, however, limited studies about the ASR effects on bond behaviour between the reinforcement steel bar and the affected concrete were found.

Chana (1989) studied the bond strength between ASR affected concrete and the embedded reinforcing steel bars by performing a series of pull-out tests. The bond strength of plain bars and deformed bars were studied. Conditions such as different concrete cover, with and without transverse reinforcement were considered. Alkalis in

reactive aggregate specimens were boosted to a total alkali level of 7 kg/m^3 Na_2O_{eq} to accelerate ASR. The author reported that at a 0.4% free expansion level, bond strength is not significantly influenced by ASR if transverse reinforcement is provided and/or the ratio of concrete cover depth to reinforcement diameter is sufficiently large. However, if the reinforcing steel bars are not restrained by transverse reinforcement and the ratio of concrete cover depth to reinforcement diameter is at about 1.5, a reduction of 40% to 50% in bond strength can be produced by ASR.

Haddad & Numayr (2007) performed pull-out tests on cylindrical specimens with a size of 75 mm (diameter) × 150 mm (height). 18 mm diameter reinforcing steel bars with 100 mm embedment length were adopted to evaluate the bond behaviour. Alkalis in cement were raised to 1.3% Na_2O_{eq} by adding KOH powder and crushed Pyrex glass was added to the concrete mix to accelerate ASR. After demolding, the specimens were water cured at 23.0 ± 2.0 °C for 40 days then immersed in a 40 °C 0.5N NaOH solution. Pull-out tests were performed at different expansion levels up to around 0.3%. A reduction as high as 44% in critical bond stress was reported by Haddad & Numayr (2007). Meanwhile, an increase in the free-end slip at failure, and a loss of 24% in bond strength were also recorded. Haddad & Numayr (2007) concluded that up to approximately 0.3% ASR expansion and corresponding crack extent, the bond strength is not significantly influenced by ASR. However, a significant reduction in bond strength is expected at higher ASR expansion levels and more severe cracking conditions.

Ahmed, Burley & Ridgen (1999) studied the influence of different lap length on bond strength for ASR affected reinforced concrete beams. Test results revealed that, for the beams with 5d lap length in tensile reinforcement, the bond strength reduction is about 6%, compared to the non-reactive control beam; for 32d lap length beam, the bond

strength reduction is about 3%. These reductions were found to be consistent with the lap length of the tensile reinforcement.

Based on the CEB-FIP MC90 bond-slip model, Huang et al. (2014) proposed a probabilistic model taking into account the effect of ASR for the bond behaviour between concrete and the embedded reinforcing steel bar. Parameters in the probabilistic model were determined through a Bayesian approach, by matching the force-displacement response between experimental results and finite element analysis results. For different levels of ASR damage, Huang et al. (2014) suggested that the bond strength increases at the early and middle ASR stages with the development of ASR, at a later stage, then, it starts to decrease when excessive ASR cracking occurs (Figure 2.10). Huang et al. (2014) also found that changes in structural responses of the ASR affected reinforced concrete elements can be attributed to this bond behaviour change due to ASR.

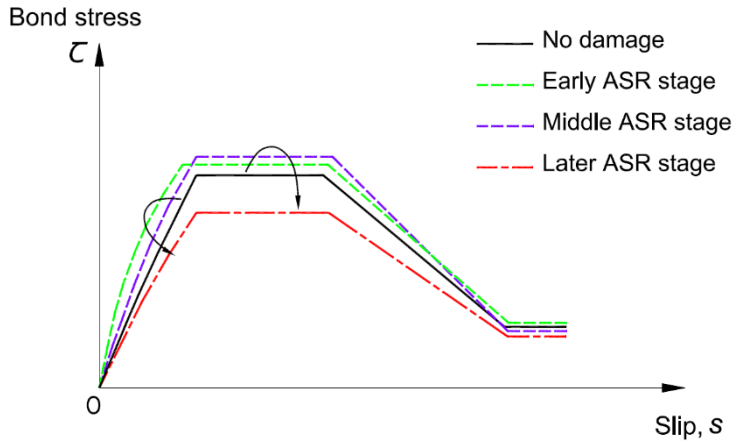

Figure 2. 10 Bond behaviour at different ASR damage levels

The ISE (1992) suggests that the reduction of bond strength is proportionately related to the concrete splitting tensile strength. The bond strength between concrete and the embedded reinforcing steel bars without links are recommended as followings:

- Deformed bars:

$$f_{bs} = \alpha(0.5 + c/d)f_t \quad (2.8)$$

where: f_{bs} is the characteristic bond strength;

α is a coefficient that generally takes as 0.6; but for corner or top cast bars, α takes as 0.43; for corner and top cast bars, α takes as 0.3;

c is the depth of concrete cover;

d is the bar diameter;

f_t represents the characteristic splitting tensile strength of the concrete affected by ASR.

- Plain bars:

$$f_{bs} = \beta f_t \quad (2.9)$$

where: β is a coefficient that generally takes as 0.65; but for corner or top cast bars, α takes as 0.47; for corner and top cast bars, α takes as 0.33.

2.5.2 Flexural Capacity

A considerable number of publications about ASR effects on the flexural capacity of the reinforced concrete beam can be found in the literature. Most of them have indicated that the flexural capacity is not compromised due to ASR. However, a study performed by Swamy & Al-Asali (1989) showed a reduction of up to around 25% for singly reinforced beams severely damaged by ASR. A critical review on publications relating to the structural performance of ASR affected members before 1989 had been made by Clark (1989). In the following sections, selected publications after 1989 will be reviewed, and a summary of the main findings from the literature will be made in Chapter 2.5.2.6.

2.5.2.1 Inoue et al. (1989)

The structural behaviour of reinforced concrete beams with reactive aggregate and different reinforcement ratios experienced a high level of ASR expansion had been studied by Inoue et al. (1989). Three beams with reactive Bronzite Andesite aggregate and three beams with non-reactive aggregate were cast. The cross-section of the beams is 200 × 200 mm and the length of the beams is 1700 mm. Three reinforcement ratios of 0.77% (2-D13), 1.2% (2-D16), and 1.74% (2-D19) was applied for both the reactive beams and non-reactive beams. All the beams had D6 stirrups in shear spans with a shear reinforcement ratio of 0.3%. Equivalent Na_2O in concrete mixes was raised to 8 kg/m^3 by adding NaCl. The beams were cured at 20 °C room temperature and 80% RH for 14 days, followed by conditioning at 40°C and 100% RH for 178 days to accelerate ASR. After that, the beams were stored in the laboratory at 20 °C room temperature and relative humidity 70% RH for two years before load testing. At the end of the accelerated ASR curing period (178-day), the expansion at the top surface of the reactive beams was reported as 0.79%, 0.65%, and 0.69% for the beams with 2-D13, 2-D16, and 2-D19 reinforcement steel bars, respectively. The recorded strains of the main reinforcement steel bars due to ASR expansion were 1384, 1075, and 917 microstrains, respectively.

Load carrying capacity tests were conducted by four-point loading with a shear span to effective depth ratio of 2.5 (a/d). The failure mode of all the beams was flexure fail except the non-reactive beam with two D19 rebars. Figure 2.11 shows the load capacity of each pair of the reactive and non-reactive beams. Although the modulus of elasticity, tensile strength, and compressive strength of the reactive concrete cylinders was reported as 48%, 59%, and 64% of that of the non-reactive cylinders, a reduction of less than 10% was observed in flexural capacity for the beams damaged by ASR, with regards to the non-reactive beams.

(a) D13-N and D13-R beams

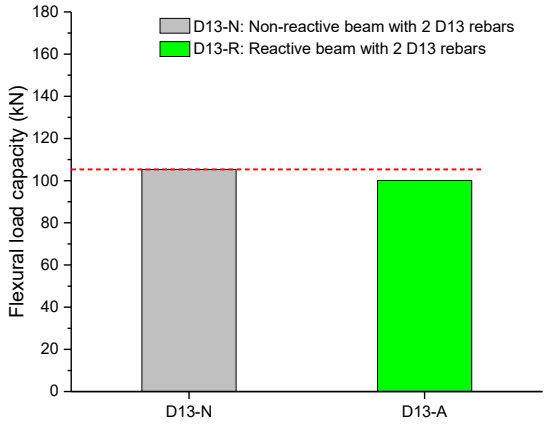

(b) D16-N and D16-R beams

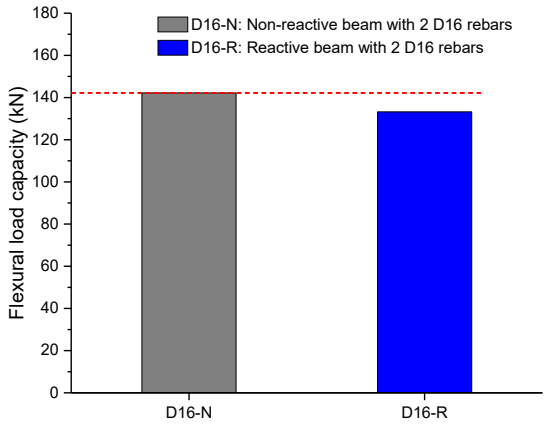

(c) D19-N and D19-R beams

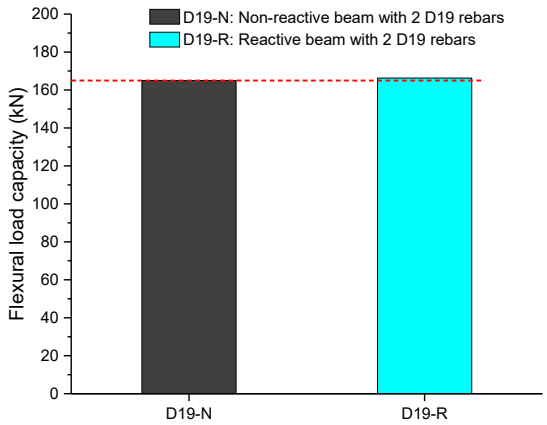

Figure 2. 11 Flexural load capacity of reactive and non-reactive beams tested by Inoue et al. (1998)

2.5.2.2 Swamy & Al-Asali (1989)

Swamy & Al-Asali (1989) studied the ASR effects on flexural capacity and deformations of small-scale reinforced concrete beams. Totally three groups including five beams were tested. Group B1 consisted of one control beam made with non-reactive aggregate. Group B2 included two identical beams with opal as reactive aggregate by replacing 4.5% of sand in the concrete mix. The third group was named B5 and consisted of two beams with fused silica as reactive aggregate replacing 15% of sand by weight. All the small-scale beams had a size of 75 mm (width) × 100 mm (height) × 800 mm (length) and were singly reinforced with two 8 mm diameter high-yield cold-worked deformed bars as main reinforcement. 6 mm diameter stirrups were supplied at shear spans of the beams to ensure flexural failure when being tested under four-point bending. In the concrete mix, a total alkali content of 5.2 kg/m^3 Na_2O_{eq} was adopted in this study. After demolding, the beams were conditioned in a fog room with 96 ± 2% RH and 20 ± 1 °C controlled temperature for about two years.

At the time of load testing, free expansion as high as around 1.7% was recorded for companion prism of B2 opal beam. Crack width up to 1 mm and an upward deflection of 6 mm were observed for the B2 opal beam. For the B5 fused silica beam, free expansion of the companion prism exceeded 0.6%. Hogging of 4 mm of the beam and 0.4 mm crack width were recorded.

Four-point bending tests showed that the failure mode of the B2 opal beam was a flexural failure, with a reduction of 25% in flexural capacity with respect to the control non-reactive B1 beam, while the flexural capacity of B1 fused silica beam decreased 15% with regards to the control B1 beam. All the tested beams exhibited flexural failure with firstly the yielding of the reinforcing steel bar then crushing of the compression zone. While the

control B1 beam failed in large deflection, the B2 and B5 beams failed with limited deflection. No shear failure or distress in bond or anchorage was observed.

At the time of load testing, the compressive strength of the severely ASR damaged B2 beam containing opal was 38% of that of the un-affected non-reactive control B1 beam. Meanwhile, the compressive strength of the ASR damaged B5 beam with fused silica was 60% of that of the non-reactive control B1 beam (Swamy & Al-Asali 1988). It implied that the decrease in flexure capacity could be attributed to heavily over-reinforcing of the beams under such circumstances.

2.5.2.3 Fan & Hanson (1998)

The effects of deleterious ASR expansion on the load-carrying capacity of reinforced concrete beams were investigated by Fan & Hanson (1998). Totally 6 reinforced concrete beams were prepared, including one non-reactive beam (#3N beam) and one reactive beam (#3R beam) with each beam having two No.3 deformed bars as main tensile reinforcement, another two non-reactive beams (#5N1, #5N2), and two reactive beams (#5R1, #5R2) with each beam reinforced by two No.5 deformed bars as main reinforcement. The size of the beams is 150 × 250 × 1500 mm. Stirrups are placed at shear spans by using D-5 wire for all the beams. The reinforcement ratio is 0.4% and 1% for beams with two No.3 deformed bars and for beams with two No. 5 deformed bars, respectively. Portland cement with 0.65% Na_2O_{eq} was used in the concrete mixing. The specimens were moist cured 14 days before subjected to a cyclic heating and cooling alkali solution to accelerate ASR. In order to measure the expansion induced by ASR, stainless steel DEMEC studs were adhered on the surface of specimens by using epoxy.

The specimens were immersed in a 0.5N sodium hydroxide solution for one year. The temperature of the sodium hydroxide was maintained at 38 °C for five to seven days then

was cooled down to room temperature at around 24 °C for two days and this cyclic heating and cooling process was applied to the end of the ASR acceleration period. In order to study the effects of ASR on the behaviour of the reinforced concrete beams under sustained service load conditions, two beams (#5N2 and #5R2) were pre-cracked by using a loading system mounted at both ends of the beams together. After that, the two beams loaded together were immersed in the sodium hydroxide solution for continuing conditioning, while the cracking load was maintained tightly to simulate the sustained service load.

During the period of conditioning, expansion and cracking of the specimens were periodically measured and checked by the authors. Longitudinal cracking was first observed on top surfaces of the beams at an expansion level around 0.08 %. At the end of immersing at one year, expansion on the top surface of beam #3R and beam #5R1 was recorded as 0.14% and 0.17%, respectively. The mechanical property of companion cylinders tested at 180 days after accelerated ASR conditioning demonstrated that, the modulus of elasticity, splitting tensile strength, and compressive strength were decreased by 31%, 38%, and 24% compared with the 28-day corresponding values, respectively. Fan & Hanson (1998) also reported that at the age of one-year, further reduction in mechanical properties was not significant.

The authors performed load capacity tests for all the six beams at the end of accelerated ASR conditioning. Four-point loading tests were conducted. All the beams exhibited a flexural failure mode. Figure 2.12 illustrates the load-carrying capacity of each pair of beams. Fan & Hanson (1998) concluded that although the under-reinforced reactive beams showed ASR expansion and cracking, the flexural load capacity was not significantly influenced. The variation of the flexural load capacity between the reactive

(a) #3N and #3R beams

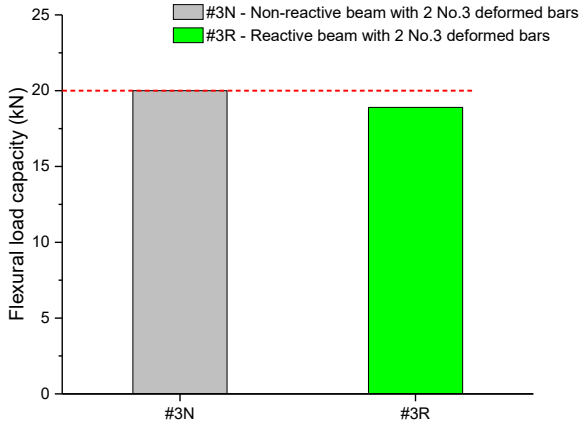

(b) #5N1 and #5R1 beams

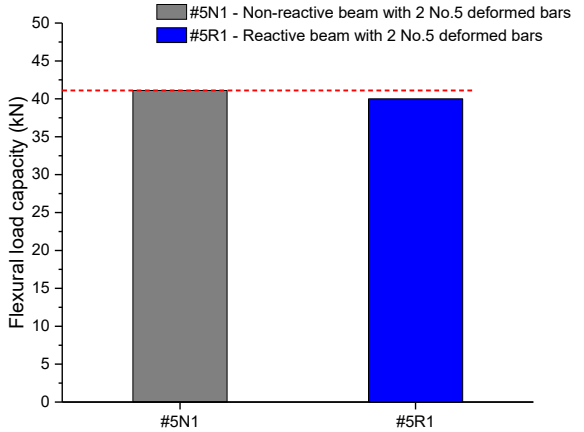

(c) #5N2 and #5R2 beams

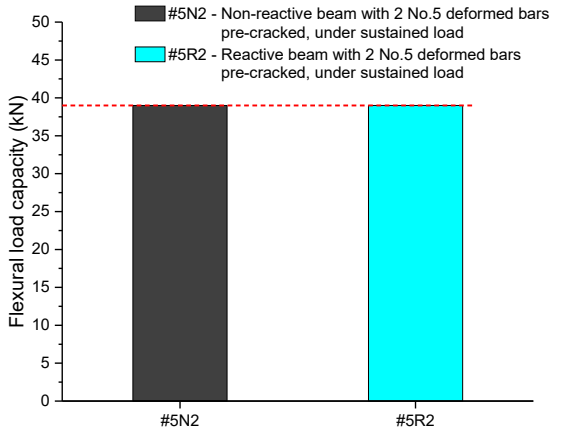

Figure 2. 12 Flexural load capacity of reactive and non-reactive beams tested by Fan & Hanson (1998)

beams and the non-reactive beams were less than 5%. Also, by comparing the flexural load capacity of the reactive beam which was pre-cracked then conditioned under sustained load with that of the reactive beam without pre-cracking, it was found that their load capacities were almost the same. Fan & Hanson (1998) thus concluded that ASR does not cause a significant detrimental influence on the flexural load-carrying capacity of the affected beam under sustained service load condition.

2.5.2.4 Monette, Gardner & Grattan-Bellew (2002)

Monette, Gardner & Grattan-Bellew (2002) performed tests on Eight reactive and seven non-reactive reinforced concrete beams to investigate the influence of ASR expansion and consequent damage on the flexure load capacity of the beams under different conditions. The cross-section of the beams is 89 × 121 mm and the length of the beams is 902 mm. All the beams were reinforced with two 8 mm diameter hot-rolled deformed reinforcing bars. Stirrups were 4.8 mm diameter hot-rolled plain reinforcing bars and were supplied for the whole length of the beams at a spacing of 63.5 mm. NaOH was used to raise the alkali content to 1.25% Na_2O_{eq} by mass of cement in the concrete mix. The beams and their companion cylinders and prisms were demolded 24 hours after casting then they were subjected to moist curing at 20 °C for 28 days.

At the age of 28 days, one non-reactive beam and two reactive beams were tested under a four-point bending test. Due to load cell problems, the authors discarded the results of the two 28-day reactive beams, so only the 28-day non-reactive beam result was recorded.

The left beams (6 reactive beams + 6 non-reactive beams) were then conditioned in a 1N sodium hydroxide solution at 38 °C for about 150 days. After that, the reactive beams were air-conditioned for another 150 days before being loaded to failure, while the non-reactive beams were kept in the laboratory for 50 days at room temperature before being

subjected to load test. During the period of 38 °C NaOH solution conditioning, two non-reactive beams and two reactive beams were subjected to sustained load, which was approximately 52% of the estimated ultimate flexural load. Another two non-reactive beams and two reactive beams were applied a cyclic load with a frequency of 0.5Hz ranging from zero to 52% of the estimated ultimate flexural load. The remaining two non-reactive beams and two reactive beams were simply immersed in the 38 °C sodium hydroxide solution without applying any load.

After conditioning in the 38 °C sodium hydroxide solution for about 150 days, free expansion of about 0.35% was recorded for the companion reactive cylinders. Expansion of the reactive beams without load measured by top gage at midspan reached about 0.4%, expansion of the reactive beams with cyclic loading at the same height was recorded about 0.2%, while for the reactive beams with sustained load, this figure was smaller than the above two conditions, recorded at around 0.1%. Cracking of reactive specimens was also recorded.

A four-point bending test was carried out afterward. All the reactive beams showed flexural failure mode and all the non-reactive beams reached full flexural capacity, but two non-reactive beams showed diagonal cracking similar to shear failure due to post steel yielding. Figure 2.13 shows the flexural load-carrying capacity of the tested beams.

Monette, Gardner & Grattan-Bellew (2002) concluded that the flexural load-carrying capacity of the under-reinforced concrete beams exposure to accelerated ASR condition, under sustained load or cyclic load condition, does not show reduction due to ASR expansion and ASR damage, with respect to that of the 28-day non-reactive datum beam. However, ASR expansion and cracking can cause a significant reduction in modulus of elasticity.

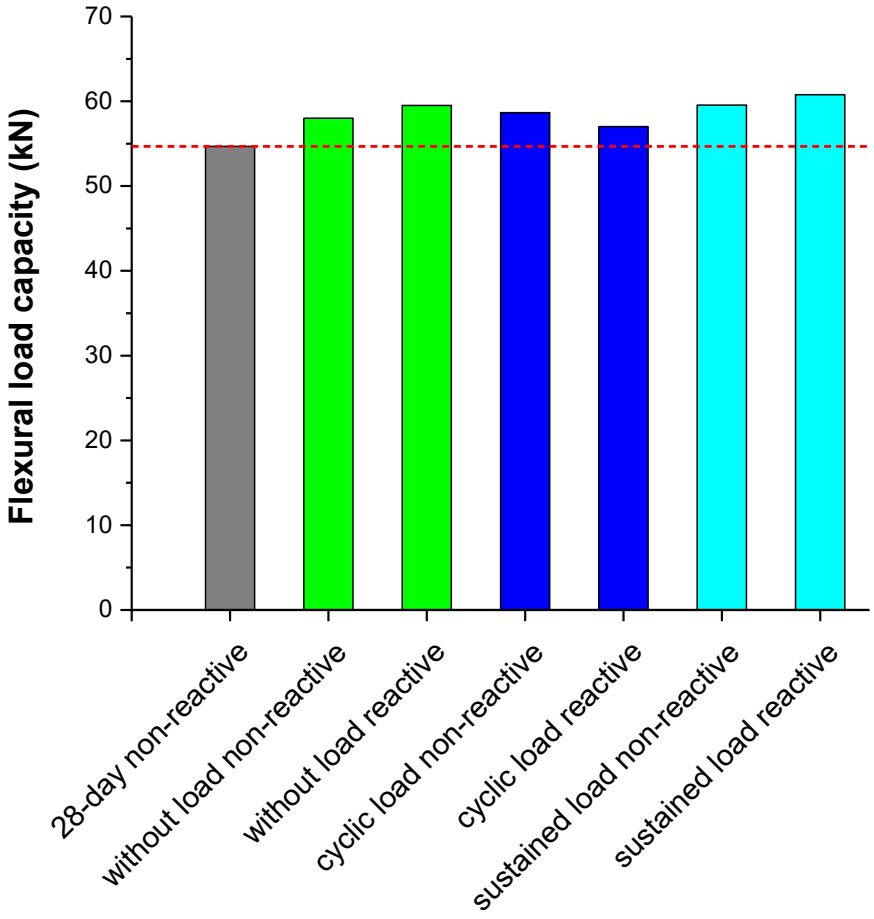

Figure 2. 13 Flexural load capacity of reactive and non-reactive beams tested by Monette, Gardner & Grattan-Bellew (2002)

2.5.2.5 Giannini (2012)

Three full-scale reinforced concrete beams were tested by Giannini (2012). One beam served as a control beam was made of non-reactive limestone coarse aggregate and non-reactive natural sand, another two beams, namely first reactive beam and second reactive beam, were made of non-reactive limestone coarse aggregate and highly reactive sand. The alkali content of the reactive beams was adjusted through adding sodium hydroxide in the concrete mix to 1.25% Na_2O_{eq} by mass of cement. The cross-section of the beams is 533 × 1067 mm and the length is 8433 mm. Five #11 rebars were provided both at the bottom and on top of the beams as longitudinal main reinforcement. Six #5 longitudinal

rebars were placed at either side of the beams as constructional reinforcement. #5 shear reinforcement was provided for the whole length of the beams with different spacing in different regions. The beams were cured in the laboratory for 15 to 74 days before outdoor exposure. During the period of outdoor exposure, a water system was used to supply sufficient moisture for the beams. In order to simulate the in-service condition stresses, a loading system was applied to provide a sustained service load for the beams.

After 20 to 22 months of outdoor exposure, large expansions for the two reactive beams were recorded. For the first reactive beam, average vertical expansion and longitudinal expansion reached 0.76% and 0.14%, respectively. The second reactive beam showed much higher expansions, with an average vertical expansion of about 1.55% and an average longitudinal expansion of around 0.2%. Giannini (2012) explained that the expansion of the first reactive beam was caused by ASR, while the expansion of the second reactive beam was due to the combined effect of ASR and Delayed Ettringite Formation (DEF), based on petrographic investigation results.

The cracking of reactive specimens was visually checked. In the middle region of the reactive beams, crack width with up to 1 mm was observed. Cracks mainly developed longitudinally along the direction of the main reinforcement.

Four-point flexure load capacity tests were conducted for the three beams after two years of outdoor exposure. The measured moment capacities of the non-reactive beam and reactive beams are shown in Figure 2.14. The first reactive beam and the second reactive beam showed an increase of 15% and 4% in moment capacity compared with the non-reactive beam. Cores were drilled from the beams for modulus of elasticity and compressive strength testing. Results showed that the compressive strength measured from the drilled cores of the first reactive beam and the second reactive beam reduced

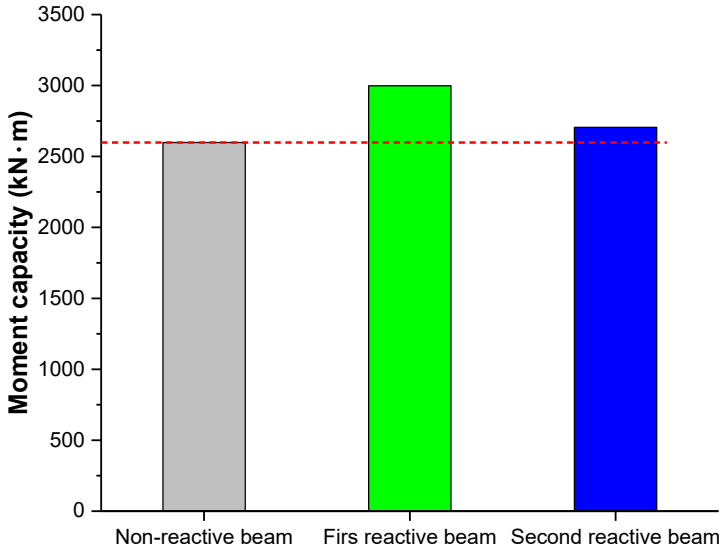

Figure 2. 14 Moment capacity of reactive and non-reactive beams tested by Giannini (2002)

about 44% and 51% compared with that of the non-reactive beam, respectively. While the modulus of elasticity decreased by about 57% and 61%, respectively. Based on the test results, Giannini (2002) concluded that:

- the reactive reinforced concrete beams exhibited higher flexural moment capacities than the nonreactive beam;
- modulus of elasticity and compressive strength obtained from drilled cores did not correlate to the flexural moment capacity;
- the flexural stiffness of the reactive beams was enhanced by the chemical pre-stressing effect induced by ASR expansion.

2.5.2.6 Summary

Clark (1989) provided a detailed review on earlier studies about the structural behaviour of ASR affected reinforced concrete members. Main findings were that, for under-

reinforced concrete beams, the flexural stiffness is not reduced, and the flexural load capacity is not significantly influenced by ASR expansion and ASR-induced damage.

Tordoff (1990) argues that while ASR does reduce the strength of the unreinforced concrete specimens, ASR expansion or cracking does not significantly influence the bending moment capacity for well-reinforced concrete beams. A similar conclusion was reported by Inoue et al. (1989), Fan & Hanson (1998). In some cases, the ASR affected beams were reported having a higher flexural capacity in comparison with the control specimens (Giannini 2012; Monette, Gardner & Grattan-Bellew 2002). However, Swamy & Al-Asali (1989) reported a reduction of up to around 25% in flexural capacity for singly reinforced beams severely damaged by ASR, which could be attributed to heavily over-reinforcing of the beams and the failure load was influenced by concrete crushing. Flexural capacity change with expansion for ASR affected reinforced concrete beams tested by various researchers is summarised in Figure 2.15.

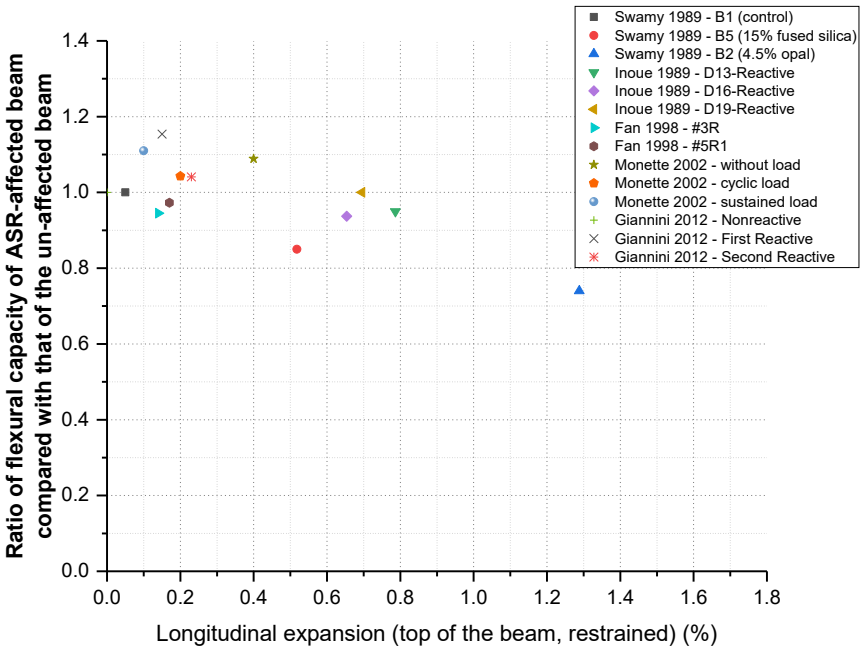

Figure 2. 15 Flexural capacity change with the expansion

Based on the short-term laboratory tests on the flexural behaviour of the ASR affected reinforced members in literature, it appears that the flexural stiffness and the flexural capacity of an under-reinforced concrete member may not exhibit significant reduction. However, these tests reveal only a short-term indication of the load-carrying capacity of the structure. The long-term flexural capacity of ASR affected reinforced concrete structures is still open to debate. In addition, the performance of the ASR-affected flexural members could also be affected by other factors, such as ASR-induced cracks, which normally have orientations along with the reinforcement, delamination, and spalling of concrete due to excessive ASR expansion, these factors could cause bond deterioration and consequently affect the performance of the structure. Furthermore, if ASR-induced cracks extend to the reinforcement and corrosion of reinforcement happen, reinforcement cross-section will be impaired and consequently, the load capacity of the affected member will be reduced. Hence, it is rather difficult to draw a general conclusion regarding the ASR effects on load-carrying capacity and structural behaviour of the affected reinforced concrete structure.

2.5.3 Shear Capacity

A limited number of publications about ASR effects on the shear capacity of the ASR affected reinforced concrete structures have been found in the literature. The results of these studies showed considerable variations. Some researchers argued that the shear resistance of the ASR affected members was enhanced due to the prestressing effect induced by ASR expansion. This ASR induced prestress has a positive effect in closing existing cracks thus improves the aggregate interlock which contributes to shear resistance (Bilodeau et al. 2016). Some, however, argued that ASR induced microcracks can have a significant detrimental influence on shear strength, which may cause the brittle

shear failure of the affected structure (Sanchez et al. 2017). Reduction as high as 25% in shear capacity due to ASR damage had been reported by den Uijl & Kaptijn (2002). The reason for these different findings could partly be attributed to the complexity of various shear stress transfer mechanisms, and partly be due to different researchers considered different conditions that may influence the shear capacity of the ASR affected reinforced concrete members, such as reinforcement layout and reinforcement ratio, with or without shear reinforcement, size of the specimen, crack width, ASR expansion or damage level.

In the following chapters, the limited publications in the literature relating to the shear capacity of ASR affected reinforced concrete members will be reviewed and classified into two categories: with transverse reinforcement and without transverse reinforcement. The main findings will be summarised in Chapter 2.5.3.3.

2.5.3.1 Shear capacity of ASR-affected reinforced concrete members with transverse reinforcement

Based on a critical review on publications relating to structural effects of ASR made by Clark (1989), relevant studies performed by Clayton, Currie & Moss (1990), and ISE (1992), for concrete members with transverse reinforcement, conclusions on the shear capacity are drawn as followings:

- When a transverse reinforcement ratio of at least 0.2% is provided, tests had revealed that the shear capacity of the ASR damaged concrete member does not show a significant decrease. Indeed, an increase of up to 47% in shear capacity had been reported.
- The enhancement in shear capacity could be attributed to the self-prestressing effects produced by the ASR expansion. However, it is not clear whether this prestress could be maintained in the long-term. Hence, a low bound value

regarding the prestressing effect is advised to evaluate the residual load capacity of the ASR affected member.

Later studies performed by Ahmed, Burley & Rigden (1998) also confirmed that the shear capacity of ASR affected reinforced concrete beams with transverse reinforcement was enhanced. In this study, beams with a size of 80 × 130 × 1300 mm were cast. Two 12 mm diameter high-tensile deformed bars were supplied as tension reinforcement for all the beams. Two 6 mm diameter mild plain reinforcing bars were provided as compression reinforcement. As for the shear reinforcement, 3.2 mm diameter mild plain reinforcing steel bars were placed at a spacing of 50 mm. The alkali content of the reactive beams was raised to 7 kg/m^3 Na_2O_{eq}. The reactive beams and the non-reactive beams were water cured 28 days at a temperature of 20 °C then kept in 40 °C water for five months to accelerate ASR. After that, four-point bending tests were carried out. A shear span to effective depth ratio of 3.6 was applied when performing load testing. Results showed that the average shear capacity of the ASR damaged beams increased by about 11.5% with respect to the non-reactive control beams. Ahmed, Burley & Rigden (1998) concluded that the self-prestressing induced by ASR expansion enhanced the shear resistance of the ASR affected beams.

The more recent study and probably also the most significant validation experiment performed by Deschenes, Bayrak & Folliard (2009) had confirmed again that the structural integrity of the ASR damaged concrete beams was well maintained. Owing to the confinement effect provided by the shear reinforcement, the shear resistance was found not significantly affected by ASR deterioration. In order to evaluate the potential loss in shear strength of the ASR affected bent caps, six near full-scale beams, including four reactive and two non-reactive beams were cast and tested at Ferguson Structural Engineering Laboratory, The University of Texas at Austin, USA. The beams had a

section of 533 × 1066 mm and a length of 8433 mm in size. A typical amount of longitudinal reinforcement was provided for the beams. The minimum amount of transverse reinforcement required by relevant design code was considered to ensure a lower bound shear failure and to maximise the ASR expansion at least restraint direction. Figure 2.16 shows the details of the reinforcement of the beams and shear span arrangement during load test.

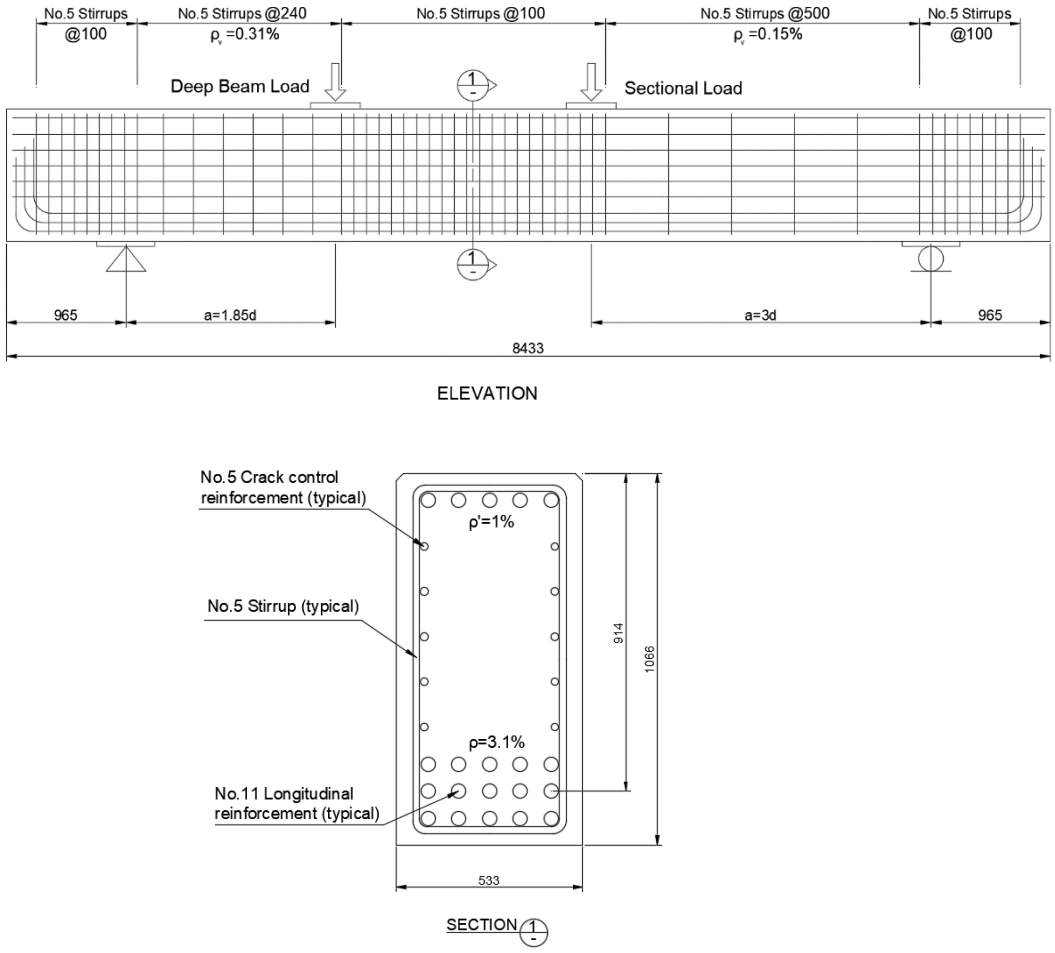

Figure 2. 16 Reinforcement detail and shear span of tested beams

(Deschenes, Bayrak & Folliard 2009)

For the reactive beams, a reactive siliceous fine aggregate and a Portland cement (high alkali cement) with 0.8% Na_2O_{eq} were adopted in the concrete mix. Furthermore, the alkali content of the concrete was adjusted to 1.25% Na_2O_{eq} by dissolving sodium

hydroxide in the mixing water. For the non-reactive beams, the concrete mix adopted non-reactive sand and low-alkali Portland cement instead.

After fabrication and initial curing, the beams and the companion cylinders were moved outdoors and subjected to outdoor exposure for the development of realistic ASR damage. A water system was adopted to intermittently supply water for the beams to simulate the severe exposure conditions in the field. A sustained load was applied to the beams to take into account the influence of the service load on the development of ASR.

Shear testing was conducted on one non-reactive beam (NR1) and two reactive beams (R1, R2) damaged by ASR after approximately one year of outdoor exposure. The transverse expansions of R1 and R2 beam exceeded the reinforcement yield strain at the time prior to testing. The shear strength of ASR damaged beam compared with that of the non-reactive beam are shown in Figure 2.17.

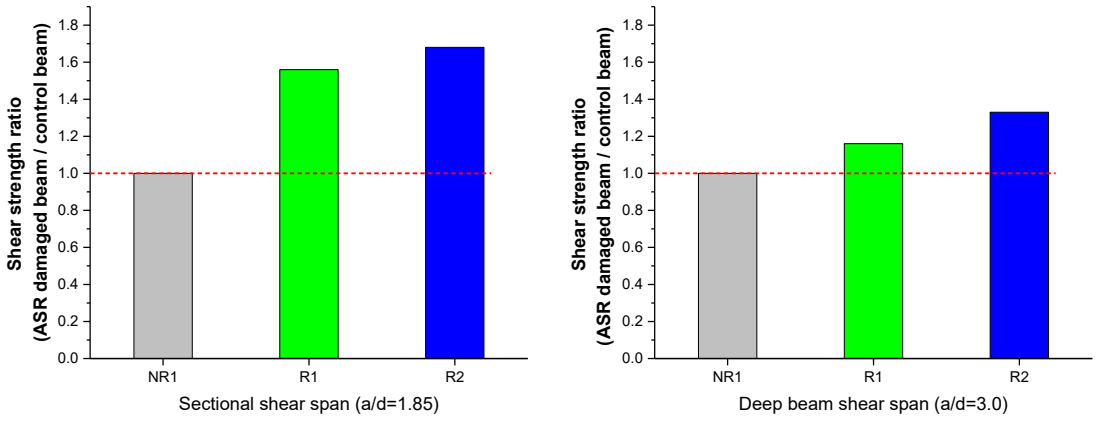

Figure 2. 17 Shear strength ratio (ASR damaged beam / control beam)
(Deschenes, Bayrak & Folliard 2009)

Conclusions were drawn by the authors as follows:

- ASR deterioration did not pose a notable effect on failure modes. The sectional shear span and the deep beam shear span were all failed by significant shear

reinforcement yielding and propagation of crack between the load and the support till loss of equilibrium.

- As a result of ASR expansion, shear reinforcement yielding was observed for the ASR affected beams, however, shear strength of the affected beams was not diminished.
- The presence of shear reinforcement and a well-detailed reinforcement cage provided a confinement effect on the ASR affected concrete, maintaining the load-carrying capacity and the integrity of the ASR damaged structure.

However, Deschenes, Bayrak & Folliard (2009) pointed out that these tests were carried out after only one year of ASR expansion. Due to the accelerated nature of the tests, whether the results are universally applicable to be used to justify the structural safety of field structures suffered from long-term ASR deterioration is still questionable. It appears that this ASR acceleration period is too short for those more severe ASR damages to occur. If longer periods of exposure and persistent ASR expansions are applied, consequences affecting the integrity of the structure may happen. First, ASR expansion builds up tensile stresses in the stirrups. These tensile stresses can surpass the yield strength of the reinforcing steel while there is no enough amount of transverse reinforcement, and this phenomenon had been observed by Deschenes, Bayrak & Folliard (2009). Secondly, in some extreme cases, fracture of reinforcing steel bars due to excessive ASR expansion could happen. Torii et al. (2008) and Miyagawa (2013) had reported that due to severe ASR expansion, fractures of reinforcing steel bars in ASR affected bridge piers, footings, and bridge pier cap beams were observed. In such a scenario, the integrity and the structural safety of the ASR damaged structure are questionable due to the loss of confinement provided by the reinforcement (Deschenes, Bayrak & Folliard 2009).

While the self-prestressing induced by ASR expansion exerts a positive impact on the shear resistance of the ASR affected members, the loss of confinement due to fracture of the transverse reinforcement would impair the shear capacity and lead to a rapid deterioration of the core concrete. The combined effect of these positive and negative impacts on shear capacity and structural performance is complex. However, through investigation of ASR effects on the shear capacity of the affected beams without shear reinforcement, the issues arising from fracture of transverse reinforcement could be analysed in an alternative approach.

2.5.3.2 Shear capacity of ASR affected reinforced concrete members without transverse reinforcement

Based on earlier experimental results, the ISE (1992) concluded that the shear capacity of ASR affected beams without transverse reinforcement showed some variation, while some of the test results demonstrated an enhancement in shear resistance, some others exhibited a reduction in shear resistance of up to around 20%. Literature review on later publications also revealed some inconsistent findings by different researchers regarding the shear capacity of the ASR damaged members without shear reinforcement. Test results of Clark & Ng (1989), Cope & Slade (1992) demonstrated that the shear resistance of the ASR affected members first increases with the increasing ASR expansion, after a certain level of expansion, then, the shear resistance decreases with the continuing increase of expansion. den Uijl & Kaptijn (2002) reported an average reduction of about 25% in shear capacity for ASR damaged beams sawn from bridges affected by ASR, while Bach, Thorsen & Nielsen (1993), Ahmed, Burley & Rigden (1998), Bilodeau et al. (2016), Allard et al. (2016) reported that the shear capacity of the ASR damaged members were not reduced due to ASR. In the following, these publications are reviewed, and the data collected will be summarised in Chapter 2.5.3.3.

Clark & Ng (1989) performed punching shear tests for slabs without shear links damaged by ASR. Four batches of 610 × 610 mm square slabs with a thickness of 80 mm were cast. Specimens of Batch 1 had 100 × 100 mm 6 mm diameter deformed bar mesh at the bottom of the slabs. Specimens of Batch 6 were reinforced with 50 × 50 mm mesh at the bottom. Batch 3 slabs were reinforced with two layers of 100 × 100 mm meshes, while batch 7 had two layers of 50 × 50 mm meshes, placed at the bottom and the top of the slabs. At the age of 28 days, punching tests were conducted for selected specimens from each batch, which were deemed as having zero expansion and thus no ASR damage. All the other specimens were then kept in 38 °C water. Expansions of the slabs and the companion cylinders were measured monthly. When the free expansion of the cylinders reached a pre-determined value, the corresponding slabs were then taken out and subjected to a punching shear test. Test results are shown in Figure 2.18.

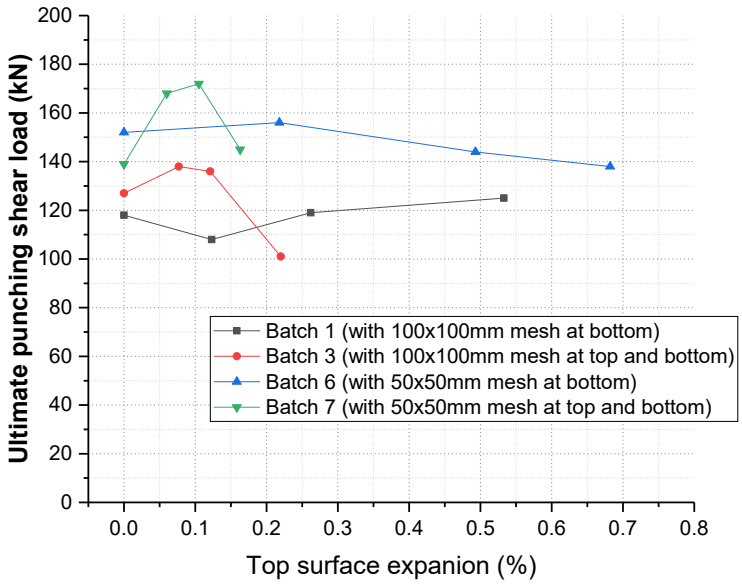

Figure 2. 18 Punching shear versus expansion of slabs (Clark & Ng, 1989)

It can be seen that the punching shear of the 4th slab of batch 3 reduced about 20% compared with the relevant 28-day reference value. It is worth to be noted that, due to the restraints provided by the bottom reinforcement and the top reinforcement, expansion at

the top surface of the slab was about 0.22%, while the corresponding free expansion of the companion cylinder reached 0.64%. For the 4th slab of batch 6, the reduction in punching shear was about 9%. Due to restraints was only provide by the reinforcement mesh at the bottom of the slab, large top surface expansion with about 0.68% was observed, which exceeded the free expansion of the companion cylinder. A clear trend shown in Figure 2.18 is that the punching shear load increases with the increase of expansion firstly, then, after a certain level of expansion, it decreases with the continuing increase in expansion.

Cope & Slade (1992) tested a series of beams with no shear reinforcement at different ratios of shear span to effective depth. Two 16 mm plain reinforcing steel bars were used to reinforce the beams with a size of 125 × 250 × 2500 mm. The beams and their companion cylinders were stored in 38 °C water to accelerate ASR. Free expansions were measured on cylinders periodically up to 433 days and when certain levels of expansion were reached, shear testing was conducted on relevant beams. Figure 2.19 illustrates the shear strength ratio between the ASR damaged beams and the control beams.

Test results demonstrated that the shear strength of the ASR affected beams increased up to about 10% compared with that of the un-damaged control beams when free expansion increased to around 0.25%. However, when free expansion reached 0.5% to 0.6%, a reduction of up to 30% in shear strength was recorded by Cope & Slade (1992).

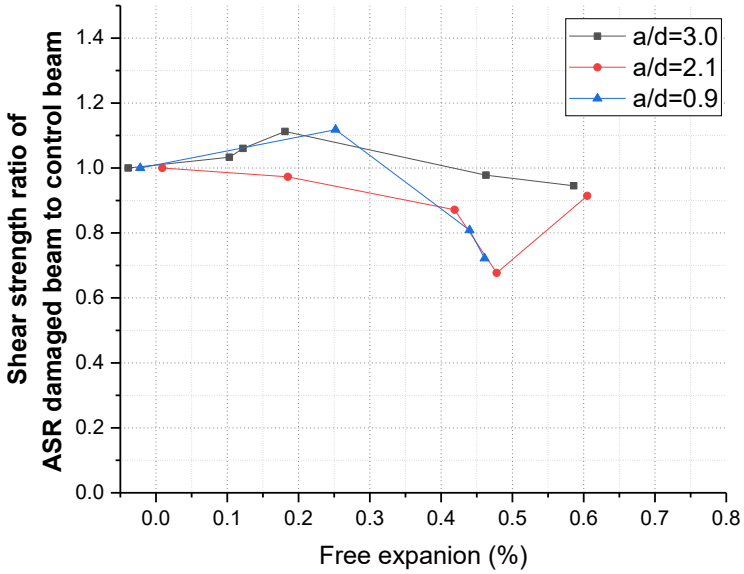

Figure 2. 19 Shear strength ratio (ASR damaged beam / control beam)

(Cope & Slade, 1992)

den Uijl & Kaptijn (2002) studied the shear capacity of six beams obtained from two 35-year-old ASR damaged slab bridges. The first two beams had a width of 600 mm, a depth ranging from 620 mm to 740 mm, and a length of 8500 mm. The other four beams were in the length of 7500 mm with a varied width from 480 mm to 570 mm, and a varied depth from 645 mm to 730 mm. The ASR-induced cracks were observed mainly orientated horizontally, due to no shear links were presented. Cores were also drilled from the two bridges in vertical, longitudinal, and transverse directions for mechanical property tests. Four-point bending tests were performed on these beams, and the first two beams with a higher reinforcement ratio (0.97% ~ 1.32%) were failed in flexure. In order to obtain the shear resistance of the left four beams which had a relative lower reinforcement ratio (0.45% ~ 0.54%), the bending resistance of the beams was enhanced by gluing steel strips to the bottom surface of the beams. Theoretical analysis of shear load capacity was also conducted. According to the shear test results and the theoretical analysis results, den

Uijl & Kaptijn (2002) concluded that the average shear capacity of the ASR damaged beams had a reduction of 25% compared with the theoretical value if there was no ASR damage. In addition, the shear tension failure was observed in the tested ASR-damaged beams due to the severe tensile strength reduction.

Bach, Thorsen & Nielsen (1993) investigated the shear strength of ASR-damaged beams without transverse reinforcement. Beams were cast with reactive and non-reactive aggregates. The beams had a size of 180 × 360 × 4300 mm and were reinforced by three T18 tensile reinforcement, two T12 compressive reinforcing steel bars. The alkali content of concrete was 0.8% Na_2O_{eq} by mass of cement. After approximately three weeks of curing at 20 °C and 100% relative humidity, specimens were then exposed to 50°C NaCl solution up to 236 weeks to promote ASR expansion. Transverse and longitudinal expansions of the specimens as well as the longitudinal free expansion of the companion prisms were measured. Beams were subjected to shear test after a different duration of NaCl solution submersion, with a shear span to effective depth ratio around 2.8. Test results showed no reduction in shear capacity for ASR damaged beams. Bach, Thorsen & Nielsen (1993) concluded that the shear strength of the specimens was not reduced even the beams were severely deteriorated by ASR. In addition, the ASR-damaged beams showed more ductility than the control specimens un-affected by ASR.

Ahmed, Burley & Rigden (1998), while performed tests on beams with transverse reinforcement as has been reviewed in Chapter 2.5.3.1, also conducted shear tests for beams without transverse reinforcement. The beams without transverse reinforcement had the same size as the beams with shear reinforcement, but only two 12 mm diameter high-tensile deformed bars were provided as tension reinforcement. Results demonstrated that the average shear capacity of the ASR deteriorated beams without shear links increased by about 8.5% compared with that of the non-reactive control beams.

Bilodeau et al. (2016), Allard et al. (2016), and Allard et al. (2018) studied the residual shear capacity of thick concrete slabs without shear links. Two sets, totally eight thick slabs were manufactured. Each set of the specimens consist of one non-reactive specimen and three reactive specimens. The slabs had a section of 610 mm in width, 750 mm in height and 4500 mm in length. Ten 25M deformed steel bars were placed in the bottom part of the slabs as the main reinforcement (ρ=1.18%). Three 10M deformed bars were arranged in the topside of the specimens as constructional reinforcement for shrinkage control. At each end of the slabs above the bearing support, three 10M rebars were provided for local strengthening to avoid concrete crushing during the loading test. No transverse shear reinforcement was provided for all the slabs. A high alkali Portland cement (1.12% Na_2O_{eq}) was used in this study. There were slight differences in concrete mixes for set 1 and set 2 specimens. In the first set, cement usage was 420 kg/m^3 while in the second set, cement usage was 370 kg/m^3. The alkali content of concrete mixes for set 2 was adjusted to 1.25% Na_2O_{eq} by dissolving NaOH pellets in the mixing water. Total alkali contents for set 1 and set 2 specimens were 4.7 kg/m^3 and 4.63 kg/m^3, respectively. After moist curing for seven days, the specimens were demolded then stored in a 38 °C environment with high relative humidity (> 95%) for up to 80 weeks (Allard et al. 2018). During the period of conditioning, longitudinal, vertical, and transverse expansion of the slabs were measured on embedded stainless-steel studs. For set 2 slabs, fibre optic sensors were also installed on the surface of the slabs for expansion measurements. When certain levels of expansion were reached, three-point loading tests were conducted on selected slabs to find the ultimate load capacity. Table 2.3 shows the test results. It was also observed that the initial flexural stiffness of the ASR affected slabs was lower than that of the non-reactive slabs. The authors explained that the lower initial flexural stiffness of the ASR affected specimens could be attributed to the microcracks and the macrocracks

induced by ASR. However, when shear cracks appeared, the flexural stiffness of the non-reactive specimen decreased suddenly, while the flexural stiffness of the reactive specimens decreased gradually with loading.

Table 2. 3 Shear capacity of slabs tested by Bilodeau et al. (2016)

Ref. Name of Tested Slabs		Average Longitudinal Expansion (%) (top of the slab)	Shear Resistances V_r (kN)	Changes in Shear Capacity * (%)
Set No.	Slab Name			
1	NR	0.01	411	--
	R1	0.08	506	23% ↑
	R3	0.15	469	14% ↑
2	NR	0.01	423	--
	R1	0.24	471	11% ↑
	R2	0.25	476	13% ↑

(∗ "↑" indicates an increase in shear capacity compared with relevant non-reactive specimen)

Mechanical property tests were performed on drilled cores. The core samples were obtained vertically and horizontally from the tested slabs. A comparison of mechanical properties between the non-reactive specimens and the reactive specimens were made. Results revealed that the average compressive strength of the reactive specimens was 36% lower than that of the non-reactive specimens, the average tensile strength reduced 44%, while the modulus of elasticity decreased by about 58%. According to the test results, the authors concluded as followings:

- The non-reactive slabs showed a higher initial flexural stiffness than the ASR affected ones, although their load-deflection behaviour was similar in overall;
- The ASR affected slabs without shear reinforcement showed a slightly higher shear capacity compared to the non-reactive specimen;

- Chemical prestressing could increase the shear strength by limiting the opening of the main critical shear crack. However, it might not be the only mechanism that contributes to the enhancing of the shear resistance;
- The extent of degradation in concrete material properties measured from drilled cores could not necessarily serve as a direct reflection of the structural performance.

These slabs were tested after about one to two years of ASR expansion when the expansion level reached about 0.25%. Again, one can see that it is a short-term exposure. For long-term ASR deteriorated reinforced concrete field structures, average shear capacity reduction as high as 25% had been reported by den Uijl & Kaptijn (2002). The conflicting findings in shear capacity of ASR affected reinforced concrete structures thus called for more extensive exploration on this issue.

Full-scale in-situ shear capacity tests were carried out on an ASR damaged bridge built in 1976 by Schmidt et al. (2014) to assess the residual shear capacity of the cantilever slab with no shear reinforcement. Four cantilever beams were cut in strips with approximately 1000 mm in width and 1330 mm in length. The fixed end had a depth of 450 mm, while the free end where the testing load was applied had a depth of approximately 270 mm. Figure 2.20 shows the test specimen size and a schematic test set-up.

Concrete cores were drilled out from the bridge at the four testing areas for mechanical property tests. The compressive strength of the ASR deteriorated concrete was found significantly decreased by about 50% due to ASR. Schmidt et al. (2014) also impregnated the specimens cut from the bridge with fluorescent epoxy to check the cracking pattern

in the samples. Figure 2.21 shows the fluorescence impregnated ASR damages in the sample. Comprehensive horizontal ASR cracks were visualized by using this method.

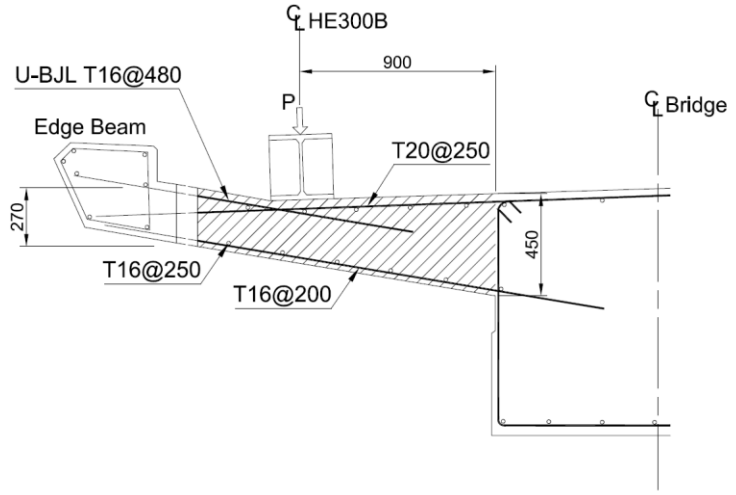

Figure 2. 20 Size of the specimen and schematic test set-up
(adapted from Schmidt et al. 2014, Hansen et al. 2016)

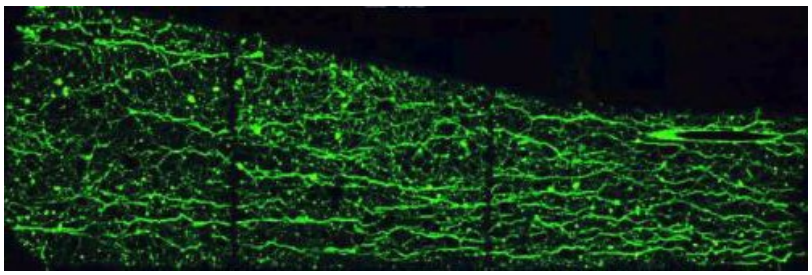

Figure 2. 21 Fluorescent impregnated beam observed under UV light
(Schmidt et al. 2014, Hansen et al. 2016)

Shear tests were carried out by applying load on the spreader beam (HE300B) 900 mm away from the fixed end. The failure loads of the four cantilever beams were measured, and the shear strength of the specimens was also predicted according to the Eurocode EN 1992-1-1, using the initial designing compressive strength of the beams. The measured shear capacities and the calculated values are shown in Figure 2.22.

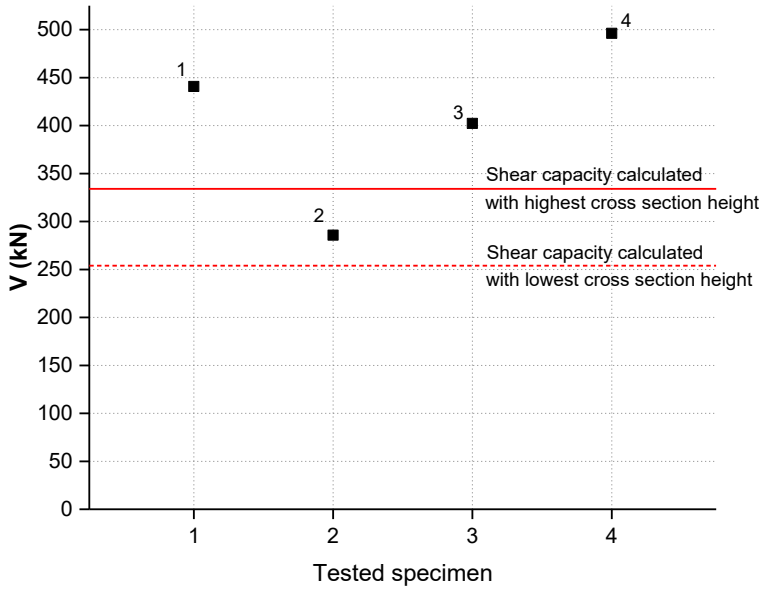

Figure 2. 22 Shear test results vs. Calculated shear capacity
(Schmidt et al. 2014)

A large variation in shear capacity between the most severely deteriorated specimen (specimen 2) and the less severely damaged specimen (specimen 4) was observed. The authors ascribed the low capacity in specimen 2 to the poor anchorage condition, lower prestressing level, and inhomogeneous of the tested beam. According to the measured shear capacities and the calculated values, Schmidt et al. (2014) concluded that it was unnecessary to demolish the bridge, and it is debatable to predict the shear capacity using the compressive strength of cores drilled from ASR damaged structures.

Hansen et al. (2016) further explored the residual shear capacity of the damaged cantilever beams mentioned above. By using an upper bound Crack Sliding Model (CSM) and the deteriorated concrete material properties, the authors predicted the residual shear capacity of the tested beams. The measured shear capacity was found approximately 30% higher than the predicted value. Hansen et al. (2016) concluded that the shear capacity was not reduced as high as the concrete compressive strength indicates, owing to the ASR-induced prestress.

More recently, Barbosa, Hansen, Hoang, et al. (2018) tested 18 beams without shear reinforcement sawn from a slab bridge built in 1967 which was severely damaged by ASR and was expected to be demolished. Nine beams failed in flexure under three-point bending, while the other nine specimens failed in shear, tested with different shear span to effective depth ratio (a/d) under four-point bending. The residual shear strength was estimated by using Eurocode 2 (EC2). The influence of concrete compressive strength, ASR-induced prestress, and different a/d ratio on the shear capacity were investigated. By comparing the calculated values with the measured results, below conclusions were drawn by Barbosa, Hansen, Hoang, et al. (2018):

- Shear strength decreases with the increase of the a/d ratio.
- Evaluation of residual shear strength according to EC2, by using the compressive strength of drilled cores and without considering the ASR-induced prestress effect normally leads to conservative results. However, with the increase in a/d ratio, this conservativeness decreases.
- ASR-induced prestress enhances the shear capacity. However, for beams with large a/d ratios, taking into consideration the ASR-induced prestress effect could result in the calculated shear strength value higher than the measured value.

2.5.3.3 Summary

Test results from literature had revealed that for reinforcement concrete members with shear reinforcement, ASR does not cause a significant reduction in shear capacity. Indeed, a slight increase in shear capacity had been reported, owing to confinement and the prestress effect induced by ASR expansion. However, at extremely large ASR expansions, fracture of the transverse reinforcement could happen, and this will

deteriorate the core concrete, damage the confinement, and ultimately impair the shear capacity.

Conflicting findings had been reported in the literature about the shear capacity of ASR damaged reinforced concrete members without shear reinforcement. While no shear reduction for ASR damaged members without shear reinforcement had been reported by some short-term laboratory tests, reductions of up to 30% in the shear capacity were recorded by some other laboratory tests. Studies on field structures severely damaged by long-term ASR revealed that there were reductions in shear capacity.

A summary of test results on shear capacity of ASR-affected reinforced concrete members with respect to the un-affected members is shown in Figure 2.23.

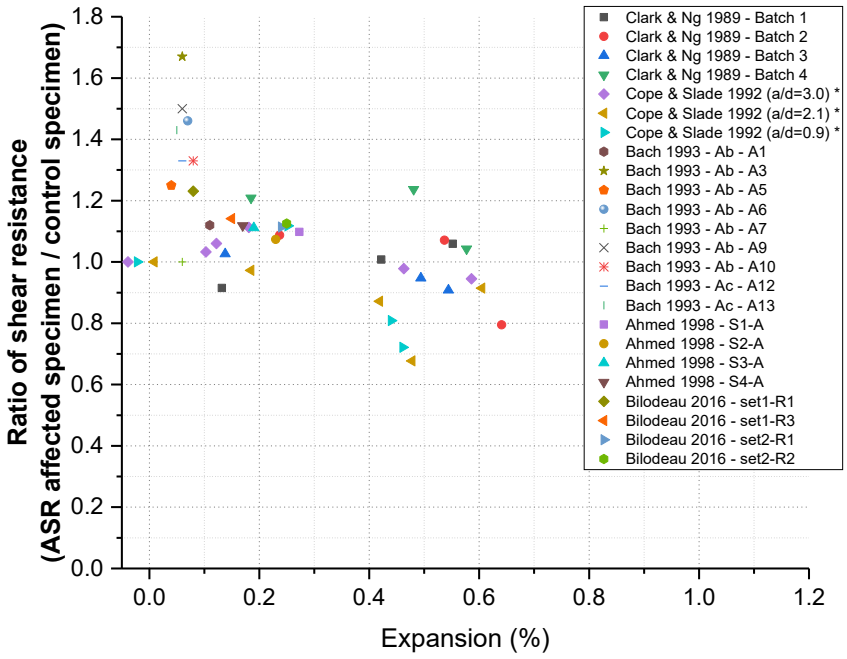

(*Free expansion)

Figure 2. 23 Shear resistance change with restrained and free expansion

It can be seen that large variations existed in test results regarding the shear strength of the ASR affected members. This could be ascribed to the various factors influencing the

shear capacity of ASR damaged reinforced members, e.g., confinement effect, self-prestress induced by ASR, ASR expansion and damage level, reinforcement detailing, deterioration in concrete mechanical properties. It is thus difficult to draw a general conclusion regarding the ASR effects on shear behaviour.

Because of the lack of universally accepted analytical methods, the prediction of residual shear resistance of ASR damaged reinforced concrete structures is a challenge. It is generally acknowledged that field load testing is the most reliable method to assess the residual shear capacity of ASR damaged structures. However, structural testing is labour intensive and time-consuming. Prediction of shear strength based on code recommendations had been performed by different researchers tentatively. Using material properties from drilled cores, and without considering the prestress effect induced by ASR expansion normally lead to conservative conclusions.

The ASR-induced prestress can enhance shear capacity. Hansen, Barbosa & Hoang (2016) investigated the impact of ASR-induced prestressing on the shear capacity of full-scale beams from severely ASR-damaged bridges. The results showed that the residual shear capacity of ASR affected slabs increased at the early stage of ASR due to the increase in the prestressing effect. When the prestressing effect reached a maximum level, the residual shear capacity decreased due to the decreasing of concrete strength. However, how the shear capacity develops as a function of long-term ASR deterioration is still unclear (see Figure 2.24).

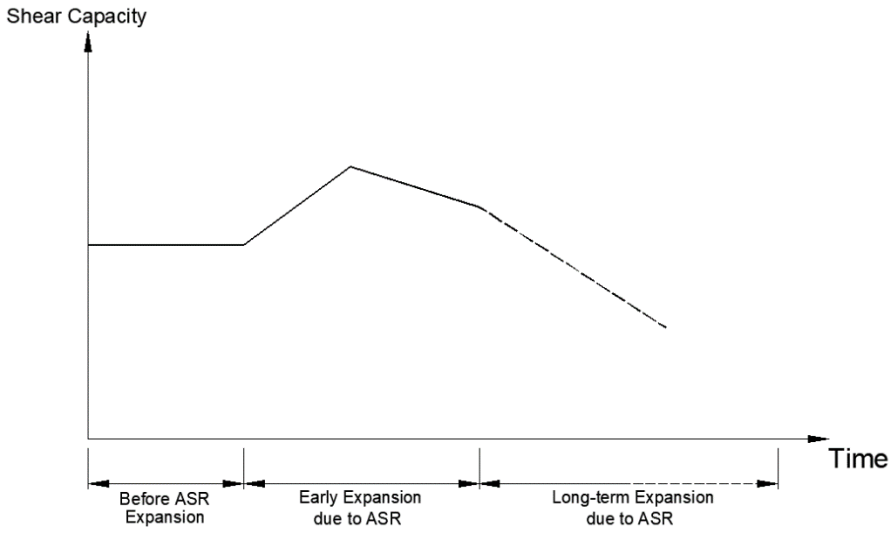

Figure 2. 24 Shear capacity of ASR affected concrete structures (Hansen, Barbosa & Hoang 2016)

2.5.4 Long-term Behaviour

The number of publications on the subject of the long-term behaviour of ASR affected structures is limited. Sustained loads, restraints by reinforcement or boundary conditions, anisotropic expansions, temperature and humidity heavily influence the long-term structural response of ASR affected structures. Efforts had been made by several researchers to predict the damage evolution caused by progressive ASR under service load and to assess the serviceability and bearing capacity of an ASR affected gravity dam (Comi, Fedele & Perego 2009). A chemo-thermo-damage model was developed in Abaqus to analyse the long-term deterioration of the structure. Figure 2.25 demonstrates the FE model used by Comi, Fedele & Perego (2009). The long-term behaviour of the affected dam under service load and progressive ASR deterioration had been simulated up to 25 years through a plain-strain finite element analysis approach. Figure 2.26 demonstrates the simulation results. The authors concluded that while a limited reduction in bearing capacity of the ASR affected dam was found, serviceability of the dam could

be severely compromised due to the reduction in structural stiffness and the consequent increase of deformations of the structure.

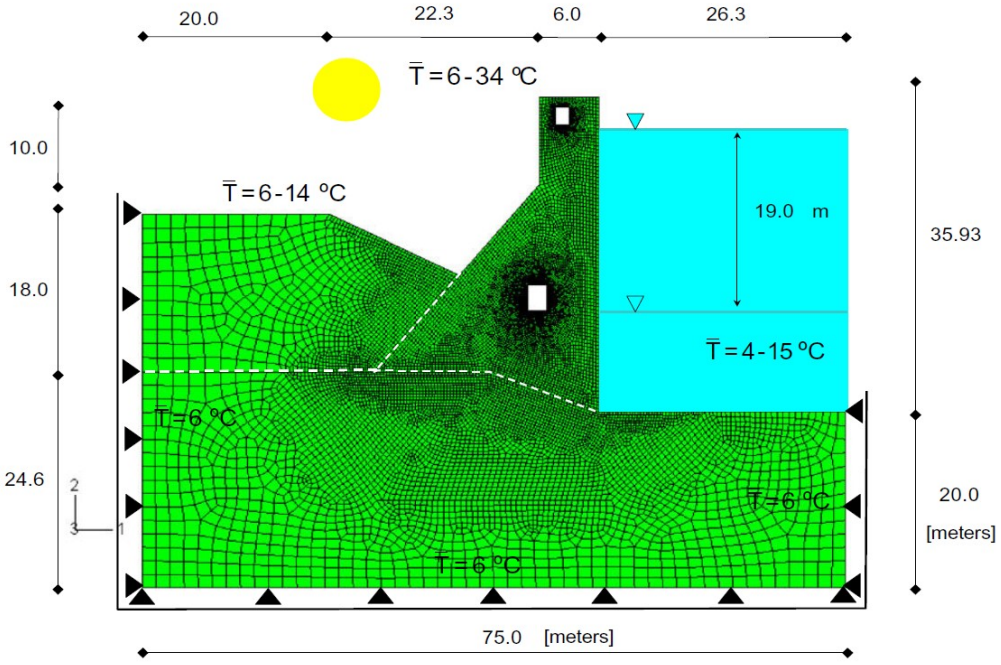

Figure 2. 25 FE model of an ASR affected gravity dam
(Comi, Fedele & Perego 2009)

Other time-dependent aging and deterioration effect, such as creep, although beyond the scope of this dissertation, plays a critical role in the long-term behaviour of reinforced concrete structures affected by ASR (Alnaggar, Di Luzio & Cusatis 2017; Grimal et al. 2008; Kawabata et al. 2017). Creep has a critical influence on the deformation of ASR affected concrete structures subjected to sustained service loads (Kawabata et al. 2017). A rheological model was developed by Grimal et al. (2008) and Grimal et al. (2010) to analyse the creep effect and ASR damage. Some researchers adopted effective modulus to consider the long-term creep effects (Multon & Toutlemonde 2006; Saouma, Perotti & Shimpo 2007). However, it is still a controversial problem on how to analyse the combined effect of creep and stress states on the long-term behaviour of ASR affected reinforced concrete structures.

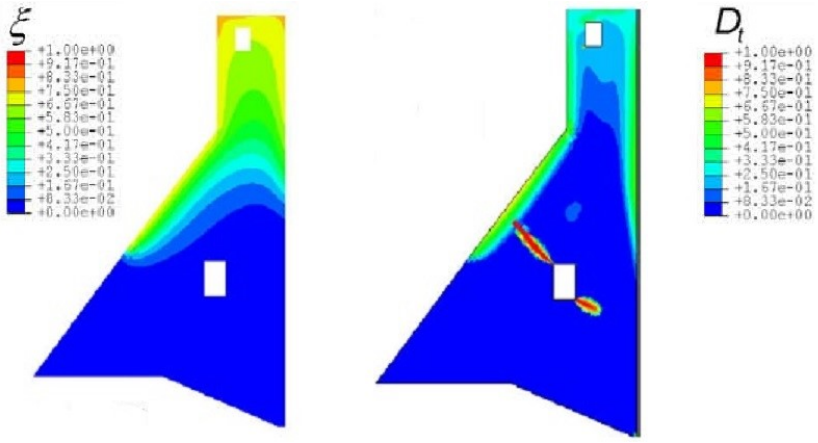

t = 3 years

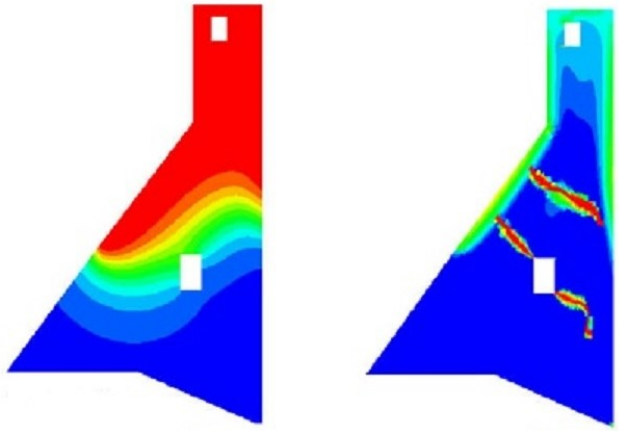

t = 7 years

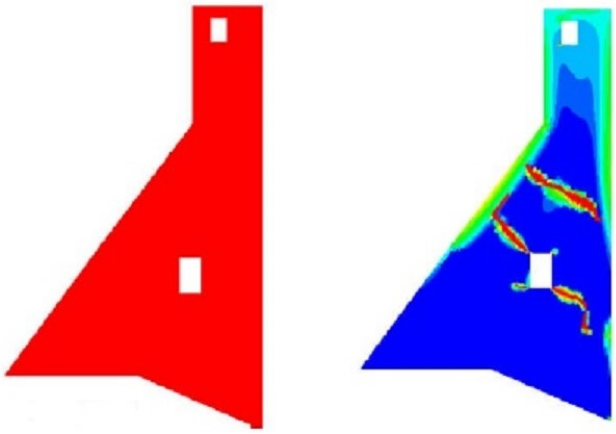

t = 25 years

Figure 2. 26 Long-term deterioration of ASR affected dam

(left column: reaction extent ξ; right column: tensile damage D_t)

(Comi, Fedele & Perego 2009)

2.6 Secondary Effects of ASR - Corrosion of Reinforcement

For ASR affected structures subjected to severe exposure conditions, such as marine environment or de-icing salts, the ASR induced cracking can facilitate the ingress of water and other aggressive chemicals thus lead to corrosion of reinforcement as secondary damage due to ASR. Carse (1996) reported an ASR affected bridge structure built in 1979 showing combined damage of ASR and subsequent corrosion of reinforcement. Longitudinal cracks in the piles of the bridge were first observed, and the primary mechanism that causing the cracks in the pile was ascribed to ASR. Due to the ASR-induced cracks in the piles and the subsequent chloride attack, reinforcement corrosion happened. Due to the combined effect of ASR and reinforcement corrosion, cracks were subsequently widened to a maximum width of 8 mm. Concerns on the load-carrying capacity of the piles were raised and a repair strategy was deployed in 1995 for this bridge, which was affected by ASR and subsequent reinforcement corrosion.

Limited publications on structural behaviour due to the combined effects of ASR and reinforcement corrosion were found in the literature. Hamada, Otsuki & Fukute (1989) performed a series of experiments with 10 years of long-term exposure under marine environment to investigate the behaviour of ASR affected concrete. The authors reported that although ASR caused a significant reduction in elastic modulus and compressive strength, the moment capacity of the test specimens with ASR and reinforcement corrosion showed limited decreasing. Kawamura, Takemoto & Ichise (1989) studied the influence of ASR on the reinforcement corrosion in concrete contaminated by sodium chloride. The authors confirmed that ASR can improve the corrosion rate. Although beyond the scope of this dissertation, the potential corrosion of reinforcement as a secondary damage due to ASR, especially pitting corrosion induced by chloride concentration, is harmful to the load capacity of the affected structure.

2.7 Accelerated Test Methods for ASR

ASR can take a very long time (5 years to even 20 years) to happen in a structure (Fernandes 2009). To ensure the suitability for concrete, aggregates from new sources are required to be assessed for their potential reactivity before being used in concrete. In order to screen the reactivity of aggregates, accelerated test methods in the laboratory are the most efficient methods. For those known reactive aggregates, mitigation of ASR, and prediction of the performance of the concrete which adopts these aggregates also need to use the accelerated test methods. In practice, the Accelerated Mortar Bar Test (AMBT), Concrete Prism Test (CPT), and Accelerated Concrete Prism Test (ACPT) are the generally accepted tests for assessing aggregates for ASR potential. In recent years, the Ultra-accelerated Autoclave Test Methods for ASR has emerged and attracted more and more attention from researchers due to its advantages in quickly determining the potential ASR for aggregates. All these tests belong to accelerated laboratory test methods, meaning that the specimens are exposed to conditions that can make the reaction rate faster than the rate which would happen in actual structures. In the following, these test methods, their advantages, and disadvantages will be reviewed.

2.7.1 80 °C Accelerated Mortar Bar Test (AMBT)

The AMBT method, which can be found in AS1141.60.1, is a rapid test for ASR. Alternative forms of the AMBT methods can also be referred to ASTM C1260, RILEM AAR-2, CSA A23.2-25A, and RMS T363. According to AS1141.60.1, the general procedure of AMBT involves: casting at least three mortar bars with a size of 25 × 25 × 285 mm following specific grading requirements for aggregates; curing the specimens in an environment with RH > 95% for 24 hours; after demoulding, record an initial comparator reading for the length of each specimen; the mortar bars are then placed in

portable water and the temperature was raised to 80 °C; the mortar bars are stored in the water for 24 hours then removed from the water and measured as zero readings; then the specimens are subjected to 1 N sodium hydroxide solution treatment; mortar bar samples remain in the 80 °C sodium hydroxide solution and are measured at specific times up to 21 days.

According to AS1141.60.1, for mortar bar expansion at 21 days less than 0.1%, the aggregates are identified as non-reactive aggregates. If the 10-day expansion value equal or greater than 0.1%, or expansion at 21 days equal or great than 0.3%, the aggregates are classified as reactive aggregates. While for those 10-day expansions less than 0.10% but the 21-day expansions fall between 0.1% and 0.3%, the aggregates are classified as slowly reactive aggregates. ASTM C1260 and RILEM AAR-2 provide a different interpretation of test results, expansions at 14 days less than 0.1% indicate an innocuous aggregate, expansions at 14 days higher than 0.2% indicate a reactive aggregate, while for expansions at 14 days fall between 0.1% and 0.2%, the aggregate is regarded as potential reactive. The RMS T363, however, adopts a lower limit 0.1% to classify the aggregate reactivity, that is, for expansions less than 0.1% both at 10 days and 21 days, aggregates are classified as non-reactive, for expansions greater than 0.1% both at 10 days and 21 days, aggregates are classified as alkali reactive, while for expansions at 10 days less than 0.1% but at 21 days greater than 0.1%, the aggregates are regarded as slowly reactive. This lower expansion limit might be due to the relative lower water to cement ratio (w/c) (0.42 to 0.45) adopted in RMS T363 with respect to 0.47 that is recommended in AS1141.60.1, ASTM C1260, and RILEM AAR-2 (Sirivivatnanon, Mohammadi & South 2016).

AMBT provides a tool for screening the reactivity of aggregates in a couple of weeks. It is suitable for testing fine aggregates. However, for testing the reactivity of coarse

aggregates, a specific grading should be satisfied by crushing the aggregates. Because crushing of aggregate can cause increasing in specific surface area of reactants and immersing the specimens in NaOH solution means an unlimited supply of alkalis, hence, AMBT could lead to false-positive results (Lu et al. 2008; Thomas et al. 2006). On the other side, Hooton & Rogers (1993), Thomas et al. (2006) had reported that some reactive aggregates were tested with false-negative results as well. However, due to its efficiency and convenience, AMBT is still a widely accepted test for screening aggregate for its reactivity potential.

2.7.2 38 °C Concrete Prism Test (CPT)

Compared to the AMBT, a more reliable test method for ASR is the Concrete Prism Test (CPT). AS1141.60.2, ASTM C1293, RILEM AAR-3, CSA A23.2-27A and RMS T364 are different forms of CPT. The AS1141.60.2 test method uses 75 × 75 × 285 mm concrete prisms. In the concrete mix, a 420 kg/m^3 cement content and a water to cement ratio (w/c) of 0.42~0.45 are recommended. As for the coarse aggregate and fine aggregate, a specific proportion and grading are also recommended. A 1.25% Na_2O_{eq} is used to artificially boost the alkali content in the concrete. The prisms are stored in 38 °C, 100% RH environment after an initial length measurement, and length measurement continues up to 52 weeks.

AS1141.60.2 classifies an aggregate as non-reactive when the average 52-week prism expansion is less than 0.3%. Whilst the expansion at 52 weeks is equal or greater than 0.3%, the aggregate is regarded as potentially reactive. RMS T364 uses the same criteria but the total alkali content in concrete is raised higher to 1.38% Na_2O_{eq} by mass of cement. ASTM 1293 adopts a 0.04% expansion limit to classify the reactivity of aggregates, while RILEM AAR-3 uses a 0.05% expansion limit as the criteria. However, RILEM AAR-3

also stated that for some slowly reactive aggregates, a lower criterion should be considered.

CPT is regarded as the most reliable method currently for determining the potential reactivity of aggregate, and the most reliable performance test method for evaluating the potential risk of ASR in concrete. CPT uses fine aggregates and coarse aggregates in standard mix combinations. It is also suitable for CPT to use the actual aggregate combination intended for job mixes. In addition, the alkali content used in CPT is at more realistic levels compared to the unlimited supply of alkalis in AMBT. Furthermore, instead of immersion of the prisms in the NaOH solution, the CPT cures the prisms in a 100%RH environment at 38 °C which is more realistic and is close to exposure conditions of field structures. However, the long test duration makes its use in practice less competitive. It takes one year to get the results for determining the potential reactivity of aggregate and two years for justifying the mitigation of ASR expansion when supplementary cementitious materials (SCMs) are used. Furthermore, the alkali leaching in the CPT could slow down the rate of expansion thus may lead to a false-negative test result.

Despite some of its disadvantages, CPT is still a widely accepted test method for ASR and is regarded as the most reliable performance test method for determining the risk of ASR expansion in the laboratory.

2.7.3 60 °C Accelerated Concrete Prism Test (ACPT)

The Accelerated Concrete Prism Test (ACPT) is an improved alternative form of the CPT for assessing the reactivity of aggregates by using fine aggregates and coarse aggregates in combination. In order to reduce the test duration, a 60 °C conditioning temperature is adopted in this test method. This test method can be found in RILEM AAR-4.1. In this

method, concrete prisms are stored in a 60 °C 100%RH environment for 20 weeks to accelerate ASR. Expansions of the specimens are measured periodically to obtain the results. RILEM AAR-4.1 recommends that at 15 weeks of age, if the average expansion is less than 0.03%, an aggregate will be identified as non-reactive; if the average expansion is greater than 0.03%, the aggregate will be identified as potentially reactive. In ACPT, the possibility of alkali leaching is more severe than in the standard CPT.

Yamada et al. (2014) proposed an alternative ACPT method to identify the reactivity of an aggregate. The proposed test method uses concrete prisms with a size of 75 × 75 × 250 mm. The total alkali content is adjusted to 5.5 kg/m^3 to accelerate ASR. Specimens are wrapped with alkali solution wetted paper and then overwrapped with thin plastic film. The specimens are stored in a 60 °C environment for 20 weeks. During this period, after each length measurement at a specific time, the same procedure of wrapping the specimens is applied. An expansion limit of 0.04% at the age of 20 weeks is suggested to classify the reactivity of the aggregate. The authors concluded that wrapping the specimens with alkali solution wetted paper can overcome the disadvantage of alkali leaching in the RILEM AAR-4.1 ACPT method.

Another alternative accelerated test method is the Miniature Concrete Prism Test (MCPT) proposed by Latifee & Rangaraju (2015). The MCPT protocol uses 50 × 50 × 285 mm concrete prisms to test the reactivity of aggregates. The maximum particle size of the aggregate used in the concrete mixture is 12.5 mm and the total alkali content is adjusted to 1.25% Na_2O_{eq} by mass of cement. The initial length of the prisms is measured after demolding and the prisms are immersed in 60 °C water for 1 day. After that, the prisms are taken out, and the length measurement is made again, then the prisms are placed in 1N sodium hydroxide solution with a temperature maintained at 60 °C. Periodical length readings are made. At the age of 56 days, an expansion threshold of 0.04% is proposed

to distinguish reactive and non-reactive of an aggregate. The periodical length measurement continues to the age of 84 days.

2.7.4 Ultra-accelerated Autoclave Test Methods for ASR

To quickly identify the ASR potential of aggregates, ultra-accelerated autoclave test methods have been used. A summary of past autoclave tests is listed in Table 2.4. Among them, the representative autoclave test method on mortar bars and concrete prism specimens are reviewed in the following sections.

2.7.4.1 Rapid Autoclave Mortar Bar Test Method (Fournier, Bérubé & Bergeron 1991)

Fournier, Bérubé & Bergeron (1991) proposed a rapid aggregate reactivity screening method by using an autoclave to identify the potential ASR. Mortar bars with a size of 25 × 25 × 285 mm were adopted in the test. The influence of different test parameters, such as alkali content, type of cement, water to cement ratio (w/c), autoclave steam curing temperature, and autoclave steam curing duration, on the mortar bar expansion, was explored. In this test, the alkali content was adjusted by adding NaOH in the mixing water. Alkali content parameters varying from 1.0% - 3.5% Na_2O_{eq} by mass of cement were studied. Five different cement types having different alkali content were investigated. The water to cement ratio (w/c) used was 0.45, 0.50, and 0.60. Five different autoclaving temperatures, between 123 °C and 190 °C were investigated, along with autoclaving durations ranging from 4 to 8 hours. Forty different types of aggregate were tested.

The expansion of mortar bars was taken before placed into the autoclave and after autoclaving when the specimens were cooled to ambient temperatures.

Table 2. 4 Summary of ultra-accelerated autoclave tests

Test Parameter	Tang, Han & Zhen (1983)	Tamura (1987)	Fournier, Bérubé & Bergeron (1991)	Nishibayashi et al. (1996)	French Standard Method (MBT/AFNORXP 18-594, 590) (Criaud et al. 1994)	Giannini & Folliard (2013)	Wood et al. (2017)
Specimen type	Mortar	Mortar	Mortar	Concrete	Mortar	Concrete	Mortar
Specimen size, mm	10×10×40	40×40×160	25×25×285	75×75×400	40×40×160	75×75×286	25×25×285
Na_2O_{eq} by mass of cement	1.5%	2.4%	3.5%	3.0%	4%	3.0%	3.5%
Temperature	150 °C	111 °C	130 °C	133 °C	127 °C	133 °C	130 °C
Duration of autoclaving	6 hours	2 hours	5 hours	4 hours	5 hours	24 hours	5 hours
Proposed expansion limit	--	--	0.15%	--	0.15%	0.08%	--

Reference concrete prisms with a size of 75 × 75 × 300 mm and 1.25% Na_2O_{eq} alkali content were also made. The concrete prisms were subjected to 38 °C 100% relative humidity conditioning. An expansion of 0.04% at six months was used as criterion to classify the reactivity of aggregate.

Test results about the influence of alkali content, water to cement ratio (w/c), autoclaving temperature, and autoclaving duration on the expansion of mortar bars are addressed as followings:

(1) Influence of total alkali content and cement (see Figure 2.27)

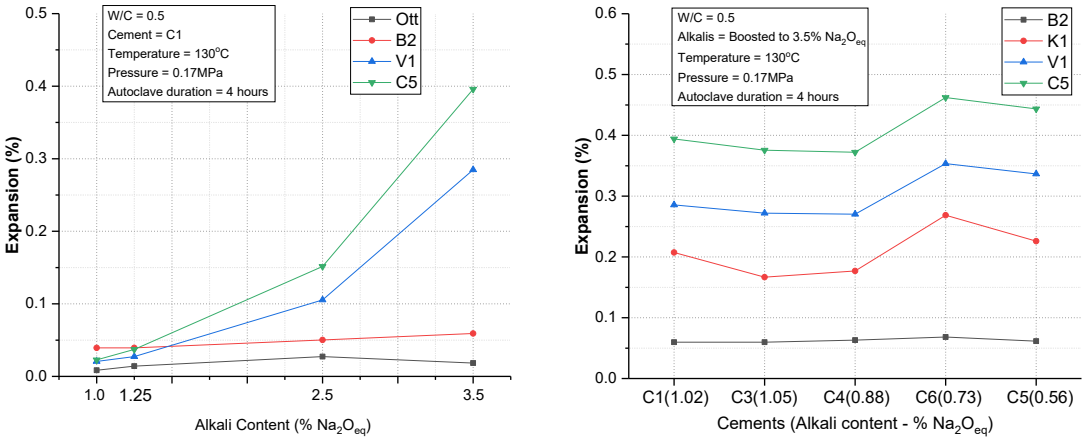

Figure 2. 27 Relation between expansion and total alkali content, different types of cement

(Fournier, Bérubé & Bergeron 1991)

It was concluded by the authors that increasing of total alkali content increased the expansion of reactive aggregates (V1 and C5) but did not affect the non-reactive aggregates (B2 and Ott).

A pessimum alkali content of 2.5% Na_2O_{eq} by mass of cement in the concrete mixes was also observed by (Nishibayashi, Yamura & Matsushita 1987).

Changing of cement type did not influence the expansion of the non-reactive aggregate (B2). However, some fluctuations in the expansion were observed for

reactive aggregates when different types of cement were used. This could be attributed to the different amounts of sodium hydroxide addition in the concrete mixes to boost the total alkali content to 3.5% Na_2O_{eq}.

(2) Influence of the water-to-cement ratio

Figure 2.28 shows the impact of the water to cement ratio (w/c) on the expansion behaviour of different types of aggregate.

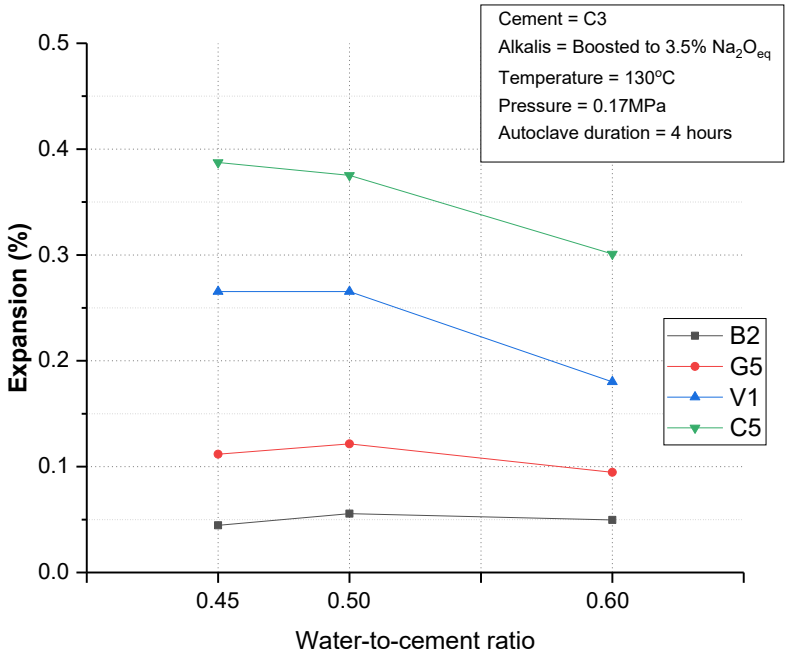

Figure 2. 28 Effect of the water-to-cement ratio on the expansion of mortar bars (Fournier, Bérubé & Bergeron 1991)

It was found that increasing of water-to-cement ratio could lead to a reduce in the expansion. This could be ascribed to the increased permeability and porosity at a higher water to cement ratio (w/c) because the increased porosity could facilitate accommodating more ASR gel thus reduced the expansion of the specimen.

(3) Influence of autoclaving temperature (see Figure 2.29)

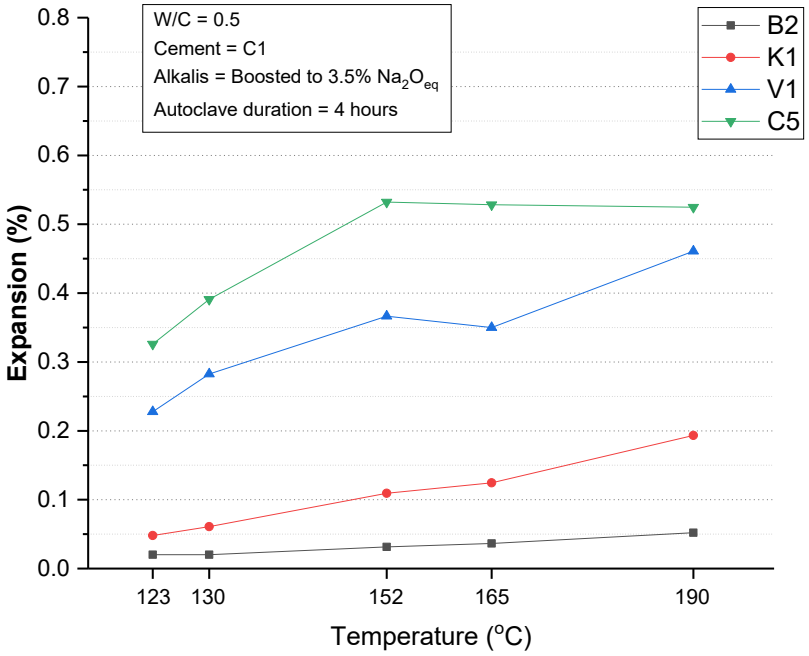

Figure 2. 29 Impact of autoclaving temperature on mortar bar expansions (Fournier, Bérubé & Bergeron 1991)

When autoclaving temperature was elevated, the expansion of reactive specimens increases (V1 and C5). But the autoclaving temperature had no significantly influence on the expansion of non-reactive specimens. For non-reactive aggregate K1 (based on the CPT results), at 152 °C autoclaving temperature condition, an expansion of greater than 0.1% was observed. Hence, an autoclaving temperature higher than 150 °C could produce excessive expansion.

(4) Influence of autoclaving duration (see Figure 2.30)

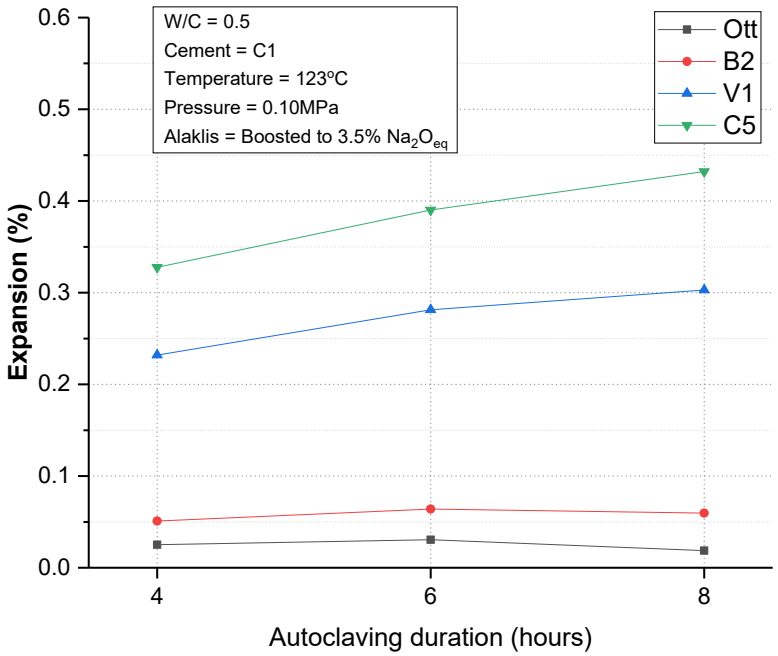

Figure 2. 30 Impact of autoclaving duration on mortar bar expansions (Fournier, Bérubé & Bergeron 1991)

With the increase of the autoclaving duration, the reactive aggregate (V1 and C5) specimens showed an increasing trend in expansion. However, the increase of autoclaving duration did not influence the expansion behaviour of non-reactive aggregate specimens (Ott and B2).

According to test results regarding the impact of different parameters on mortar bar expansions, a final autoclave mortar bar test procedure as shown in Figure 2.31 was proposed by the authors. The final proposed test procedure involved raising the total alkali content of the mortar bars to 3.5% Na_2O_{eq} by mass of cement. A water to cement ratio (w/c) of 0.5 was suggested for the mortar bars and five hours autoclaving at 130 °C was adopted.

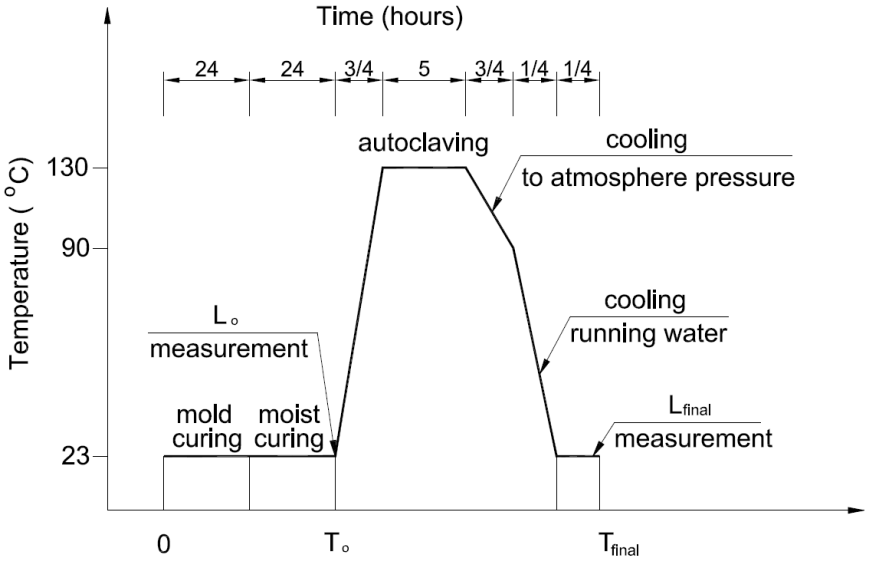

Figure 2. 31 Laval/CANMET autoclave mortar bar test procedure

(Fournier, Bérubé & Bergeron 1991)

After comparing with the CPT results, Fournier, Bérubé & Bergeron (1991) reported an overall efficiency of 93% of the autoclave test results, which means that 37 out of 40 aggregates showed the same results. A 4.4% coefficient of variation was reported for the series of autoclave mortar bar tests. For this accelerated autoclave mortar bar test, an expansion threshold of 0.15% was also proposed to classify the reactivity of aggregates by Fournier, Bérubé & Bergeron (1991).

2.7.4.2 Rapid Autoclave Concrete Prism Test (Giannini & Folliard 2013)

Giannini & Folliard (2013) carried out a series of autoclave tests based on concrete prisms (75×75×286 mm) to distinguish the reactivity of aggregates. The whole test program consists of two stages. Stage one involves testing of benchmark aggregates, including three reactive aggregates and two non-reactive aggregates, to study the influence of various autoclaving parameters on the expansion of the concrete prisms, and to finalize the autoclave test parameters for the second phase tests. The investigated parameters included: total alkali content of 2.0%, 2.5%, and 3.0% Na_2O_{eq} by mass of cement;

different duration of autoclaving with 4, 6 and 24 hours at a temperature of 133 °C. The test procedure of the autoclave concrete prism test was proposed by Giannini & Folliard (2013) as followings:

- Curing specimens in moulds for 24 hours after casting;
- Demolding specimens then moist curing the specimens for another 24 hours;
- After initial length readings, specimens are subjected to 4, 6, or 24 hours of autoclaving at 133 °C;
- Removing specimens from the autoclave, taking the final length measurements after the specimens were cooled to 23 °C under running cold water.

In the first phase test program, below four concrete mixtures were tested:

- F1+C1 combination: using non-reactive fine aggregates F1 and non-reactive coarse aggregates C1 in the concrete mixture;
- F2+C1 combination: using highly reactive fine aggregates F2 and non-reactive coarse aggregates C1 in the concrete mixture;
- F3+C1 combination: moderately to highly reactive fine aggregates F3 and non-reactive coarse aggregates C1;
- F1+C2 combination: non-reactive fine aggregates F1 and moderately to highly reactive coarse aggregates C2 in the concrete mixture.

After testing the F1+C1 and F2+C1 combinations, it was found that the total alkali content of 2.0% Na_2O_{eq} by mass of cement could only produce limited expansion for highly reactive aggregates F2. Thus, the authors eliminated the 2.0% Na_2O_{eq} parameter for the rest of the testing. Expansion of the four combinations under autoclave accelerated condition is shown in Figure 2.32.

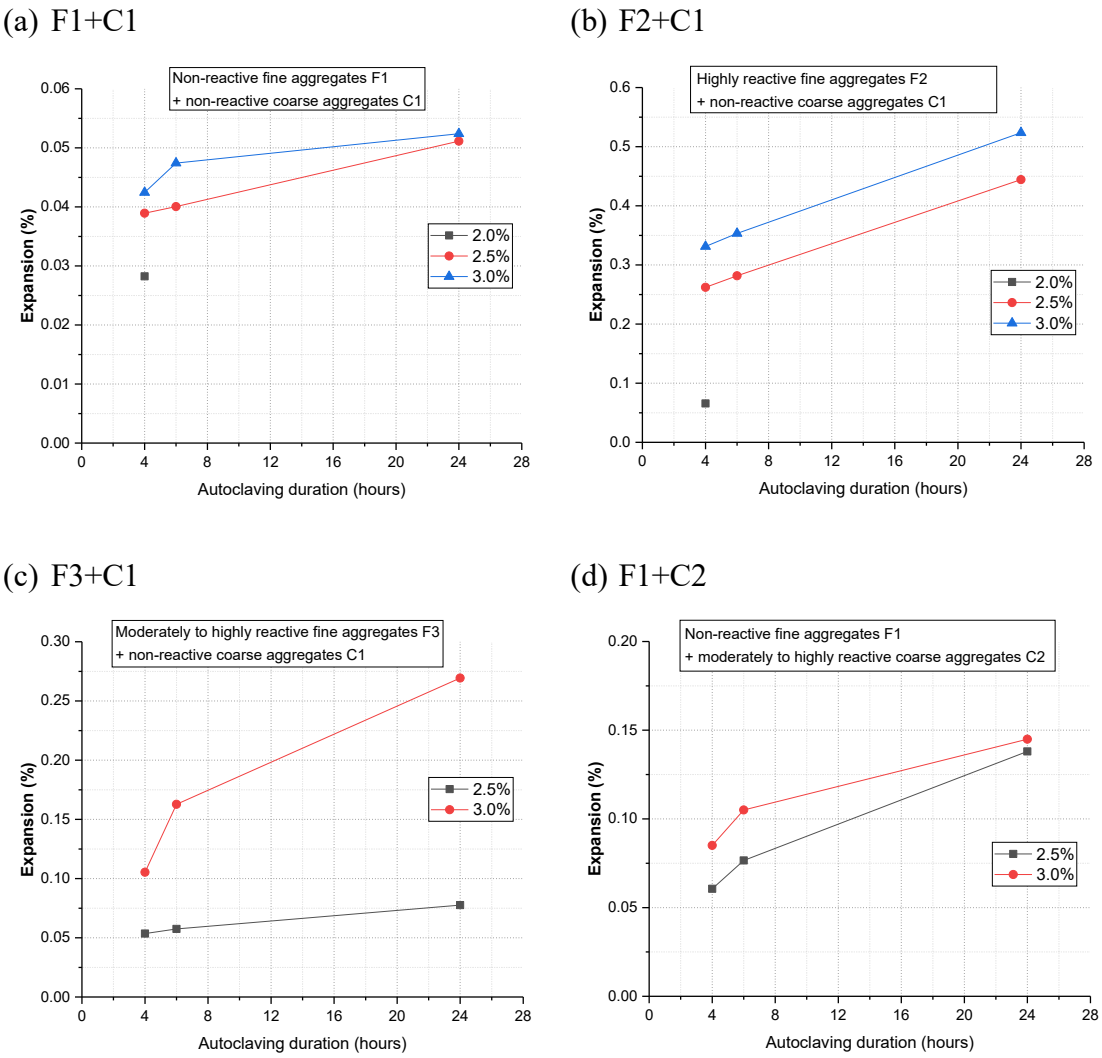

Figure 2. 32 Expansions of different mixtures under various alkali contents and autoclaving durations at 133 °C (Giannini & Folliard 2013)

According to the first stage test results, Giannini & Folliard (2013) proposed the optimal test parameters to be: 3.0% Na_2O_{eq} alkali content, 24 hours autoclaving duration, and 133 °C autoclaving temperature. The expansion limit to distinguish the reactivity of aggregates was proposed as 0.08%.

The second stage of the test involved investigating the reactivity of another six aggregates by using the proposed autoclave concrete prism test method. By comparing the test results with the ASTM C1293 results, the proposed autoclave concrete prism test successfully identified the reactivity of all the six aggregates, while the ASTM C1260 gave a false

result for one aggregate and two inconclusive results for two aggregates. Giannini & Folliard (2013) made conclusion that the proposed ultra-accelerated autoclave concrete prism test appeared to be suitable for screening the potential reactivity of aggregates. The authors also recommended that more aggregates to be tested by using this method in the future, particularly for those slowly expanding aggregates.

2.7.4.3 Summary

Grattan-Bellew (1997) provided several criteria for a reliable ultra-accelerated test that can be used for classification of aggregate reactivity. First of all, the test period should not exceed several weeks, and the results should be obtained within a few days as much as possible; secondly, it should avoid complicated operations and does not involve expensive equipment; third, it should be able to correctly distinguish most of the aggregate (greater than 90%) for the reactivity and non-reactivity; fourthly, the reaction product produced in the ultra-accelerated test should be similar to that produced in the CPT test and the field structure affected by ASR; last but not least, the expansion limit should be higher than 0.05%. After reviewed existing autoclave accelerated mortar bar tests, Grattan-Bellew (1997) concluded that these test methods showed good correlation and considerable promise results. However, Shayan, Ivanusec & Diggins (1994) compared the expansion of five types of sand by storing mortar bars in 1N sodium hydroxide solution at 80 °C and using the autoclave accelerated test method, found that the autoclave accelerated test with 3.5% alkali boosting and 127 °C for 4 or 5 hours, failed to detect the slowly reactive sand. More investigations on the influence of various parameters on different aggregate types are needed.

The studies performed by Giannini & Folliard (2013) showed promising results in screening the reactivity of aggregates by using the ultra-accelerated autoclave test.

However, more research needs to be conducted on the performance of "job mixes" by using an ultra-accelerated autoclave test for assessing the potential risk of ASR.

2.8 Numerical modelling of ASR

Over the past few decades, various numerical models including the macroscopic model or microscopic model have been proposed to simulate the ASR deterioration and structural response due to ASR (Pan et al. 2012; Saouma 2014). Esposito & Hendriks (2017) summarised the ASR models based on different classification levels, ranging from ASR product level to structural member and structure level. The early finite element models utilised the equivalent temperature load to simulate the ASR expansion. For this reason, in the input parameters, the thermal coefficient of concrete was defined as a variable (Esposito & Hendriks 2017). Thereafter, researchers started to develop comprehensive models to depict the kinetics of the chemical reaction.

Ulm et al. (2000) developed a thermo-chemo-mechanical model based on governing micro-mechanisms of ASR expansion, which took into account the ASR kinetics and ASR swelling pressure (see Figure 2.33).

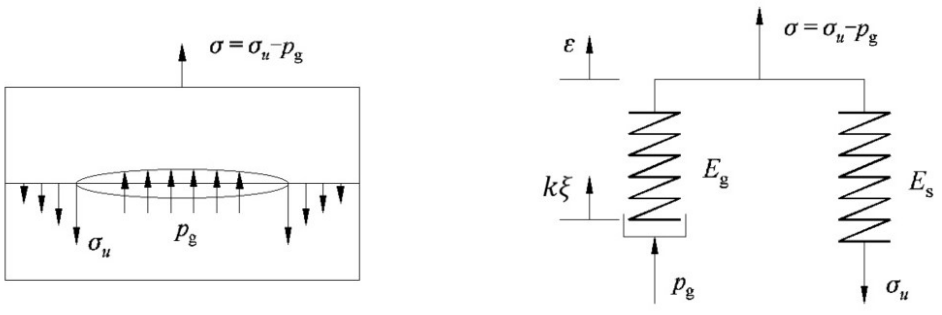

Figure 2. 33 Rheological model by Ulm et al. 2000

In this model, σ is the total stress acting on the material at the macroscopic level, ε is the total strain, E_g and E_s represent the spring moduli of the chemo-mechanical device, σ_μ

denotes the stress in the elastic spring E_s, and p_g represents the swelling pressure in the chemical device, $k\xi$ denotes the ASR induced strain. $\xi \in [0,1]$ represents the degree of the chemical reaction, assuming it is proportional to the volume increase of the ASR product. Ignoring the free expansion space where the ASR gel can freely swell, from the stress equilibrium in the above chemo-elastic device, one can obtain:

$$\sigma = \sigma_\mu - p_{\mathrm{g}} = E_s\varepsilon + E_{\mathrm{g}}(\varepsilon - k\xi) \tag{2.10}$$

Where: $\sigma_\mu = E_s\varepsilon;\ p_{\mathrm{g}} = -E_{\mathrm{g}}(\varepsilon - k\xi)$.

Free energy can be written in the form of:

$$\Psi = \frac{1}{2}\left[E_s\varepsilon^2 + E_{\mathrm{g}}(\varepsilon - k\xi)^2\right] + \mathrm{g}(\xi) \tag{2.11}$$

Function $\mathrm{g}(\xi)$ represents the free energy in chemical pressure cell. Based on Equation 2.11, one can verify the stress equilibrium:

$$\sigma = \frac{\partial\Psi}{\partial\varepsilon} = E_s\varepsilon + E_{\mathrm{g}}(\varepsilon - k\xi) \tag{2.12}$$

The authors suggested that in massive concrete structures such as dams, heat diffusion plays a major role in driving ASR deterioration, with a combination of the reaction kinetics. While in thin-wall slender concrete structural elements, moisture distribution was of more concern.

Esposito & Hendriks (2016) proposed a multiscale model to assess the concrete material degradation caused by ASR. At the macroscopic scale, the concrete was considered as a homogeneous material. At microscopic scale the microstructure of concrete was modelled by an elastic matrix-cracks system formed by aggregates and cement paste. The model was analytically solved by adopting damage criterion based on linear fracture mechanics theory and the concept of representative elementary volume. Results showed that it can

predict well the macroscopic deterioration of concrete subjected to uniaxial loading. However, an overestimation of the stiffness degradation was reported, and the authors suggested a reconsideration of the elastic assumption for model modifications.

Alnaggar, Di Luzio & Cusatis (2017) took into account aging effects such as creep and shrinkage in the concrete, and the coupling effects between creep, shrinkage, and ASR, proposed a more sophisticated model under the framework of the Lattice Discrete Particle Model (LDPM). The authors adopted a multi-physics formulation to analyse the progress of humidity, temperature, cement hydration and ASR in both space and time. The analysis was further extended to cracking of the concrete, creep, and shrinkage using physics-based formulations. With calibration by available experimental data of individual lab size specimens, the model showed its ability to capture the ASR formation and expansion for full scale beam elements. However, Alnaggar, Di Luzio & Cusatis (2017) explained that due to lack of experimental data on bond-slip behaviour between reinforcing steel bar and concrete, the rebar-concrete slippage phenomenon was neglected although the authors suggested that at a high level of stress, partial bond loss, reinforcement slippage or rebar yielding could happen.

The ASR models introduced above are few models in the literature claiming to be able to simulate the complicated ASR effects on structures. There are many other models in literature as summarised by Esposito & Hendriks (2017). Although these models try to simulate and predict the ASR effects in a different way from microscopic scale to the macroscopic scale, much still needs to be explored in predicting the structural behaviour for ASR affected structures perhaps by bridging the scale from the microscopic scale to macroscopic scale with the help of increased computational power and technology advancement.

Chapter 3

Accelerated Autoclave Test for Assessing Alkali-Silica Reaction of Concrete

3.1 Overview

Alkali silica reaction (ASR) in concrete is a deleterious reaction that occurs due to the reaction between alkalis in the pore solution and reactive forms of silica found in some aggregates. ASR can result in expansion and cracking which has the potential to reduce mechanical properties of the concrete. Figure 3.1 shows extensive cracking in the superstructure of a bridge severely damaged by ASR. There have been concerns about the structural integrity and the residual load capacity of the structure due to ASR damage in the concrete.

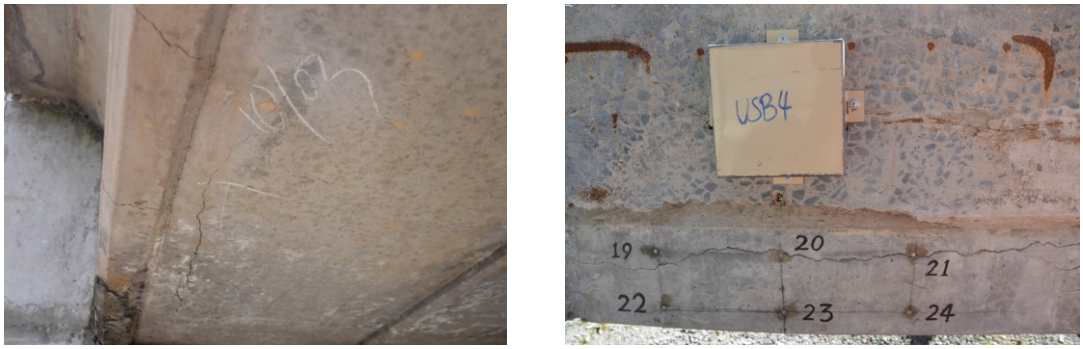

Figure 3. 1 Cracking of bridge beams due to ASR

The presence of cracking and damage due to ASR in the bridge has resulted in the demolition and replacement of the superstructure (see Figure 3.2). A comprehensive understanding of the cause of ASR, the extent of damage, and the consequent influence on the residual load-carrying capacity of the concrete members are needed. Research relating to ASR deterioration of bridge girders is carried out at the University of Technology Sydney.

ASR is one of the major durability issues affecting concrete structures in the world (Rajabipour et al. 2015). Alkalis in concrete basically initiate ASR, mostly from Portland

Figure 3. 2 ASR affected bridge beams from a demolished bridge deck

cement as well as other internal and external sources which causes a high concentration of alkalis within the pore solution. The alkalis initially attack some siliceous phases in aggregates and produce an expansive gel, consequently causing expansion and cracking of concrete which ultimately reduces the mechanical properties (Stanton 1940). In the existing two laboratory test methods, namely AS 1141.60.1 accelerated mortar bar test (AMBT) and AS 1141.60.2 concrete prism test (CPT), AMBT can produce results within 21 days. CPT, however, takes one year for OPC concrete mixes and two years for mixes with supplementary cementitious materials. In both methods, aggregates are crushed to give specific gradings. Also, the AMBT test requires handling NaOH solution at 80 °C.

In order to test concrete mixes as used in the field and also to study reinforced concrete elements, an ultra-accelerated test method is required. An autoclave environment is suitable for this purpose. Autoclave test methods for ASR have been investigated by several researchers (see Table 2.4). In these autoclave test methods, the mixes were

boosted with alkalis between 1.5 to 4.0% by mass of cement, and maximum temperatures used were kept between 111 °C and 150 °C. The duration of the test was between 4 to 24 hours for concrete prisms and 2 to 6 hours for mortar bars.

In this chapter, a multi-cycle autoclave test method for ASR is investigated. In this method, concrete specimens with and without alkali boosting under ultra-accelerated autoclave test condition have been tested. Expansion and deterioration caused by ASR in concrete are investigated using an autoclave to simulate long-term deterioration. Results obtained within a short period, clearly show large expansions and deterioration levels for concrete made with reactive aggregates. Details of the multi-cycle autoclave test method, adopting 130 °C and duration of 5 hours for each cycle, are presented in the following sections.

3.2 130 °C Autoclave Test Program

3.2.1 Materials and Mix Proportions

Aggregates which are considered as the most reactive (aggregate B) and least reactive (aggregate C) were chosen for these experiments. A non-reactive fine aggregate (Sydney Sand) was used in this study.

Two types of general-purpose Portland cement with similar equivalent alkali contents (Na_2O_{eq}) of 0.52% (cement 1) and 0.50% (cement 2) by mass of cement were used for all mixes. Equivalent alkali content was calculated as $Na_2O + 0.658K_2O$. The cement oxide composition analyses are provided in Table 3.1.

To increase the Na_2Oeq content in the system, sodium hydroxide (NaOH) pellets with a purity of 98% were added to the mixing water 24 hours prior to the mixing as dissolution of NaOH generates heat. Two types of coarse aggregates were tested. Non-reactive sand

(Sydney Sand) was used as a fine aggregate in the concrete mix. The alkali levels were boosted to equivalent Na_2O levels of 3% and 5% by mass of cement. An un-boosted mix was also cast and tested for comparison. Concrete prisms of 75 × 75 × 285 mm in size were prepared to determine ASR expansion. Nine concrete prisms were cast for each mix. The mix proportions are shown in Table 3.2.

Table 3. 1 Oxide composition of Portland cement used in the mixes

Oxide Composition	Weight Percentage (%)	
	Cement 1	Cement 2
CaO	62.78	64.18
SiO_2	19.66	19.67
Al_2O_3	5.11	4.78
Fe_2O_3	3.04	3.10
SO_3	2.68	2.37
MgO	1.14	0.91
K_2O	0.43	0.41
TiO_2	0.26	0.22
Na_2O	0.24	0.23
P_2O_5	0.12	0.06
Mn_2O_3	0.07	0.12
LOI	4.06	4.09
Total	99.9	100.1
Na_2O_{eq}	0.52	0.50

Table 3. 2 Concrete mix proportions

Material	Concrete mix		
	Un-boosted (kg/m^3)	With 3% Na_2O_{eq} boosting (kg/m^3)	With 5% Na_2O_{eq} boosting (kg/m^3)
20 mm Aggregate	1134	1134	1134
Sand (non-reactive)	610	610	610
Cement 2	440	440	440
Water	175	175	175
NaOH pellets added	--	14.491	26.083
Na_2O_{eq} (Calculated)	2.2	13.2	22.0

3.2.2 Specimen Fabrication and Autoclave Test Procedure

After casting and demolding (the following day), the specimens (9 specimens each batch) were cured in water at a temperature of 23.0 ± 2.0 °C for 3, 7, and 28 days of age (3 identical specimens were cured for a specific age).

The autoclave expansion tests were carried out on saturated prisms at 3, 7, and 28 days of age. For the expansion test at each age, e.g., at the age of 3 days, after initial length measurements, a set of 3 concrete prisms were placed in the autoclave (Figure 3.3).

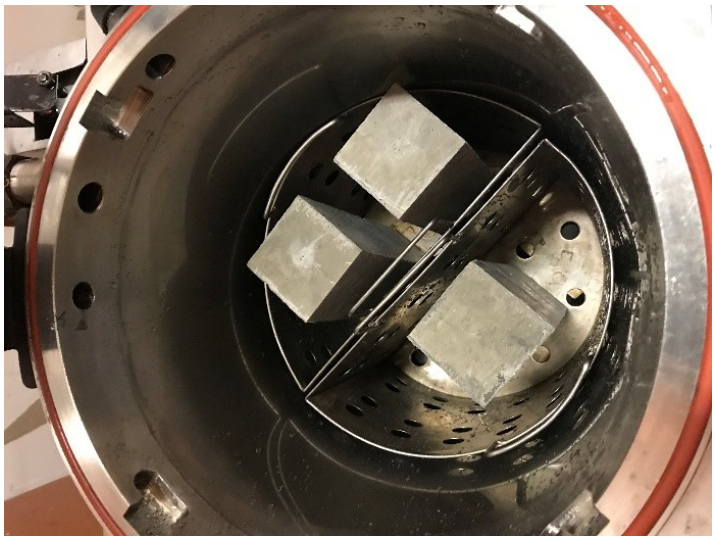

Figure 3. 3 Test specimens in an autoclave

The temperature cycle shown in Figure 3.4 was applied. The maximum temperature and pressure were maintained at 130 °C and 170 kPa, respectively, for 5 hours. The autoclave chamber had sufficient water at the base during the test and the specimens were kept in a saturated vapour environment in the pressurised chamber of the autoclave. When the specimens were cooling down, the relative humidity of the chamber was kept at 100%. The following day, the specimens were removed from the autoclave and the length reading was recorded while the specimens were in a saturated condition. The specimens were then returned to the autoclave and further 2 cycles were applied over the 2

consecutive days. After each cycle, the length readings were recorded. Also, the specimens were examined for cracks. The entire 3 cycles were applied over 3 successive days. The same procedure was repeated for another 2 sets of specimens, commencing at the ages of 7 and 28 days.

The temperature-time relationship and the pressure-time relationship for one cycle of autoclaving are shown in Figure 3.4.

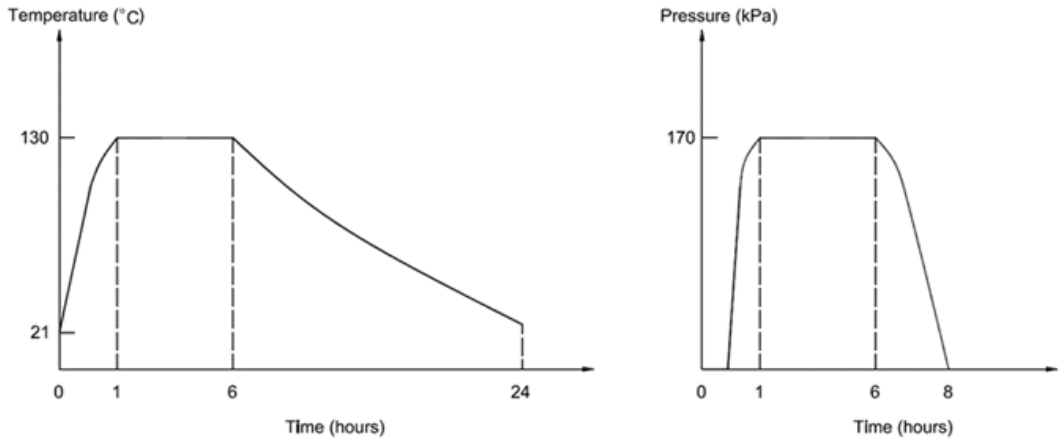

Figure 3. 4 Temperature-time and pressure-time relationships for one cycle of autoclaving

3.2.3 Expansion of Concrete Prisms

Figure 3.5 shows the expansion of concrete prisms cast with reactive aggregate B and boosted to 3% Na_2O_{eq} by mass of cement after autoclave testing at the ages of 3, 7, and 28 days.

The expansion after autoclave testing at the ages of 3, 7, and 28 days for concrete prisms cast with reactive aggregate B and with total alkali content boosted to 5% Na_2O_{eq} by mass of cement, is illustrated in Figure 3.6.

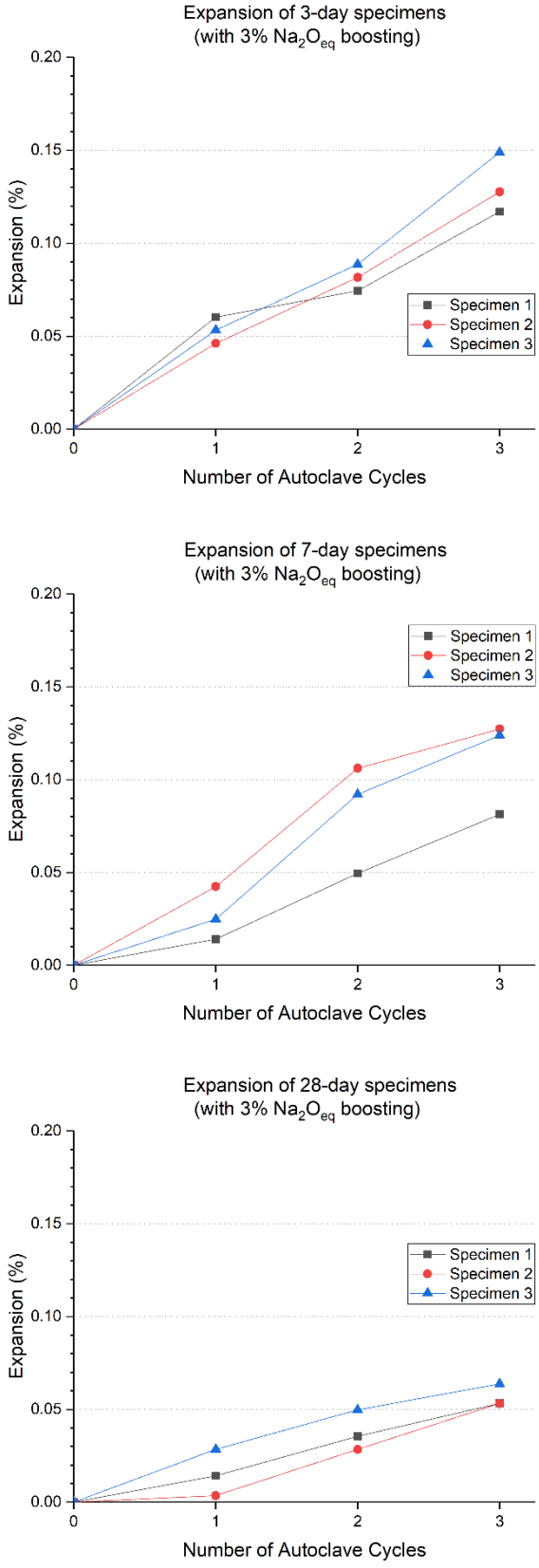

Figure 3. 5 Expansion of reactive aggregate B prisms with 3% Na_2O_{eq} boosting after autoclaving at ages of 3, 7, and 28 days

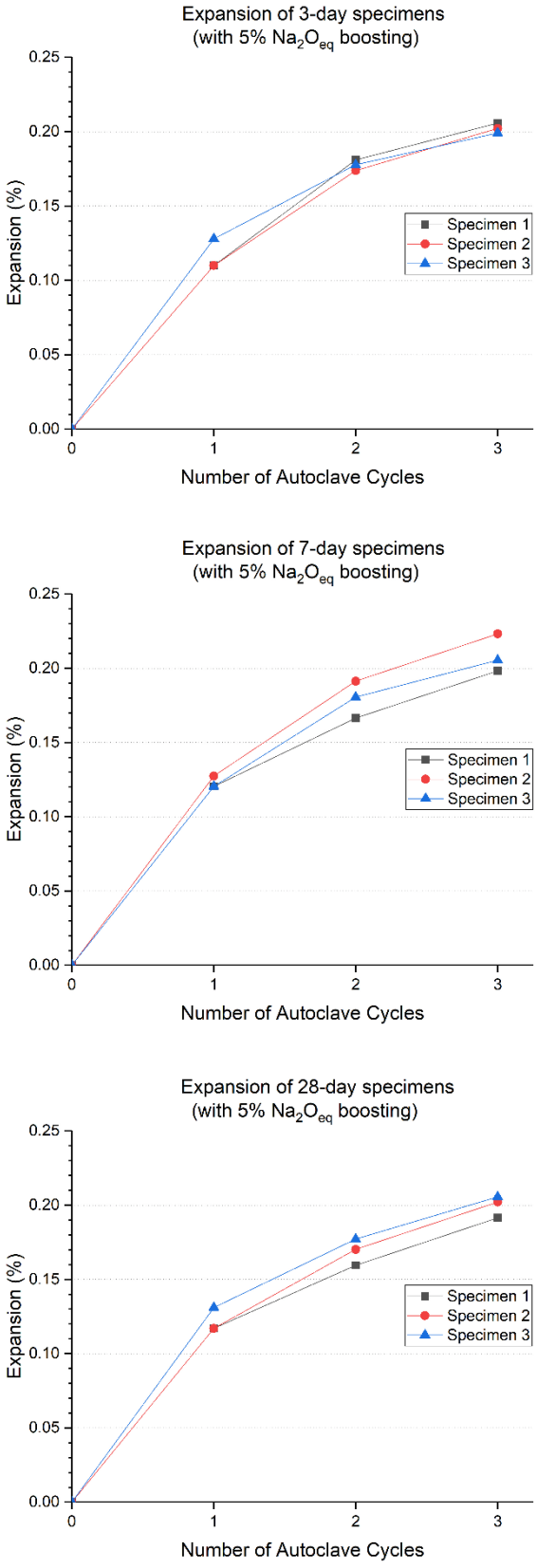

Figure 3. 6 Expansion of reactive aggregate B prisms with 5% Na_2O_{eq} boosting after autoclaving at ages of 3, 7, and 28 days

3.2.4 Testing of Mechanical Properties

Deterioration of concrete mechanical properties due to the combined effect of thermal, pressure, and potential ASR under 130 °C autoclave accelerated testing conditions are investigated. It is worth noting that alkali boosting by the addition of sodium hydroxide can cause substantial reductions in compressive strength and modulus of elasticity.

Smaoui et al. (2005) studied the influence of alkali loading on the mechanical properties of concrete. The authors carried out tests on low-alkali and high-alkali concrete specimens made with non-reactive limestone coarse aggregates and non-reactive granitic sand. The alkali content in the low-alkali concrete mixture was 0.63% Na_2O_{eq} by mass of cement. In the high-alkali concrete mixture, alkali content was boosted to 1.25% Na_2O_{eq} by mass of cement through adding extra NaOH. Mechanical property test results (Table 3.3) had revealed that there is a reduction in compressive strength, tensile strength, and modulus of elasticity for high-alkali concrete. As can be seen from Table 3.3, at the age of 28 days, the reduction in compressive strength, tensile strength, and modulus of elasticity for high-alkali concrete reach 16.6%, 13.4%, and 9.4% with regards to the low-alkali concrete, respectively. The authors interpreted that the reduction in strength and stiffness was due to the higher porosity of the concrete caused by high alkali loading. This indicates that increasing the alkali content in the concrete mixture can cause a significant reduction in compressive strength, tensile strength, and modulus of elasticity, although the aging of concrete in high-alkali concrete, increases the compressive strength, tensile strength, and modulus of elasticity considerably.

When alkali content is boosted to a 3% level, there will be a more significant reduction in the mechanical properties of the concrete. Details can be found in Chapter 4.4.6 of Chapter 4.

Table 3. 3 Comparison of mechanical properties between low-alkali and high-alkali concrete (Smaoui et al. 2005)

Mechanical property	Age (days)	(1) Low-alkali concrete (0.63% Na_2O_{eq})	(2) High-alkali concrete (1.25% Na_2O_{eq})	((2) - (1)) / (1) (%)
Compressive strength (MPa)	3	42.6	31.4	-26.3
	7	43.6	34.9	-20.0
	28	49.9	41.6	-16.6
	90	57.4	46.8	-18.5
	180	58.5	51.7	-11.6
Direct tensile strength (MPa)	3	2.82	2.28	-19.1
	7	2.93	2.63	-10.2
	28	3.14	2.72	-13.4
	90	3.33	3.10	-6.9
	180	4.12	3.49	-15.3
Modulus of elasticity (GPa)	3	35.6	33.8	-5.1
	7	39.7	35.3	-11.1
	28	39.4	35.7	-9.4
	90	38.8	41.0	--
	180	39.9	38.7	-3.0

Hence, to eliminate the influence of alkali loading on the mechanical properties of the tested specimens, investigation of mechanical properties degradation under 130 °C autoclave condition focuses on specimens without alkali boosting (see Table 3.2 Concrete mix proportions). Concrete cylinders (100 mm dia. × 200 mm) and prisms (100 × 100 × 340 mm) of actual concrete mixes (Grade 40 concrete) are cast. The specimens are made with reactive aggregate B or least reactive aggregate C. The maximum aggregate size is 20 mm. Specimens are subjected to 130 °C autoclave conditions after 28 days of water curing at 23 ± 2 °C. After autoclaving, compressive strength tests for cylinders and

flexural strength tests for the prisms are conducted. Below tests are also conducted on specimens after 28 days of water curing:

- Compressive strength tests on 28-day cylinders, following AS 1012.9;
- Flexural strength tests on 28-day prisms, as per AS 1012.11.

Cylinders made with non-reactive coarse aggregates are also tested for compressive strength and modulus of elasticity, after 90 days of water curing at 23 ± 2 °C and subsequent 130 °C autoclave conditioning.

- Modulus of elasticity tests on 90-day non-reactive cylinders, as per AS 1012.17.

  Modulus of elasticity tests are carried out at the age of 90 days of water curing for non-reactive aggregate concrete cylinders. At the age of 90 days, 6 specimens are placed in Zirbus LVSA 50/70 autoclave (see Figure 3.7) to study the combined effect of thermal and pressure on the mechanical properties of the concrete. After each cycle of autoclaving, two cylinders are taken out of the autoclave then modulus of elasticity tests are conducted.

- Compressive strength tests on 90-day non-reactive cylinders

  Compressive strength tests are conducted at the age of 3, 7, 28, and 90 days of water curing. At the age of 90 days, 6 specimens are put in the autoclave (see Figure 3.7). After each cycle of autoclaving, two specimens are taken out of the autoclave then modulus of elasticity tests are performed first and followed by the compressive strength tests.

Figure 3. 7 Non-reactive concrete cylinders (90-day) in Zirbus LVSA 50/70 autoclave

3.3 Results and Discussion

3.3.1 Expansion and cracking of specimens

Significant expansions were observed at all ages (see Figure 3.8). For concrete prisms cast with aggregate B and boosted to 3% Na_2O_{eq} by mass of cement, average expansion of 3-day specimens (after 3 cycles of autoclaving) reached 0.131%. The average expansion of 7-day specimens was 0.111% and the average expansion of 28-day specimens showed the smallest expansion of 0.057%. This is mainly due to the strength development of the concrete with age. However, for concrete prisms boosted to 5% Na_2O_{eq} by mass of cement after 3 cycles of autoclaving at ages of 3, 7 and 28 days, average expansions of the specimens were 0.2%, 0.209% and 0.2%, respectively. As can be seen that with alkali boosting to 5% Na_2O_{eq} by mass of cement, specimens of 3, 7 and 28 days showed similar levels of significant expansion. Besides, the expansion in concrete caused by ASR increases with the increase of Na_2O_{eq}, regardless of the age of concrete.

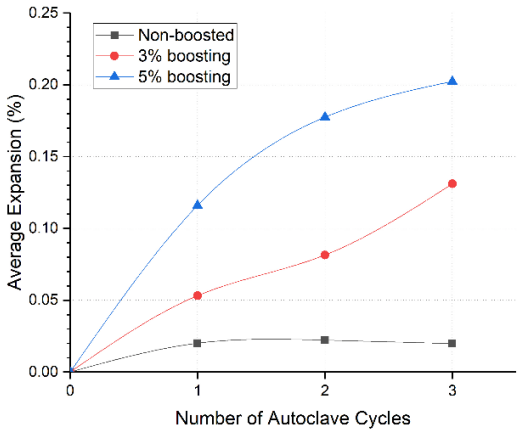

(a) Average expansion at the age of 3 days

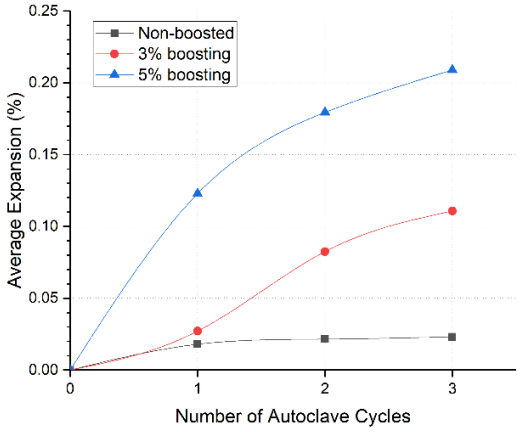

(b) Average expansion at the age of 7 days

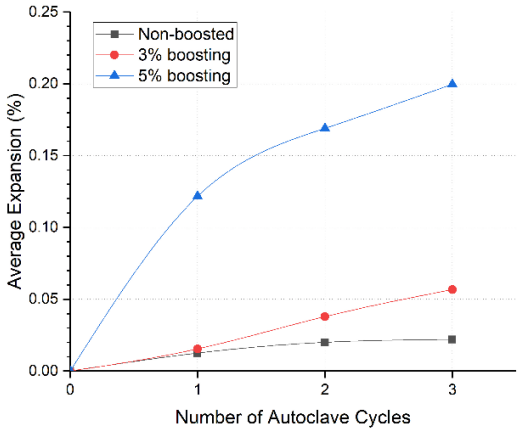

(c) Average expansion at the age of 28 days

Figure 3. 8 Average expansion (of 3 specimens made with aggregate B) at the ages of 3, 7 and 28 days

For concrete made with both aggregates B and C, without additional alkali boosting, the expansion of the specimens (after 3 cycles of autoclaving) was very small, varying from 0.02% to 0.03%. Hence un-boosted concrete specimens may not show sufficient levels of expansion with only 3 cycles of autoclaving. Therefore, it is not possible to test and compare non-boosted concrete specimens under 3 cycles of ultra-accelerated autoclave test conditions. The effect of more numbers of cycles on the expansion of the specimens needs further investigation.

The crack patterns of prisms made of aggregate B, with 3% Na_2O_{eq} boosting (after 3 cycles of autoclaving) at the ages of 3, 7, and 28 days are shown in Figure 3.9. Similar map cracking patterns were observed for prisms with 5% Na_2O_{eq} boosting.

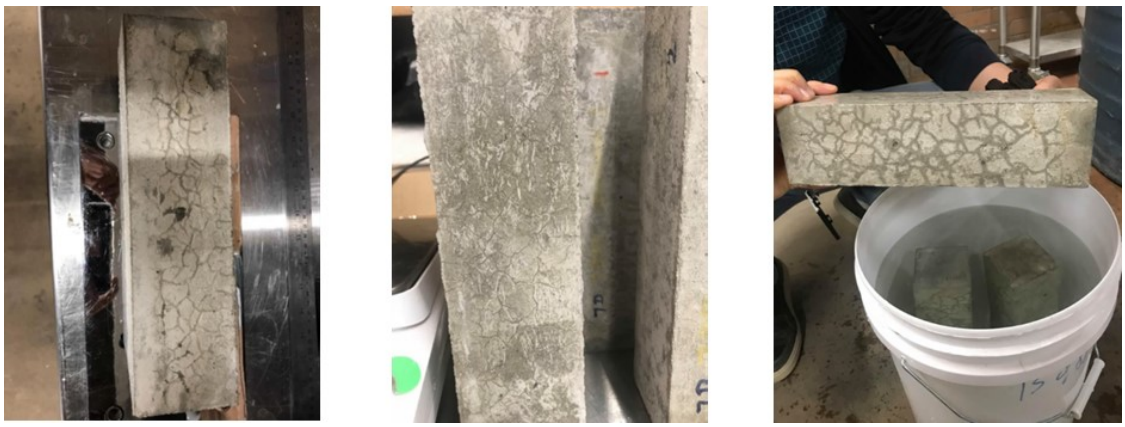

Figure 3. 9 Crack patterns of reactive aggregate B prisms with 3% Na_2O_{eq} boosting after 3 cycles of autoclaving at ages of 3, 7, and 28 days

3.3.2 Compressive Strength Testing Results

The compressive strength of non-autoclaved and autoclaved specimens without alkali boosting is compared in Figures 3.10.

By comparing the compressive strength results, it can be seen that there is a significant reduction between 30% and 35% for both mixes with aggregate B and mixes with aggregate C after 1 to 3 cycles of autoclaving. Ultra-accelerated autoclave test at 130 °C

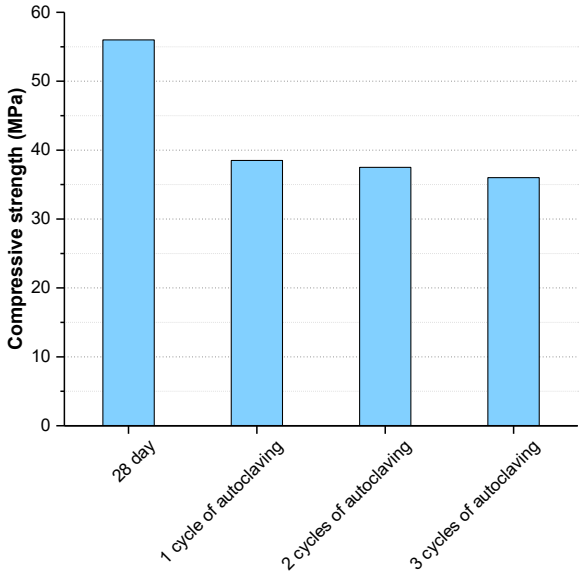

(a) Aggregate B cylinders

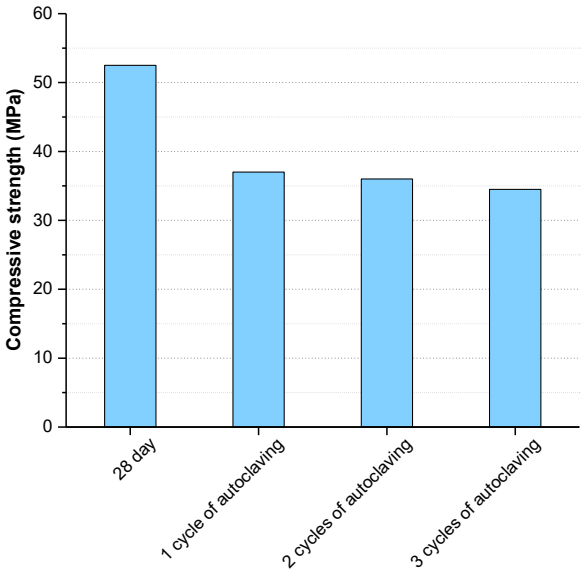

(b) Aggregate C cylinders

Figure 3. 10 Compressive strength of 28-day value and after 1, 2, 3 cycles of 130 °C autoclaving

and 170kPa can provide damage levels similar to field exposure over 20 years within a very short period of seven days. Hence, this method will provide a useful accelerated testing regime for simulating ASR damage.

3.3.3 Flexural Strength Testing Results

The flexural strength of non-autoclaved and autoclaved specimens without alkali boosting is compared in Figures 3.11.

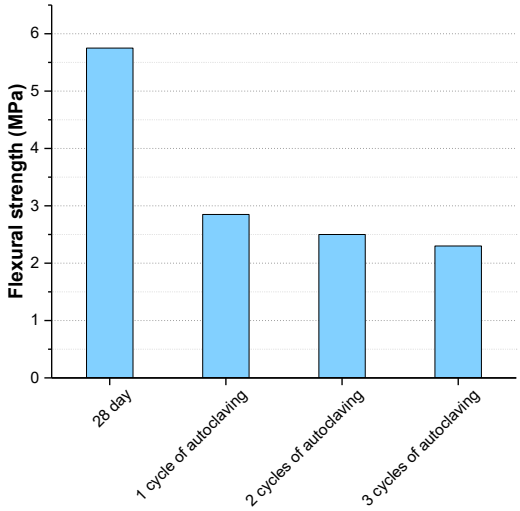

(a) Aggregate B prisms

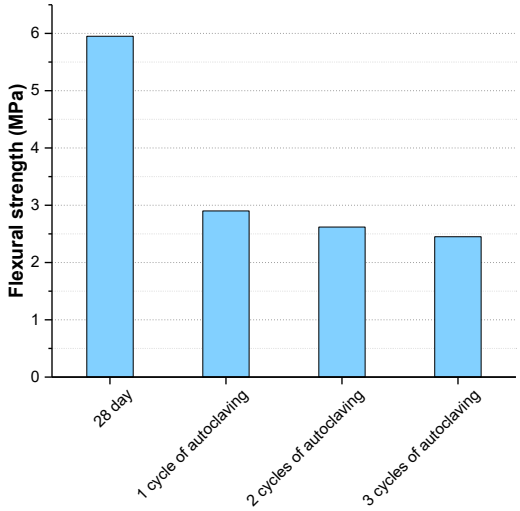

(b) Aggregate C prisms

Figure 3. 11 Flexural strength of 28-day value and after 1, 2, 3 cycles of 130 °C autoclaving

By comparing the flexural strength results, it can be seen the percentage of reductions is considerably more than the compressive strength reductions. The flexural strength

reductions after 1 to 3 cycles of autoclaving reached 50% to 60% compared to the 28-day value. These results are in line with long-term reductions reported in Table 2.2. Hence, ultra-accelerated method using autoclave can provide a tool to study long-term mechanical reduction due to ASR in actual structures.

3.3.4 Modulus of Elasticity Test on 90-day Non-reactive Cylinders

Table 3.4 summarised the modulus of elasticity test results on 90-day non-reactive cylinders and the modulus of elasticity after subsequent 1, 2, 3 cycles of 130 °C autoclaving. Calculation of modulus of elasticity is based on the secant modulus averaged from the second and third cycles of the load test.

Table 3. 4 Modulus of elasticity of 90-day non-reactive cylinders

Conditioning	Modulus of elasticity (GPa)	Reduction (%)
After 90 days of water curing	40.7	--
After 1 cycle of autoclaving	34.4	15.5
After 2 cycles of autoclaving	30.9	24.1
After 3 cycles of autoclaving	29.4	27.8

Figure 3.12 shows the combined effect of temperature and pressure of 1,2,3 cycles of autoclaving on the modulus of elasticity in comparison with the modulus of elasticity at the age of 90 days without autoclaving. After 1 cycle of 130 °C autoclaving, the reduction on modulus of elasticity of the 90-day non-reactive cylinders is 15.5%. After 2 and 3 cycles of 130 °C autoclaving, the reduction of modulus of elasticity reached 24.1% and 27.8%, respectively. This implies that, for non-reactive specimens, 1, 2, 3 cycles of 130 °C autoclaving can cause a significant reduction in stiffness of concrete due to the high autoclave temperature and autoclave pressure.

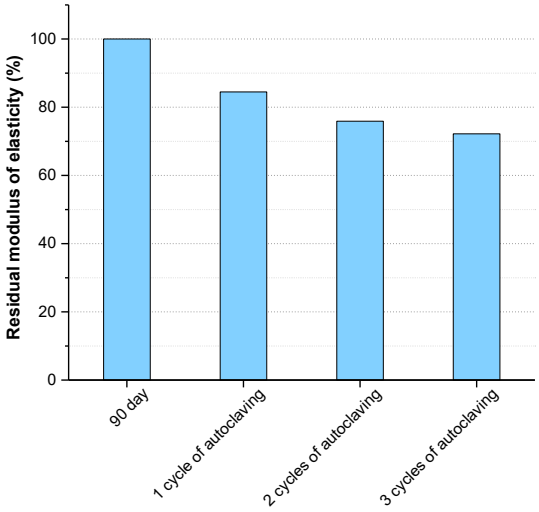

Figure 3. 12 Residual modulus of elasticity compared to the 90-day value after 1, 2, 3 cycles of 130 °C autoclaving

3.3.5 Compressive Strength Test on 90-day Non-reactive Cylinders

Figure 3.13 illustrates the compressive strength of non-reactive cylinders tested at the age of 90 days and followed by 1, 2, 3 cycles of 130 °C autoclaving.

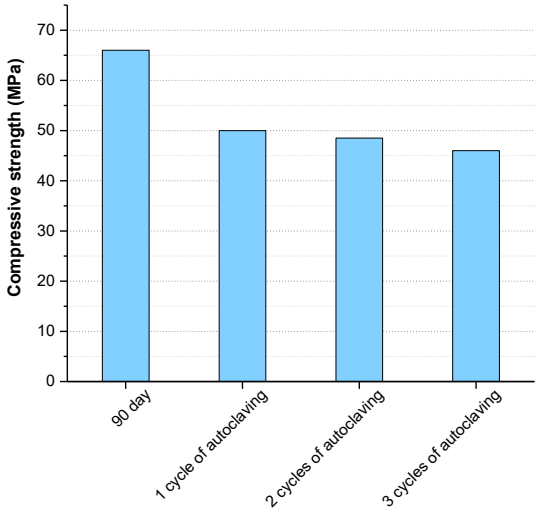

Figure 3. 13 Compressive strength of non-reactive concrete cylinders tested at the age of 90 days and after 1, 2, 3 cycles of 130 °C autoclaving

Figure 3.13 clearly shows that the compressive strength of the non-reactive specimens decreased significantly after 130 °C autoclaving. The reduction of compressive strength

after 1, 2, 3 cycles of autoclaving reached 24.0%, 26.5%, and 30.3%, respectively, compared with the 90-day value before autoclaving. This again indicates that, for non-reactive specimens, 1, 2, 3 cycles of 130 °C autoclaving can have a significant detrimental effect on the strength of the specimens due to the high autoclave temperature and autoclave pressure.

3.3.6 SEM Observation of 90-day Non-reactive Cylinders after Autoclaving

Microscopic observations on samples of autoclaved specimens under scanning electron microscope (SEM) are performed. Figure 3.14(a) shows the microcracking observed in paste of 90-day cylinder subjected to 1 cycle of 130 °C autoclaving with pressure of 170kPa. Figure 3.14(b) demonstrates the microcracking in the paste and around an aggregate. The specimen was exposed to 3 cycles of 130 °C autoclaving with a pressure of 170kPa. These microcracking are reckoned responsible for the reductions in modulus of elasticity and compressive strength of the concrete subjected to 130 °C autoclaving. Other mechanisms may also contribute to the reductions in mechanical properties due to 130 °C autoclaving with a pressure of 170kPa, such as changing of hydration products, alteration of porosity or pore structure. These mechanisms need further investigation.

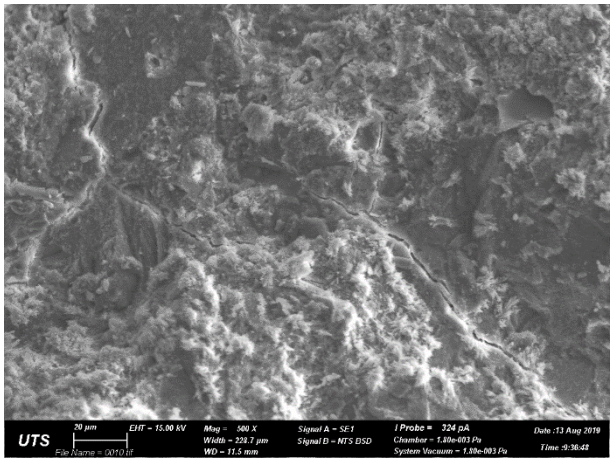

(a) After 1 cycle of autoclaving at 130 °C and 170kPa

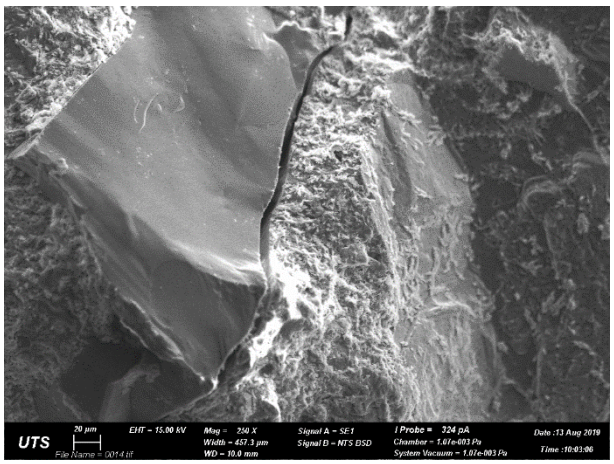

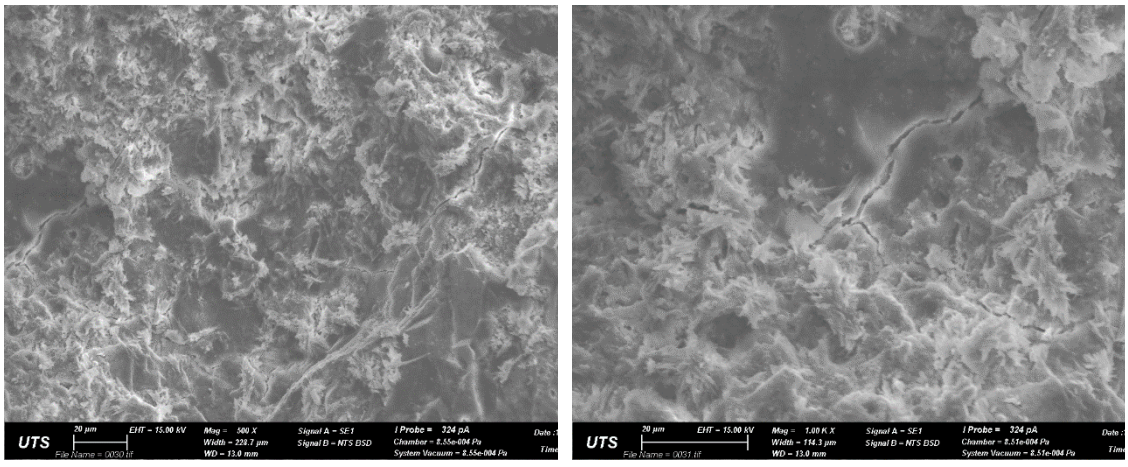

(b) After 3 cycles of autoclaving at 130 °C and 170kPa

Figure 3. 14 Microscopic observation on samples of autoclaved specimens by SEM

3.4 Summary

The ultra-accelerated autoclave test, on prisms of actual concrete mixes with appropriate alkali boosting, is able to simulate expansion and cracking caused by ASR within a short period of time.

With appropriate alkali boosting, the 130 °C autoclave test method could be used for screening the potential ASR of aggregates within a short period of time. It can also cause damage to the concrete and reductions in concrete mechanical properties in a short period of time which could be utilised to simulate long-term deterioration of concrete.

The multi-cycle 130 °C autoclave test method appears to be suitable for simulating damage of concrete and for investigating the subsequent consequences on load capacity of the damaged reinforced concrete members.

However, the correlation between the reduction of mechanical properties of concrete under multi-cycle 130 °C autoclave conditions and deterioration of concrete caused by long-term ASR expansion needs further investigation.

In order to simulate deterioration due to ASR and to study the reinforced concrete elements, a new autoclave test method is investigated to reliably reflect the performance of concrete affected by ASR. In the following chapter, the development of an innovative autoclave test method for identifying the potential reactivity of aggregates and also as a reliable performance test that can be used to determine the risk of ASR expansion is introduced.

Chapter 4

Novel Accelerated Test Method for ASR by Using an Autoclave

4.1 Overview

Alkali-silica reaction (ASR) is one of the most harmful long-term distresses for reinforced concrete structures as observed worldwide (Rajabipour et al. 2015). This chemical reaction between certain forms of reactive siliceous minerals in aggregates and alkali hydroxides in the pore solution, produces an alkali-silica gel that swells by imbibing water from the surrounding environment. This swelling causes expansion and cracking of the concrete, leading to a reduction in mechanical properties, and ultimately resulting in the lower durability and performance of the affected structure (Ulm et al. 2000). Deleterious ASR in hardened concrete occurs under the following conditions. Aggregates need to have a certain amount of reactive siliceous minerals; sufficient alkalis should exist in concrete pore solution; adequate moisture and calcium ions should be available (Thomas 2018). It can take 10-15 years for ASR damage to be developed in structures (Fernandes, Noronha & Teles 2004; Miyagawa et al. 2006; Torii et al. 2008). Hence, in order to ensure that the aggregate is suitable for concrete, it is required to be assessed for its ASR potential, prior to being used in the concrete mix.

For assessing the reactivity of aggregates, currently, there are four accelerated laboratory test methods available, namely, accelerated mortar bar test (AMBT), concrete prism test (CPT), accelerated concrete prism test (ACPT), and ultra-accelerated autoclave test. The potential reactivity of the aggregates can be identified within a few days if the autoclave test is used whereas the duration of CPT can be up to one year. The standard AMBT, such as AS 1141.60.1, ASTM C1260 and RILEM AAR-2, involves crushing of the aggregate to specific grading and immersion of NaOH solution at 80 °C. Although AMBT can

provide results within 21 days, both false positive and false negative results had been reported (Lu et al. 2008; Thomas et al. 2006). By examining the accuracy of different test methods, Sirivivatnanon, Mohammadi & South (2016) concluded that the improved AS 1141.60.1 is a relatively reliable accelerated test method in screening 'reactive' and 'slowly reactive' aggregates, while ASTM C1260 was found to be more reliable in classifying the non-reactive aggregates. With evidence from field performance, CPT test is currently recognised as the most reliable test method for identifying the reactivity of aggregates and the most reliable performance test for assessing the potential risk of ASR in concrete (Sirivivatnanon, Mohammadi & South 2016). The long test duration of CPT, which takes one year for ordinary Portland cement (OPC) concrete mixes and two years for mixes with Supplementary Cementitious Materials (SCMs) for mitigation purposes, however, limits its application in practice. In addition, mixes used in real structures often have mix proportions different to the specific aggregate grading, cement contents and water-to-cement ratio as specified in AS 1141.60.2, ASTM C1293, or RILEM AAR-3, and hence the standard CPT also has its limitations. ACPT refers to accelerating the CPT by increasing the testing temperature from 38 °C to 60 °C (Kawabata et al. 2018; Latifee & Rangaraju 2015; Yamada et al. 2014). Among the ACPT methods, RILEM AAR-4.1 recommends a test duration of at least 20 weeks. In addition, alkali leaching in ACPT is of concern (Lindgård et al. 2013). In ultra-accelerated autoclave tests carried out to date, the mixes were boosted with alkalis between 1.5 to 4.0% by mass of cement, and maximum temperatures used by different researchers varied between 100 °C and 150 °C. For mortar bars, duration of autoclaving was 2 to 6 hours, while for concrete prisms, duration of the autoclaving was between 4 to 24 hours (Giannini & Folliard 2013; Nishibayashi et al. 1996; Nishibayashi, Yamura & Matsushita 1987; Tamura 1987; Tang, Han & Zhen 1983; Wood et al. 2018). However, in spite of extensive research on ASR

over a period of approximately 80 years, there is still a need for a reliable and rapid test method for testing the reactivity of aggregates. Also, there is a need for a reliable performance test method that can rapidly assess the potential risk of ASR (Thomas 2018).

For the purpose of rapidly testing concrete mixes as used in the field and for studying reinforced concrete elements by accelerating ASR within a short period of time, an ultra-accelerated test method is needed. This chapter introduces the development of a novel accelerated autoclave test method for assessing the potential risk of ASR. In the first phase, experiments are conducted on mortar specimens to accelerate ASR within a short period of time by using an autoclave to investigate the influence of different temperatures, duration/cycles and different alkali dosage on expansion. The experimental program and test results are introduced in Chapter 4.2 and Chapter 4.3. In the second phase, the novel accelerated test method is applied to concrete specimens. Expansion of concrete prisms, external and internal cracking are recorded. Microscopic observation including scanning electron microscope (SEM) and confocal laser scanning microscope confirmed that the expansion occurs in the accelerated test is caused by ASR. Tests on the mechanical properties of concrete specimens under the accelerated ASR test method are conducted. Details are provided in Chapter 4.4. Main findings are presented in Chapter 4.5.

4.2 Phase I Experimental Program – Mortar Specimens

4.2.1 Materials and Mix Proportions

A general-purpose Portland cement with an alkali content of 0.50% Na_2O_{eq} was used in the mixing as binder material. The chemical composition of the general-purpose Portland cement was examined by X-ray florescence and is provided in Table 4.1. Equivalent alkali content (Na_2O_{eq}) of cement was calculated as $Na_2O+0.658*K_2O$. In addition, a technical grade sodium hydroxide (NaOH) pellets with a purity of 98% were added into the mixing

water and pre-dissolved in a fraction of the mixing water before mixing, to adjust the alkali contents (Na_2O_{eq} by mass of cement) in the mortar.

Table 4. 1 Chemical composition of general-purpose Portland cement (wt.%)

	CaO	SiO_2	Al_2O_3	Fe_2O_3	SO_3	MgO	K_2O	N_2O	LOI	Na_2O_{eq}
Cement	64.18	19.67	4.78	3.10	2.37	0.91	0.41	0.23	4.09	0.50

Two types of aggregates were used in this study, one is the highly reactive aggregate, namely dacite aggregate, and another is the non-reactive aggregate as a reference to demonstrate the efficacy of the proposed accelerated test method. The dacite aggregate is crushed from the dacite coarse aggregate and the non-reactive aggregate is crushed from the non-reactive coarse aggregates. Both two types of crushed aggregates have the same grading as shown in Figure 4.1. The chemical compositions of the reactive dacite aggregate and non-reactive aggregate are presented in Table 4.2. It is worth to mention that, for reference specimens, crushed non-reactive aggregates and general-purpose Portland cement were used in the mix proportion, while for reactive specimens, crushed reactive dacite aggregate and general-purpose Portland cement were adopted.

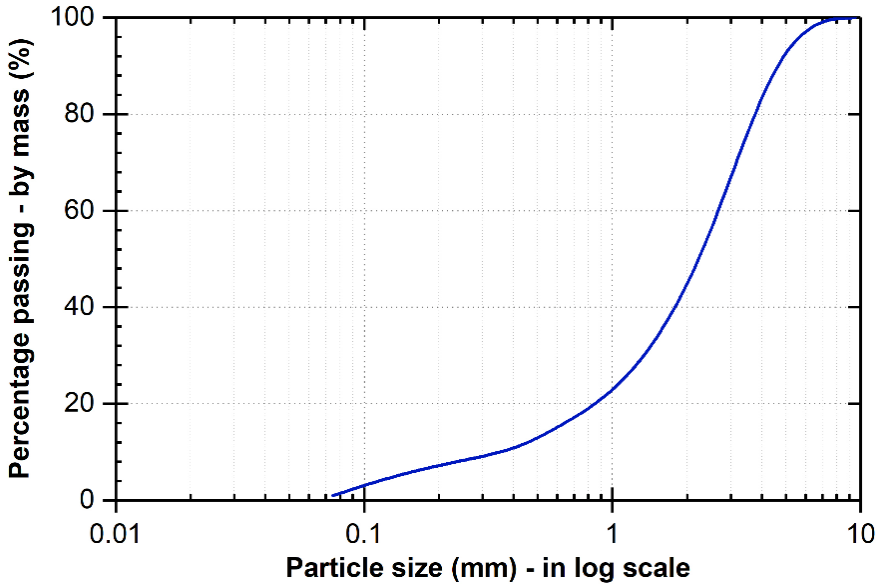

Figure 4. 1 Grading curve of crushed aggregates

Table 4. 2 Chemical composition of the aggregates (wt. %)

Aggregate	CaO	SiO_2	Al_2O_3	Fe_2O_3	MgO	TiO_2	Na_2O	K_2O	LOI
Dacite aggregate	2.35	68.38	13.25	3.32	1.30	0.36	2.41	3.84	4.52
Non-reactive aggregate	9.04	43.22	14.47	12.15	8.97	2.98	4.01	1.81	1.34

The mix proportions for preparing mortar specimens adopted in this study is one part of cement to 2.25 parts of dacite aggregates or non-reactive aggregates with the maximum particle size 4.75 mm. the water-to-cement ratio is 0.4, instead of 0.47 as stated in the AS 1141.60.1. Also, in order to boost the alkali content in the mortar specimens, sodium hydroxide (NaOH) pellets were added to the mixing water 24 hours prior to the mixing to increase the alkalis of different mortar specimens to 2.5%, 3.0% and 3.5% Na_2O_{eq} by mass of cement.

4.2.2 Specimen Fabrication and Steam Warming Procedure

The mortar mixing procedure follows ASTM C305, that is: place all the mixing water in the bowl of Hobart mixer; add cement then mix at a slow speed for 30s; add dacite aggregates or non-reactive aggregates and mix at slow speed for 30s; shift to medium speed and mix for 30s; stop the Hobart mixer for 90s; then finally finish mixing using medium speed for 60s.

After casting, the mortar specimens (25 × 25 × 285 mm) with embedded stainless studs at two ends were kept in a 23 °C 90%RH temperature-humidity controlled cabinet for 24 hours then demoulded, and the initial measurements (length and mass) were conducted. The initial length of the mortar bars was measured by a digital comparator. The specimens were then cured in 23 °C 90%RH temperature-humidity controlled cabinet for another 24 hours, thereafter, the specimens were taken out and put into the autoclave for steam warming.

In order to accelerate ASR, a testing regime of 3 cycles at a specific temperature was adopted. To study the influence of different temperatures on the expansion of mortar bars, two temperature conditions, 70 °C and 80 °C, were applied. Each cycle of steam warming duration is 60 hours and totally three cycles of steam warming were applied. The pressure inside the autoclave chamber is kept at atmospheric pressure. Figure 4.2(a) shows the temperature-time relationship of steam warming for three cycles. Figure 4.2(b) shows the characteristic temperature and corresponding absolute pressure in the autoclave chamber when 80 °C steam warming is applied. The temperature in the autoclave chamber is heated up to 80 °C in less than 10 minutes. The temperature quickly stabilizes at 80°C with minor variations and the pressure is maintained at 1000mbar. This is achieved by the independent steam pot of the autoclave injecting steam into the chamber automatically and controlling the temperature while keeping the chamber in a fully saturated condition during the entire test period. At the end of each cycle, the expansion of the mortar bars, due to the accelerated ASR were recorded and the next cycle was applied.

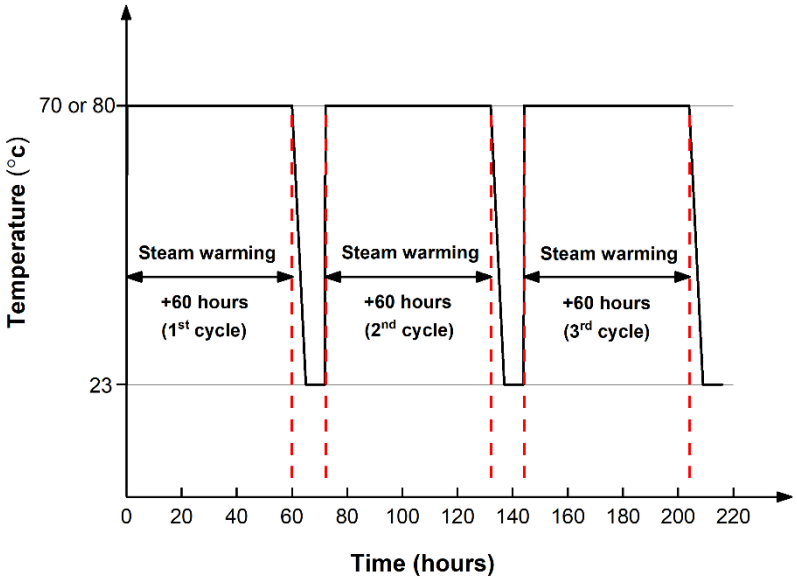

(a). Time-temperature cycles adopted for conditioning the specimens

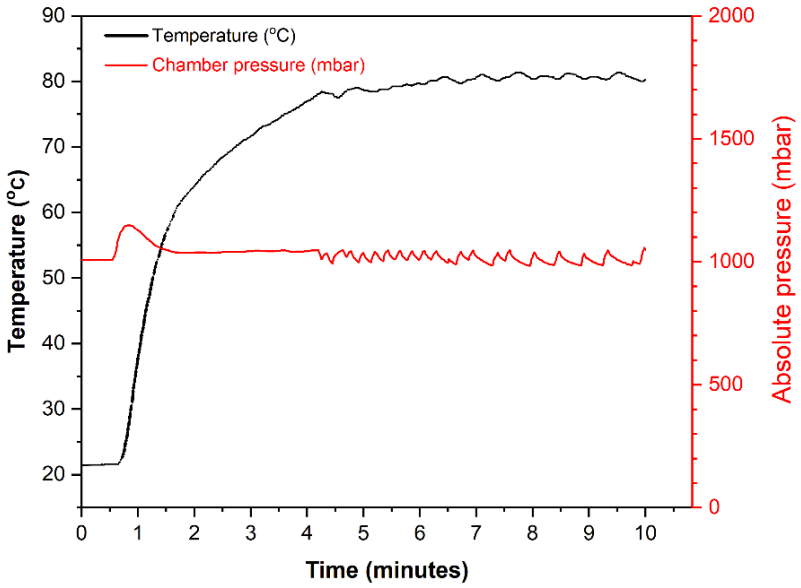

(b). Characteristic temperature and absolute pressure in autoclave chamber with 80°C steam warming (at the beginning of each cycle)

Figure 4. 2 Temperature and pressure in the autoclave chamber adopted for the multi-cycle accelerated test

4.2.3 Expansion Measurements

Initial lengths of the mortar bars were measured and recorded using a digital comparator after demoulding. After each cycle of steam warming in an autoclave, the specimens were

taken out of the autoclave and cooled down to room temperature at 23 ± 2 °C then the lengths of the specimens were measured and recorded again using the digital comparator. Changes in length were used to calculate the expansion of the specimens after 1, 2, and 3 cycles of autoclave steam warming.

4.3 Results and Discussion for Phase I Experiments

4.3.1 Expansion of Mortar Bars

Expansion of the mortar bars from the time of demoulding and after 3 cycles of autoclave steam warming is shown in Figure 4.3. Three replicate specimens for each alkali loading were tested. Each data point is the average expansion of three specimens. After 3 cycles of 70 °C steam warming in the autoclave, a total expansion of about 0.24% was recorded. After 3 cycles of 80 °C steam warming, total expansion reached 0.35% to 0.39%. In addition, it was observed that expansion increased with the increase of steam warming duration/cycles. However, this parameter has no effect on non-reactive aggregate specimens. The influence of alkali content and the influence of steam warming temperature will be discussed in the following sections.

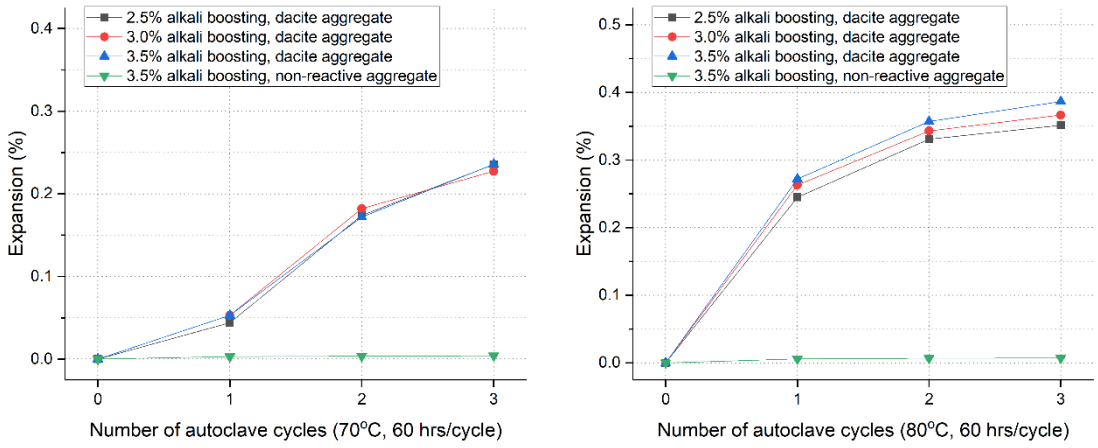

(a) 70 °C (b) 80 °C

Figure 4. 3 Expansion of specimens after steam warming in an autoclave

4.3.2 Influence of Total Alkali Content (2.5%, 3.0%, 3.5%)

At 80 °C steam warming cycles, the expansion of reactive dacite aggregate mortar bars increased with the increase of total alkali content from 2.5% to 3.5% Na_2O_{eq} (see Figure 4.4). However, at 70 °C autoclave steam warming cycles, this trend is not significant (see Figure 4.3(a)). For non-reactive aggregate mortar bars, the increasing of the total alkali content, from 2.5% to 3.5% Na_2O_{eq}, has no effect on the expansion of the specimens.

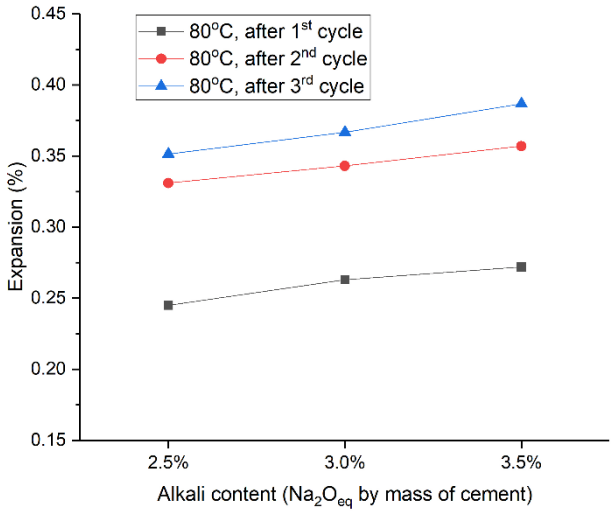

Figure 4. 4 Expansion – Alkali content relationship (80 °C autoclave steam warming)

By performing autoclave test for ASR using a large cooking pressure pot at 100 °C to 130°C, Nishibayashi, Yamura & Matsushita (1987) reported that expansion of specimens increased with increasing of total alkali content of the mixes when alkali content was over 1.0% Na_2O_{eq} and decreased when alkali content was higher than 3.0% Na_2O_{eq}. The maximum expansion occurred when alkali content was about 2.5% Na_2O_{eq}. However, the authors suggested a total alkali content of 1.5% Na_2O_{eq} in the proposed test procedure. Through chemical analysis, the authors also confirmed that the reaction products were same as that from the normal accelerated test at 38 °C and 100% RH. Fournier, Bérubé & Bergeron (1991), however, observed that expansion of reactive specimens was significantly improved when the alkali content was raised from 2.5% Na_2O_{eq} to 3.5%

Na_2O_{eq}, but this parameter had no effect on the behaviour of non-reactive aggregates. The authors proposed a rapid autoclave mortar bar test method with 3.5% Na_2O_{eq} alkali loading. Wood et al. (2018) investigated the influence of alkali loading on the expansion of mortar bars subjected to a 130 °C autoclaving temperature and a 5 hours autoclaving duration. The authors reported that 2.5% Na_2O_{eq} alkali loading failed to distinguish the potential reactivity between non-reactive and reactive aggregates, while increasing the alkali content from 3.5% to 4.5% had minimal effect for promoting expansion of mortar bars. Therefore, Wood et al. (2018) recommended a 3.5% Na_2O_{eq} alkali loading for autoclave mortar bar test..

4.3.3 Influence of Temperature on Expansion (70 °C and 80 °C)

The influence of steam warming temperature (70 °C and 80 °C) on expansion of mortar bars is studied. For reactive dacite aggregate specimens after 3 cycles of autoclaving, when the steam warming temperature in the autoclave was increased from 70 °C to 80°C, it was observed that the average expansion of mortar bars was improved by a factor of 1.49, 1.61 and 1.64 for mixes with 2.5%, 3.0% and 3.5% alkali content, respectively. Hence, temperature increase from 70 °C to 80 °C can significantly accelerate the ASR for reactive aggregates. This suggests that steam warming temperature at 80 °C is more efficient than testing at 70 °C for rapid ASR testing by using an autoclave. Nishibayashi, Yamura & Matsushita (1987) performed autoclave testing at higher temperature and observed that, higher autoclaving temperature under pressures can produce larger expansion for mortar bars than steam curing under atmospheric conditions (100 °C); and the expansion under steam curing condition was higher than that in boiling water.

4.3.4 Microscopic Observation for Assessment of ASR

Petrographic examination under the SEM on samples from mortar bars subjected to 3 cycles of 80 °C steam warming in an autoclave is conducted. ASR gel is Ca-Alkali(Na,K)-Si-H_2O in general. As H_2O is unable to be detected by scanning electron microscope and energy dispersive spectrometry (SEM-EDS), Ca, Na, K and Si are the indicators that ASR gel is present (Gavrilenko et al. 2007; Godart, de Rooij & Wood 2013; Leemann et al. 2011; Thaulow, Jakobsen & Clark 1996). Figure 4.5 shows the ASR gel formation in cracking through an aggregate, after 3 cycles in the autoclave. Gel lining pore of cement paste was also observed. Figure 4.6 shows gel lining a pore of the cement paste and presenting sponge-like surface microtexture. ASR gel around aggregate was observed as well. Figure 4.7 demonstrates ASR gel at aggregate-cement paste interface.

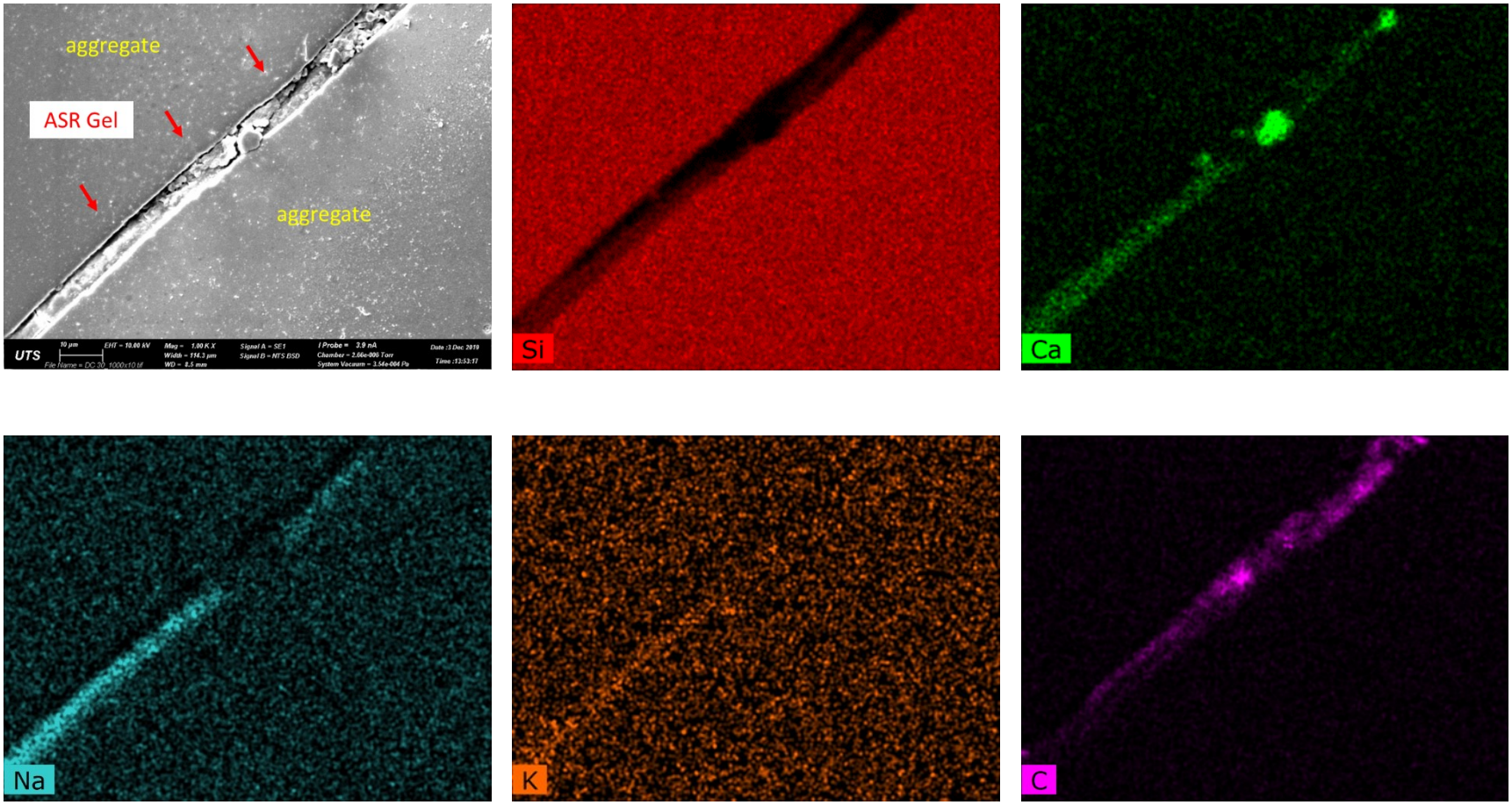

Figure 4. 5 SEM-EDS map of ASR gel within an aggregate

(Notable presence of carbon, can be from resin)

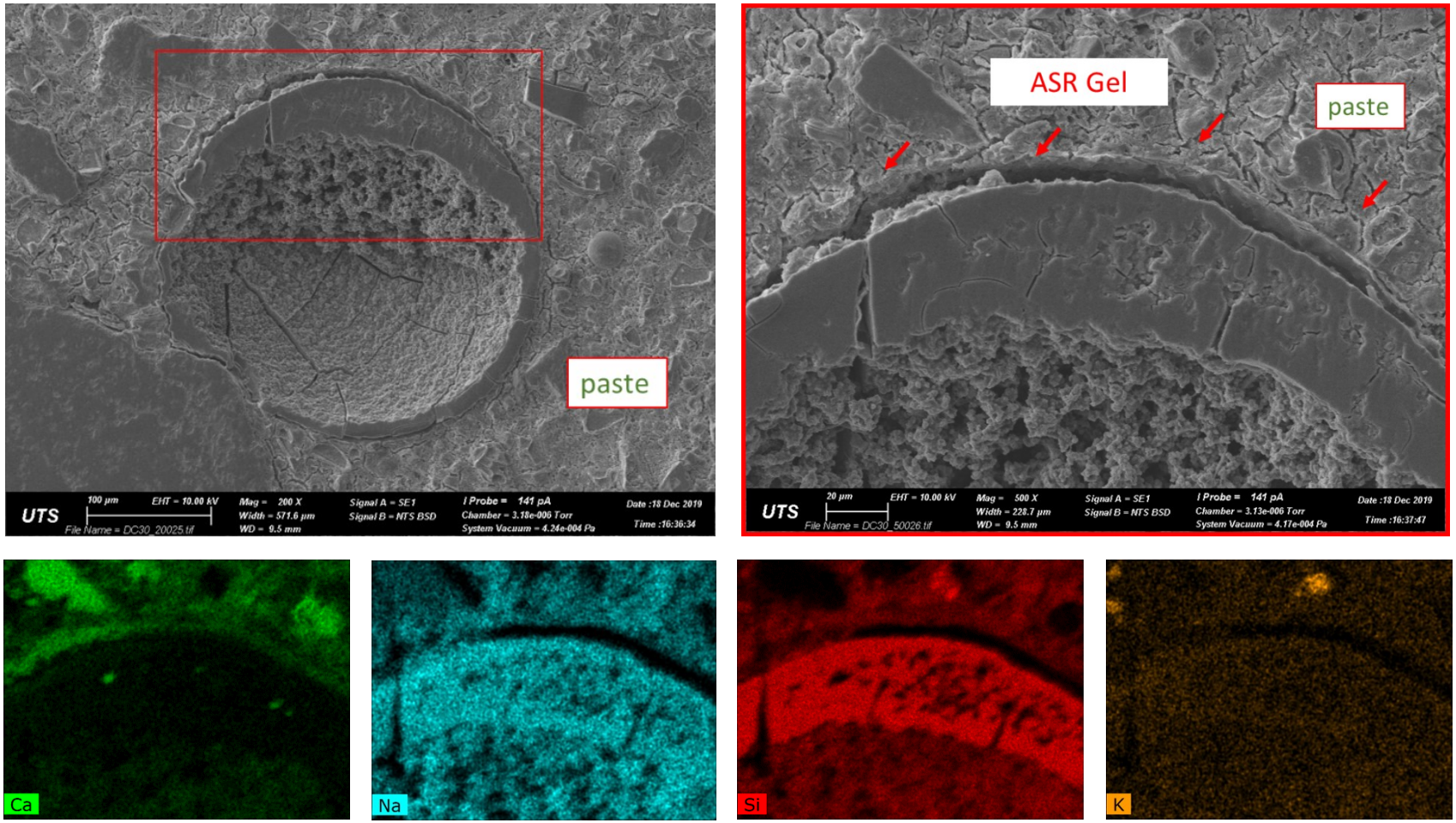

Figure 4. 6 SEM-EDS map of ASR gel lining pore with sponge-like morphology

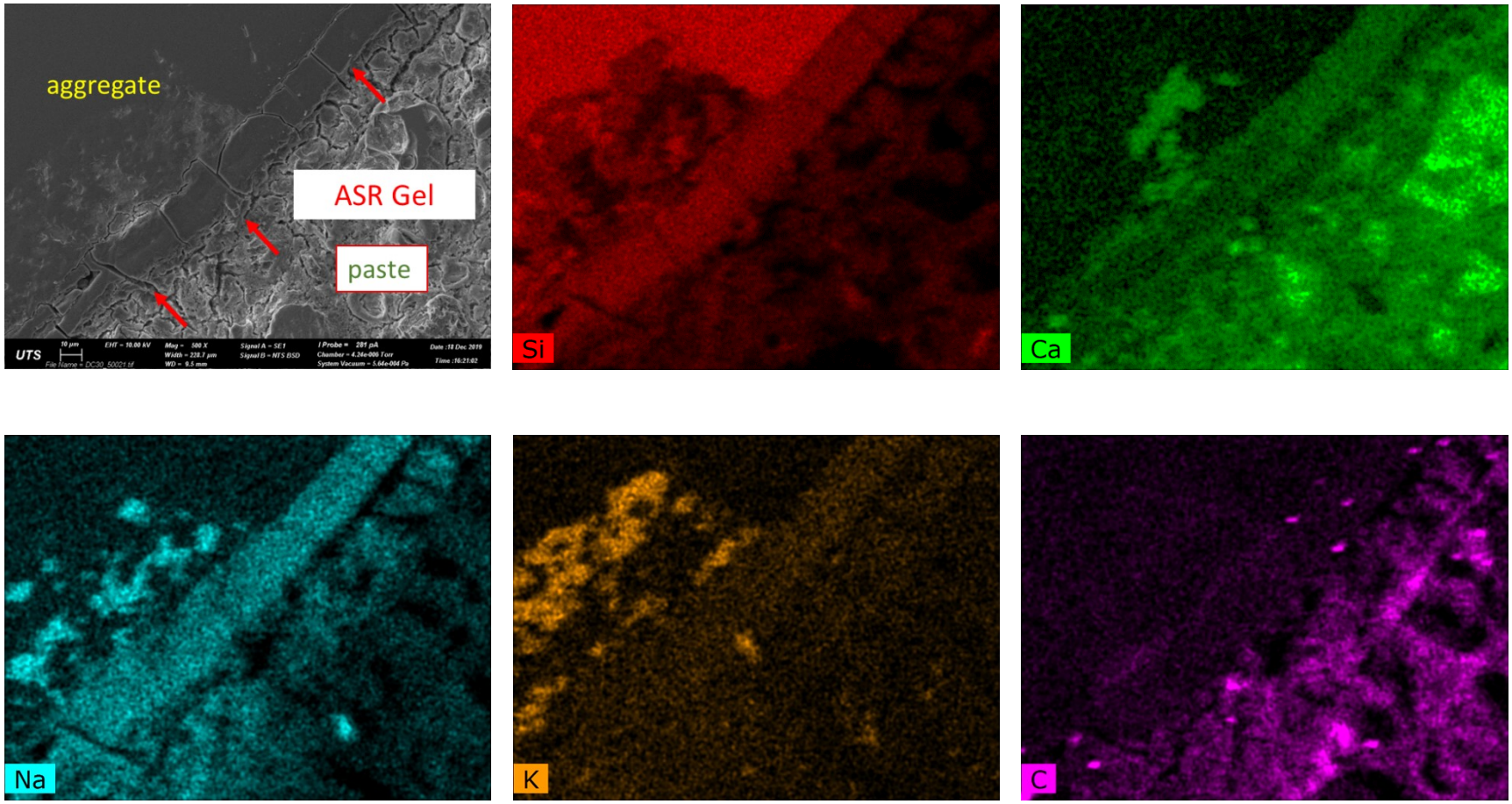

Figure 4. 7 SEM-EDS map of ASR gel at aggregate-cement paste interface

(Notable presence of carbon, can be from resin)

4.3.5 Summary of Phase I Experimental Program

Through the phase I experimental program on mortar bars specimens, a new accelerated test for ASR using an autoclave is established. Main findings and the proposed test procedure are summarised as follows:

- Under various test conditions, expansion values of the mortar bars made with reactive dacite aggregates increased with increasing of steam warming temperature and autoclave duration/cycles. Tests at 80 °C steam warming temperature demonstrated that expansion values of the reactive dacite aggregate mortar bars increased with increasing of the total alkali content of the mix.
- The proposed final test procedure is 80 °C, 60 hours per cycle and totally three cycles of steam warming using an autoclave.
- The proposed test method is suitable for preliminary test to identify the potential reactivity of aggregate. However, more tests on different aggregate types which include highly reactive, moderate reactive and slowly reactive aggregates need to be conducted. Correspondence between the test results obtained from the new accelerated autoclave test and the expansion of field concrete needs further investigation.
- Based on test results of mortar bar specimens at phase I, it is expected that the proposed test method could also be applied to concrete mixes. Through accelerated autoclave test, significant expansion within a short test duration is expected for concrete prisms which could simulate long-term expansion in concrete structures subjected to severe exposure conditions.

4.4 Phase II Experimental Program – Concrete Specimens

4.4.1 Materials and Mix Proportions

The same type of general-purpose Portland cement with equivalent alkali content (Na_2O_{eq}) of 0.50% by mass of cement was used for all concrete specimens. The equivalent alkali content (Na_2O_{eq}) of the cement was calculated as $Na_2O+0.658*K_2O$. The cement oxide composition analysis is provided in Chapter 4.2.1 (Table 4.1).

In all the concrete mix, a non-reactive dune sand, namely Sydney sand, was used. Figure 4.8 gives the grading information of Sydney sand adopted in this study.

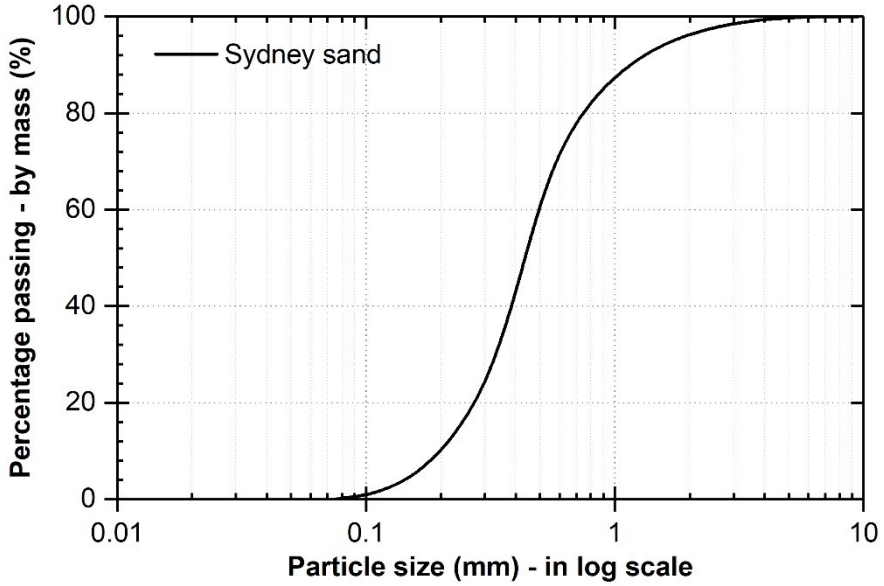

Figure 4. 8 Cumulated PSD of fine aggregates (Sydney sand)

As for the coarse aggregate, a highly reactive dacite aggregate was used in the concrete mixes. The chemical composition of reactive dacite aggregates is given in Chapter 4.2.1 (Table 4.2). The maximum particle size of coarse aggregate used is 20 mm. Figure 4.9 shows the grading information of the coarse aggregate.

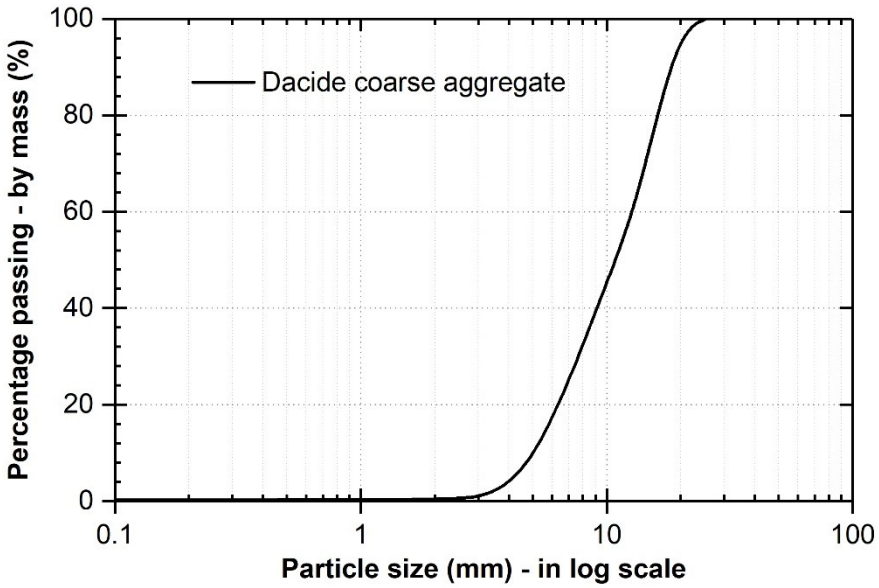

Figure 4. 9 Cumulated PSD of coarse aggregates (dacite aggregate)

The mix proportions used for concrete specimens is given in Table 4.3.

Table 4. 3 Mix proportions per cubic metre of concrete

Material	Concrete mix with 2.5% Na_2O_{eq} boosting (kg/m^3)	Concrete mix with 3% Na_2O_{eq} boosting (kg/m^3)
20 mm dacite aggregate (highly reactive)	1160	1160
Sydney sand (non-reactive)	620	620
Cement	520	520
Water	192.5	192.5
NaOH pellets added	13.69	17.12
Na_2O_{eq} (Calculated)	13.0	15.6

Following the accelerated test procedure proposed in phase I, two representative alkali loading, 2.5% and 3.0%, were applied to the concrete mix. Although previous results revealed that the expansion increases with the total alkali content of the mix containing reactive aggregates, the mechanical properties of the concrete can be significantly reduced by the increasing of the alkali content with addition of sodium hydroxide (Smaoui

et al. 2005). Therefore, for studying the mechanical properties of reinforced concrete affected by ASR, a lower alkali content is preferred. In this study, the 2.5% alkali loading was chosen to investigate the change of mechanical properties under the accelerated test condition.

4.4.2 Specimen Fabrication and Steam Warming Procedure

To boost the alkali content in the concrete mix to 2.5% and 3.0% Na_2O_{eq} by mass of cement, sodium hydroxide pellets with purity of 98% were added to the mixing water 24 hours prior to mixing of the concrete. The mixing water with sodium hydroxide was contained in closed plastic containers left in the laboratory overnight at about 23 °C. This is to avoid the heat generated during the dissolution of the sodium hydroxide pellets so that the mixing water for concrete mixing was at about 23 °C. The concrete was mixed in a horizontal pan mixer with a capacity of 70 litres. Figure 4.10 shows the pan mixer used for concrete mixing. The concrete mixing procedure follows the Australian Standards for mixing and preparing concrete specimens (AS 1012.2:2014). For the 3.0% Na_2O_{eq} boosting mix, three prisms with embedded stainless-steel studs were cast, while for the mix with 2.5% alkali loading, twelve cylinders and three prisms were cast. The size of the cylinders was 100 mm (diameter) by 200 mm (height), and that of the prisms was 75 × 75 × 285 mm.

Figure 4. 10 70L Pan mixer

Specimens were demolded after one day from casting, and then the initial length and mass of the prisms were recorded for expansion and mass change measurement. Thereafter, all specimens were stored in a temperature-humidity controlled cabinet maintained at 23 °C and relative humidity of 90% RH. At the age of 28 days, three cylinders were tested for the modulus of elasticity and then compressive strength, in accordance with AS 1012.17 and AS 1012.9, respectively. Meanwhile, the length and mass of all the prisms were measured.

The accelerating tests started at the age of 28 days, using an autoclave with a chamber volume of 153 litres (Zirbus LVSA 50/70, shown in Figure 4.11). All the prisms and the remaining nine cylinders were placed in the top and bottom baskets of the autoclave (see Figure 4.12), respectively. Before the specimens were placed in the baskets, a stainless-steel washbasin was put beneath the bottom basket first. This is to collect any small particles that may fall from the specimens during autoclaving, and to avoid the potential

risk of these small particles being discharged in the drainage system which may cause damage of the machine.

Figure 4. 11 Zirbus LSVA 50/70 autoclave used for the test

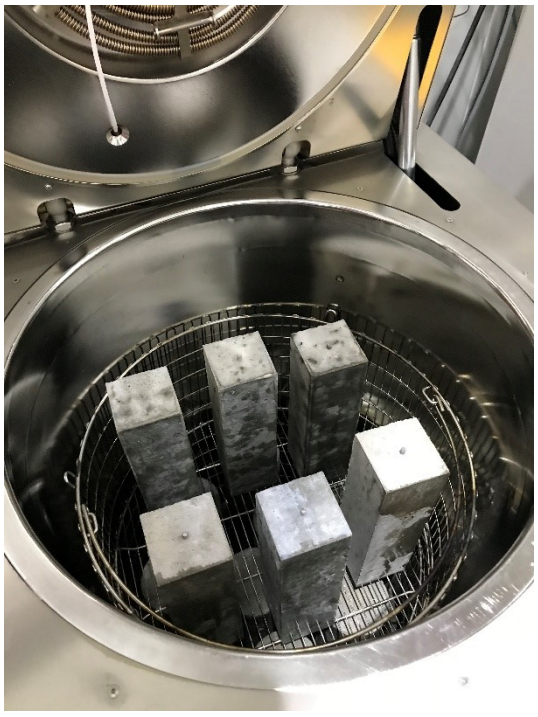

Figure 4. 12 Specimens as placed in the autoclave

In order to accelerate ASR for the concrete specimens, the same autoclaving cycles used in Chapter 4.2.2 was adopted. The maximum steam warming temperature used is 80 °C. Each cycle of steaming warming duration is 60 hours and totally three cycles are applied. Figure 4.13 shows the temperature-time relationship of steam warming for three cycles.

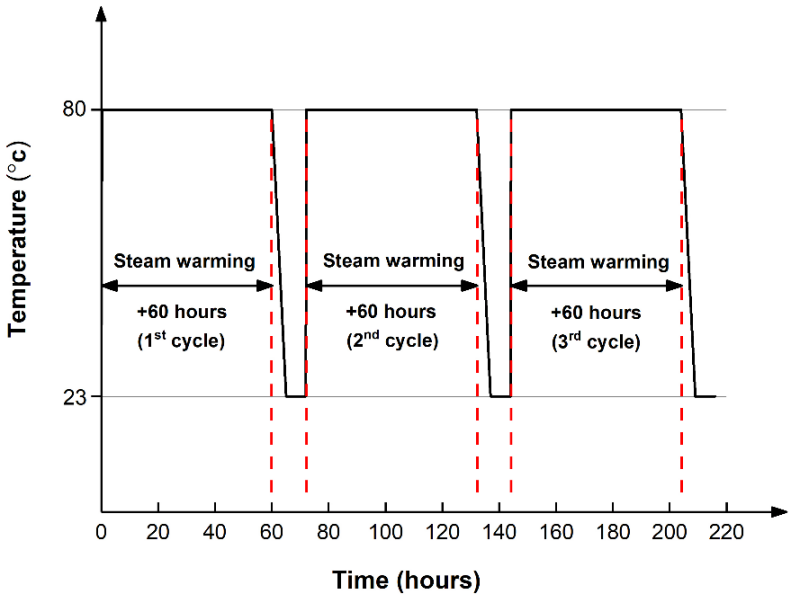

Figure 4. 13 Time-temperature cycles adopted in the autoclave chamber

At the end of each cycle, three cylinders were taken out from the autoclave for testing of modulus of elasticity and compressive strength, whilst the expansion and the mass of the prisms were measured. It is worth to mention that the mass of the prisms was recorded immediately after the specimens were taken out, while the length of the prisms was measured after the specimens were cooled down to room temperature at 23 °C.

4.4.3 Expansion and Mass Change

Figure 4.14 shows the expansion of the concrete prisms after 28 days of curing in the temperature-humidity controlled cabinet and after each cycle of autoclaving. During storage up to the age of 28 days in the temperature-humidity controlled cabinet, a slight shrinkage of 0.019% was observed. The expansion increases with the autoclaving cycles. The expansion of prisms with 2.5% Na_2O_{eq} boosting was 0.05% after one cycle, while

this value was raised to 0.18% after three cycles. Similar phenomenon was confirmed by the results obtained from specimens with 3.0 % Na_2O_{eq} boosting, expansion increasing from 0.07% to 0.22% after 3 cycles. In addition to the autoclaving cycles, the expansion was increased with the alkali content. Moreover, the effect of alkali content on expansion under the same cycle was enhanced by the increasing of cycles in the scope of this study. As can be seen from Figure 4.14, when only one cycle (60 hours) was applied, the difference of expansion between two mixes was 0.02%, while that difference reached 0.04% after three cycles (180 hours). Effects of more cycles on the expansion of specimens needs further investigation.

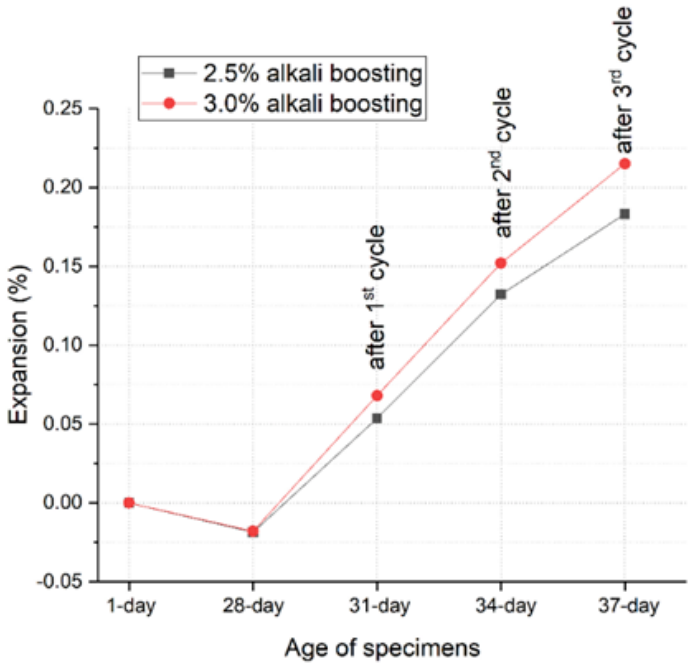

Figure 4. 14 Expansion of concrete prisms after 3 cycles in the autoclave

The accompanying mass change of the prisms is shown in Figure 4.15. As mentioned before, the ASR expansion is caused by gel swelling after absorbing water. Different mass gain would be expected in prisms with different expansion. The mass change of prisms was measured immediately after being taken out from the autoclave. This operation was to reduce the influence of moisture evaporation on the mass measurement. The results

showed that the mass of prism increases with increasing autoclaving cycles, and the prisms with higher alkali loading exhibited higher mass gain, which agreed well with the expansion results in Figure 4.14. Interestingly, after 28 days of curing in the humidity cabinet, a slight mass gain of about 0.05% was observed when there is no expansion in prisms, which could be attributed to the continued hydration of the cement during this period. As can be seen from Figure 4.15, in the first two cycles, the mass gain of prisms increased significantly with the increasing of autoclaving cycles, from about 0.05% to 0.38% for specimens with 2.5% alkali loading, and to 0.46% for specimens with 3.0% alkali content, respectively. However, this trend was slowed down afterwards, as minor mass gain was recorded for specimens with 2.5% and 3.0% alkali loading when the third cycle was applied. It should be mentioned that the hydration of the unreacted cement possibly continued during the autoclaving cycles, which could contribute part of the mass again. In addition, presence of water in cracks could also contribute to the mass gain. Therefore, the measured mass gain could be attributed to the combination of continued hydration, the presence of water in cracks and ASR gel formation.

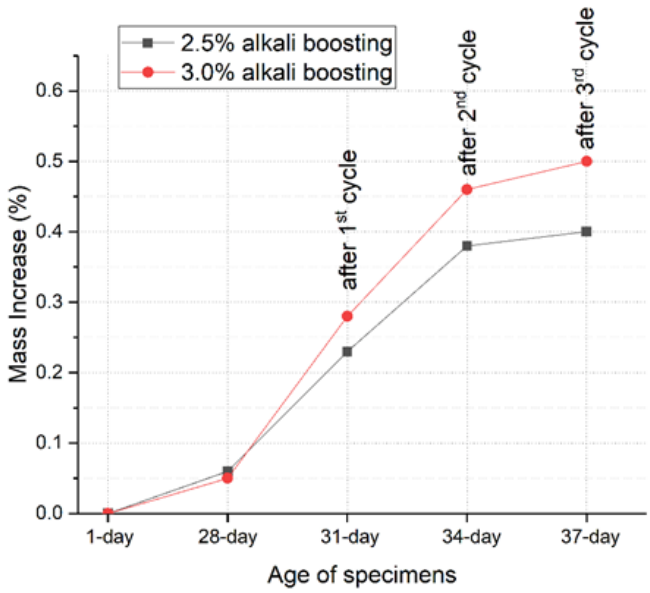

Figure 4. 15 Mass change of concrete prisms after 3 cycles in the autoclave

4.4.4 Cracking of Specimens

The map crack in concrete cylinders and prisms at the end of third autoclaving cycle, with 2.5% Na_2O_{eq} boosting, are shown in Figures 4.16 and Figure 4.17. Some white exudations were also found on surface of concrete specimens after 3 cycles in the autoclave.

Figure 4. 16 External cracks on cylinder after 3 cycles in the autoclave

Figure 4. 17 External map cracking on prism after 3 cycles in the autoclave

Enlarged micrographs of internal cracks and microscope observation by SEM are discussed in Chapter 4.4.5.

4.4.5 Microscopic Observation

The objective of microscopic observation is to confirm that the expansion under accelerated test method was caused by ASR. Microscopic observation was performed by using laser confocal scanning microscope and scanning electron microscope.

Prisms experienced three autoclaving cycles were sliced into small samples using a Struers Labotom-15 cutting machine with cooling water. The sample with internal cracks was examined using an Olympus LEXT OLS5000 confocal laser scanning microscope. An abundant of reaction product was observed inside the aggregate particle, as shown in Figure 4.18.

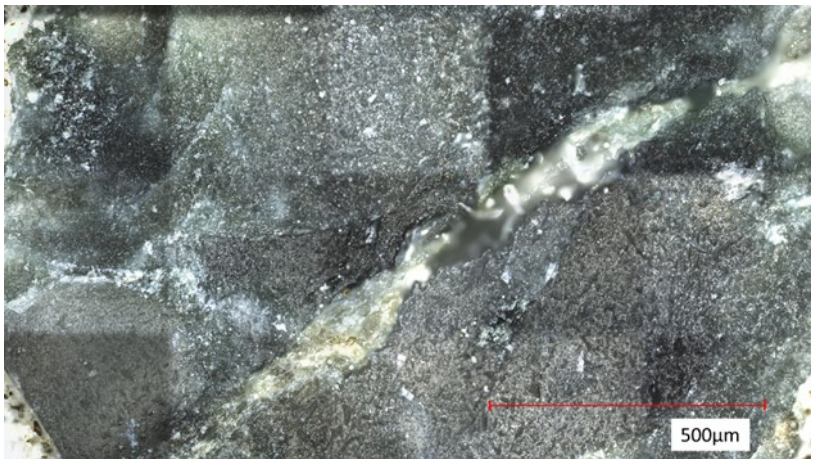

Figure 4. 18 Internal cracks and ASR gel in aggregate from concrete prism after 3 cycles in the autoclave observed using laser confocal scanning microscope

SEM-EDS analysis was performed on polished concrete samples to investigate the chemical composition of ASR gel. Figure 4.19 shows the results of the elemental mapping obtained by SEM-EDS analysis. As it can be seen, the ASR gel was composed of Ca, Si and alkali (Na and K).

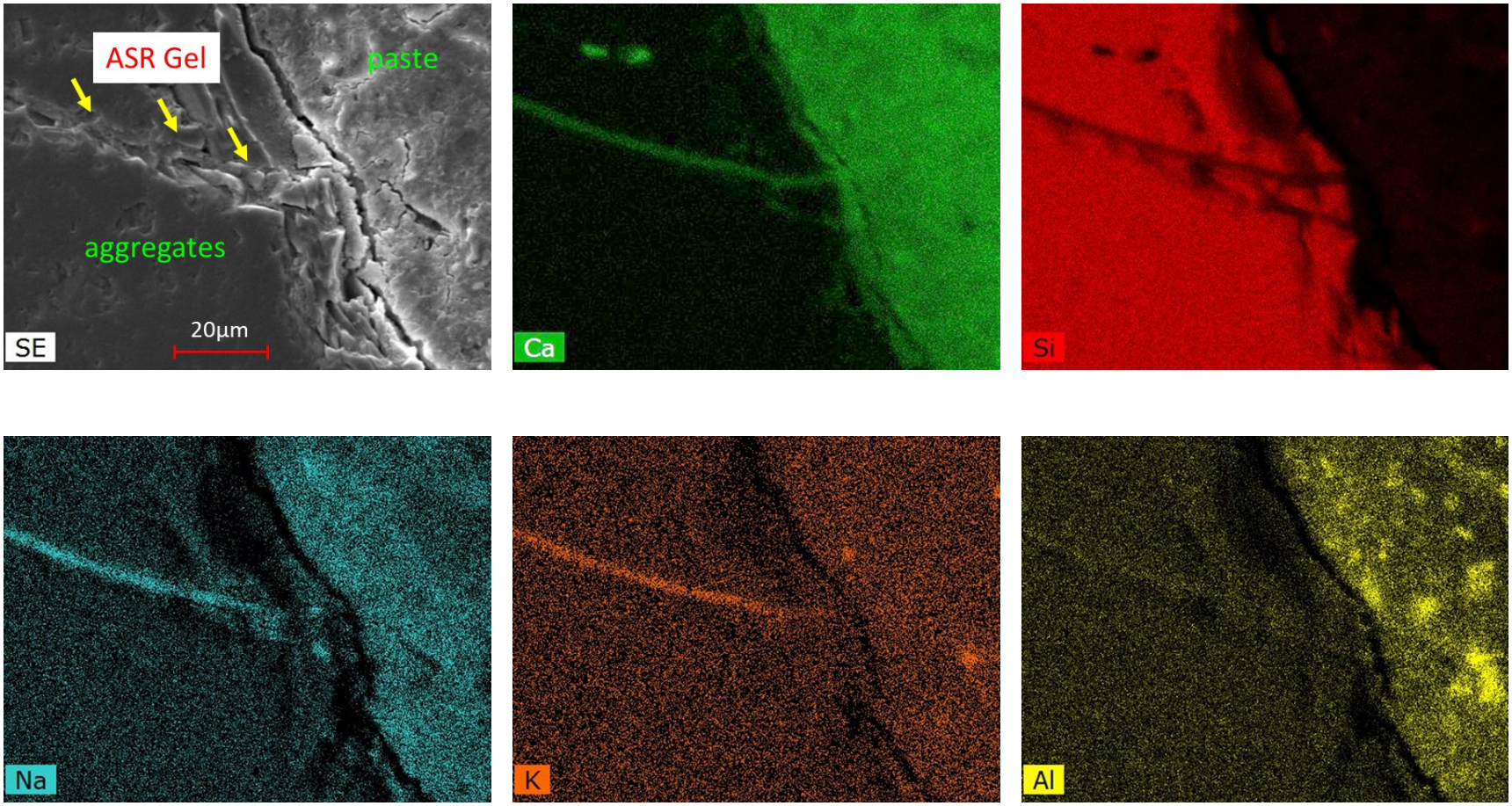

Figure 4. 19 SEM-EDS map of ASR gel formed in an aggregate

ASR products with typical rosette-type morphology and plate-like morphology were observed by Zeiss Evo LS15, and Zeiss Supra 55VP SEM from samples extracted from prisms with 2.5% alkali boosting after 3 cycles of autoclaving. Figure 4.20, 4.21, and 4.22 show the SEM images of ASR products observed.

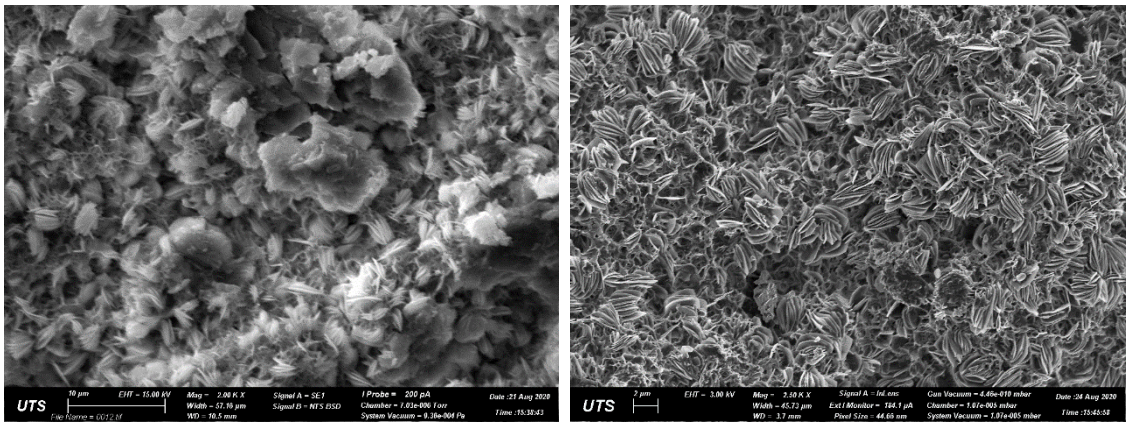

Figure 4. 20 SEM images showing ASR products with rosette-like morphology (sample from 80°C accelerated autoclave test)

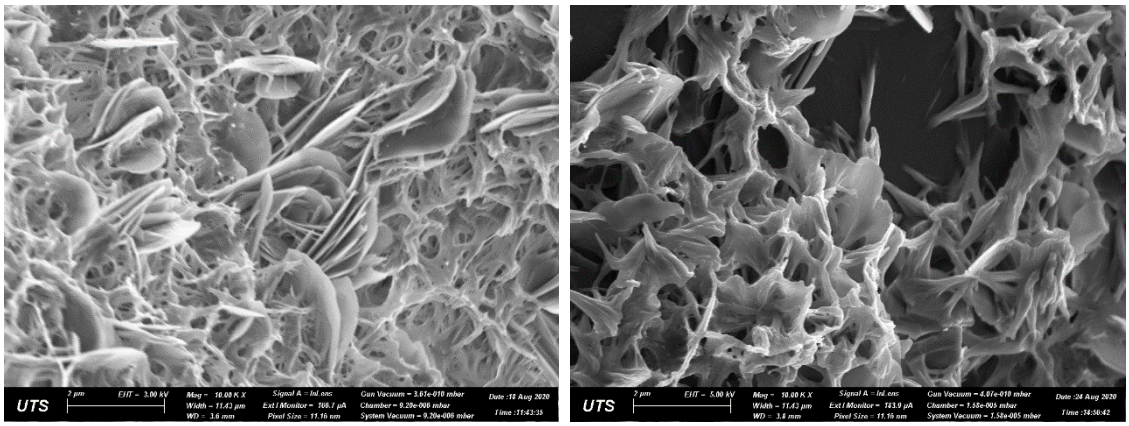

(a) plate-like morphology (b) network-like morphology

Figure 4. 21 SEM images showing ASR products with network and plate-like morphology (sample from 80°C accelerated autoclave test)

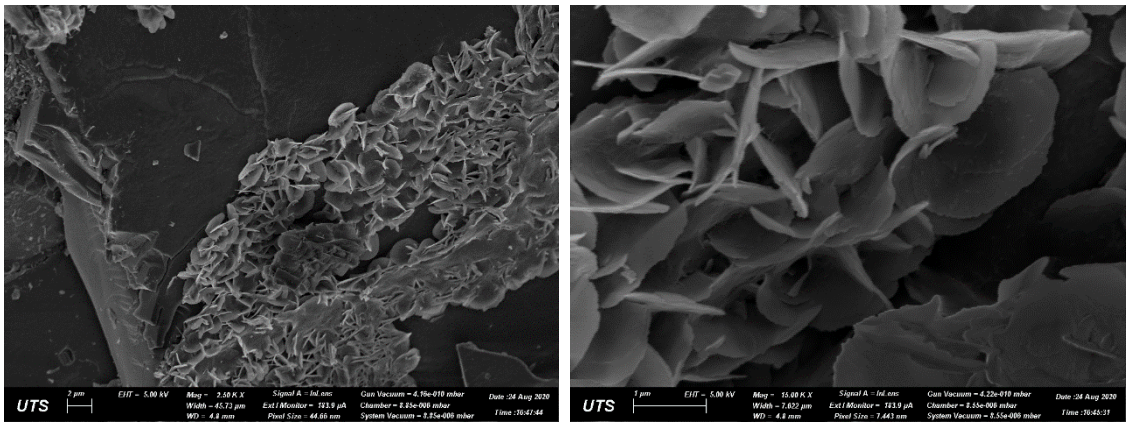

Figure 4. 22 SEM images showing ASR products with crystalline morphology (sample from 80°C accelerated autoclave test)

4.4.6 Mechanical Properties of Concrete under Accelerated ASR Test

Influence of alkali boosting by adding sodium hydroxide pellets in the mixing water on the 3, 7 and 28-day compressive strength of concrete cylinders are shown in Figure 4.23. Results are obtained from separate tests. The concrete mix proportions are presented in Table 4.3. It should be noted that for concrete without alkali boosting, there is no additional sodium hydroxide being added in the mixing water, while for the concrete with 2.5% and 3.0% alkali boosting, 13.69 kg/m^3 and 17.12 kg/m^3 of sodium hydroxide pellets are added in the mixing water, respectively (see Table 4.3). As can be seen from Figure 4.23, for concrete with 2.5% and 3.0% alkali boosting, the 28-day compressive strength decreased 42% and 49% compared to that of the specimens without alkali boosting, respectively.

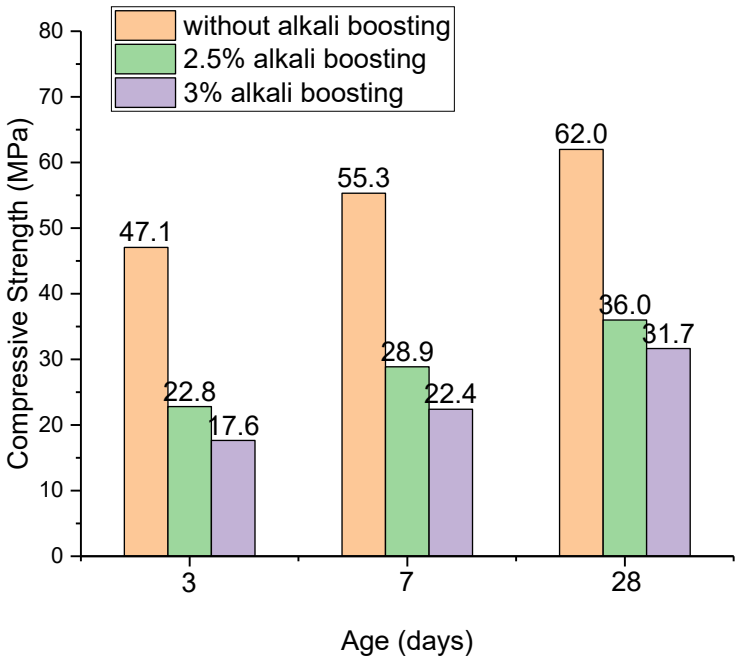

Figure 4. 23 Influence of alkali loading on compressive strength of concrete cylinders tested at age of 3, 7 and 28 days

Figure 4.24 presents effects of autoclaving cycles on compressive strength and elastic modulus of cylinders with 2.5% alkali boosting. The compressive strength increased until the end of the second cycle and showed a decreasing trend thereafter. It can be observed that the compressive strength initially increased with the increasing of expansion at relatively low expansion level in this study, which was consistent with previous findings (Gautam et al. 2017; Larive 1998). As can be seen from Figure 4.24, up to expansion level about 0.13%, the compressive strength was improved by 15.3% and 23.6% after the first and second cycle respectively, with respect to the 28-day compressive strength. The continued hydration under 80 °C autoclaving condition could have effect on the increase of the compressive strength. This effect needs further investigation. Thereafter, the compressive strength showed a decreasing trend while expansion keeps increasing. The gain in compressive strength dropped to 16.7% as the expansion developed to 0.18% at the end of the third cycle. It is expected that the compressive strength will continue to

decrease with the increasing of expansion in concrete. This trend had already been reported by Gautam et al. (2017). The authors observed a maximum reduction of 4-6% in compressive strength at 365-day compared with 28-day value when expansion reached 0.24-0.35%.

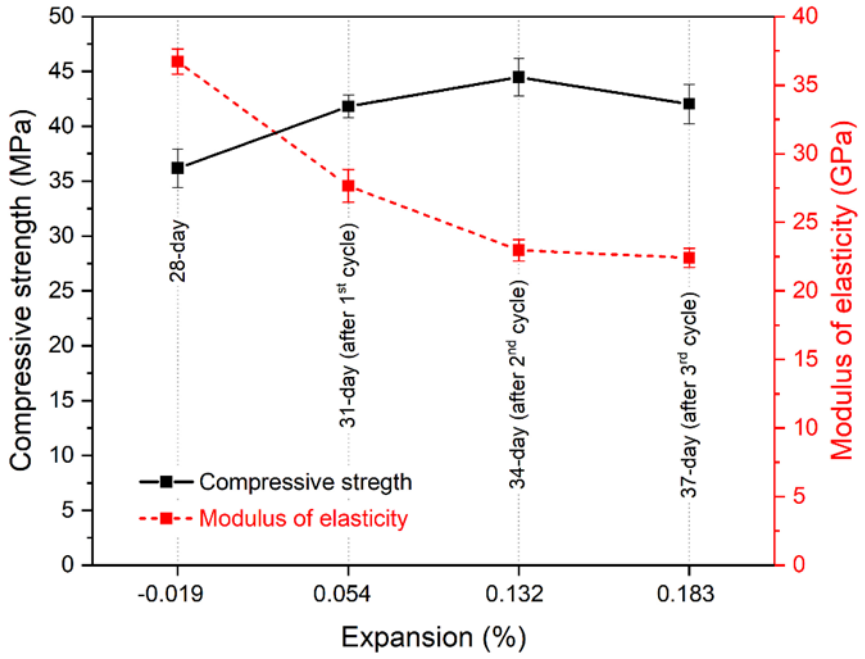

Figure 4. 24 Change in compressive strength and modulus of elasticity of concrete cylinders with 2.5% alkali boosting after 3 cycles in the autoclave

Modulus of elasticity is generally regarded as the most sensitive mechanical property affected by ASR. Prior to compressive strength tests, three cylinders was tested after each cycle to obtain the modulus elasticity and the results were presented in Figure 4.24. The modulus of elasticity was observed systematically reduced with autoclaving cycles. With respect to the modulus elasticity at 28 days, a reduction of 24.5%, 37.9% and 39.0% was recorded after 1, 2 and 3 cycles, respectively. The degradation of the modulus elasticity is due to the microcracking caused by accelerated ASR.

4.5 Comparison of Expansion Results

Refer to classification of aggregate reactivity recommended in ASTM C1778-20 (see Table 4.4), the reactivity of dacite aggregate used in this study is evaluated. Based on the expansion results of dacite aggregate tested under 80 °C steam warming cycles with alkali boosting, and the AMBT and CPT expansion results from previous study, a comparison of the expansion obtained from these tests was made for classify the reactivity of dacite aggregate.

Table 4. 4 Aggregate reactivity classification (ASTM C1778-20)

Aggregate reactivity level	Reactivity description	1-year expansion (CPT, ASTM C1293)	14-day expansion (AMBT, ASTM C1260)
R0	Non-reactive	<0.04%	<0.10%
R1	Moderately reactive	≥0.04%, <0.12%	≥0.10%, <0.30%
R2	Highly reactive	≥0.12%, <0.24%	≥0.30%, <0.45%
R3	Very highly reactive	≥0.24%	≥0.45%

4.5.1 Comparison of AMBT and 80 °C Autoclave Test Results

Figure 4.25 compares the expansion of mortar bars with dacite aggregates tested under 80 °C autoclave treatment condition and the AMBT test condition. The average 14-day expansion of mortar bars tested by Tapas (2020) is 0.292% which is very close to 0.3%, but well below the 0.3% limit regulated in the ASTM C1778-20 for classification of moderately reactive and highly reactive aggregate. While the average 14-day mortar bar expansion results from Cement Concrete & Aggregates Australia (CCAA) is 0.47% for this type of aggregate, which is well above the 0.45% threshold for classifying the highly reactive and very highly reactive aggregate. Under the current 80 °C autoclave treatment

condition, for mortar bars with 2.5-3.5% alkali boosting, the average expansion is 0.35-0.39%, after 3 cycles of 80 °C autoclave treatments. As can be seen, the expansion yielded

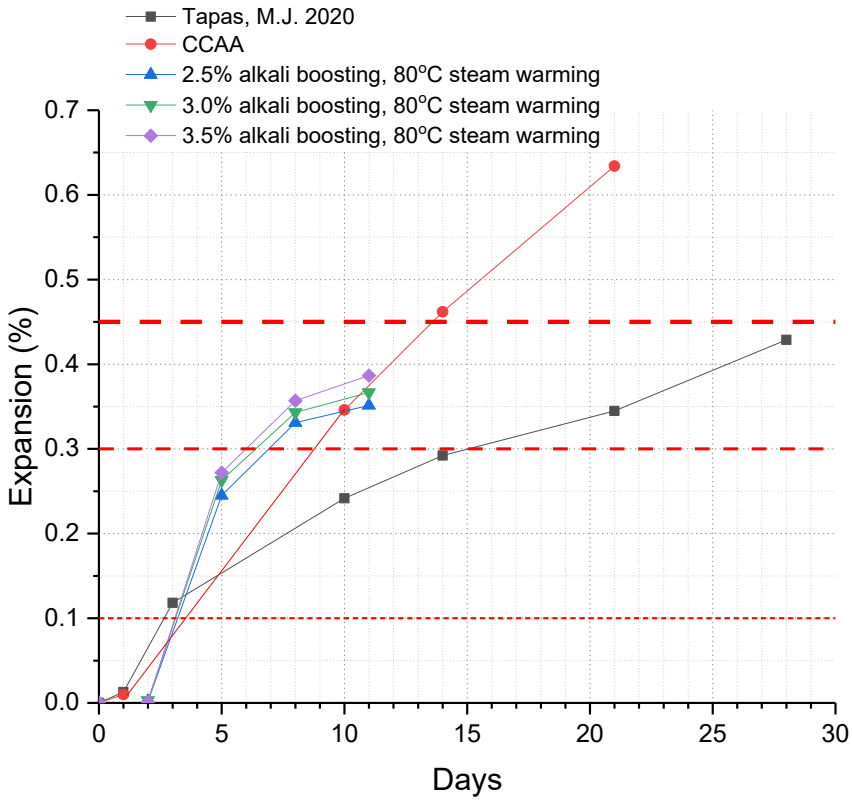

Figure 4. 25 Comparison of expansion results between 80°C autoclave treatment with alkali boosting and AMBT for dacite aggregate mortar bar

from the current 3-cycle 80 °C autoclave test was greater than 0.3% and lower than 0.45%. These expansions were obtained at the age of 11 days. Hence, refer to Table 4.4, it can be concluded that the used dacite aggregate is highly reactive.

4.5.2 Comparison of CPT and 80 °C Autoclave Test Results

Figure 4.26 compares the expansion of concrete prisms containing dacite aggregate with 2.5% alkali boosting tested under the 80 °C autoclave cycles and the 1-year CCAA CPT result for dacite aggregate prisms. The CCAA 1-year CPT expansion is 0.233%. To investigate the influence of more cycles on the expansion of concrete prisms, 3 more

cycles were run. While the expansion after 3 cycles was 0.18%, after totally 6 cycles of 80 °C autoclave, the expansion of the prisms reached 0.228%. Refer to Table 4.4 and the expansion results of CCAA, it can be concluded that the used dacite aggregate is highly reactive.

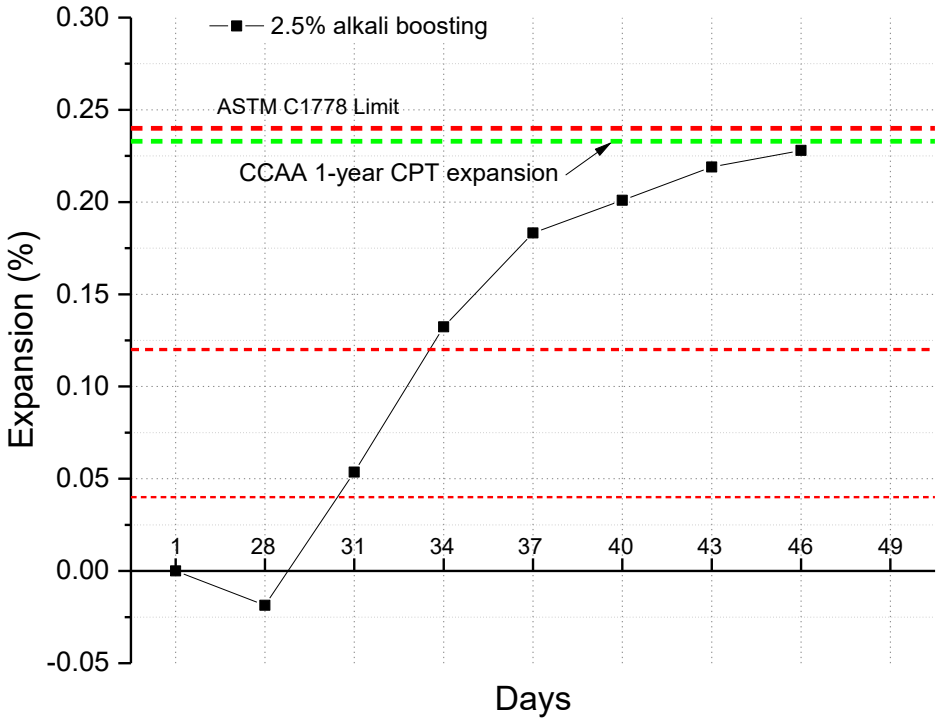

Figure 4. 26 Comparison of expansion results between 80°C autoclave treatment with 2.5% alkali boosting and CPT for dacite aggregate prism

It can be seen from Figure 4.26 that, after 3 cycles, the expansion is approaching the upper limit with the increasing cycles. However, both of the expansion after 3 cycles and after 6 cycles are located between 0.12% and 0.24%. Therefore, by considering the aforementioned mortar bar expansion results and the current concrete prism expansion results, it can be confirmed that the used dacite aggregate is highly reactive.

4.5.3 Summary

The proposed multi-cycle 80 °C autoclave test, with 60 hours per cycle and 2.5% alkali boosting, successfully identify the reactivity of dacite aggregate. In addition, according to the ASTM C1778 recommendation, the used dacite aggregate is classified as highly reactive. By comparing the proposed multi-cycle 80 °C autoclave test and the standard AMBT and CPT test, the 80°C autoclave test has unique advantages in testing concrete prisms and mortar bars. In the mortar bar test, although the test duration takes 11 days from casting, which is close to the 14 days in the AMBT test, it can test the specimens by avoiding the immersion of 1N 80 °C NaOH solution. In the concrete prism test, the test duration can be significantly shortened with regards to the 1-year test duration in standard CPT test. However, more tests on different types of aggregate with known field performance, or AMBT, CPT results, are needed. This will help validate the proposed multi-cycle 80 °C autoclave test in classifying the aggregate with very highly reactive, highly reactive, moderately reactive or non-reactive, in accordance with the recommendations of ASTM C1778.

4.6 Concluding Remarks

An accelerated test method for assessing the potential risk of alkali-silica reaction in concrete using an autoclave is proposed in this study: a testing regime of 3 cycles of steam warming at 80 °C using an autoclave, with 60 hours per cycle. Basing on the method, the effects of temperature, alkali loading and autoclaving cycles on the ASR expansion of mortar bars and concrete prisms were investigated. Afterwards, SEM-EDS analysis was conducted to confirm the ASR products. Furthermore, the method was adopted to study the mechanical properties degradation caused by ASR in concrete. The main conclusions can be drawn as follows:

(1) For mortar bars containing dacite aggregate subjected to autoclaving cycles, the expansion was slightly affected by increasing alkali loading from 2.5% to 3.5% when the steam warming temperature was at 70 °C, and the maximum expansion was 0.23% at the end of three cycles. While the expansion was significantly increased by increasing the alkali content as the temperature was elevated to 80 °C, and a maximum expansion of 0.39% was recorded in a short period.

(2) Although increasing the alkali content and autoclaving temperature could achieve higher expansions, to study the mechanical properties of ASR affected concrete, controlling alkali content in concrete and autoclaving temperature is necessary, because high alkali content by addition of NaOH and high autoclaving temperature affect the mechanical properties of OPC concrete. Therefore, an alkali content of 2.5% by mass of cement and a temperature of 80 °C are recommended for using autoclaving cycles to test ASR.

(3) As revealed by the expansion measurements and mechanical properties assessment performed on concrete, the multi-cycle autoclave test method appears to be suitable for investigating ASR deterioration of actual concrete mixes within a short period of time. For concrete prisms containing dacite aggregate with 2.5% alkali boosting, a maximum expansion of 0.18% was achieved after 3 cycles of autoclaving. The compressive strength showed an initial increase under low expansion followed by a reduction under higher expansion, while the modulus of elasticity systemically decreased with the increasing expansion.

(4) Potential degradation of mechanical properties, bond deterioration, and ultimately the residual load capacity of ASR affected reinforced concrete structures can be simulated using the proposed accelerated ASR test method.

Chapter 5

Flexural and Shear Behaviour of Small-scale Reinforced Concrete Beams Affected by ASR

5.1 Overview

Concerns about the safety of the ASR damaged reinforced concrete structures have driven the demand of accurately assessing the residual load capacity of the deteriorated structure. A conservative prediction of the residual load capacity may lead to the decision of demolishing a functioning structure, while an overestimation of the residual load capacity could result in keeping a structure in a dangerous condition operational and jeopardising the safety of the public. Therefore, it is critical to evaluate the residual load capacity of ASR affected structure accurately.

Conventionally, field load testing on real structures (Blight et al. 1989; Imai et al. 1987), are employed to assess the residual load capacity of ASR affected structures. Such methods, however, are labour intensive, time consuming and may cause further damage to the structure. Large-scale in-situ field exposure testing have also been conducted by different researchers (Deschenes, Bayrak & Folliard 2009; Giannini 2012; Karthik, Mander & Hurlebaus 2018; Liu et al. 2017). These tests provided valuable information and results for reference on evaluating the residual load capacity of ASR affected members. The long test duration of these tests, however, could be the primary factor that limited its application in investigating the influence of ASR on flexural and shear behaviour of the affected reinforced concrete elements. During the decades of extensive research on ASR in the past, more efforts have been dedicated through controlled laboratory conditions to investigate the flexural and shear behaviour on small-scale to full-scale reinforced concrete specimens (Ahmed, Burley & Rigden 1998; Bilodeau et al.

2016; Fan & Hanson 1998; Fujii et al. 1986; Inoue et al. 1989; Koyangi et al. 1996; Monette, Gardner & Grattan-Bellew 2002; Swamy & Al-Asali 1989). Some researchers modified mix with adding fused silica (Majlesi 1994; Swamy & Al-Asali 1989), but whether the modification is suitable for representing actual concrete mix is arguable. Some researchers tested specimens with up to 10 years of field exposure to accelerate ASR (Hamada, Otsuki & Fukute 1989) and these tests took very long time, therefore, a quick test method is needed. Although a commonly accepted accelerated method to rapidly and reliably assess the residual load capacity of ASR damaged structures is still unavailable, previous research have revealed some valuable findings about the stiffness and strength of ASR damaged reinforced concrete structures.

With regards to flexural behaviour, an enhancement in the flexural stiffness of the ASR damaged reinforced concrete beam was observed, compared with that of the non-reactive specimen due to the chemical prestress effect (Giannini 2012; Inoue et al. 1989). Due to this effect, the cracking loads of the ASR affected reinforced concrete beams were reported higher than that of the non-reactive ones (Inoue et al. 1989; Koyangi, Rokugo & Ishida 1986). Despite significant reduction in mechanical properties and severe cracking of concrete due to ASR, the flexural load capacity was found not significantly compromised, with some even slightly increased (Fan & Hanson 1998; Giannini 2012; Inoue et al. 1989; Koyangi et al. 1996). In addition, under various loading conditions (e.g., sustained loading or cyclic loading), the flexural capacity of ASR damaged beams showed no significant difference when compared to the non-reactive beams (Fan & Hanson 1998; Monette, Gardner & Grattan-Bellew 2002). In contrast, some other researchers (Swamy & Al-Asali 1989), reported a reduction of up to about 25% in flexural capacity, and considerable losses in flexural stiffness for severely damaged beams with high level of ASR expansion (e.g., at 1.6% expansion levels).

Whereas for the shear behaviour, when transverse reinforcement is adequate and well-functioning, an increasing in the shear capacity can be expected. This is attributed to the chemical prestressing and confinement effects, and these aspects have already been reported by different researchers in the literature (Ahmed, Burley & Rigden 1998; Deschenes, Bayrak & Folliard 2009). For ASR damaged members without shear reinforcement, some inconsistent findings have been reported. Test results of Ahmed, Burley & Rigden (1998), Bach, Thorsen & Nielsen (1993), Bilodeau et al. (2016) showed that shear strength of the ASR damaged beams was improved even when there were no stirrups. While Clark & Ng (1989), Cope & Slade (1992) demonstrated that the punching shear strength of the reactive specimens initially increased with the increasing expansion. This trend started to decrease when the expansion reached certain level (0.2-0.3%). Upon reaching a free expansion of 0.5-0.6%, a reduction of 30% in punching shear strength was reported. Cope & Slade (1992) observed the same trend when the authors tested beams for shear strength.

The enhancement in the structural performance with regards to flexural behaviour and shear behaviour of ASR damaged members, e.g., flexural stiffness, cracking load and shear strength, is attributed to the chemical prestressing effect induced by ASR expansion and the confinement effects (Deschenes, Bayrak & Folliard 2009; Giannini 2012). Karthik, Mander & Hurlebaus (2018) reported that the load carrying capacity of the specimen with severe ASR damage after five years of field exposure exhibited higher load carrying capacity relative to the undamaged control specimen, even though the deteriorated concrete showed significant reduction in mechanical properties. Also, it was observed that the severely deteriorated specimen was much stiffer than the slightly damaged specimen, moderately damaged specimen, and the undamaged control specimen, due to the higher chemical prestressing effects caused by ASR expansion. It is

worth to note that all these tested specimens are well reinforced with appropriate reinforcement arrangement.

Although full-scale field load testing and field exposure testing are considered as the most reliable methods in determining the flexural and shear capacity of ASR affected structures, these tests usually take long time, require abundant resources, and need a lot of manpower. Therefore, a reliable and rapid accelerated laboratory test is preferred.

In this chapter, the novel accelerated test using an autoclave with 80 °C steam warming is applied to study the flexural and shear behaviour of small-scale reinforced concrete beams affected by ASR. The beams are singly reinforced with two levels of reinforcement ratios. For simplicity, no shear reinforcement is employed for these beams. Load carrying capacity tests on small-scale reinforced concrete beams are conducted. Moreover, mechanical properties of ASR affected concrete under accelerated tests are investigated. Free expansion is measured and recorded on prisms with embedded stainless studs at two ends of the prism. In addition, digital imaging correlation (DIC) technique is applied to investigate the load-deflection behaviour of these beams in flexure.

5.2 Experimental Program

5.2.1 Materials and Mix Proportions

The cement used is the same type of general-purpose Portland cement with equivalent alkali content (Na_2O_{eq}) of 0.50% by mass of cement. As for the fine aggregate, a non-reactive sand, Sydney sand, was used. While for the coarse aggregate, a highly reactive Dacite aggregate with a maximum particle size of 20 mm was used. The chemical composition of reactive Dacite aggregates is provided in Table 4.2 of Chapter 4. As for

the reinforcement, deformed bars with 5 mm diameter (N5) and with 8 mm diameter (N8) were used.

The mix proportions used for all small-scale beams, cylinders and prisms is given in Table 5.1. In the concrete mixes, total alkali content is raised to 2.5% Na_2O_{eq} by mass of cement through adding extra sodium hydroxide in the mixing water. This is for promoting ASR in the accelerated test, and meanwhile to avoid too significant reduction in the 28-day concrete strength due to the addition of NaOH in the mix.

Table 5. 1 Mix proportions per cubic metre of concrete

Material	Concrete mix with 2.5% Na_2O_{eq} boosting (kg/m^3)
20 mm Dacite aggregate (highly reactive)	1160
Sydney sand (non-reactive)	620
Cement	520
Water	192.5
NaOH pellets added	13.69
Na_2O_{eq} (Calculated)	13.0

5.2.2 Specimen Fabrication

Twelve small-scale reinforced concrete beams with size of 100 × 100 × 340 mm were fabricated. Six beams were reinforced with two 5 mm diameter deformed bars (N5) obtained from a steel wire mesh, the other six beams were reinforced with two 8 mm diameter deformed bars (N8) obtained from a steel mesh, as the main reinforcement, respectively. The reinforcement ratios for the two series of small-scale beams are 0.39% and 1.0%, respectively. No transverse reinforcement is provided for the beams. Concrete cover of the beams is maintained at 20 mm. Details of reinforcement of the beams are shown in Figure 5.1.

The concrete mixing procedure follows the Australian Standards AS 1012.2:2014 and a 70L horizontal pan mixer was used for the mixing. During the cast of the small-scale beams, fresh concrete was poured in two layers into the steel moulds with reinforcing bars inside (see Figure 5.2). A vibrating table was used to compact the fresh concrete thoroughly for 30s after the moulds were filled with the first layer of concrete, followed by the second layer, which was vibrated for 30s again. Afterwards, the top surface of the beams was levelled with a trowel (see Figure 5.3).

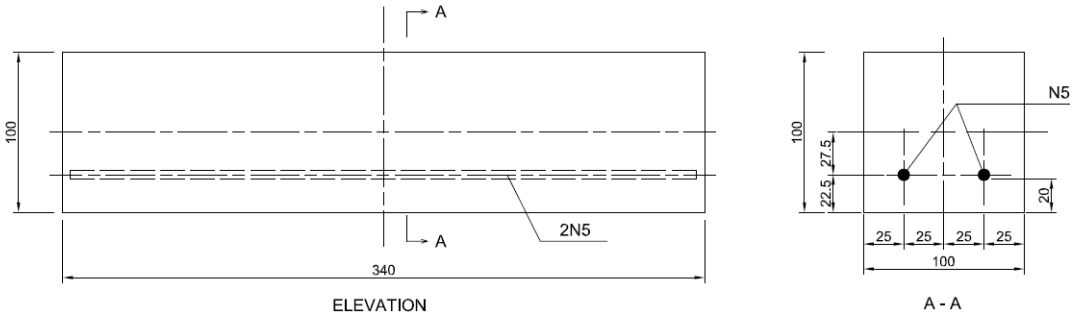

(a) Beam with two N5 deformed bars (all dimensions are in mm)

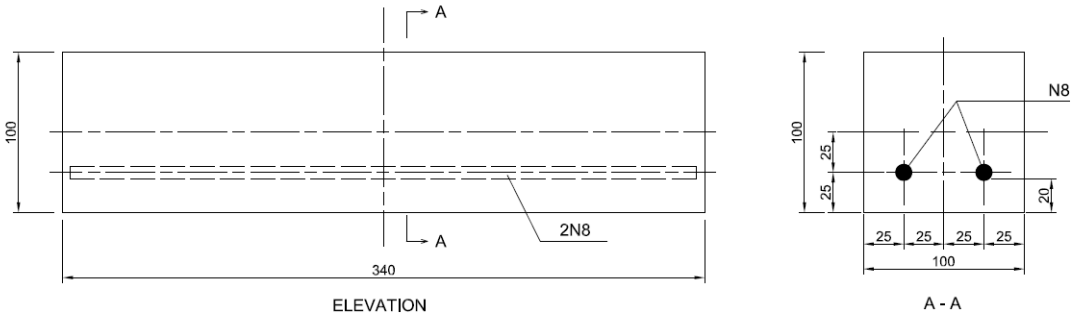

(b) Beam with two N8 deformed bars (all dimensions are in mm)

Figure 5. 1 Detail of reinforcement of small-scale reinforced concrete beam

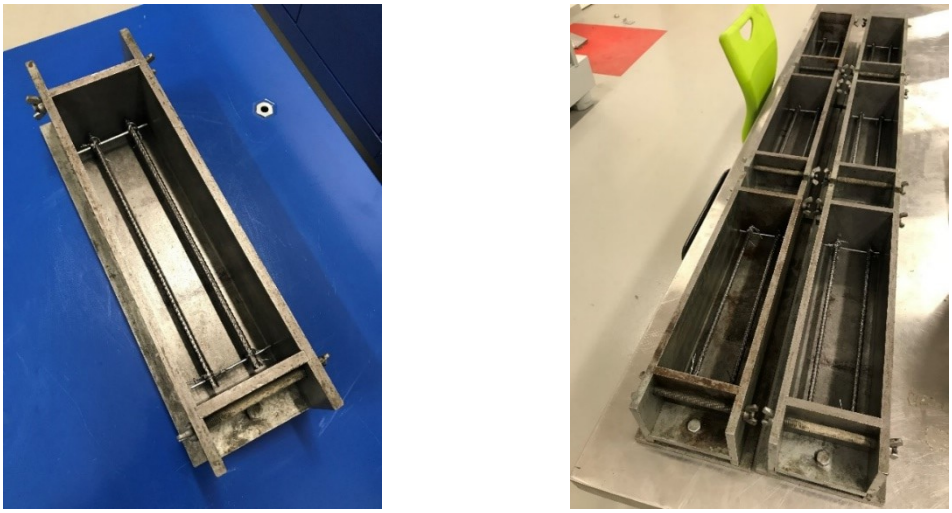

Figure 5. 2 Reinforcing steel bars in steel moulds

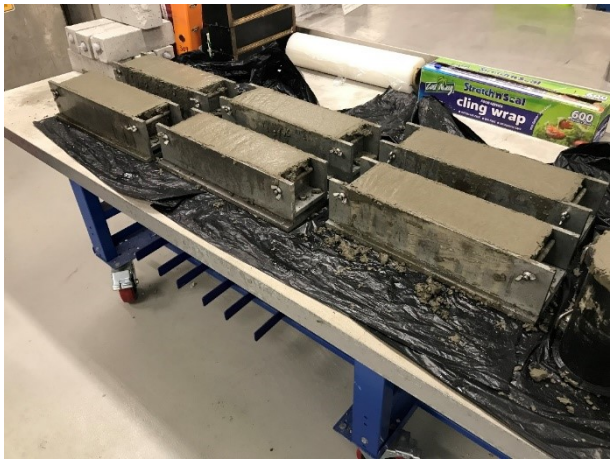

(a) Beams with two N5 deformed bars

(b) Beams with two N8 deformed bars, cylinders and prisms

Figure 5. 3 Specimens cast for flexural and shear test

Plain Ø100 mm (diameter) × 200 mm cylinders and 75 × 75 × 285 mm size prisms were also cast. The cylinders were used for mechanical properties test and the prisms were used for free expansion measurement.

Due to the limited capacity of the autoclave for accommodating the specimens, the twelve small-scale reinforced concrete beams were cast in two batches and tested separately.

After casting, the specimens were covered with plastic sheets and kept in the laboratory at a room temperature of 23 °C for 24 hours. At the following day after casting, the specimens were demoulded. In order to measure the free expansion of the concrete prisms, an initial length reading by using a digital comparator was made on the prisms with embedded stainless-steel studs, after demoulding. This initial length was used to calculate the subsequent ASR expansion of the prisms. An initial mass reading of the prisms was also recorded. The recorded initial mass reading is for analysing the corresponding mass change under accelerated ASR test. All the specimens were then moved into a temperature-humidity controlled cabinet which was maintained at 23 °C and 90% RH. At the age of 28 days, the specimens were removed from the temperature-humidity controlled cabinet and subjected to tests as described in Chapter 5.2.3 to Chapter 5.2.6.

5.2.3 ASR Acceleration

The prisms were taken out of the humidity cabinet and the lengths and masses were recorded and then placed in the autoclave (Zirbus LVSA 50/70 model with a chamber volume of 153 litres) for accelerated temperature cycles. Selected number of cylinders were also placed in the autoclave as shown in Figures 5.4.

The ASR acceleration adopted 3 cycles at a steam warming temperature of 80 °C. Each cycle of steaming duration is 60 hours and totally three cycles of steaming were applied.

It should be noted that, at 80 °C steam warming temperature, the pressure inside the autoclave chamber was maintained at atmospheric pressure. The temperature-time relationship of steam warming for three cycles is shown in Figure 4.2 of Chapter 4.

Figure 5. 4 Specimens as placed in the Zirbus LVSA 50/70 autoclave

The expansion of the prisms at the end of each cycle was recorded to assess the ASR reaction. In parallel, at the end of each cycle, selected number of cylinders were taken out for mechanical property testing. One reinforced concrete beam was taken out for load carrying capacity testing.

5.2.4 Expansion and Mass Change Measurements

Initial length and mass readings of the prisms with embedded studs were recorded for expansion measurements and change of mass after demoulding. All the specimens were then stored in 23 °C and 90% RH temperature-humidity controlled cabinet until testing.

At the age of 28 days the specimens were taken out from the cabinet. Lengths and masses

of the prisms were recorded again. The specimens were then placed in the autoclave for accelerating ASR.

After each cycle of autoclaving, the prisms were taken out of the autoclave and an immediate measurement on masses of the prisms were made. Afterwards, the prims were cooled down to room temperature at 23 °C then the lengths were recorded. Figure 5.5 shows the length measurement of the prisms.

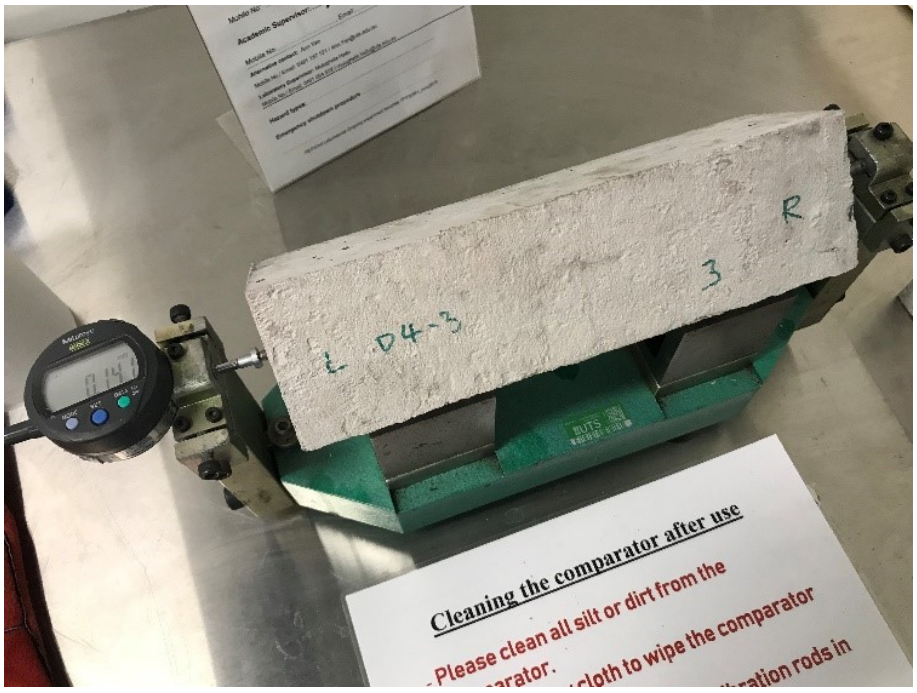

Figure 5. 5 Length measurement using a comparator

5.2.5 Testing of Mechanical Properties

Modulus of elasticity and compressive strength tests on Ø100 mm (diameter) × 200 mm cylinders with 2.5% Na_2O_{eq} by mass of cement alkali loading were performed previously in Chapter 4. First, after 28 days of moist curing in a humidity cabinet (23 °C, 90%RH), totally three cylinders were tested for obtaining the 28-day modulus of elasticity according to AS 1012.17:2014. The cylinders were then tested for compressive strength following procedure recommended by AS 1012.9:2014. After each steam warming cycle,

totally three cylinders were tested for modulus of elasticity then compressive strength. Figure 5.6 shows the set up for modulus of elasticity test for cylinder.

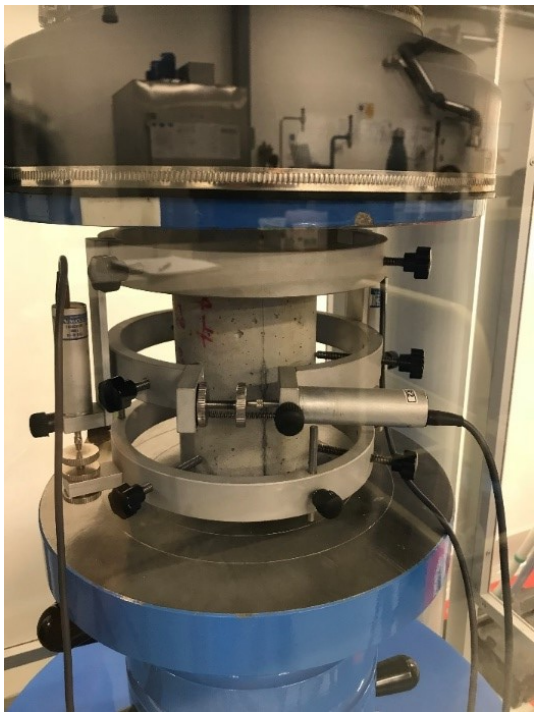

Figure 5. 6 Modulus of elasticity test on 100 mm diameter 200 mm height cylinder

Splitting tensile strength tests on cylinders are performed to study the changing of splitting tensile strength under accelerated autoclave test condition. At the age of 28 days, three cylinders are tested for splitting tensile strength after being moist cured in a humidity cabinet (23 °C, 90%RH), as per recommendation of AS 1012.10:2014. Selected number of cylinders are then placed into the autoclave for 80 °C steam warming cycles. After each cycle of steam warming, selected number of cylinders are taken out of the autoclave for splitting tensile strength testing. For each steam warming cycle, totally three cylinders were tested for splitting tensile strength. Figure 5.7 demonstrates the splitting tensile strength test of cylinder.

Figure 5. 7 Splitting tensile strength test

5.2.6 Load Capacity Test under Four-Point Loading

Figure 5.8 illustrates a schematic four-point loading set up for testing for the load carrying capacity of the small-scale reinforced concrete beams. The cross-section of the small-scale reinforced concrete beams is 100 mm by 100 mm and the length is 340 mm. The span length is 300 mm and it is divided in three 100 mm intervals. Locations of the support points and the loading points were marked on the beam prior to test setting up. To measure the displacement and strain, and also to capture the crack propagation during flexural load testing, a real-time DIC system Mercury RT® was used in this study. As the surface of reinforced concrete beam has weak texture information, marking is necessary to provide distinctive texture for DIC. Therefore, the side surface of the beam between the two loading points is marked with dots roughly at an interval of 5 mm to 10 mm using a marking pen. By this way, it can create contrast on the beam surface and facilitate the capturing of movement of the beam by DIC during load testing.

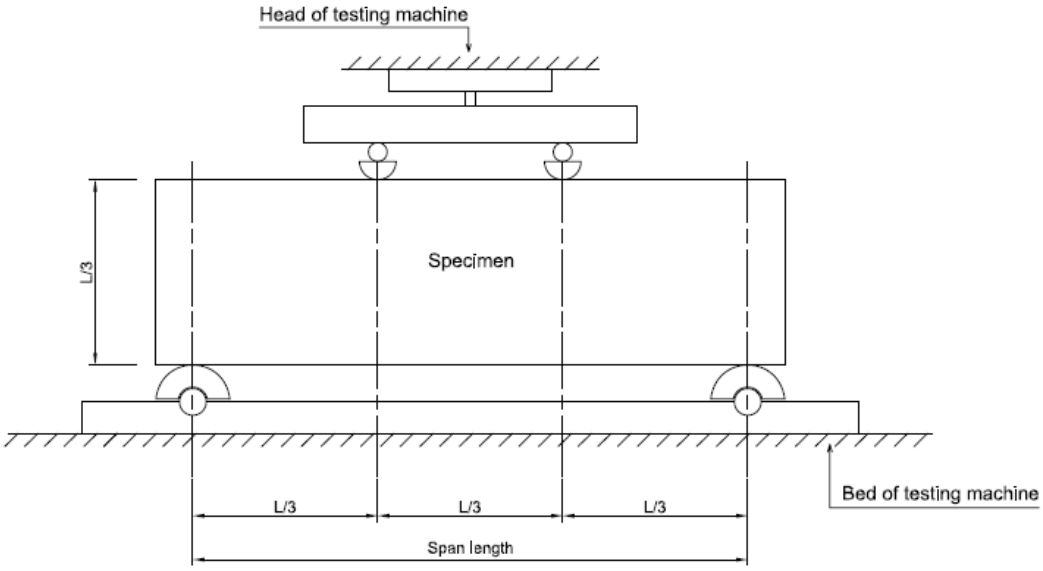

Figure 5. 8 Schematic test set up for load capacity test (adapted from ASTM C78)

Two-dimensional DIC (2D-DIC) as illustrated in Figure 5.9 was adopted in the test to perform the in-plane displacement and strain measurement. As a non-contacting image-based technique, DIC has its distinctive advantages, such as convenient in experimental setting up, high resolution and easy to operate. The unique advantages of DIC have made this technique prevalent in different areas of applications for full-field displacement and strain measurement, including experimental mechanics, material science, civil engineering and some other new areas.

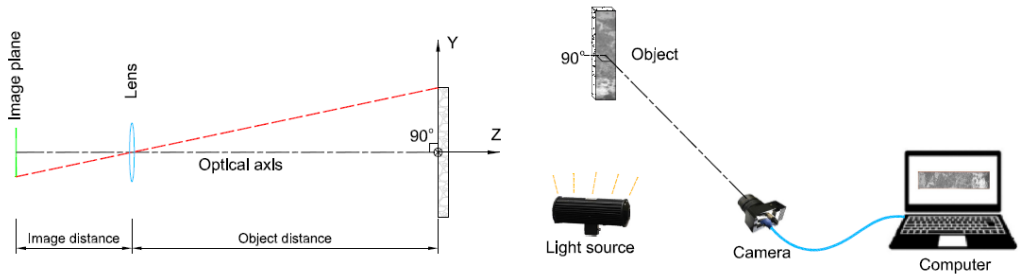

Figure 5. 9 2D-DIC imaging systems

After the beam was placed over the roller supports, with a span of 300 mm, the upper loading head of the test machine was then lowered down. Initial load reading from the

test machine was controlled between 0.5kN to 1kN to ensure the loading apparatus was securely in touch with the beam. Then, the 2D-DIC system was set up. First, a mono camera was selected, and two light sources were turned on and pointed towards the area of measurement. Second, aperture and focus of the camera were adjusted appropriately to ensure the images captured by the camera can provide sufficient information for correlation. Third, camera calibration for distortion compensation was performed and a coordinate system was properly set for measurement. Afterwards, the area of interest (AOI) was defined. Appropriate point probes for displacement measurement, line probes for measuring the change of distance between points, and area for full-field measurements if needed were also applied.

Deflection of the beam at midspan is also measured by a laser sensor located beneath the beam to capture the load-deflection of the beam when loading to fail. A loading rate with 0.1 mm/min is adopted to test the beam to failure under displacement-controlled mode.

Figure 5.10 shows the setup of the load carrying capacity test of small-scale reinforced beams tested under four-point loading.

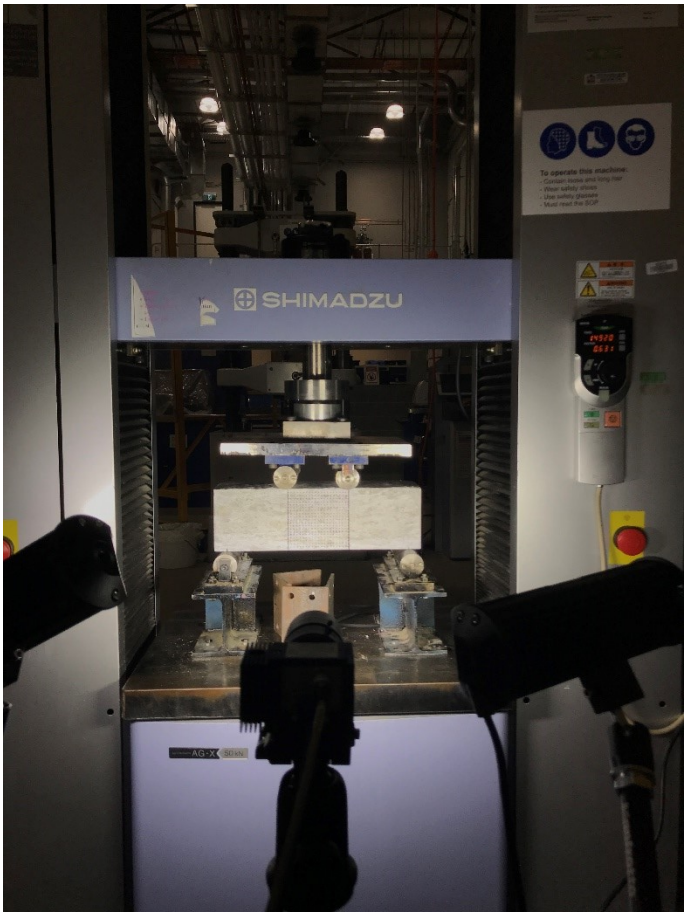

Figure 5. 10 Testing of reinforced concrete beams under four-point loading with 2D-DIC system

5.3 Results and Discussion

5.3.1 Cracking of Specimens

The crack patterns of concrete cylinders and small-scale reinforced concrete beams, with 2.5% Na_2O_{eq} boosting after 3 cycles in the autoclave are shown in Figures 5.11 to 5.12. As can been seen, the external cracks on the surface of concrete cylinders and small-scale reinforced concrete beams are map pattern hairline cracks, which resemble the crack pattern on ACPT specimen after 6 months reported by (Gautam & Panesar 2017).

Figure 5. 11 Crack pattern of cylinders after 3 cycles of autoclaving

Figure 5. 12 External cracks on reinforced beam after 3 cycles in the autoclave

White exudations can be observed on surface of the specimen after each autoclaving cycle. Figure 5.13 shows the typical white exudation on the surface of small-scale reinforced concrete beam.

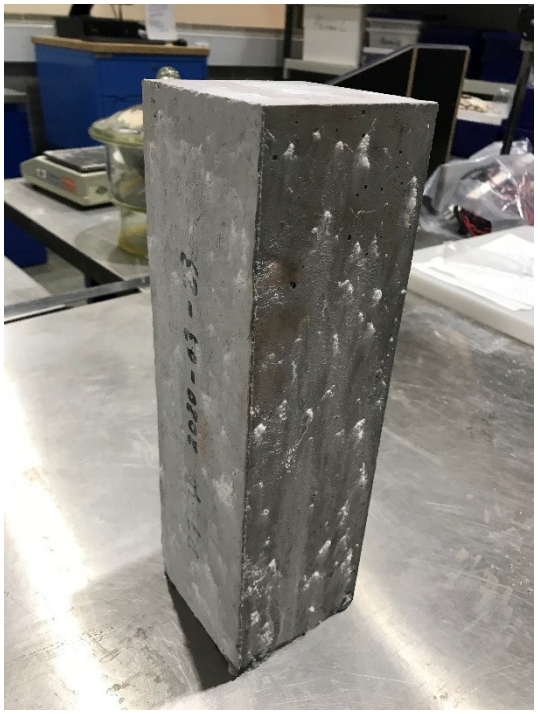

Figure 5. 13 White exudation on surface of small-scale reinforced concrete beam after 2nd cycle of autoclaving

5.3.2 Length Change of Concrete Prisms

Length change of the three concrete prisms from the time of demoulding and after 3 cycles in the autoclave is shown in Figure 5.14. In the temperature-humidity controlled cabinet, during storage up to the age of 28 days, a slight shrinkage of 0.019% was recorded. After that, the specimens were subjected to 80 °C steam warming cycles in autoclave. It can be seen that the length of the prisms increases with the steam warming cycles. After the 3 cycles in the autoclave, a total average expansion of about 0.18% was recorded.

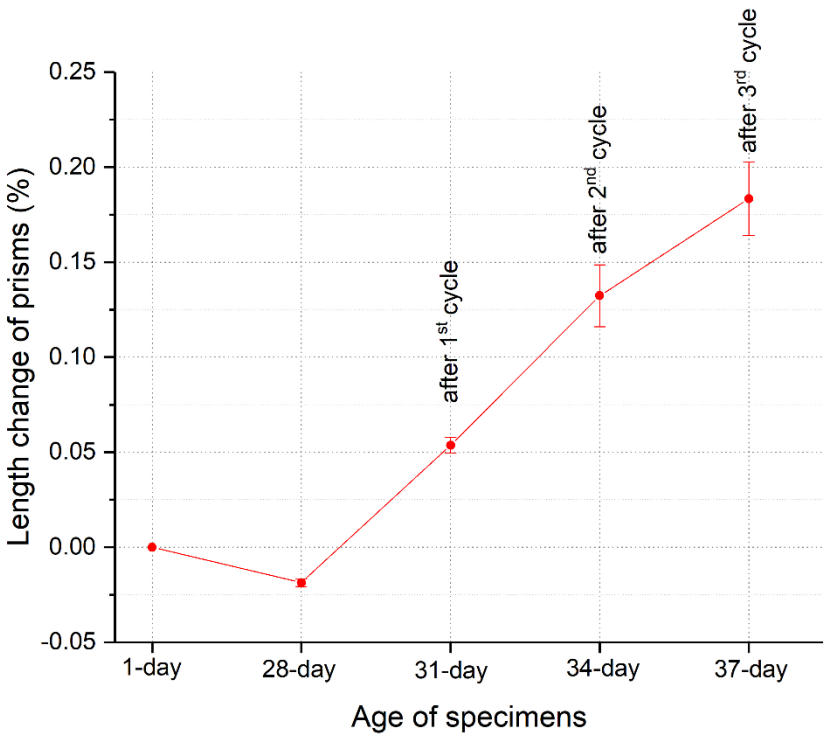

Figure 5. 14 Length change of concrete prisms after 3 cycles in the autoclave

5.3.3 Modulus of Elasticity

Figure 5.15 shows the change of modulus of elasticity after 1, 2 and 3 cycles of 80°C autoclaving compared with the 28-day value. With respect to the modulus elasticity at 28 days, a reduction of 24.5%, 37.9% and 39.0% was recorded after 1, 2 and 3 cycles, respectively. The reduction in modulus of elasticity could be attributed to the microcracking of the material due to accelerated ASR.

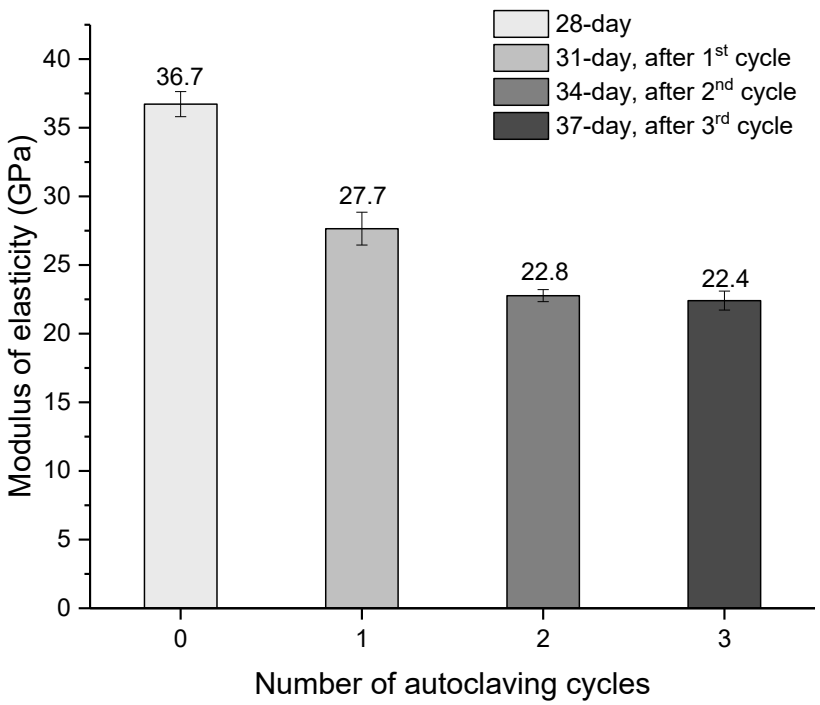

Figure 5. 15 Change in modulus of elasticity of concrete cylinders

Details of modulus of elasticity test results can be found in Table B.1 of Appendix B. The stress-strain behaviour obtained from modulus of elasticity tests are recoded in Appendix B Figure B.1 to Figure B.4.

5.3.4 Compressive Strength

Figure 5.16 shows the change in compressive strength of cylinders after 1, 2 and 3 cycles of 80°C autoclaving compared with the 28-day value. The compressive strength test results are given in Table B.2 of Appendix B.

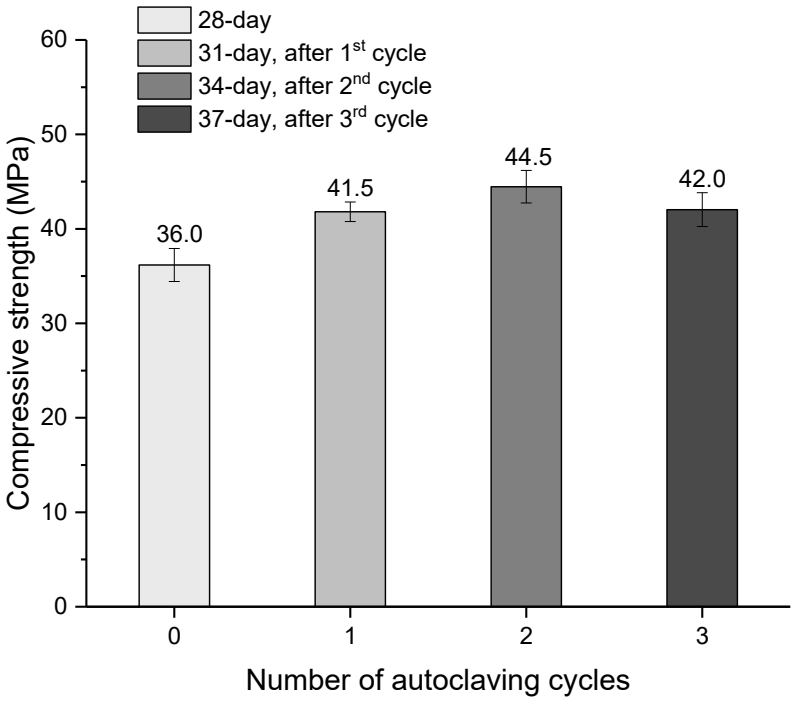

Figure 5. 16 Change in compressive strength of cylinders

For concrete with 2.5% alkali boosting, after 3 cycles of 80 °C autoclaving, no dis-earnable changes in compressive strength were noticed compared to the 28-day compressive strength. As it can be seen that, up to expansion level about 0.13%, the compressive strength was improved by 15.3% and 23.6% after the first and second cycle respectively, with respect to the 28-day compressive strength. Thereafter, the compressive strength showed a decreasing trend while expansion keeps increasing. The gain in compressive strength dropped to 16.7% as the expansion developed to 0.18% at the end of the third cycle. It is expected that the compressive strength will continue to decrease with the increasing of expansion in concrete.

5.3.5 Splitting Tensile Strength

Splitting tensile strength test are performed for cylinders after 28 days of moist curing in a humidity cabinet (23 °C, 90%RH). The rest cylinders are then put into an autoclave for 80 °C steam warming cycles. After each cycle of autoclaving, totally three cylinders were

tested for splitting tensile strength. Figure 5.17 shows the change in splitting tensile strength of cylinders after 1, 2 and 3 cycles of 80°C autoclaving compared with the 28-day value. Results of splitting tensile strength tests are provided in Table B.3 of Appendix B.

Similar to compressive strength, for concrete with 2.5% alkali boosting, it was observed that the splitting tensile strength increased initially with the autoclaving cycles, after 2nd cycle of autoclaving, it started to show a decreasing trend.

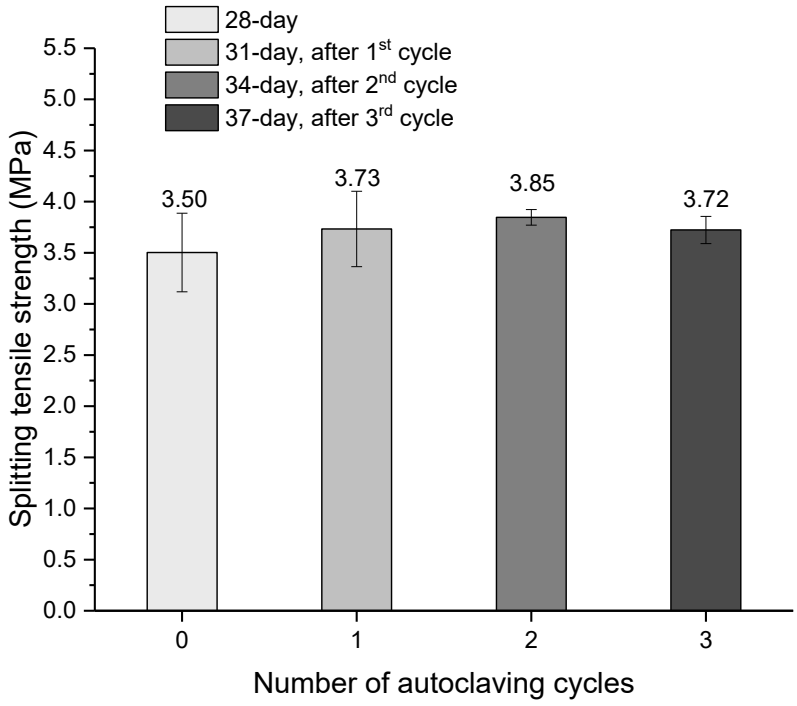

Figure 5. 17 Change in splitting tensile strength

5.3.6 Load Capacity of Reinforced Concrete Beams

5.3.6.1 Test results of the small-scale beams with two N5 rebars

The load capacity test value of the small-scale reinforced concrete beams with two N5 reinforcing bars are given in Table 5.2 and Figure 5.18. Load capacity test results of

small-scale reinforced concrete beams with two N5 reinforcing bars revealed that flexural capacity is not significantly influenced under accelerated test.

Table 5. 2 Load capacity test results of N5 rebar beams

Testing time	Small-scale RC Beam Name	Load (kN)	Failure mode (Flexural/Shear)
28-day (without autoclaving)	D7-1 (28-day)	35.05	Flexure
	D7-2 (28-day)	39.55	Flexure
	Average	37.30	Flexure
after 1 cycle 80 °C autoclaving	D7-3 (1 cycle)	36.54	Flexure
after 2 cycles 80 °C autoclaving	D7-4 (2 cycles)	37.49	Flexure
after 2 cycles 80 °C autoclaving	D7-5 (3 cycles)	36.43	Flexure

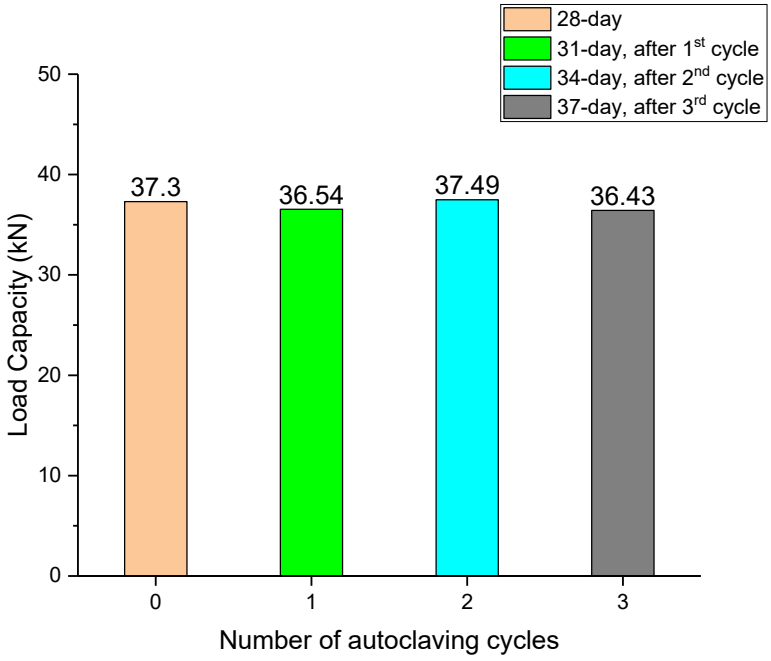

Figure 5. 18 Load capacity test results of small-scale reinforced concrete beam with two N5 deformed bars

Figure 5.19 to 5.23 show the experimental load versus mid-span deflection curves and the failure mode of the small-scale reinforced concrete beams with two N5 reinforcing bars, under four-point loading. It can be seen that all the small-scale reinforced concrete beams with two N5 reinforcing bars are failed in flexure. Flexural cracks can be observed between the point loadings of the loading head. The flexural crack develops from the tension side with the increasing loading and gradually extend upwards. Upon yielding of the reinforcing bars, deflection of the beams keeps increase while the load shows no increasing. In addition, there is no sudden failure occurred for all the small-scale reinforced concrete beams with two N5 reinforcing steel bars.

(a)

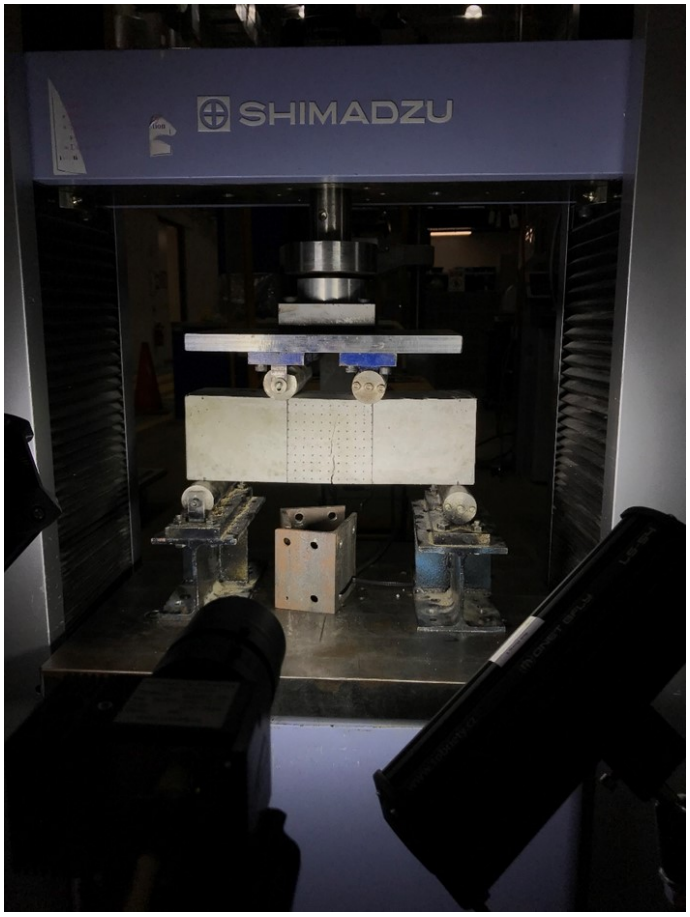

(b)

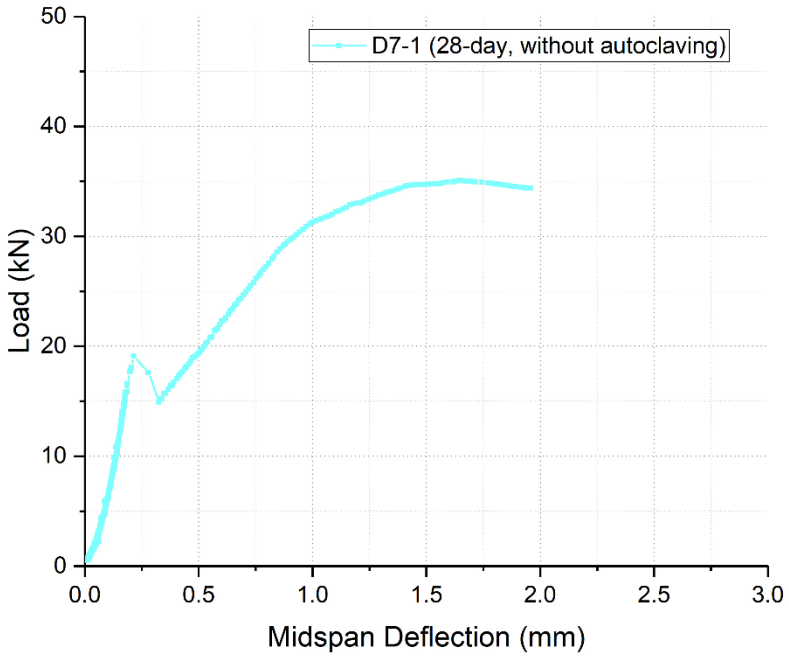

Figure 5. 19 Beam D7-1: (a) Failure mode; (b) Load-displacement curve

(a)

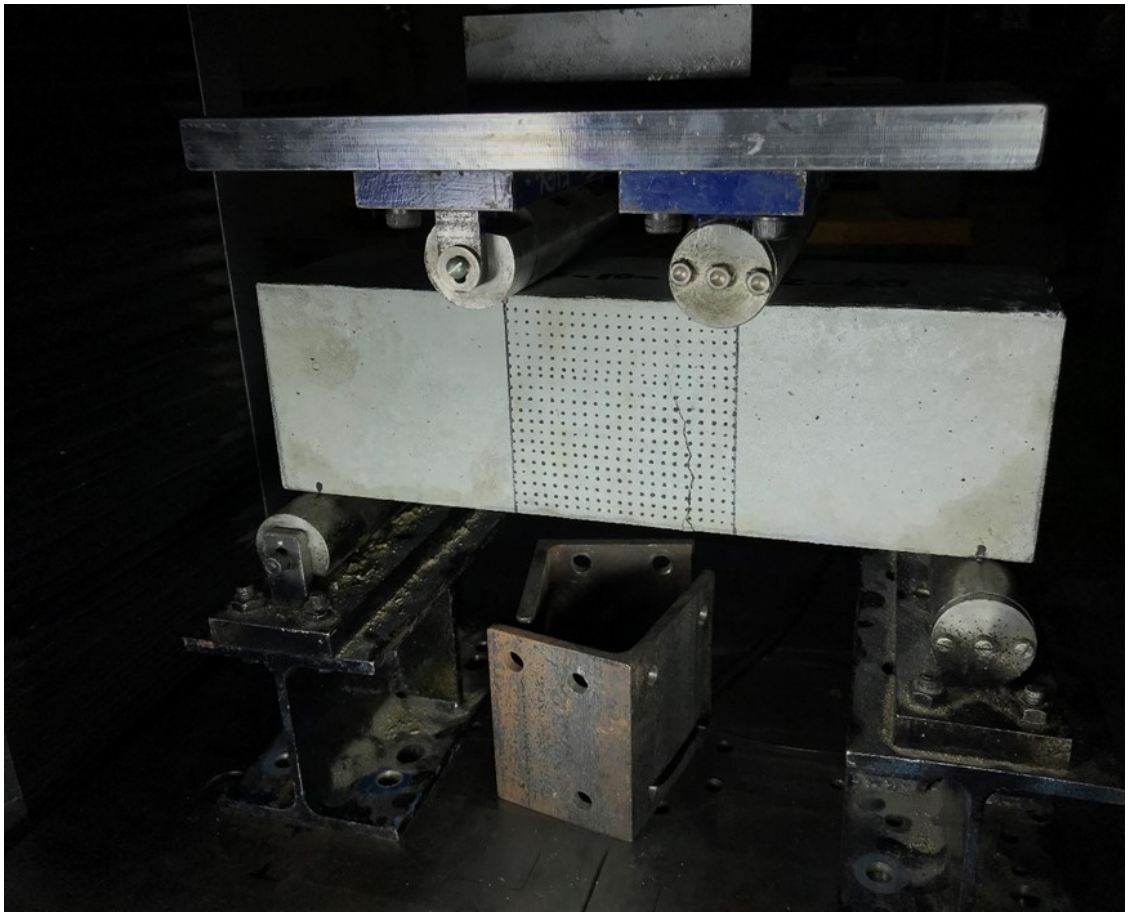

(b)

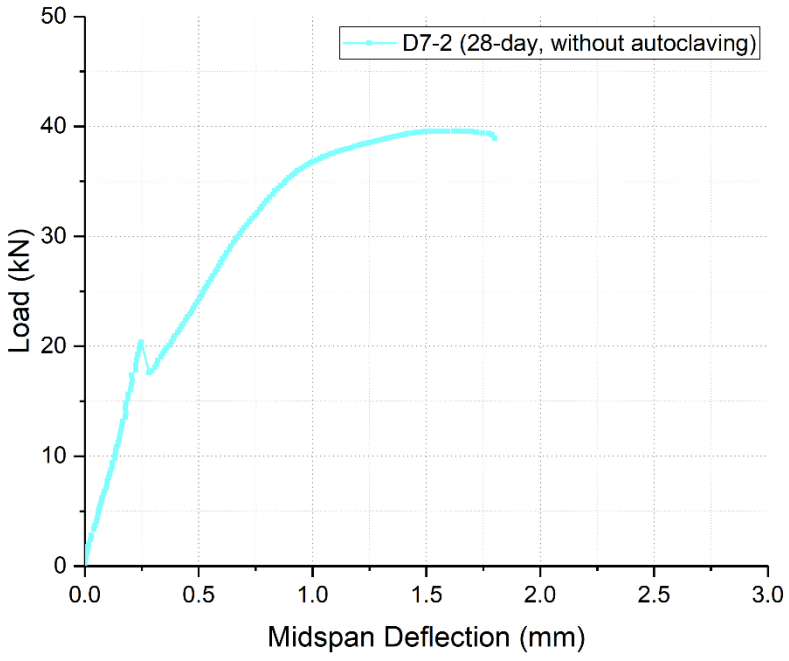

Figure 5. 20 Beam D7-2: (a) Failure mode; (b) Load-displacement curve

(a)

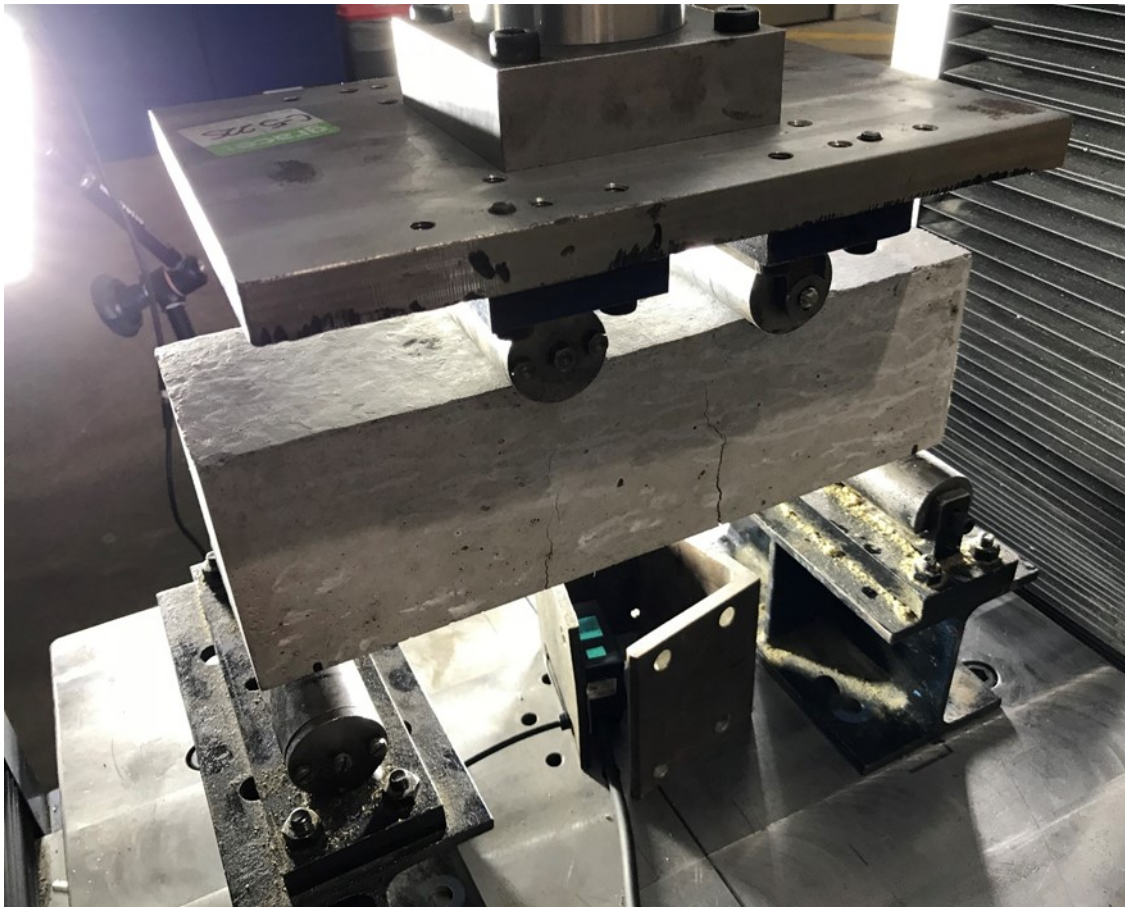

(b)

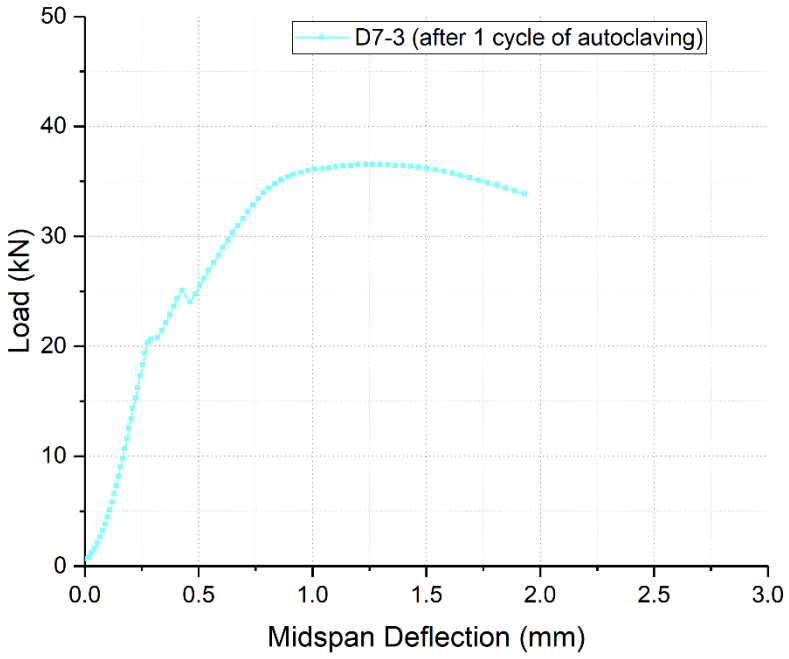

Figure 5. 21 Beam D7-3: (a) Failure mode; (b) Load-displacement curve

(a)

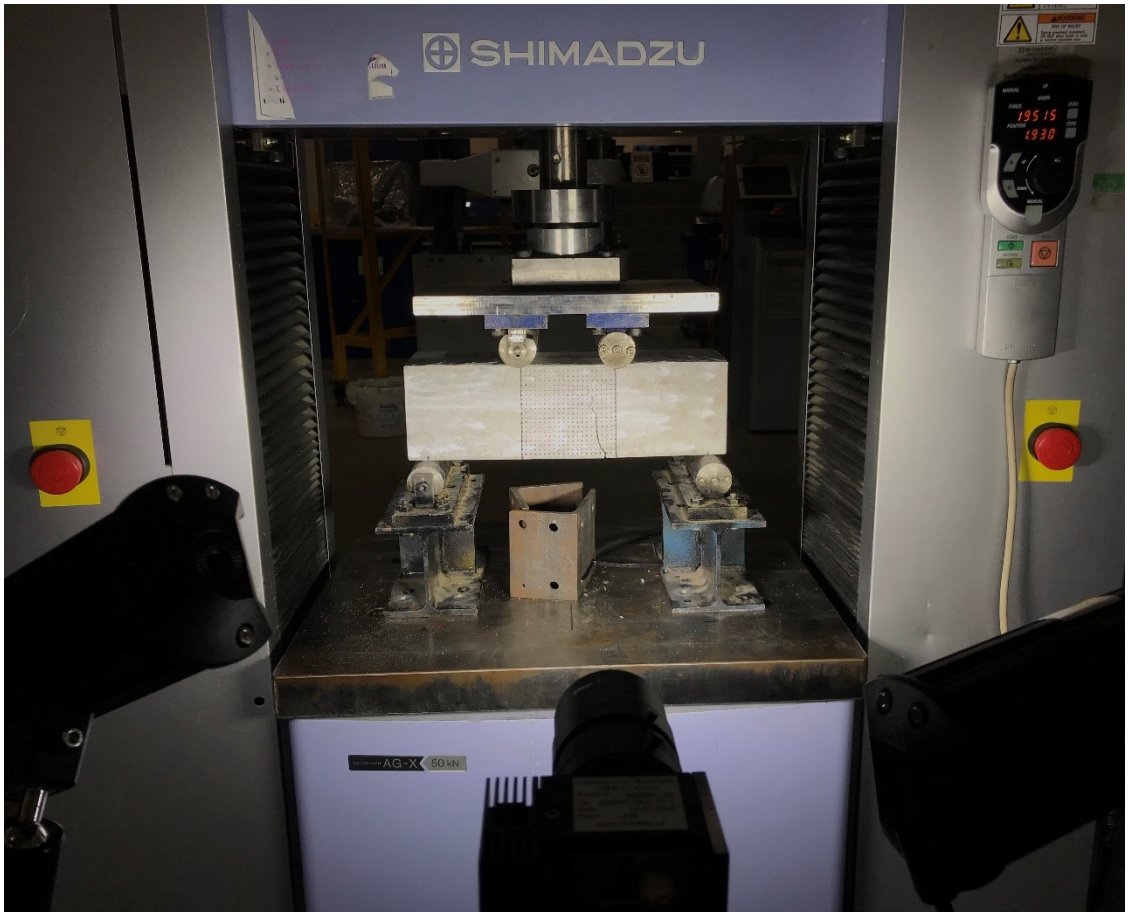

(b)

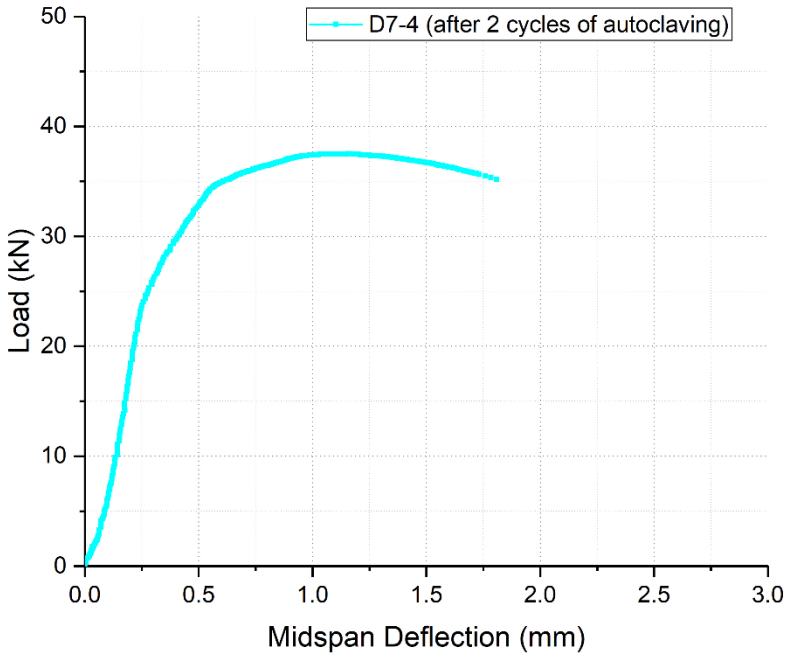

Figure 5. 22 Beam D7-4: (a) Failure mode; (b) Load-displacement curve

(a)

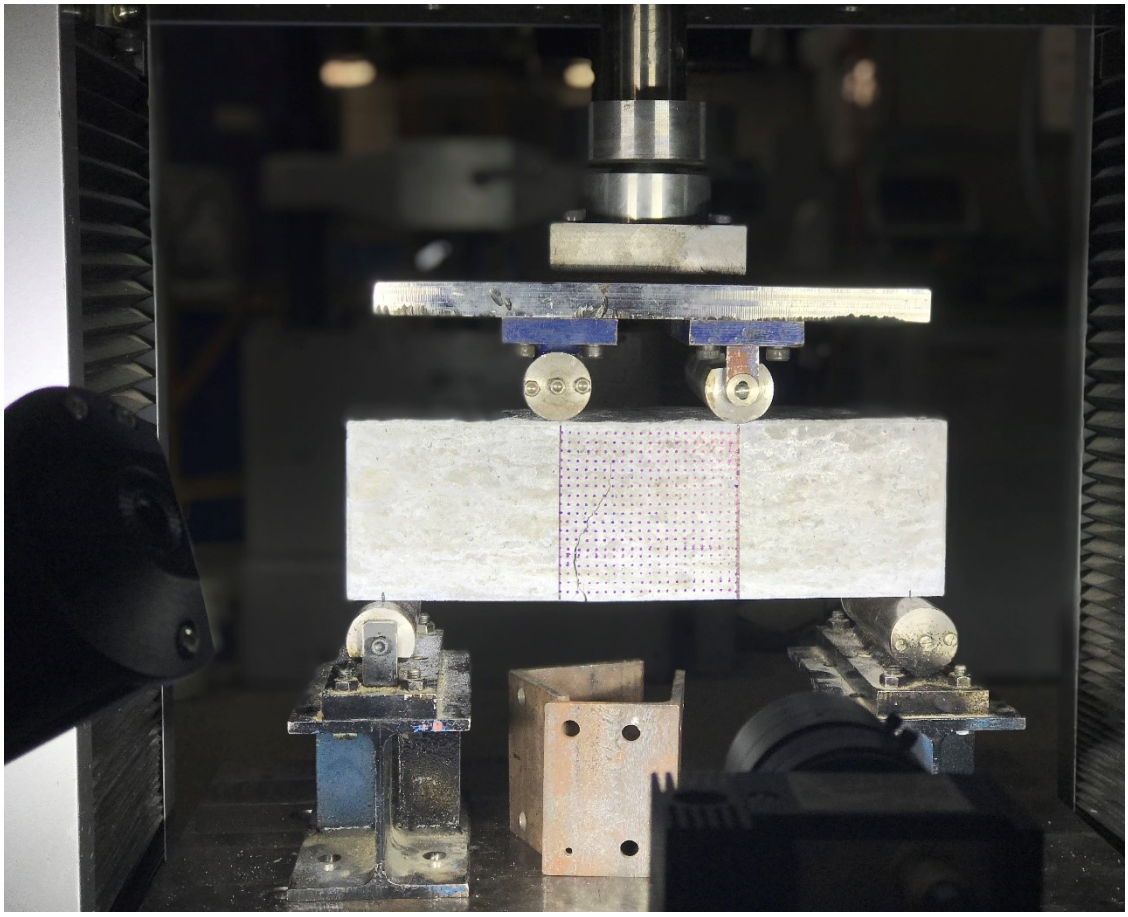

(b)

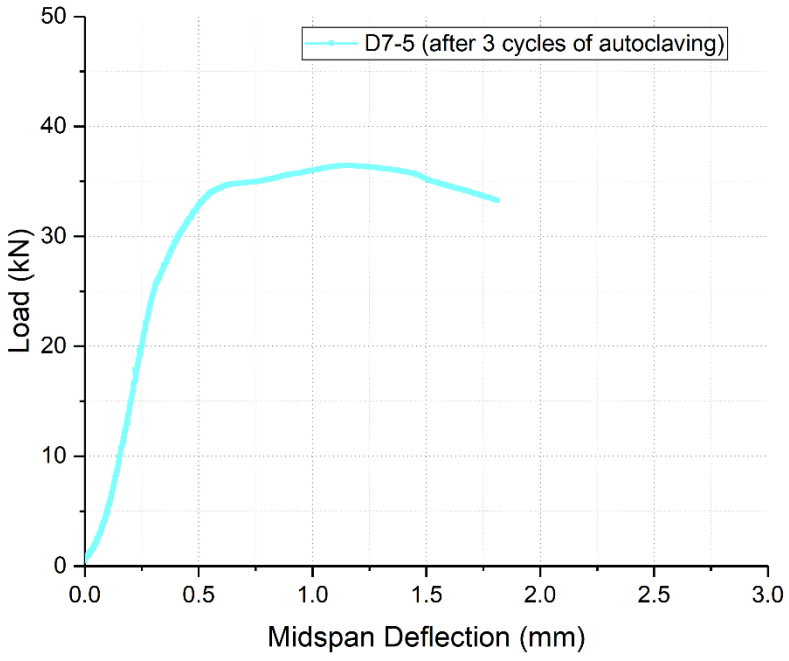

Figure 5. 23 Beam D7-5: (a) Failure mode; (b) Load-displacement curve

5.3.6.2 Test results of small-scale beams with two N8 rebars

Load capacity test results for the small-scale reinforced concrete beams with two N8 deformed reinforcing bars are shown in Table 5.3 and Figures 5.24 to 5.29.

Table 5. 3 Load capacity test results of N8 rebar beams

Test time	Small-scale RC Beam Name	Load (kN)	Failure mode (Flexural/Shear)
28-day (without autoclaving)	D4-1 (28-day)	46.88	Shear
	D4-2 (28-day)	51.20	Shear
	Average	49.04	Shear
after 1 cycle 80 °C autoclaving	D4-3 (1 cycle)	60.85	Shear
after 2 cycles 80 °C autoclaving	D4-4 (2 cycles)	57.37	Shear
after 2 cycles 80 °C autoclaving	D4-5 (3 cycles)	53.16	Shear

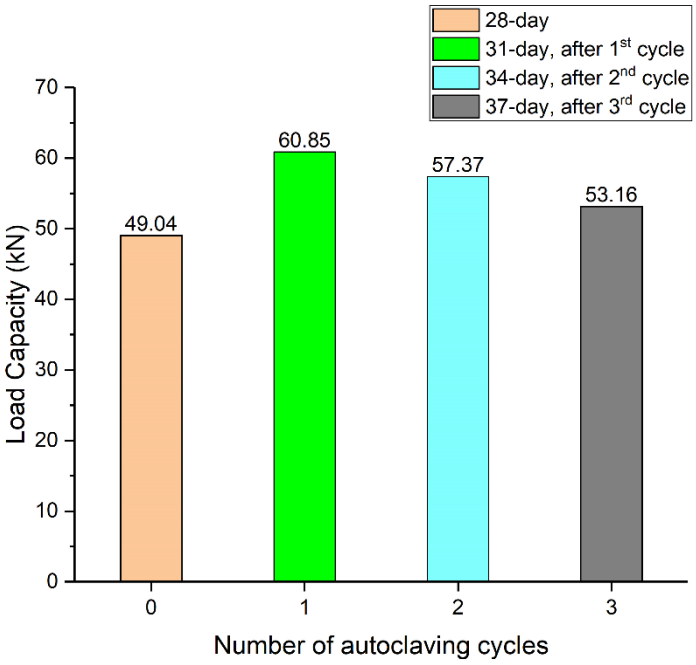

Figure 5. 24 Load capacity test results of small-scale reinforced concrete beam with two N8 deformed bars

(a)

(b)

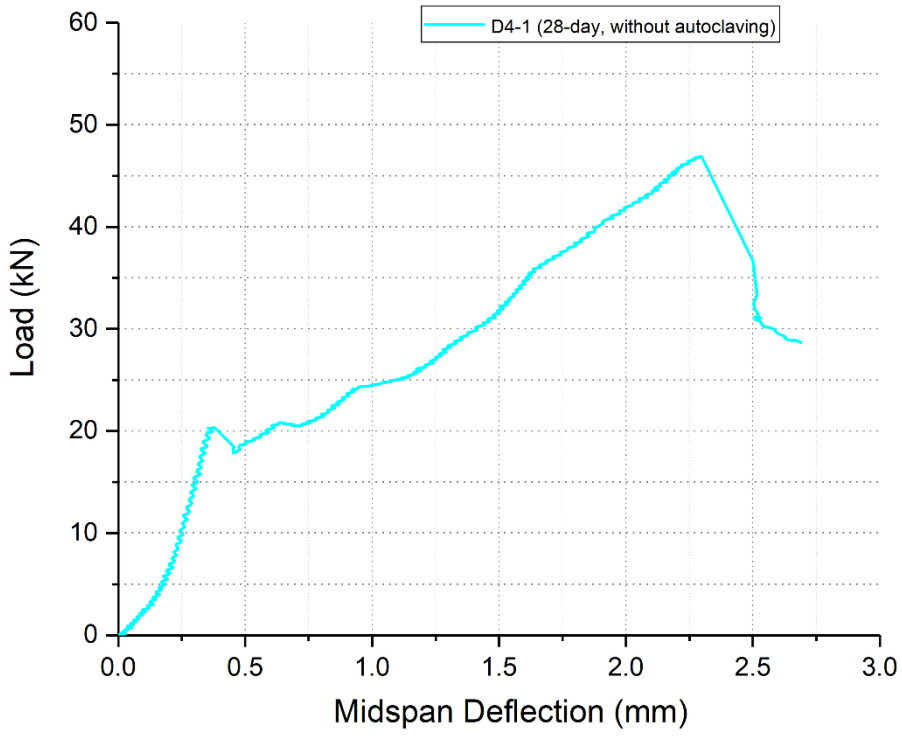

Figure 5. 25 Beam D4-1: (a) Failure mode; (b) Load-displacement curve

(a)

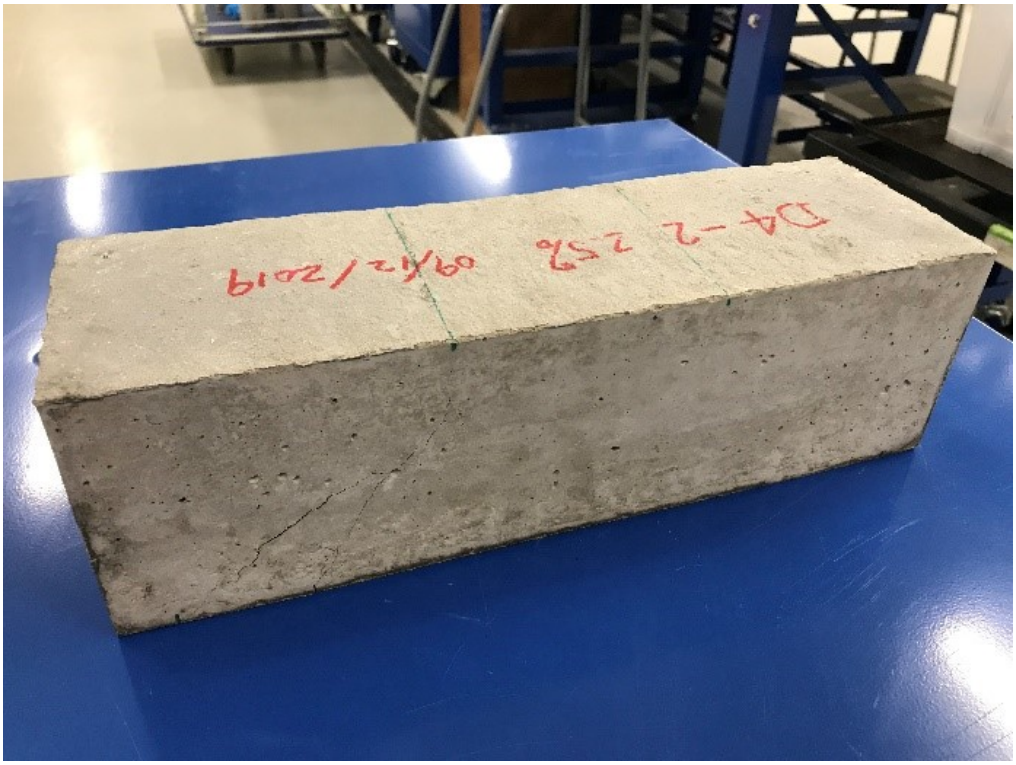

(b)

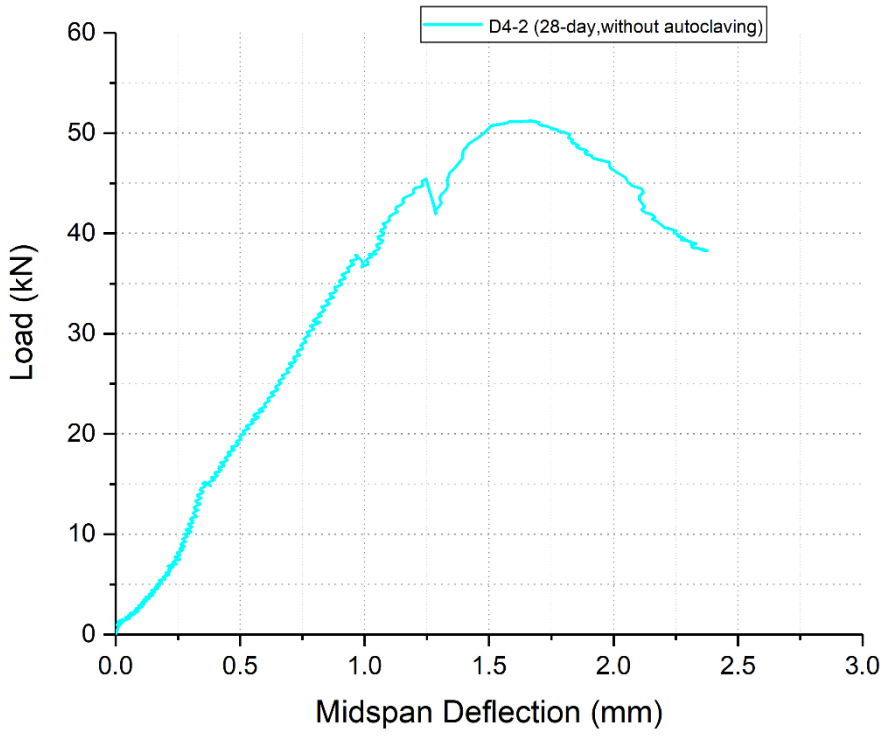

Figure 5. 26 Beam D4-2: (a) Failure mode; (b) Load-displacement curve

(a)

(b)

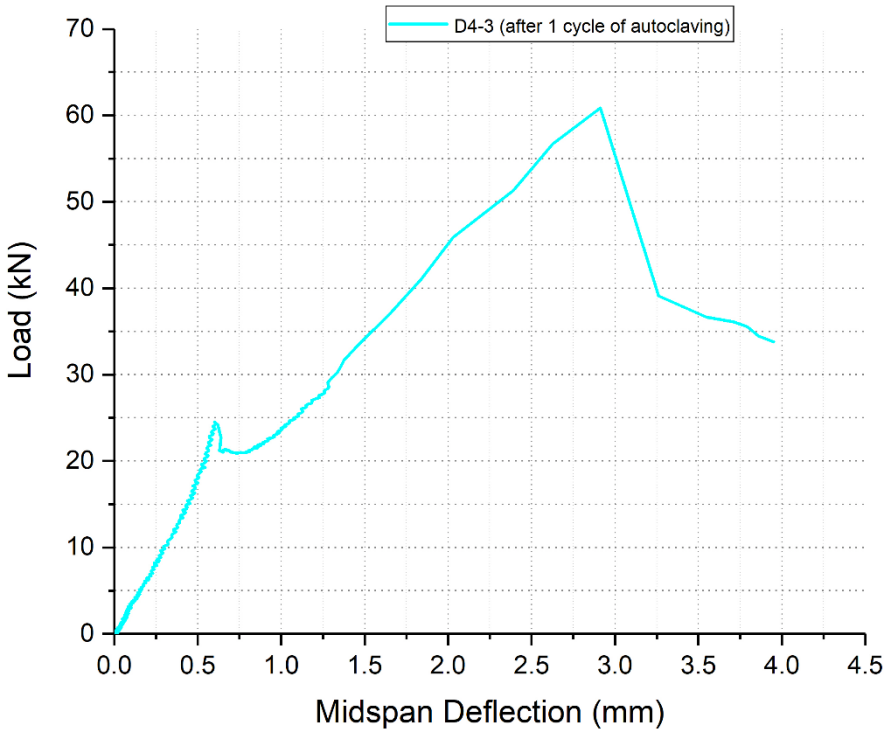

Figure 5. 27 Beam D4-3 after 1 cycle of autoclaving: (a) Failure mode; (b) Load-displacement curve

(a)

(b)

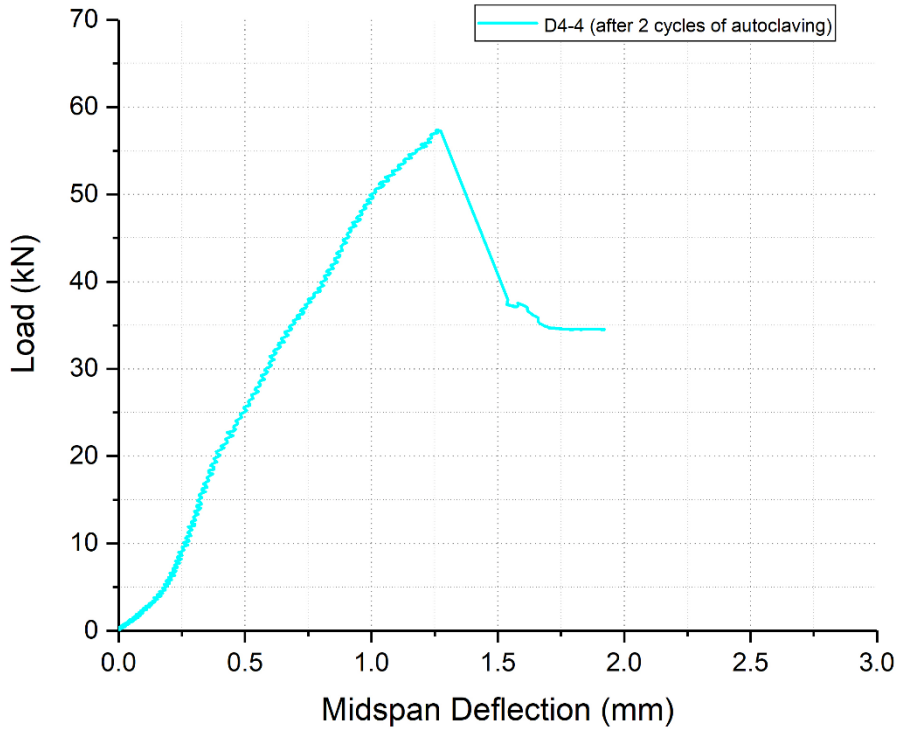

Figure 5. 28 Beam D4-4 after 2 cycles of autoclaving: (a) Failure mode; (b) Load-displacement curve

(a)

(b)

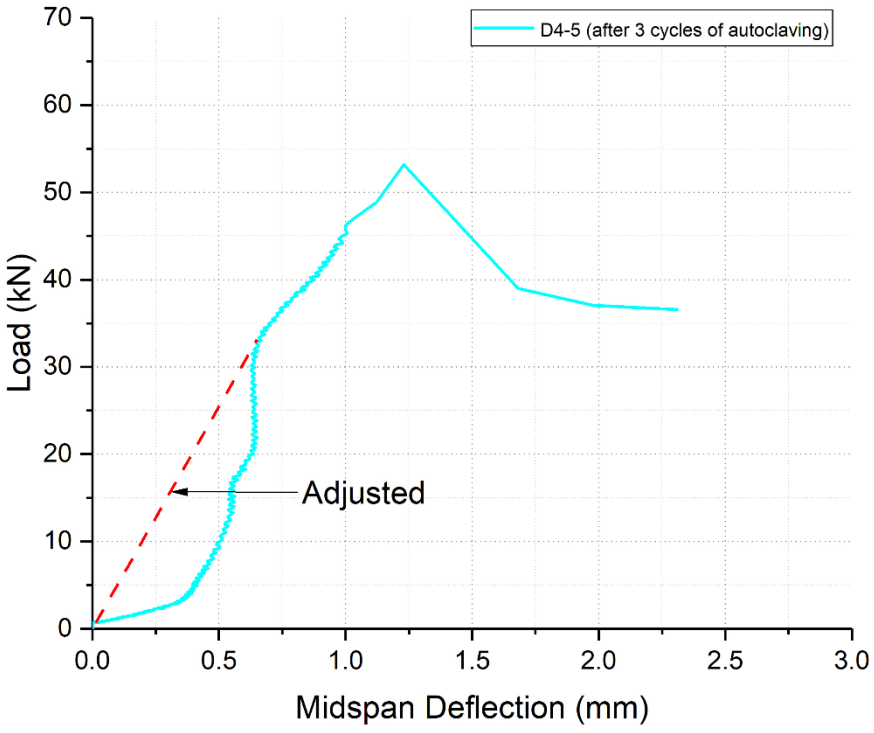

Figure 5. 29 Beam D4-5 after 3 cycles of autoclaving: (a) Failure mode; (b) Load-displacement curve

Load carrying capacity test on small-scale reinforced concrete beams with two N8 deformed reinforcing bars showed that all the beams failed in shear. For the two beams tested at the age of 28-day without autoclaving, the first beam (D4-1) initially exhibited flexural crack between the two loading points when the load reached 20kN, afterwards, the flexural crack developed with the increasing load. When the load increased to 46.88 kN, the beam failed suddenly in shear, with diagonal shear crack from the supporting point to the loading point (Figure 5.25). However, there was no flexural crack on the second beam during loading. Upon the load reaching 51.20kN, the second beam also failed in sudden shear failure. Shear cracks can be observed between the supporting point and the loading point (Figure 5.26). Due to flexural crack, beam D4-1 showed more ductility than beam D4-2, as can be seen from the load-deflection curves, beam D4-1 recorded a 2.8 mm mid-span deformation before sudden shear failure, whereas beam D4-2 experienced a 1.6 mm mid-span deflection before sudden shear failure. Similar to beam D4-1, flexural crack first appeared between the two loading points when beam D4-3 was subjected to loading. But the crack loading of beam D4-3 showed a 25% improvement than that of the beam D4-1, with a recorded value of about 25kN. This could be attributed to the prestress effect due to ASR expansion, as beam D4-3 had experienced one cycle of 80 °C autoclaving. In addition, shear capacity of beam D4-3 showed about 20% higher than the average shear capacity of beam D4-1 and beam D4-2. Moreover, beam D4-3 exhibited similar ductility relative to beam D4-1 (Figure 5.27). Beam D4-4 (after 2 cycles of 80 °C autoclaving) and beam D4-5 (after 3 cycles of 80 °C autoclaving) showed similar response when subjected to loading. No flexural crack was observed, and the two beams all failed suddenly in shear failure, with diagonal crack extended from the supporting point to the loading point. Although the failure loads of beam D4-4 and beam D4-5 are still higher than the average shear capacity of beam D4-1 and beam D4-2, ductility of

beam D4-4 and beam D4-5 showed a decreasing trend, compared to that of the beam D4-2. However, the flexural stiffness of beam D4-4 and beam D4-5 was enhanced with regards to beam D4-1, beam D4-2 and beam D4-3. This again could be attributed to the prestress effect due to larger ASR expansion, as beam D4-4 and beam D4-5 experienced 2 cycles and 3 cycles of 80 °C autoclaving, respectively (Figure 5.28 and 5.29).

5.5 Summary

In order to study the effect of ASR on the flexural and shear capacity of the ASR-affected reinforced concrete beams, this chapter performed load capacity tests on small-scale reinforced concrete beams at the age of 28 days and subsequent 1, 2 and 3 cycles of 80°C autoclaving, with 60 hours per cycle. After 3 cycles of 80 °C autoclaving, an average free expansion of about 0.18% was recorded. Based on the test results, main findings are summarised as follows:

(1) The cracking load of the beams subjected to 1, 2 and 3 cycles of 80 °C autoclaving was improved compared to that of the 28-day specimens, due to the prestressing effect induced by ASR expansion.

(2) Although modulus of elasticity of concrete cylinders decreased about 24.5%, 37.9% and 39.0% after 1, 2 and 3 cycles compared to the 28-day value, respectively, the flexural stiffness of the beams subjected to 1, 2 and 3 cycles of 80 °C autoclaving does not show any measurable reduction due to the presence of reinforcement.

(3) Shear resistance of small-scale beams with two N8 reinforcing bars was increased after 1, 2 and 3 cycles of 80°C autoclaving, compared with their 28-day counterparts. Again, this could be attributed to the prestressing effect due to ASR expansion.

(4) The beams reinforced with two N5 reinforcing bars are all failed in flexure. Flexural capacity of the beams subjected to 1, 2 and 3 cycles of autoclaving, is not significantly influenced by the extent of ASR achieved in the current accelerated autoclave test.

Results suggest that the chemical prestressing induced by ASR expansion could have beneficial effects on strength and stiffness of the affected structure. However, experiment is performed under accelerated test within a short period, long-term field exposure and subsequent more severe ASR expansion could have significant detrimental effect on the flexural and shear behaviour of the affected structure. In field structures, due to the combined effect of live load, dead load, severe environmental exposure condition, and ASR, cracking widths could be larger than in laboratory accelerated test. Larger cracking width not only imposes appearance warning of the ASR affected structure, it may also affect the bond between reinforcement and concrete, increase the risk of corrosion of reinforcement, and ultimately influence the capacity of the affected structure.

Chapter 6

Bond Behaviour Between Reinforcing Steel Bar and ASR Affected Concrete

6.1 Overview

The bond between reinforcing steel bars and the surrounding concrete has vital influence on the performance of reinforced concrete structures, thereby affecting the service life and load-carrying capacity of the structure. The bond failure between concrete and reinforcing steel bar can cause the failure of load transfer between the steel bar and surrounding concrete, affect the resistance of the structure members, and may further lead to the failure of the entire structure, resulting in loss of asset or fatal injuries (Amleh 2000).

6.1.1 Effect of ASR on Bond Characteristics

As mentioned earlier, the bond performance of reinforced concrete is significantly influenced by the strength of the surrounding concrete (Lundgren 2005; Yalciner, Eren & Sensoy 2012), and also the presence of longitudinal crack in concrete cover (Desnerck, Lees & Morley 2015; Tepfers 1979). Previous studies have revealed that ASR can cause cracking of concrete owing to the swelling of ASR gel when it absorbs water, and degradation of mechanical properties of the affected concrete (Barbosa, Hansen, Hansen, et al. 2018; Clark 1990; Esposito et al. 2016; Smaoui et al. 2006). Therefore, concerns about bond between reinforcing steel bar and ASR affected concrete were raised. However, limited publications with regards to this issue have been reported in literature and the results of these studies varied considerably, with even some conflicting findings.

While Swamy & Al-Asali (1989) reported that no distress in bond or anchorage was observed even at 1.3% and 0.52% unrestrained ASR expansion level, Bach, Thorsen & Nielsen (1993) reported that the anchorage strength was reduced due to ASR deterioration and a 20-30% of loss in anchorage strength was recorded through pull-out tests. The reason of these seemingly conflicting findings could be attributed to the different reinforcement details adopted in these studies. When good anchorage and transverse reinforcement were applied, no reduction or a smaller reduction in bond strength for deformed bars would be expected, as ASR expansion will cause tensile stress in the transvers reinforcement, thus confine the concrete and enhance its ability to restrain the splitting cracks (Clark 1989).

After systematically studied the effect of different parameters on bond strength by performing pull-out tests, Chana (1989) reported that if transverse reinforcement exists, ASR does not appear to have detrimental effect on the bond strength, up to a 0.4% unrestrained expansion level. Whereas there is no transverse reinforcement, ASR does reduce the bond strength. When concrete cover to diameter ratio is 1.5, the reduction in bond strength can reach 40-50%. These findings are consistent with results of the pull-out tests presented by Clark (1989), which showed that the reduction in bond strength was less than 10% when transverse reinforcement was supplied, while in condition of no transverse reinforcement was present, the bond strength was approximately halved due to the presence of ASR cracking.

In terms of the influence of ASR expansion level on the bond strength deterioration between reinforcing steel bar and the affected concrete, Haddad & Numayr (2007) investigated the bond strength change with respect to expansion for 18 mm diameter deformed bars using two types of reactive concrete mixes (Mix A and Mix B) with different mix proportions. Pull-out tests were performed at different stages and the change

in bond strength with expansion is shown in Figure 6.1. As can be seen that the bond strength between reinforcing steel bar and the Mix A concrete increases first with the increasing of expansion (to 0.28% unrestrained expansion level). This phenomenon could be attributed to the higher compressive strength of the Mix A. When expansion reaches 0.31%, a reduction of 11% in bond strength is recorded. For Mix B concrete, due to the lower compressive strength and the higher reactive nature of the mix, the bond strength appears to decrease constantly with the increasing expansion in general. At unrestrained expansion of 0.29%, a reduction of 24% in bond strength is achieved. The authors concluded that higher expansion level and severer ASR cracking are needed to cause more significant reduction in the bond strength.

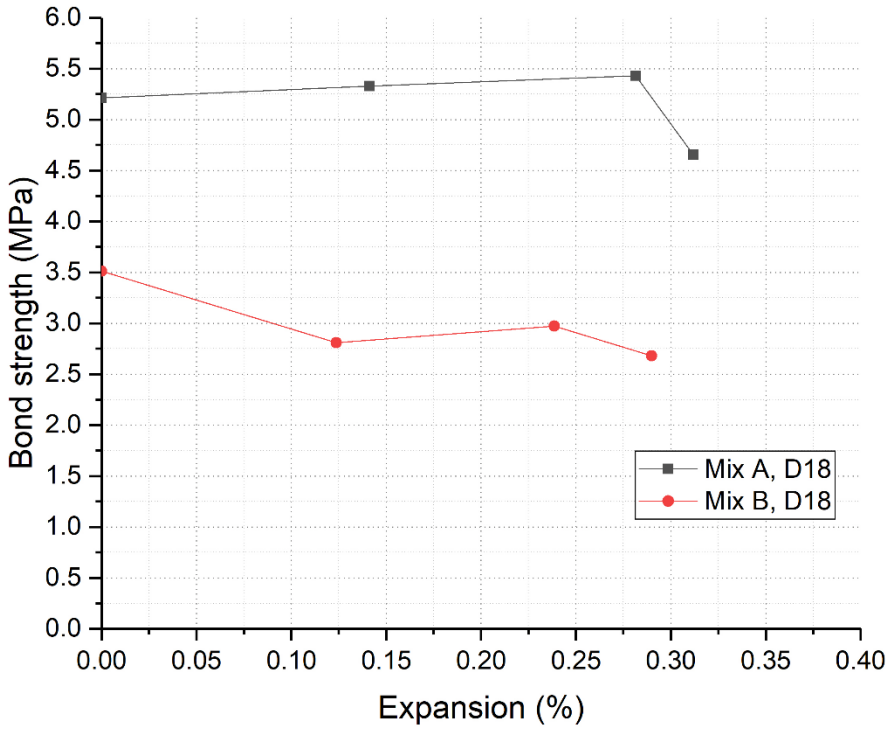

Figure 6. 1 Change in bond strength with expansion (Haddad & Nymayr 2007)

Study performed by Li et al. (2020) revealed that the bond strength increased initially with ASR expansion, afterwards the bond strength decreased with the continuing increasing of the expansion. The authors conducted pull-out tests on specimens with

different deformed bar diameters and embedment lengths. Specimens were cured at 20 ± 2 °C and 90 ± 5% RH condition for 28 days then were subjected to 1 mol/L 80 °C NaOH solution to accelerate ASR up to 170 days. At different expansion levels, pull-out test was performed. Results of bond strength change with respect to the restrained expansion is shown in Figure 6.2. Comparing to the 28-day bond strength values, reductions in bond strength for deformed bars with different diameters D12, D16 and D20 were recorded as 17.6%, 34.5% and 30.4%, corresponding to restrained expansion of 0.34%, 0.32% and 0.28%, respectively.

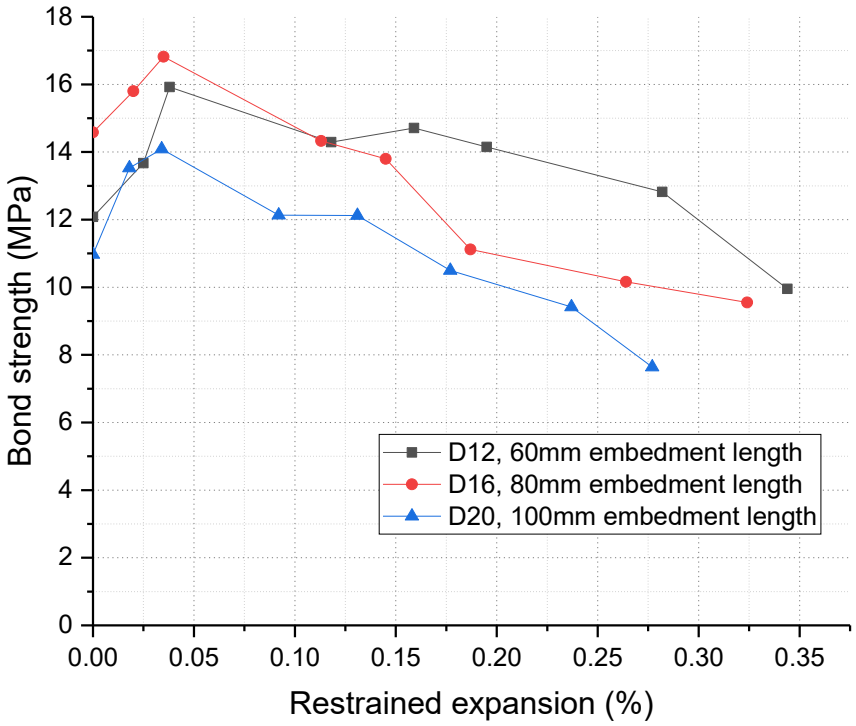

Figure 6. 2 Change in bond strength with restrained expansion (Li et al. 2020)

Based on the force-displacement response of specimens subjected to load testing, Huang et al. (2014) developed a probabilistic model to study the effect of ASR on steel-concrete bond behaviour. Through a Bayesian approach, parameters in the bond-slip model were calibrated. It was found that at early or middle ASR stage, when specimens exhibited intermediate levels of ASR expansion, the bond stiffness and strength were improved; at

later ASR stage, upon reaching certain level of expansion and extensive ASR cracking, the bond strength started to decrease.

However, the fundamental mechanism of bond deterioration between reinforcing steel bar and ASR affected concrete is still unclear. Gardoni et al. (2012) reported that, through petrographic analysis, a layer of ASR gel was found at the interface of rebar and concrete. Concerns was raised about this gel formation and the subsequent expanding and cracking, which could cause debonding of the reinforcing steel bar and concrete as shown in Figure 6.3. Studies performed by Beglarigale & Yazıcı (2013) about the effect of ASR on the bond characteristics, between steel fibre and cement based mortar matrix, revealed that the bond strength was significantly enhanced due to the ASR gel congestion at the steel fibre – matrix interface. Nevertheless, the influence of ASR gel at the steel-concrete interface on bond deterioration is not well understood and needs further investigation.

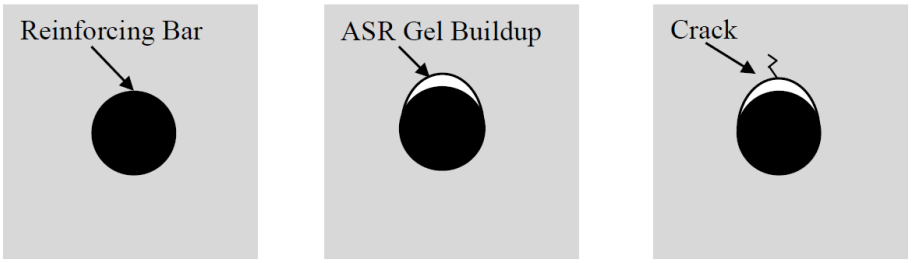

Figure 6. 3 ASR gel formation at steel-concrete interface and its effect on bond (Gardoni et al. 2013)

6.1.2 Pull-out Test

Due to the complexity of the interaction between reinforcing steel bar and concrete in the structure under load, the stress state of the bond between reinforcing steel bar and concrete is complicated. In order to investigate the bond behaviour between reinforcing steel bar and concrete, different types of tests have been used by many researchers (Ahmed, Burley & Ridgen 1999; Castel & Foster 2015; Chana 1989; Majlesi 1994). These tests can be

categorized in four categories, include pull-out tests, beam-end tests, bond beam tests and standard tension tests. Although different experimental studies may use the similar type of specimens, details of specimens may vary in different studies. Among the various test methods, pull-out test is usually used as a test method for comparing the bonding performance under various conditions. Pull-out test is not intended for directly representing the bond between reinforcing steel and concrete in concrete beams, except for the end of the beam, where the stress state can be reflected by pull-out test. Although pull-out test has its limitations, it is widely accepted for studying the relative bond resistance rather than the absolute bond strength value, due to its simplicity and easy to perform. Hence, pull-out test is performed for assessing the effect of different level of ASR on the bond behaviour between reinforcing steel bar and ASR-affected concrete in this study.

Figure 6.4 illustrates a schematic diagram of pull-out test with a reinforcing steel bar embedded in a concrete specimen. The specimen is sitting on a fixed support and load is

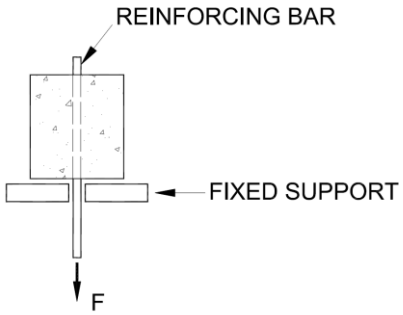

Figure 6. 4 Schematic pull-out test diagram (Castel & Foster 2015)

applied to the reinforcing bar to pull it out from the concrete specimen. Slip of the bar is normally measured at the free end, and also the active end (loading end) in some research (Li et al. 2020).

The bond stress at different loading stage is determined by Equation 6.1 assuming that the bond stress is uniformly distributed along the embedded length.

$$\tau_s = \frac{F}{\pi \cdot l_d \cdot d} \tag{6.1}$$

Where τ_s is the bond stress at different stage;

F is the applied load;

d is the diameter of the reinforcing bar;

l_d is the embedded length of the bar.

In fact, the actual bond stress is not uniformly distributed along the embedded length of reinforcing steel bar. In order to measure the local strain along the steel bar, efforts had been made by installing strain gauges internally in reinforcing steel bar when performing pull-out tests (Kankam 1997; Lee & Mulheron 2015). By this way, the bond stress distribution along the length of the embedded bar can be obtained. In practice, however, the average bond resistance is approximately represented by the average maximum bond stress τ_{max} by assuming that it is uniformly distributed along the embedded bar length. This approximation is appropriate when short embedment length is adopted in the pull-out test. Leonhardt (1964) analysed the influence of the embedment length on the distribution of bond stress and revealed that, for short embedment length, the average maximum stress τ_{max} can be used to represent the maximum bond resistance approximately (Figure 6.5).

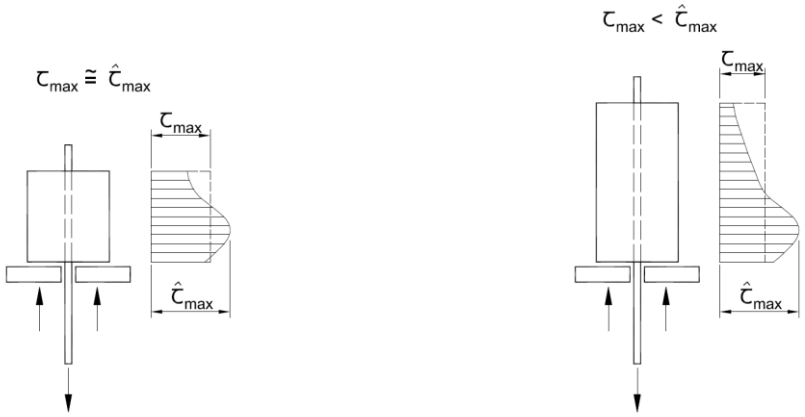

a) With short embedment length b) With long embedment length

Figure 6. 5 Influence of embedment length on bond stress distribution (Leonhardt, 1964)

6.1.3 Bond-slip Model (CEB-FIP Model Code 1990)

For monotonic loading, CEB-FIP Model Code 1990 recommended an analytical model to calculate the bond stresses between reinforcing steel bar and concrete (Figure 6.6).

By using this analytical bond stress - slip model, the bond stress can be calculated using Equation 6.2 to 6.5.

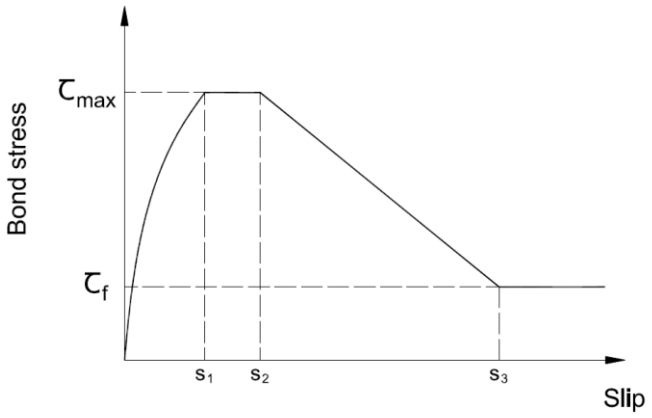

Figure 6. 6 Bond stress – slip model (CEB-FIP Model Code 1990)

For $0 \leq s \leq s_1$: $\tau = \tau_{max}(s/s_1)^{\alpha} \quad 0 \leq \alpha \leq 1$ (6.2)

For $s_1 < s \leq s_2$: $\tau = \tau_{max}$ (6.3)

For $s_2 < s \leq s_3$: $\tau = \tau_{max} - (\tau_{max} - \tau_f)[(s - s_2)/(s_3 - s_2)]$ (6.4)

For $s_3 < s$: $\tau = \tau_f$ (6.5)

Formula 6.2 refers to the ascending curve representing the phase where the lugs of the reinforcing steel bar squeeze the concrete matrix and develop microcracks and cause the concrete to locally break. In this phase, the bond stress increases non-linearly up to τ_{max}. Equation 6.3 is applied for confined concrete only, representing the developing of the concrete breaking and shearing off between the lugs of the steel bar. Equation 6.4 represents the decreasing in bond resistance as a result of the occurrence of splitting cracks along the bars. Equation 6.5 refers to the final stage in which the residual bond capacity is maintained at certain level by the presence of transverse reinforcement.

A brief overview of ASR effects on bond characteristics, test method for measurement of bond strength and factors affecting the bond behaviour is presented. ASR may lead to deterioration of concrete materials and the formation of a weak layer of ASR gel at the interface of steel-concrete matrix, which could cause reduction in the bond stiffness and bond strength. In addition, excessive expansion due to the internal swelling caused by ASR may result in cracking of concrete, which not only accelerate the deterioration of concrete materials, but may also affect the bond behaviour and anchorage capacity of the reinforcement in concrete. Different types of accelerated ASR test had been used by different researchers to investigate the impact of ASR on bond. However, it is still not clear how the ASR gel formation at steel-concrete interface and the cracking due do ASR influence the bond behaviour. In this chapter, a novel accelerated test method is applied

to accelerate ASR for cylindrical pull-out test specimens. Pull-out tests are then performed to investigate the bond behaviour between reinforcing steel bar and ASR-affected concrete. Details are introduced in the following sections.

6.2 Experimental Program

A testing programme for investigating the effect of ASR on bond behaviour is introduced in this section. The purpose of this investigation is to study the influence of different levels of ASR damage on the bond behaviour between reinforcing steel bar and the concrete. Responses of specimens in pull-out test under ultra-accelerated ASR condition are obtained.

6.2.1 Materials and Mix Proportions

In the concrete mixing and casting, for all the pull-out test specimens, cylinders (Ø100 × 200 mm) and prisms (75 × 75 × 285 mm), the same type of general-purpose Portland cement with equivalent alkali content (Na_2O_{eq}) of 0.50% by mass of cement is used. The chemical compositions of the general-purpose Portland cement can be found in Table 4.1 of Chapter 4.

For fine aggregate in the mix, a non-reactive sand, named Sydney sand, is adopted. For the coarse aggregate, a highly reactive Dacite aggregate with a maximum particle size of 20 mm is used in concrete mix. The grading curve of Sydney sand and reactive Dacite aggregate used in this study are illustrated in Figure 4.8 and Figure 4.9, respectively. The chemical compositions of the reactive Dacite aggregate are presented in Table 4.2.

All the pull-out specimens use the same mix proportions as for the small-scale reinforced concrete beams. The mix proportions are provided in Table 5.1 of Chapter 5. The alkali content in the concrete mix is boosted to 2.5% Na_2O_{eq} by mass of cement. To boost the

alkali content, sodium hydroxide pellets were added in the mixing water 24 hours prior to the mixing.

Nominal 8 mm diameter cold worked deformed bars are used in this study. Tensile strength tests are performed in the laboratory to determine the yield stress and the ultimate tensile strength of the reinforcing bars. The measured yield stress f_y is 560 MPa and the measured ultimate tensile strength f_u is 645 MPa. The stress–strain curve of the reinforcing bar is shown in Figure 6.12 (see Chapter 6.2.5).

Figure 6.7 shows the rib pattern of the used reinforcing steel bars in this study. The steel bar has three longitudinal ribs, which divides the circular section of the reinforcing steel bar into three equal parts, with one transverse rib in each part. The maximum rib height of the transverse ribs is measured as 0.515 mm using an Olympus LEXT OLS5000 laser confocal scanning microscope. Each series of transvers ribs are parallel, with an angle of 47 ° to the longitudinal ribs.

Figure 6. 7 Rib pattern of 8 mm diameter deformed bar

6.2.2 Specimen Fabrication

6.2.2.1 Pull-out test specimen design

Cylindrical reinforced concrete specimens with a diameter of 75 mm and a height of 130 mm are designed for this study. Deformed reinforcing steel bar with a diameter of 8 mm is centrally placed in the specimen as shown in Figure 6.8 and Figure 6.10. The bond length for all pull-out test specimens is 50 mm. An 80 mm long PVC sleeve with an inner diameter of 12 mm is provided as shown in Figure 6.8. All the pull-out specimens are cast in Ø75 mm × 150 mm steel cylindrical moulds.

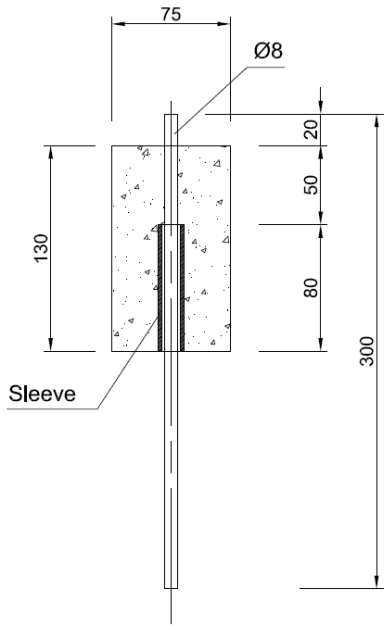

All dimensions are in mm.

Figure 6. 8 Pull-out test specimen design (50 mm bond length specimen)

6.2.2.2 Preparing the rebars with tubes

Figure 6.9 shows the reinforcing steel bars with 50 mm long tubes ready for casting the pull-out test specimens. The inner diameter of the tube is 12 mm while the outer diameter is 16 mm. At the two ends of the tube, gaps between the tube and the reinforcing steel bar are sealed with silane sealer.

Figure 6. 9 Reinforcing steel bars with 80 mm long tubes

6.2.2.3 Mixing and casting of specimens

Figure 6.10 shows the rebars sitting in steel moulds ready for concrete casting. It is worth to be noted that, at the bottom of each cylindrical steel mould, a 20 mm thick circular plywood with a Ø9 mm hole in the centre is placed above the steel base of the moulds, so that the reinforcing bars can be held in a vertical position by the circular plywood.

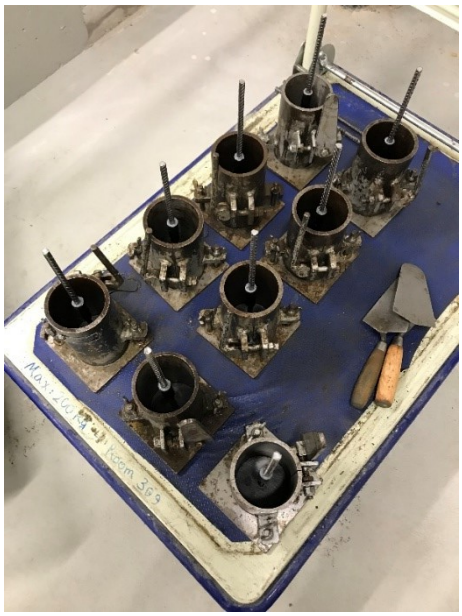

Figure 6. 10 Rebars sitting in steel moulds ready for concrete casting

A laboratory pan mixer with a capacity of 70 litres is used to cast all the pull-out specimens, the control Ø100 mm × 200 mm plain cylinders, and the 75 × 75 × 285 mm size prisms. The control cylinders are used for testing the mechanical properties of the concrete and the prisms with embedded stainless studs at two ends are for expansion measurements. To avoid high temperature of the mixing water due to the dissolution of the sodium hydroxide pellets, mixing water with sodium hydroxide is prepared 24 hours prior to the mixing and is stored in closed plastic containers left in the laboratory overnight at about 23 °C. The concrete mixing follows the procedure recommended by AS 1012.2:2014. After 1 minute of mixing of the coarse aggregates, the fine aggregates and the cement, the prepared mixing water is added, and the mixing continues for 2 minutes, then rest for 2 minutes and mix for another 2 minutes.

The workability of the concrete is checked by performing a slump test. The measured slump is 65 mm. Afterwards, the moulds are placed with three layers of concrete in sequence. A vibrating table is used to compact the concrete immediately after each layer is placed. Figure 6.11 shows the specimens cast for the pull-out test.

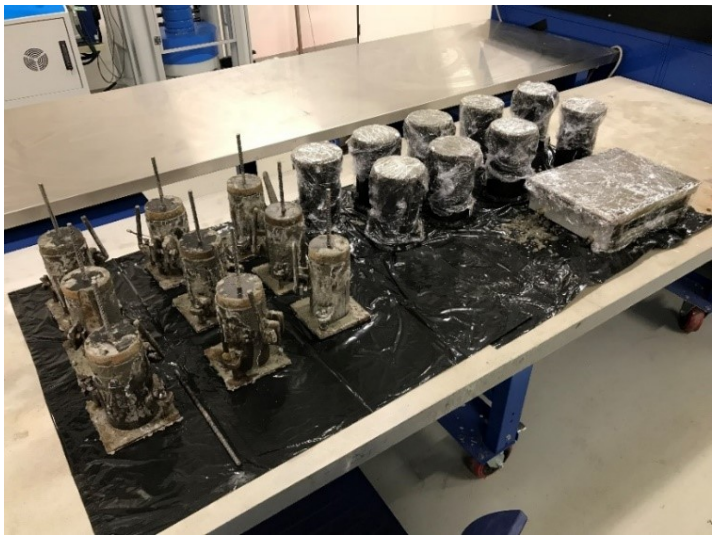

Figure 6. 11 Pull-out Specimens and cylinders + prisms

6.2.2.4 Curing of specimens

After casting, all the specimens were kept in the laboratory, and covered with plastic sheets, at a room temperature of 23 °C. After 24 hours from casting, the specimens were demoulded and then stored in a temperature-humidity controlled cabinet. The temperature-humidity controlled cabinet was maintained at 23 °C and 90% relative humidity. At the age of 28 days, the pull-out specimens were taken out from the temperature-humidity controlled cabinet. Two pull-out test specimens, D7-1 and D7-2, were tested for 28-day bond behaviour. The left specimens were subjected to ASR acceleration and then pull-out tests. Details are described in the following sections.

6.2.3 ASR Acceleration

The same ASR accelerated test procedure was adopted to accelerate ASR using the Zirbus LVSA 50/70 autoclave for the pull-out test specimens at the age of 28 days. That is, steam warming at a temperature of 80 °C using the autoclave for 3 cycles with 60 hours each cycle. The temperature-time relationship of steam warming is shown in Figure 4.2. The ASR acceleration for different pull-out test specimens is presented in Table 6.1.

Table 6. 1 ASR acceleration for pull-out test specimens

Pull-out specimen type	ASR acceleration		Pull-out test specimen
50 mm embedment length	80 °C steam warming cycles (60 hrs/cycle)	0 cycle	D7-1, D7-2 (tested at 28-day)
		1 cycle	D7-3, D7-4
		2 cycles	D7-5, D7-6
		3 cycles	D7-7, D7-8, D7-9
	Immersing in 38 °C 1M NaOH solution after steam warming cycles		D7-9

6.2.4 Testing of Mechanical Properties

Selected numbers of cylinders were tested for modulus of elasticity, compressive and splitting tensile strengths of the concrete at 28 days. After each cycle of autoclaving, selected numbers of cylinders were tested for determining the modulus of elasticity, compressive strength and the splitting tensile strength.

In the test program of this study, nominal 8 mm diameter deformed reinforcing steel bars are used for all the pull-out test specimens. The 8 mm diameter deformed bars are obtained from a steel mesh made with cold worked deformed bars. Figure 6.12 shows the stress-strain curve of the 8 mm diameter cold worked deformed bar obtained from tensile strength test in the laboratory. The measured yield stress f_y of the 8 mm diameter deformed bar is 560 MPa, and the measured ultimate tensile strength f_u is 645 MPa.

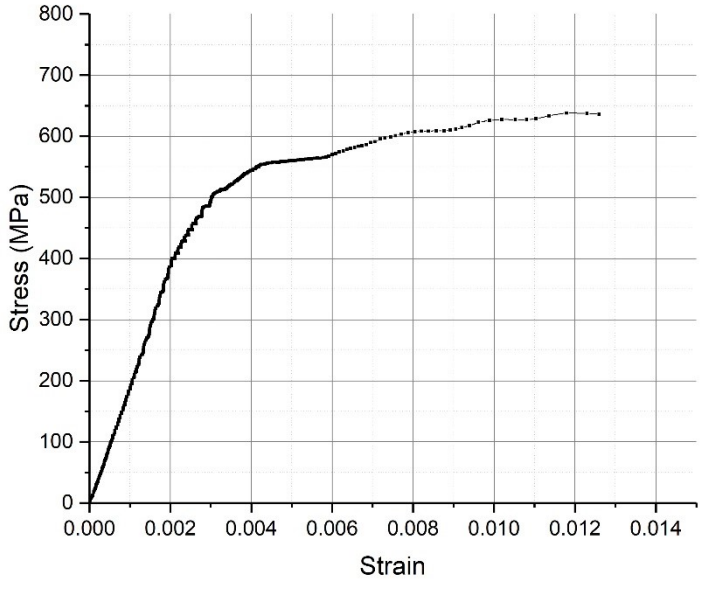

Figure 6. 12 Stress-strain curve of reinforcing steel bar

6.2.5 Pull-out Test

The pull-out tests are performed at the age of 28 days and after each cycle of autoclaving.

Figure 6.13 illustrates a schematic diagram of pull-out test set up. A test frame was designed to accommodate the specimen when performing the pull-out test using an UH-500_{kN}XR universal test machine. During the pull-out test, the cylindrical specimen is supported by a steel plate. The tensile force is applied on the reinforcing steel bar, and a constant displacement rate of 0.1 mm/min is adopted during the tests. Two linear variable differential transformers (LVDTs) are used for displacement measurements, one for measuring the displacement of the reinforcing steel bar at the free end, and another for measuring the displacement of the concrete surface at the free end. Figure 6.14 demonstrates the pull-out test load frame and instrumentation for measurements.

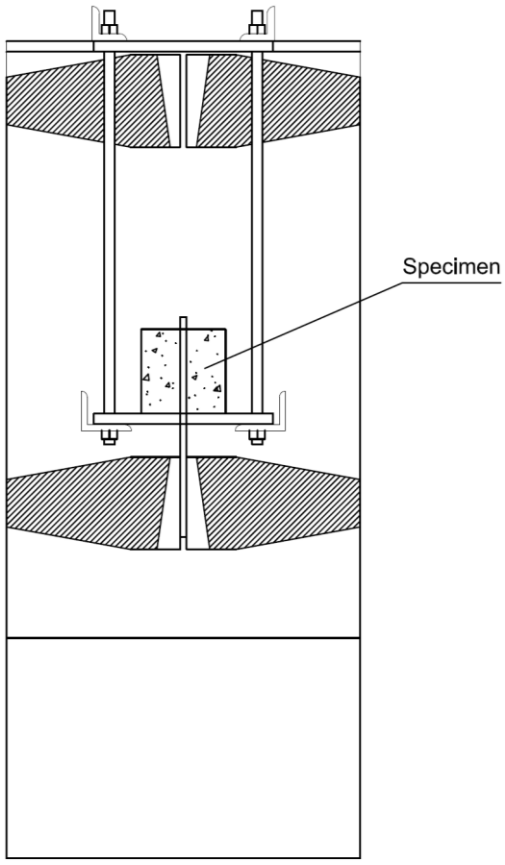

Figure 6. 13 Schematic diagram of pull-out test set up

Figure 6. 14 Instrumentation and test set-up for the pull-out tests

6.2.6 SEM Examination for Steel-Concrete Interface

The microstructure of the steel-concrete interface is studied by using Zeiss EVO SEM equipped with an EDS detector located in the Microstructural Analysis Unit (MAU) of Science at UTS. Small pieces of samples are taken from the steel-concrete interfacial zone and subjected to SEM observation. Details are introduced in Chapter 6.3.4.

6.3 Results and Discussion

6.3.1 Mechanical properties

Modulus of elasticity, compressive strength and splitting tensile strength of cylinders tested at the age of 28 days, after 1, 2 and 3 cycles of autoclaving at the age of 31, 34 and 37 days are provided in Table B.1 to Table B.3 (see Appendix B). The test results are summarised in Table 6.2. As can be seen from Table 6.2, the scatters of the measured mechanical properties are reasonably low.

Table 6. 2 Average compressive strength, modulus of elasticity and splitting tensile strength at 28-day and after 1, 2 and 3 cycles of autoclaving

	28-day	After 1st cycle	After 2nd cycle	After 3rd cycle
f_c (MPa)	36.0	41.5	44.5	42.0
COV	0.049	0.025	0.039	0.043
E_c (GPa)	36.7	27.7	22.8	22.4
COV	0.025	0.043	0.019	0.031
f_t (MPa)	3.50	3.73	3.85	3.72
COV	0.109	0.099	0.020	0.036

6.3.2 Bond Strength

The ultimate bond strength is calculated using Equation 6.1 by assuming that the bond stress is uniformly distributed along the short embedment length. The corresponding force F adopted in the calculation is the ultimate load, or the peak load recorded during the pull-out tests.

The free end slip of the reinforcing steel bar is calculated as:

$$S_{free} = S_{bar} - S_{concrete} \tag{6.6}$$

Where S_{free} is the free end slip of the reinforcing steel bar, mm;

S_{bar} is the displacement of the free end of steel bar, measured by LVDT, mm;

$S_{concrete}$ is the displacement of the concrete, measured by LVDT, mm.

Test results obtained from the pull-out tests are presented in Table 6.3. Test results are categorized in peak load, ultimate bond strength, the corresponding free end slip, and failure modes. In terms of failure mode, PO represents the pull-out of rebar failure, SP denotes the concrete splitting failure. The bond stress – free end slip curves for all the tested specimens are provided in the following Chapter 6.3.3.

Table 6. 3 Pull-out test results

Specimen	f_t (MPa)	Peak load (kN)	Ultimate bond stress τ_u (MPa)		Free end slip (mm)		Failure mode
			τ_u	Average	S_{free}	Average	
D7-1 (28-day)	3.50	21.08	16.78	17.25	0.92	0.88	PO
D7-2 (28-day)		22.26	17.72		0.85		PO+SP
D7-3 (1 cycle)	3.73	21.48	17.10	16.91	0.63	0.55	PO+SP
D7-4 (1 cycle)		20.99	16.71		0.46		SP
D7-5 (2 cycles)	3.85	21.84	17.39	17.96	0.71	0.65	PO+SP
D7-6 (2 cycles)		23.29	18.54		0.58		PO+SP
D7-7 (3 cycles)	3.72	23.46	18.68	18.90	0.38	0.45	PO+SP
D7-8 (3 cycles)		24.03	19.13		0.52		PO+SP

6.3.3 Bond Stress - Slip Relationship

Pull-out tests are performed using an UH-500_{kN}XR universal test machine. During the tests, two linear variable differential transformers (LVDTs) are applied. One LVDT is used to measure the displacement of the reinforcing steel bar at the free end, and another LVDT is to measure the displacement of the concrete surface at the free end. The pull-out load versus the readings of the LVDTs are electronically collected and recorded. The relative displacement between the reinforcing steel bar and the surrounding concrete is calculated as the free end slip of the reinforcing steel bar. Based on the information of the applied load and the corresponding free end slip, the bond stress – free end slip relationship is plotted.

6.3.3.1 Bond stress - slip relationship of 28-day specimens

Two specimens with 50 mm bond length are tested at the age of 28 days, after being cured at 23 °C and 90% RH condition in a temperature-humidity controlled cabinet. Figure 6.15

shows the bond stress – free end slip relationships of the tested specimens. The failure mode of specimen D7-1 is the pulling-out of the reinforcing steel bar, while failure mode of specimen D7-2 is concrete splitting.

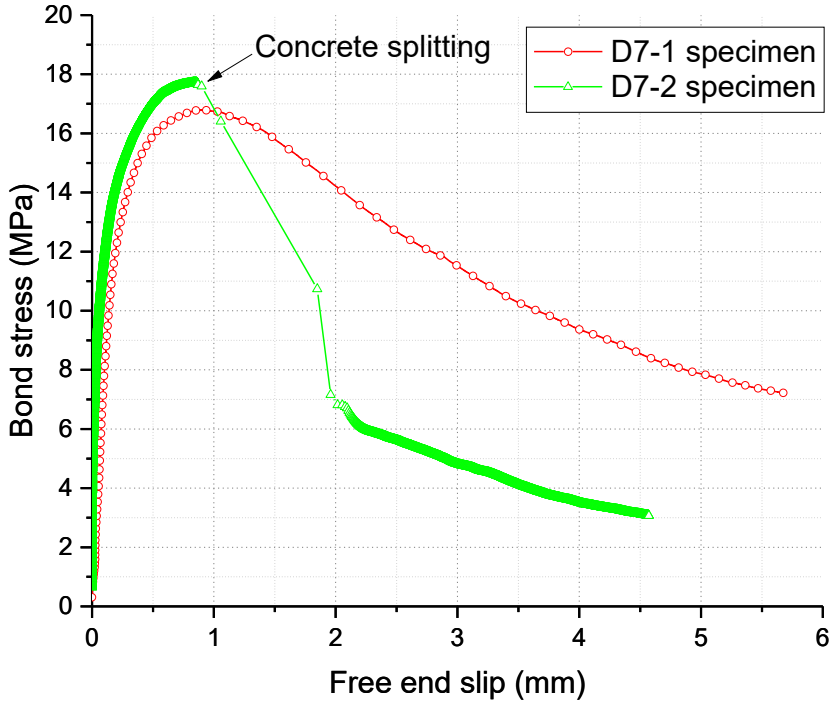

Figure 6. 15 Bond stress – slip relationship
(specimens with 50 mm bond length, tested at the age of 28 days)

6.3.3.2 Bond stress - slip relationship of autoclaved specimens

After 1 cycle of 60 hours autoclaving at 80 °C, the specimens are taken out of the autoclave. The pull-out tests are performed for two pull-out specimens with 50 mm bond length, D7-3 and D7-4, after the specimens are cooled down to room temperature at 23°C. The remaining specimens are then put back into the autoclave again and are subjected to the second and third cycle of 80 °C autoclaving. After each cycle, two pull-out test specimens are tested.

Figure 6.16 shows the bond stress – free end slip relationship of D7-3 and D7-4 and their failure mode after 1 cycle of 80 °C autoclaving. The failure mode of D7-3 is the pull-out of the rebar followed by concrete splitting. The failure mode of D7-4 is due to the splitting of concrete.

(a) Bond stress – slip relationship

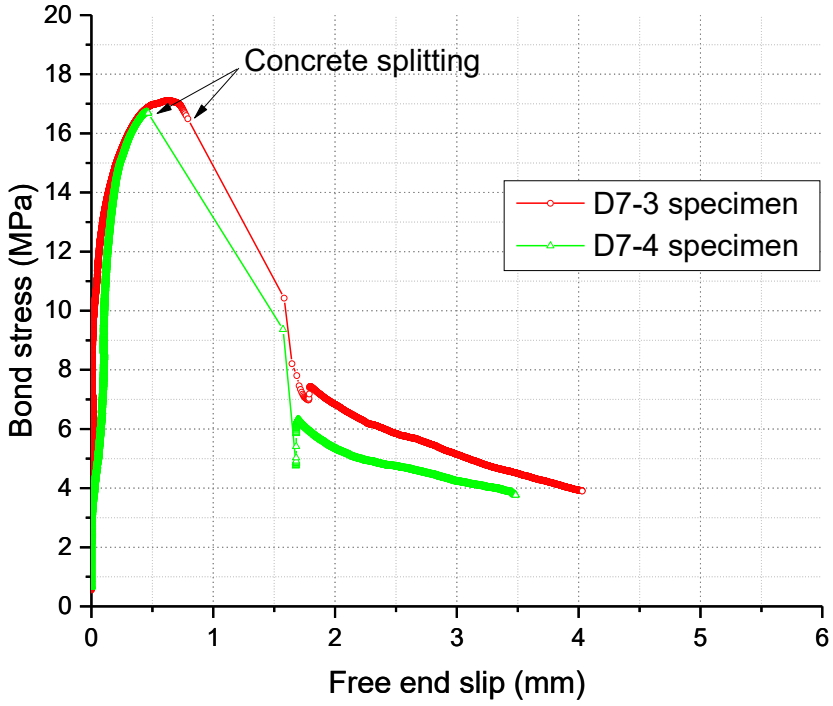

(b) Failure mode of D7-3 and D7-4

Figure 6. 16 Bond stress – slip relationship and failure mode (specimens with 50 mm bond length, tested after 1st cycle of autoclaving at 80 °C)

Figure 6.17(a) shows the bond – free end slip relationship of D7-5 and D7-6 after 2 cycles of 80 °C autoclaving. Their failure modes are shown in Figure 6.17(b). Both specimens are failed in pull-out of the steel bar and subsequent concrete splitting.

(a) Bond stress – slip relationship

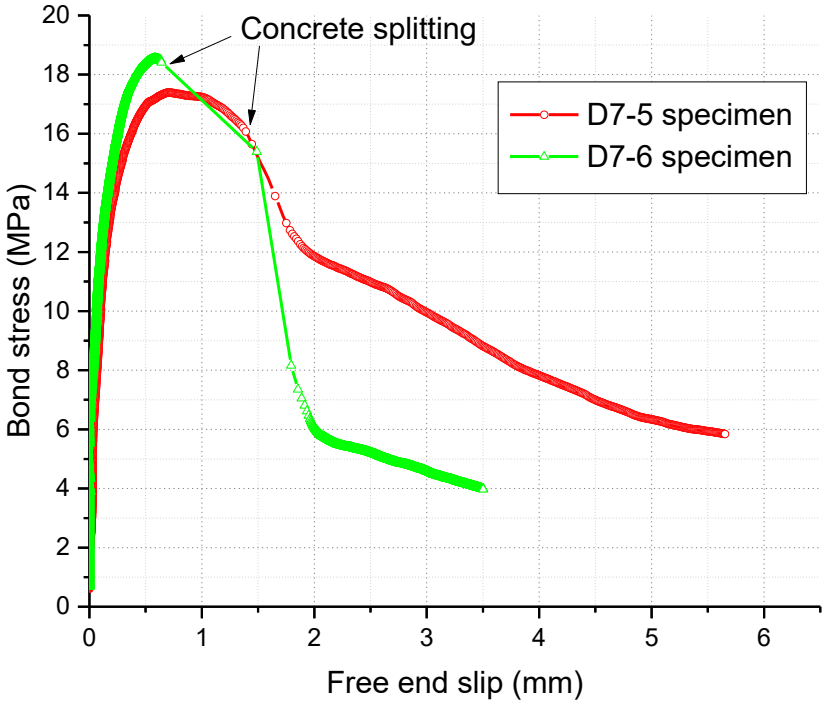

(b) Failure mode of D7-5 and D7-6

Figure 6. 17 Bond stress – slip relationship and failure mode (specimens with 50 mm bond length, tested after 2nd cycle of autoclaving at 80 °C)

Figure 6.18(a) shows the bond – free end slip relationship of D7-7 and D7-8 after 3 cycles of 80 °C autoclaving. Figure 6.18(b) shows the failure mode of D7-7 and D7-8. Both specimens are failed in the pull-out of the rebar and then concrete splitting.

(a) Bond stress – slip relationship

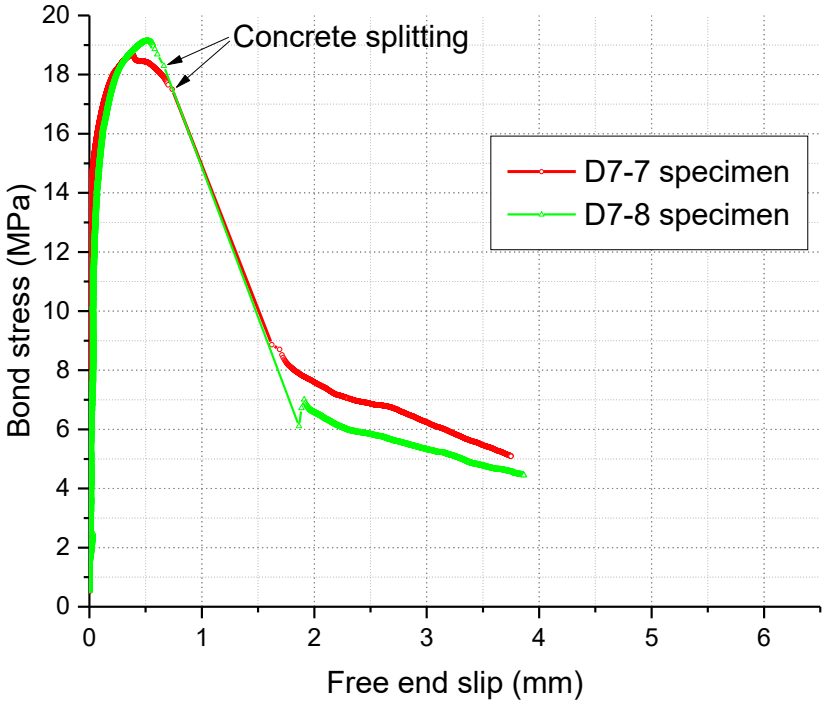

(b) Failure mode of D7-7 and D7-8

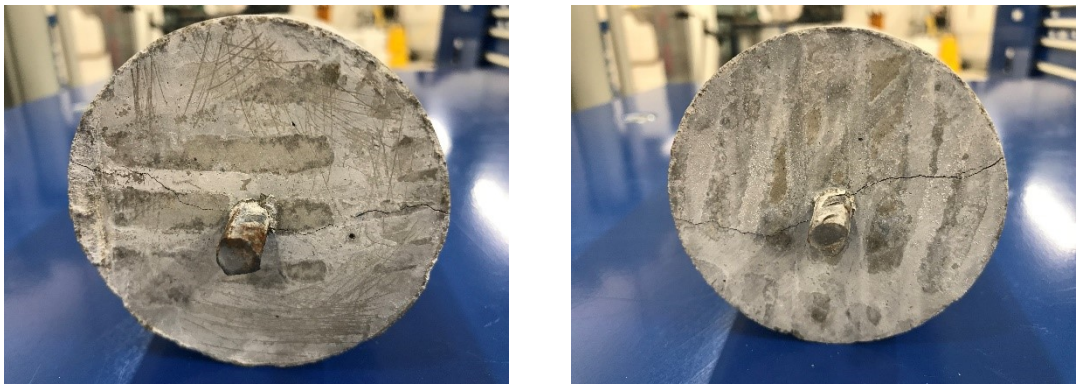

Figure 6. 18 Bond stress – slip relationship and failure mode (specimens with 50 mm bond length, tested after 3nd cycle of autoclaving at 80 °C)

6.3.4 Microstructural Investigation

The microstructure of the steel-concrete interfaces and the morphology of the ASR gel were investigated. Figure 6.19 shows ASR products with cracked platy-crystals morphology present in a pore at the steel-concrete interface.

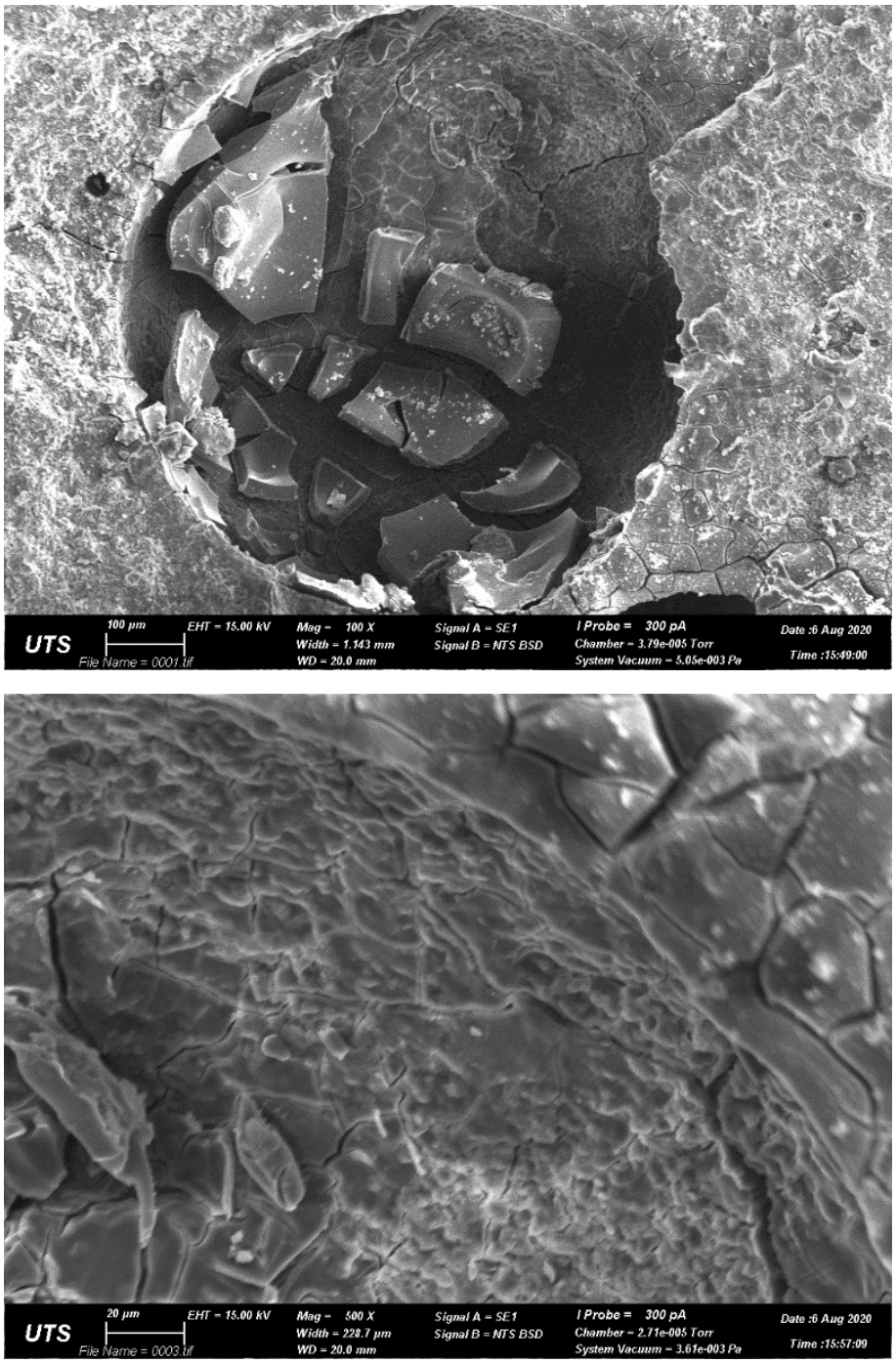

Figure 6. 19 SEM image of ASR gel with cracked platy-crystal morphology

6.4 Summary

Through pull-out test under accelerated ASR test condition and microstructural investigation by SEM, main findings on bond behaviour between reinforcing steel bar and ASR affected concrete are drawn as followings:

(1) Up to free expansion level of about 0.18%, the bond strength between the deformed reinforcing steel bar and the ASR affected concrete is improved.

(2) Compared to the 28-day specimens without accelerated ASR, the bond stiffness is enhanced.

(3) While compressive strength and tensile strength affect the bond behaviour of reinforcing steel bar and concrete, ASR gel formation and congestion at interface of steel and concrete may contribute to the improvement of bond strength.

The results of this study indicated that, up to certain level of expansion under accelerated ASR test condition, ASR gel can form at the steel-concrete interface and fill the pores of the concrete matrix, leading to an improvement in the bond strength and stiffness. However, in long-term field exposure conditions, excessive ASR expansion could cause macrocracks in concrete, especially longitudinal cracking align with main reinforcement. In addition, under combined effect of live load, dead load, and severe field exposure condition, the ASR induced cracking in field structures could be exaggerated, resulting in larger crack widths than those occurred in the accelerated laboratory test. Therefore, bond deterioration in severely damaged field structures could be significantly different to the results of early ASR stage observed in the accelerated laboratory test.

Chapter 7

Fabrication and Monitoring of Large-scale ASR-affected Beams

7.1 Overview

Various experiments have been conducted by different researchers to investigate the expansion of ASR-affected plain and reinforced concrete elements, the restraint effect of reinforcing steel bar, and the effect of sustained loading (Deschenes, Bayrak & Folliard 2009; Fan & Hanson 1998; Inoue et al. 1989; Karthik, Mander & Hurlebaus 2018; Koyangi et al. 1996; Multon & Toutlemonde 2010; Swamy & Al-Asali 1989; Wald, Martinez & Bayrak 2017). These experiments were carried out on concrete specimens by using different concrete mixes, under different environmental exposure conditions, and different restraint configurations. Size of specimens varied from small-scale elements to full-scale large members. The influence of the applied loading, the effect of restraint provided by reinforcement, and the moisture condition on ASR expansion behaviour, and load carrying capacity of the ASR affected reinforced concrete members have been intensively explored. However, the long-term effect of ASR on the behaviour of the affected reinforced concrete structure is still lacking research. In this chapter, efforts are made by casting full-scale 3 m long plain and reinforced concrete beams to study the long-term behaviour of ASR-affected concrete structures. Ultimately, the load carrying capacity of ASR-affected reinforced concrete beams will be obtained by laboratory testing, and these results will be used to verify the analytical model developed at UTS.

Methodology adopted in this study include:

(1) Alkali content of the concrete mix is artificially boosted to 1.25% Na_2O_{eq} by mass of cement;

(2) Specimens are moved into 38 °C climate chamber to accelerate ASR by supplying water, after 28 days of moist curing at 23 °C, to simulate real-life ASR damaged structures.

Due to the time constraints in this study, this chapter will only introduce the fabrication of the plain and reinforced concrete beams, and the expansion measurements up to 360 days. Currently, the beams are stored in the 38 °C climate chamber at UTS Tech Lab. Further research on the long-term behaviour of the ASR-affected plain and reinforced concrete beams is underway.

7.2 Specimen Fabrication and Conditioning

Totally five full-scale 3 m long beams are fabricated and currently stored in the 38 °C climate chamber at UTS Tech Lab. Among them, one is a plain concrete beam made with highly reactive Dacite aggregates, three of them are reinforced concrete beams made with highly reactive Dacite aggregates, and the fifth beam is a reinforced concrete beam made with non-reactive aggregates. Reference name of the beams, casting date and the date of moving into 38 °C climate chamber are shown in Table 7.1.

Table 7. 1 Full-scale 3 m long beams

Ref. Name of Beam	Reinforced/Plain	Reactive/Non-Reactive	Casting Date	Date of Moving into Climate Chamber
R1	Plain	Reactive	28/03/2019	25/04/2019
R2	Reinforced	Reactive	04/04/2019	02/05/2019
R3	Reinforced	Reactive	09/04/2019	07/05/2019
R4	Reinforced	Reactive	23/04/2019	21/05/2019
NR1	Reinforced	Non-Reactive	30/04/2019	28/05/2019

7.2.1 Specimen Design and Reinforcement Detailing

All the beams are designed to have a length of 3 meters, and with a cross-section of 150

mm (width) × 300 mm (height).

Geometry of beam and reinforcement details are shown in Figure 7.1. Two N16 deformed reinforcing steel bars are placed at the tension side, and two N10 deformed reinforcing steel bars are designed to be placed at the compression side of the beam. Grade R250N round reinforcing steel bars with 6.5 mm diameter are selected as stirrups. Distance of stirrups is 205 mm. Totally 15 sets of stirrups are arranged for one 3 m long reinforced concrete beam.

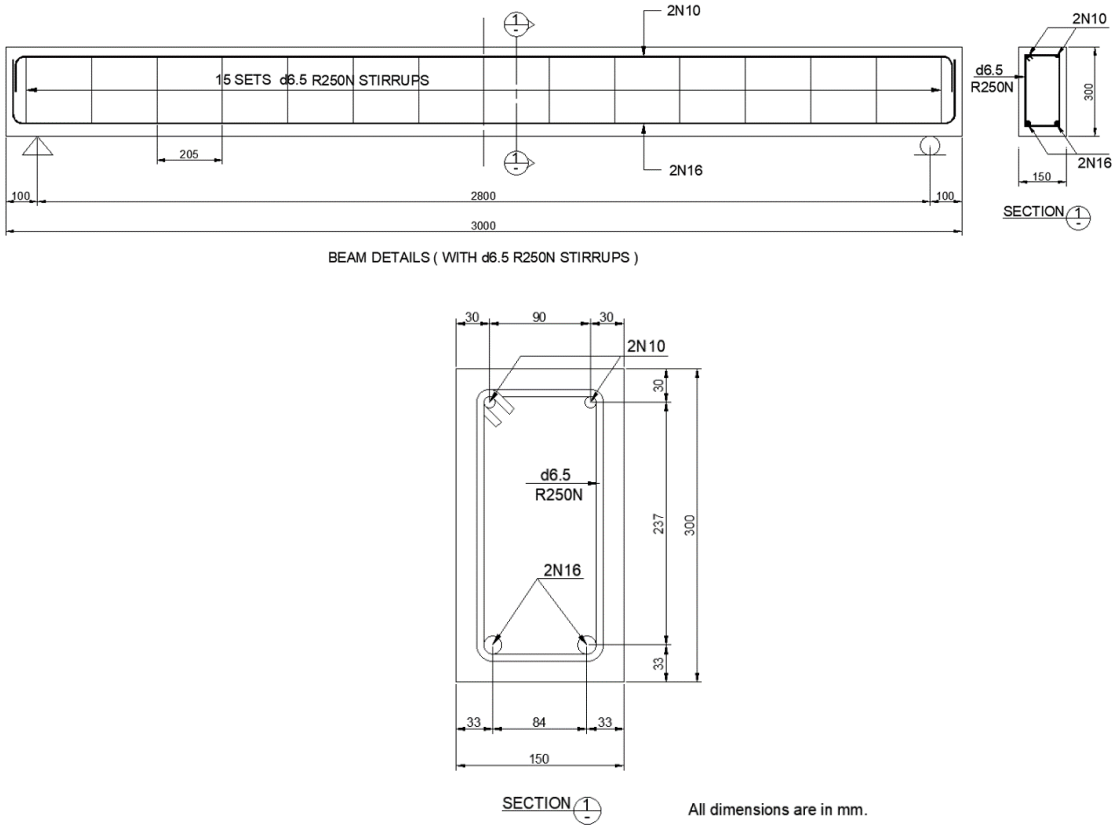

Figure 7. 1 Reinforcement details of full-scale 3 m long reinforced concrete beam

7.2.2 Materials and Mix Proportions

The same general-purpose Portland cement with an alkali content of 0.50% Na_2O_{eq} was used in the mixing for all the beams and their companion cylinders and prisms. The companion cylinders are used for testing the modulus of elasticity and compressive

strength, which is performed at the age of 7, 28, 90, 180 and 360 days, while the companion prisms are used for measuring the free expansion.

Chemical composition of the general-purpose Portland cement used in the mixing is provided in Table 4.1 (Chapter 4.2.1 of Chapter 4).

Two types of coarse aggregate, one is the highly reactive Dacite aggregates, another is the non-reactive aggregates, are used for casting reactive and non-reactive specimens. The chemical composition of these two types of coarse aggregate are demonstrated in Table 4.2 (Chapter 4.2.1 of Chapter 4). As for the fine aggregate, a non-reactive dune sand, namely Sydney sand, is adopted in all the concrete mixing. The mix proportions are shown in Table 7.2. For reactive aggregate beams, the calculated Na_2O_{eq} by mass of cement is 5.5 kg/m^3. For non-reactive beams, the calculated Na_2O_{eq} by mass of cement is 2.2 kg/m^3.

Table 7. 2 Concrete mix proportion for 3 m long full-scale beams

Material	Concrete mix with 1.25% Na_2O_{eq} boosting for reactive aggregates beams (kg/m^3)	Concrete mix without alkali boosting for non-reactive aggregates beams (kg/m^3)
20 mm Aggregate	1134	1134
Sand (non-reactive)	610	610
Cement	440	440
Water	175	175
NaOH pellets added	4.347	--
Na_2O_{eq} (Calculated)	5.5	2.2

Technical grade sodium hydroxide pellets with purity of 98% were used to raise the alkali content of concrete mix to 1.25% Na_2O_{eq} by mass of cement. Due to the dissolution of NaOH generates heat, in order to make sure that the temperature of the mixing water is kept at room temperature before mixing, the mixing water with sodium hydroxide was

prepared 24 hours prior to the mixing, cooled down, and stored in sealed plastic containers left in the laboratory at 23 °C ready for use.

7.2.3 Concrete Mixing and Placement

The concrete was mixed using a horizontal pan mixer with a capacity of 70 litres. Three drums were used to cast one beam and its companion specimens. This is due to the volume of one drum of fresh concrete is not enough for casting the beam. After mixing of the first drum, following the mixing procedure recommended by AS 1012.2:2014, the drum was lifted and moved to side of the mould then starting to place the concrete in the mould. Meanwhile, the mixing of the second drum of concrete started and the procedure repeated. Totally three consecutive mixing and casting were adopted to cast the beam and its companion specimens. Concrete mixing and slump test are shown in Figure 7.2 and Figure 7.3. Placement of concrete is shown in Figure 7.4 to Figure 7.5. A hand-held concrete vibrator is used to compact the concrete.

Figure 7. 2 Concrete mixing using a 70L pan mixer

Figure 7. 3 Slump test

Figure 7. 4 Concrete placement for plain concrete beam

Figure 7. 5 Concrete placement for reinforced concrete beam

7.2.4 Curing and Demolding of Beams

After casting, the reinforced concrete beams were covered with wet hessian cloth and plastic sheets, stored in the laboratory at a temperature of 23 ± 2 °C for 7 days then demolded. After demolding, the beams were moist cured by covering with wet hessian cloth and plastic sheets for another 21 days before being moved into the 38 °C climate chamber. In order to keep the moisture, the hessian cloth covering the beam was checked regularly and wetted one time per day. The companion cylinders and prisms were demolded at the following day after casting then wrapped with plastic foil and put together with the beams. Figure 7.6 shows the moist curing of beams and companion specimens.

Figure 7. 6 Moist curing of beams and companion specimens in the laboratory at a temperature of 23 ± 2 °C

The plain concrete beam was demolded at the age of 28 days on a moveable work bench which is equipped with heavy duty wheels (see Figure 7.7). After demolding, the plain concrete beam was initially supported by seven uniformly distributed 20 mm diameter stainless-steel rods. After the beam was successfully demolded, all the middle supports were then removed, and the beam became a simply supported beam as shown in Figure 7.9.

Figure 7. 7 Demolding of R1 beam – reactive plain concrete beam

7.2.5 38 °C Climate Chamber Conditioning

After 28 days of moist curing at 23 ± 2 °C in the laboratory by covering the beams with wet hessian cloth and plastic sheets, the beams were moved into the 38 °C climate chamber. Figure 7.8 shows the transporting of reinforced concrete beam into the climate chamber. Two trolleys were used to move the beam into the climate chamber. A third trolley was used to lift and set the beam in place. While for the plain concrete beam, it was transported into the climate chamber together with the moveable work bench.

Temperature of climate chamber is controlled at 38 °C, while the relative humidity of the climate chamber is kept at 20%. It should be noted that, 20% relative humility environment is not conducive to the acceleration of ASR, as the development of ASR requires sufficient moisture. Hence, special water supply was provided to promote the ASR for the beams stored in the 38 °C climate chamber. The details are given in Chapter 7.3.2.

(a) Transporting beam using two trolleys

(b) Lifting and placing beam using a third trolley

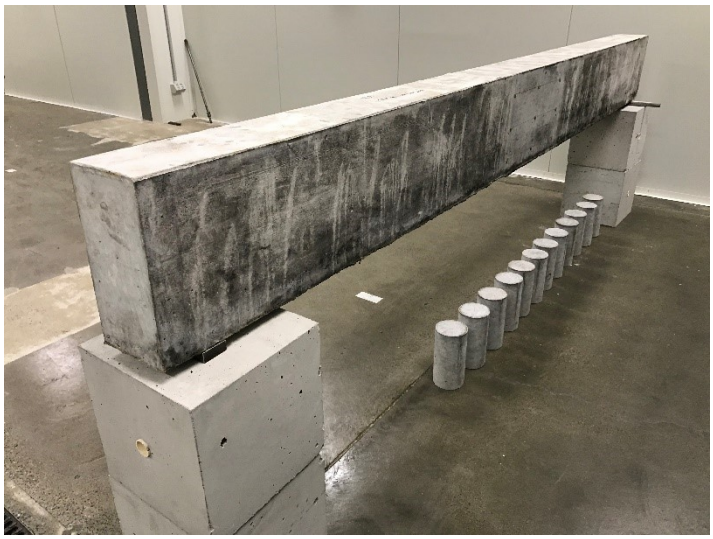

(c) Reinforced concrete beam in place inside climate chamber

Figure 7. 8 Moving reinforced concrete beam into 38 °C climate chamber

7.3 Experimental Program

The whole experimental plan includes the expansion measurements for the beams, ASR acceleration by storing the beams and their companion specimens in 38 °C climate chamber and supplying of water, testing of mechanical properties for match-cured cylinders and prisms, and long-term monitoring of ASR affected beams under sustained loading. Details of experiments are introduced in the following sections.

7.3.1 Expansion Measurements

In order to measure the free expansion of the companion prisms, stainless steel studs were embedded in two ends of the prisms when casting the specimens. After demolding, the initial length of the prisms was measured using a digital comparator and recorded. Before the specimens were moved into the 38 °C climate chamber, the length of the prisms was also measured and recorded, at the age of 7, 14, 21 and 28 days. After the specimens were moved into the 38 °C climate chamber, length changing was measured at 90, 180, 270 and 360 days to record the expansion due to ASR.

Demountable mechanical strain gauge (DEMEC) was used to measure the surface expansion of the beams up to 12 months. Before the beams were moved into the 38 °C climate chamber, DEMEC points were adhered on the concrete surface of the beams. An initial measurement was made and recorded before the beams were moved into the climate chamber. After 7 days being stored in the climate chamber, the DEMEC readings were performed again and recorded. These readings are used to calculate the surface expansion of the beams. Arrangement of DEMEC disc points are shown in Figure 7.9 to Figure 7.13.

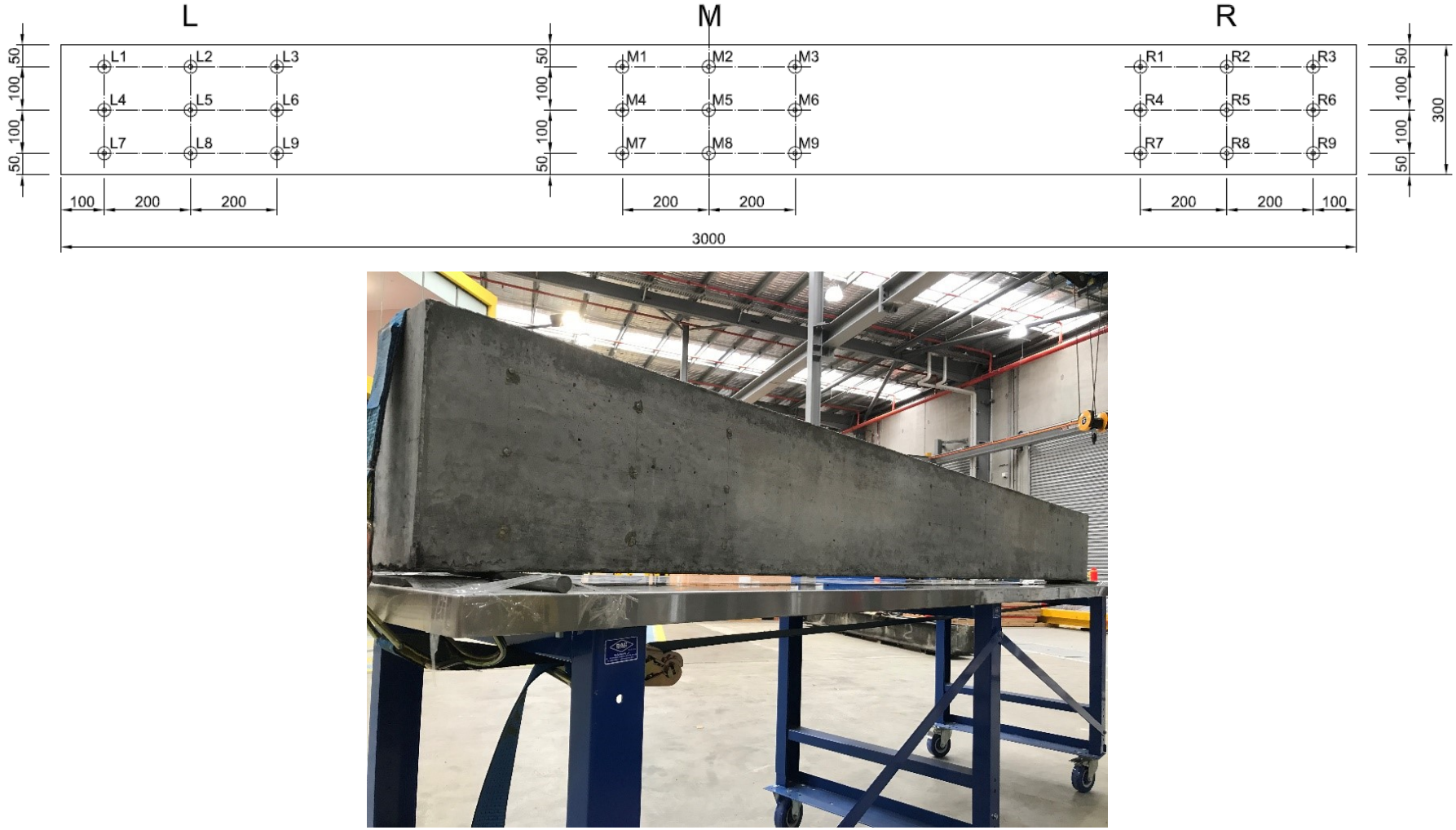

Figure 7. 9 DEMEC points arrangement (R1 beam – reactive plain concrete beam)

Figure 7. 10 DEMEC points arrangement (R2 beam – reactive reinforced concrete beam)

Figure 7. 11 DEMEC points arrangement (R3 beam – reactive reinforced concrete beam)

Figure 7. 12 DEMEC points arrangement (R4 beam – reactive reinforced concrete beam)

Figure 7. 13 DEMEC points arrangement (NR1 beam, non-reactive reinforced concrete beam, flipped over)

For cylinders, DEMEC points were adhered on the surface of 4 cylinders for measurement of the expansion caused by ASR (Figure 7.14).

Figure 7. 14 DEMEC points adhered on surface of cylinder and length measurement

7.3.2 ASR Acceleration

In order to accelerate ASR in the laboratory, different acceleration method have been used by different researchers. A common way to accelerate ASR in laboratory is by means of immersing the specimens in alkali solution, then raising and maintaining the temperature of the alkali solution to certain temperature level (Bach, Thorsen & Nielsen 1993; Fan & Hanson 1998; Swamy 1997). Some other researchers adopted the acceleration method by immersing the specimens in hot water, normally 38 °C (Jones & Clark 1996). Other acceleration methods can also be found in literature, such as putting the specimens above water at elevated temperature (Kagimoto, Yasuda & Kawamura 2014), storing specimens in high humidity fog room with controlled temperature (Koyangi, Rokugo & Uchida 1992; Swamy & Al-Asali 1989), covering specimens with impermeable polyethylene tarpaulin to maintain high humidity conditions (Bilodeau et al. 2016), or wrapping specimens with wet cloth containing alkali solution (Kawabata et al. 2019), sprinkling sodium hydroxide solution to burlap-wrapped specimens (Saouma & Hariri-Ardebili 2020). To promote ASR to high level of expansion, in some studies, chemical substances

such as fused silica (Majlesi 1994; Swamy & Al-Asali 1989), NaCl were added to the mixture (Ha, Fukada & Torii 2017).

To address the effect of different moisture conditions on the ASR damaged structures, Multon & Toutlemonde (2010), Morenon et al. (2019) studied the ASR expansion and flexural capacity of plain and reinforced concrete beams subjected to different moisture conditions. Figure 7.15 shows the water supplying conditions for the tested beams at two phases. In the first phase, the lower part of the beams was immersed in water, while the upper surface of the beams was subjected to 30% RH atmosphere and the duration of the first phase was 428 days. Afterwards, in the second phase of the experiment, water was supplied at the upper surfaces of the beams up to 700 days. During the entire test period, the temperature was maintained at 38 °C. The authors found that moisture condition has significant impact on the ASR expansion.

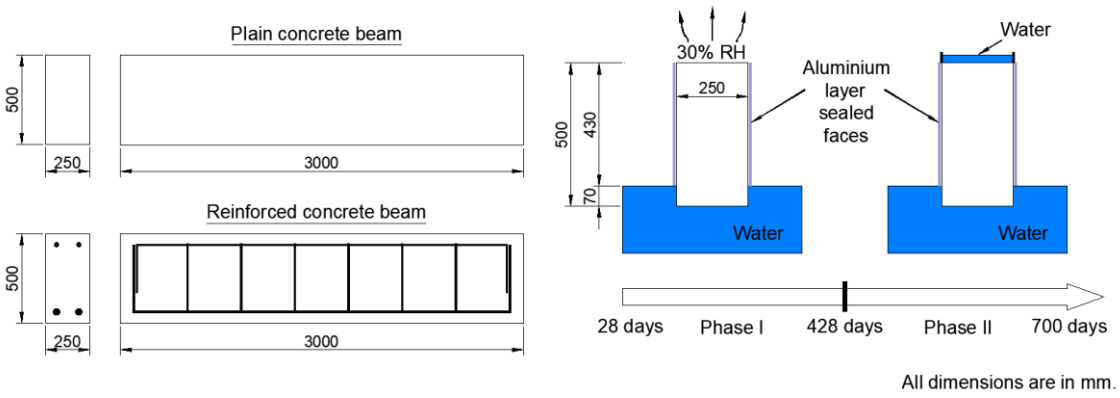

Figure 7. 15 Water supplying conditions of plain concrete beam and reinforced concrete beams tested by Multon & Toutlemonde (2010)

To further address the importance of water supply in accelerating ASR, it should be noted that water can be absorbed by ASR gel thus cause the swelling of the gel which generates pressure to the concrete matrix, resulting in the cracking of the affected material. In addition, water can also act as the 'carrier' of aggressive chemical substances such as

chloride ions, which may cause further damage to the structure, e.g., corrosion of reinforcement.

In real concrete structures, moisture condition plays a critical role in the evolution of ASR. Parts of a concrete structure, for example, the outer faces of beams or columns, which is exposed to moisture, tend to crack and damage more severely due to ASR than other parts of the structure that are protected from the weather. To simulate the exterior beam with outer faces exposed to moisture condition and study the effect of water on the ASR expansion, a water supply method for accelerating ASR of the concrete beams is adopted in this study. Figure 7.16 shows a schematic diagram of the water supply for the beams. In order to supply water at the side surface, the beams are flipped over and simply supported, afterwards, a shallow water tank is built on the side surface of the beams for supplying water. Figure 7.17 shows the water supplying of the plain concrete beam (R1 reactive beam), which is flipped over, simply supported and placed on the moveable work bench. Figure 7.18 demonstrates the water supplying for the R3 reactive reinforced concrete beam, which is also flipped over. The beam is simply supported by concrete blocks. R2 and R4 reactive reinforced concrete beams have the similar set up for supplying of water.

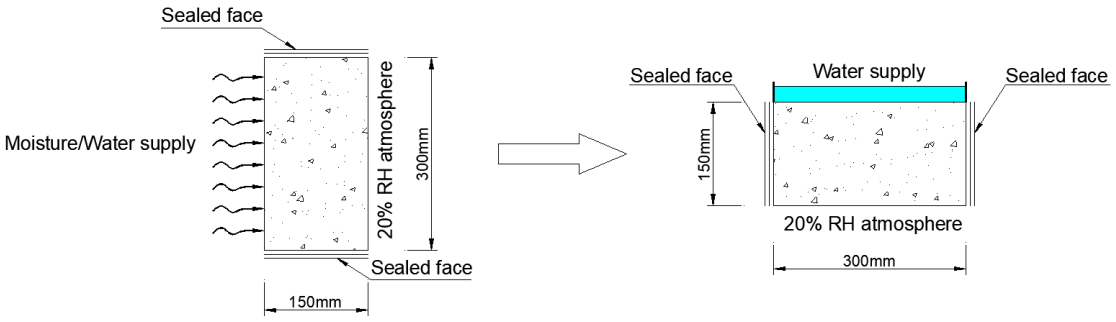

Figure 7. 16 Schematic diagram of supplying water to the beams

Figure 7. 17 Water supply of R1 beam – plain concrete beam, simply supported

Figure 7. 18 Water supply of R3 beam – reinforced concrete beam
(similar set up for R2 and R4 reinforced concrete beams)

Water was added to the shallow water tanks on the side surfaces of the beams three times per week manually. This is to ensure that the side surface of the beam is maintained in saturated condition by continuous water supplying. Expansion and cracking of the beams caused by ASR will be introduced in Chapter 7.5.

7.3.3 Testing of Mechanical Properties for Companion Cylinders

Match-cured cylinders and prisms cast with each beam specimen are listed in Table 7.3.

Table 7. 3 Companion cylinders and prisms of 3 m long full-scale beams

Ref. Name of Beam	Reinforced/Plain	Reactive/Non-Reactive	Number of Cylinders (Ø100×200 mm)	Number of Prisms (75×75×285 mm)
R1	Plain	Reactive	18	--
R2	Reinforced	Reactive	18	--
R3	Reinforced	Reactive	4	18
R4	Reinforced	Reactive	9	3
NR1	Reinforced	Non-Reactive	14	3

The cylinders are used for testing of modulus of elasticity and compressive strength of the concrete at 7, 28, 90, 180 and 360 days. Nine prisms were cast with embedded stainless-steel studs at two ends of the prism for expansion measurements.

All the match-cured cylinders and prisms were demolded at the following day after casting then wrapped with plastic foil and put together with the beams. After 28 days they were moved in the 38 °C climate chamber with the beams. The plastic wrapping was then unwrapped, and the specimen was immersed in water. It should be noted that the way of supplying water to the match-cured specimens is different to that of the 3 m long beams. There could be some difference in the mechanical properties between the match-cured specimens and the 3 m long beams due to the difference in water supplying. Actual material properties of the 3 m long beams should be determined by testing of cores drilled from the beams later. However, to study the effect of ASR on mechanical degradation of the concrete material, modulus of elasticity and compressive strength test on these match-cured cylinders are still necessary to be conducted.

7.4 Results and Discussion

7.4.1 Match-cured Specimens

After casting, the specimens were moist cured for 28 days at a temperature of 23 °C ± 2.0°C in the laboratory. Then the specimens were moved into 38 °C climate chamber accompanying with the 3 m long beams to accelerate the ASR.

Modulus of elasticity test and compressive strength test were conducted for cylinders at the age of 7 days, 28 days and 90 days, 180 days (six months), 360 days (one year). Results and discussions are introduced in the following sections.

7.4.1.1 Modulus of elasticity test for companion cylinders

Modulus of elasticity test were performed for:

- Three cylinders after 7 days of moist curing at 23 ± 2.0 °C (B8-2, R2-2, R2-3);
- Four cylinders after 28 days of moist curing at 23 ± 2.0 °C (B8-23, B8-24, R4-1, R4-2);
- Three 90-day cylinders (cylinders were moved into 38 °C climate chamber after 28 days of moist curing at 23 ± 2.0 °C, B8-10, B8-23, B8-24);
- Three 180-day (6 months) cylinders (B8-11, B8-23, B8-24);
- Four 360-day (one year) cylinders (R1-7, R1-8, R2-7, R2-8).

Results of Modulus of elasticity test are shown in Figure 7.19 and Table 7.4.

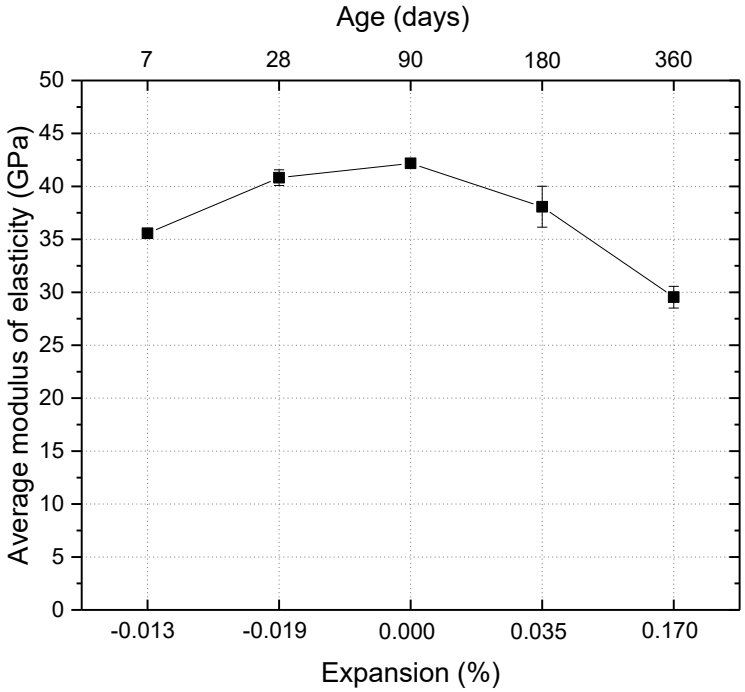

Figure 7. 19 Change in modulus of elasticity of cylinders with 1.25% alkali loading

Table 7. 4 Modulus of elasticity of cylinders with 1.25% alkali loading

Test age of cylinders	Cylinder Name	Modulus of elasticity (GPa)
7-day	B8-2	36.03
	R2-2	35.18
	R2-3	35.48
	Average	35.6
28-day	B8-23 (kept for MOE test)	40.48
	B8-24 (kept for MOE test)	40.30
	R4-1	40.58
	R4-2	41.93
	Average	40.8
90-day	B8-23 (kept for MOE test)	42.45
	B8-24 (kept for MOE test)	42.01
	B8-10	42.06
	Average	42.0
180-day	B8-23 (kept for MOE test)	36.09
	B8-24 (kept for MOE test)	39.95
	B8-11	38.20
	Average	38.0
360-day	R1-7	29.58
	R1-8	28.76
	R2-7	28.84
	R2-8	30.97
	Average	29.5

It is observed that the modulus of elasticity of the match-cured cylinders kept increasing up to 90 days of age when cured in the 38 °C climate chamber with the 3 m long beams. At the age of 90 days, the measured free expansion of the cylinders in average is around 0.0% (see Figure 7.39 in Chapter 7.4.4.1). Afterwards, the modulus of elasticity of the match-cured cylinders starts to decrease, compared to the 28-day modulus of elasticity. At the age of 360 days, with relevant free expansion about 0.17%, the modulus of elasticity was found decreased about 30%, comparing to the 90-day value. The reduction in modulus of elasticity can be attributed to the ASR damage, including microcracking and macrocracking caused by ASR expansion.

7.4.1.2 Compressive strength test for companion cylinders

Compressive strength tests were conducted on:

- Three cylinders after 7 days of moist curing at 23 ± 2.0 °C (R1-1, R1-2, R1-3);
- Six cylinders after 28 days of moist curing at 23 ± 2.0 °C (R1-4, R4-1, R4-2, R4-3, B8-4, B8-5);
- Six 90-day cylinders (cylinders were moved into 38 °C climate chamber after 28 days of moist curing at 23 ± 2.0 °C, B8-8, B8-9, B8-10, B8-14, B8-15, B8-16);
- Three 180-day (6 months) cylinders (B8-11, B8-17, B8-18);
- Four 360-day (one year) cylinders (R1-7, R1-8, R2-7, R2-8).

Results of compressive strength test are shown in below Figure 7.20 and Table 7.5.

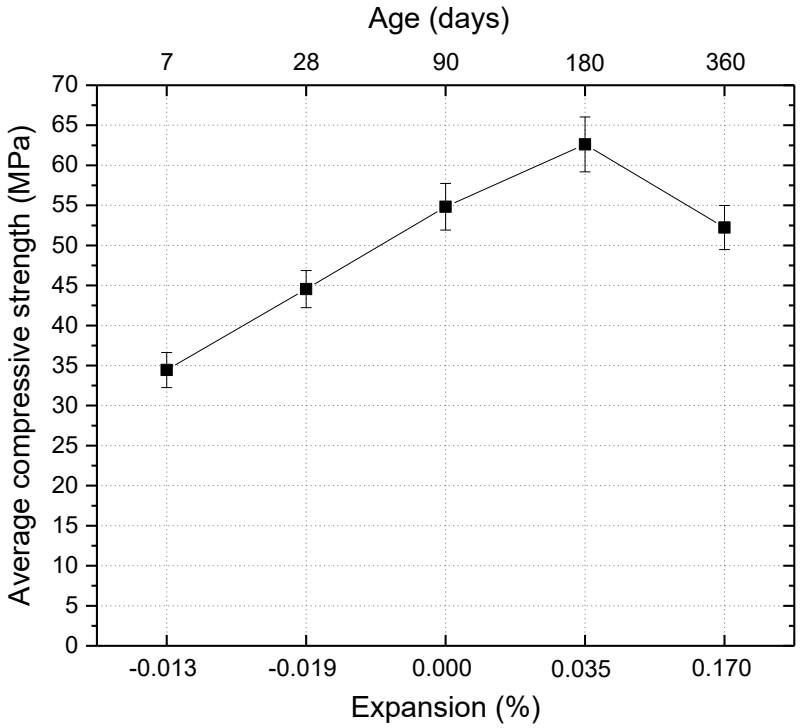

Figure 7. 20 Change in compressive strength of cylinders with 1.25% alkali loading

Table 7. 5 Compressive strength of cylinders with 1.25% alkali loading

Test age of cylinders	Cylinder Name	Compressive Strength (MPa)
7-day	R1-1	33.37
	R1-2	36.96
	R1-3	33.00
	Average	34.5
28-day	R1-4	43.30
	R4-1	44.47
	R4-2	43.90
	R4-3	43.24
	B8-4	43.19
	B8-5	49.18
	Average	44.5
90-day	B8-8	52.19
	B8-9	50.89
	B8-10	54.12
	B8-14	57.87
	B8-15	57.73
	B8-16	56.17
	Average	54.5
180-day	B8-11	58.77
	B8-17	63.67
	B8-18	65.38
	Average	62.5
360-day	R1-7	54.93
	R1-8	52.72
	R2-7	52.90
	R2-8	48.39
	Average	52.0

As can be seen from Figure 7.20, the compressive strength of cylinders with 1.25% alkali loading kept increasing up to 6 months of age while being stored in the 38 °C climate chamber with the 3 m long beams. At the age of 6 months, the average free expansion measured on cylinders and prisms is around 0.035%. After that, the compressive strength starts to show a decreasing trend. However, up to 360 days (one year), with free expansion level around 0.17%, the compressive strength of the tested cylinders is still higher than the 28-day compressive strength. This strength gaining could be attributed to the

continuing of hydration of the cement. With higher level of expansion, a reduction in compressive strength is expected.

7.4.2 Visual Observations

7.4.2.1 Cracking of cylinders and prisms

The crack patterns of concrete cylinders, with 1.25% Na_2O_{eq} boosting after one year of being stored in the 38 °C climate chamber together with the 3 m long beams are shown in Figure 7.21 and Figure 7.22. As can be seen, macrocracks with crack width around 0.2 mm appeared on the surface of the cylinder after the specimens were stored in the 38 °C climate chamber for 1 year. These ASR-induced cracks are thought to be responsible for the degradation of the mechanical properties of the ASR-affected concrete material. Correlation between the ASR-induced cracks and the degradation of the mechanical properties are being investigated currently at the University of Technology Sydney.

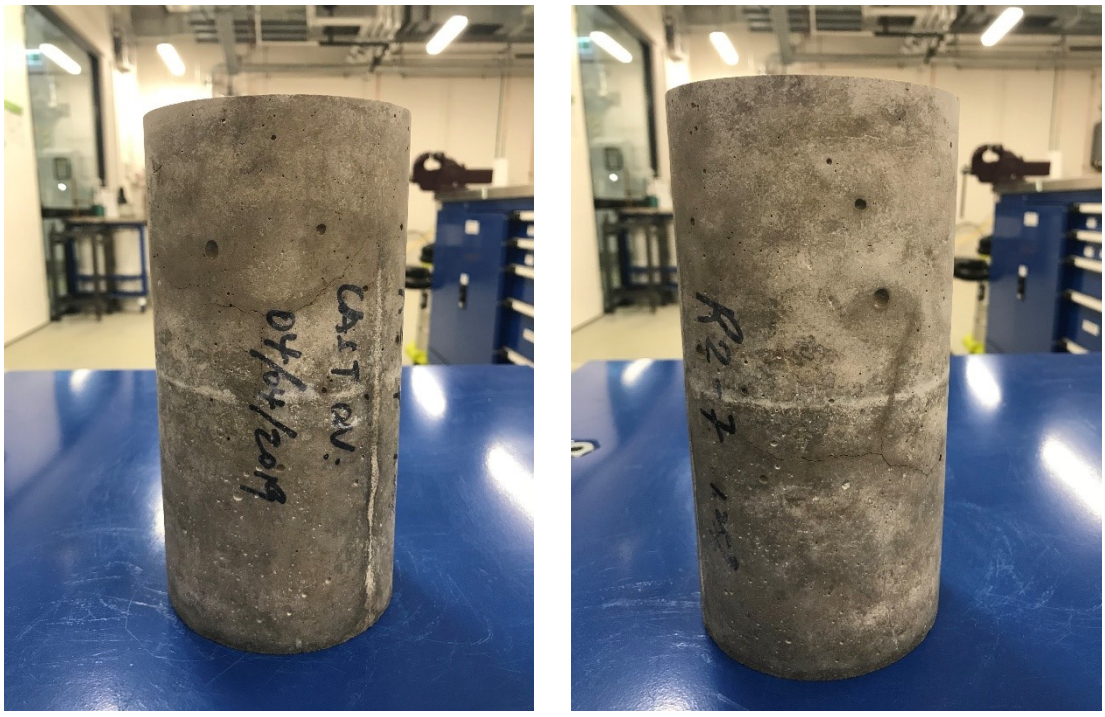

Figure 7. 21 External cracks on cylinders after 1 year of immersing in water and stored in 38 °C climate chamber (without autoclaving specimen)

Figure 7. 22 External cracks on cylinders at the age of 500 days, immersed in water and stored in 38 °C climate chamber, without autoclaving specimens

At the age of six months, one cylinder was placed in LVSA50/70 autoclave and subjected to 130 °C for 5 hours. After one cycle of autoclaving, the specimen was put back in the 38 °C climate chamber and immersed in water again. At the age of one year, this autoclaved cylinder shows more severe cracking than the other specimens. Figure 7.23 shows the crack pattern of this specimen.

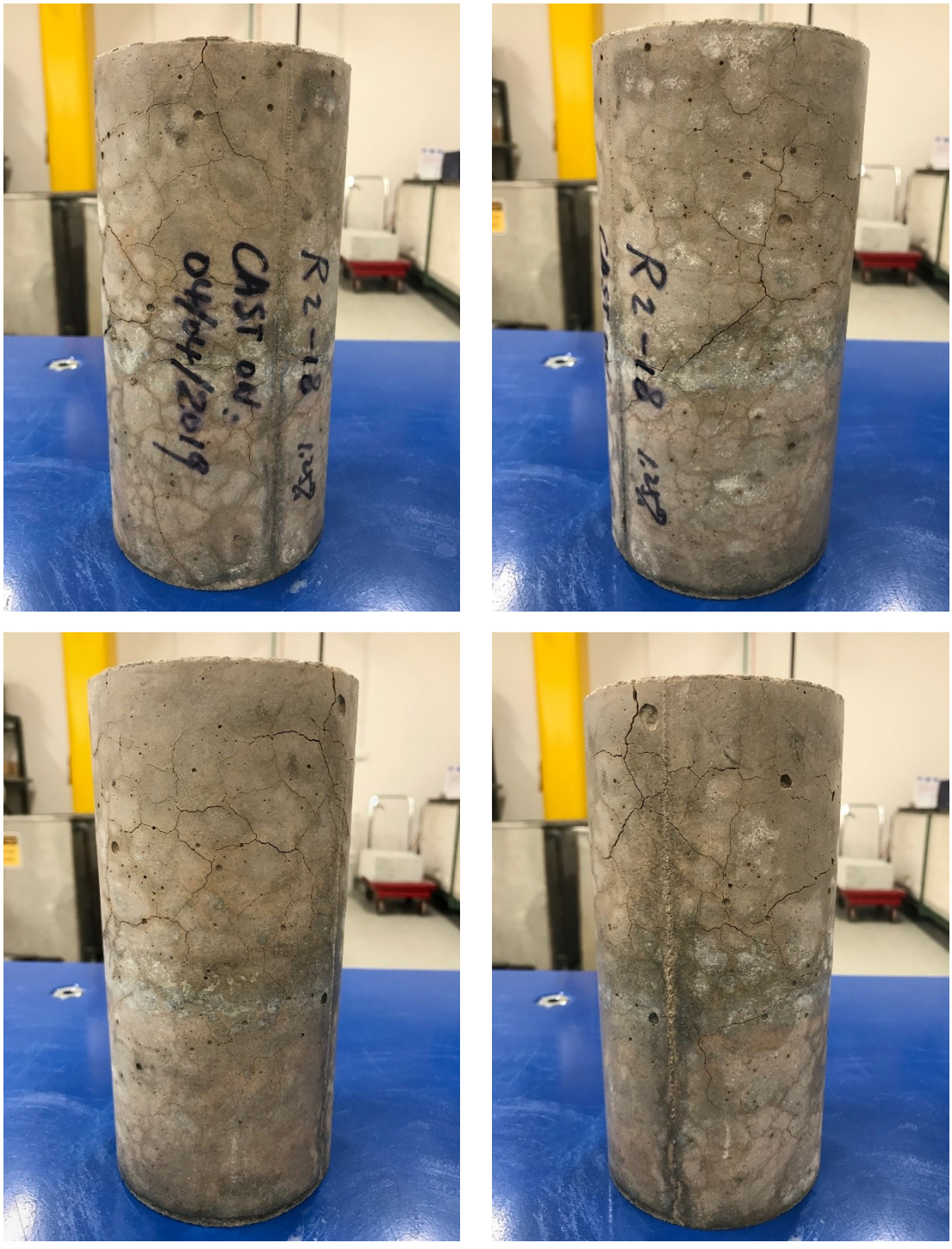

Figure 7. 23 External cracks on cylinders after 1 year of immersing in water and stored in 38 °C climate chamber (with 130 °C autoclaving for 5 hours at the age of 180-day)

The crack pattern observed from the autoclaved cylinder is similar to the crack patter of cylinders exposed to field conditions for more than five years at Texas A&M University

Riverside campus reported by Karthik, Mander & Hurlebaus (2016b). (see figure 7.24). By comparing the extent of damage of cylinders with and without autoclaving, it can be concluded that the 130 °C autoclaving has significant effect on ASR acceleration. Significant damage, which is similar to that caused by long-term field exposure conditions, can be achieved with greatly shortened period of time.

a) b)

Figure 7. 24 Comparison of cylinders at the age of more than 5 years cured in: (a) fog-room with 100%RH at 23 °C and (b) field exposure conditions (Karthik, Mander & Hurlebaus 2016b)

Figure 7.25 shows the cracking pattern on prism at the age of 500 days. As can be seen, after 500 days of immersing in water and stored in the 38 °C climate chamber, the prism exhibited map cracking on its surfaces.

Figure 7. 25 External cracks on prism (after 500 days of immersing in water and stored in 38 °C climate chamber)

7.4.2.2 Cracking of 3 m long beams

Figure 7.26 shows the surface of R1 plain concrete beam after the beam was moved into the 38 °C climate chamber. Cracking pattern of the R1 plain concrete beam is shown in Figure 7.27 to Figure 7.30. Cracking on the wetting surface was first observed after five months of being stored in the 38 °C climate chamber by supplying water to one side surface of the beam as shown in Figure 7.27 and 7.28. After one year, from the date of casting, extensive map cracking eventually developed on the wetting surface of the plain concrete beam. As the wetting surface is under compression along the length of the beam due to the current setting-up, some cracks aligned with the stress direction can also be observed. Some white staining can be also seen on the wetting surface of the beam in these photographs.

Figure 7. 26 R1 beam surface (photo taken on 03/05/2019 after the beam was moved into the 38 °C climate chamber)

Figure 7. 27 Cracking on R1 beam surface
(photo taken on 30/09/2019, 6th month)

Figure 7. 28 Cracking on R1 beam surface
(photo taken on 30/09/2019, 6th month)

Figure 7. 29 Map cracking on R1 beam surface
(photo taken on 31/03/2020, 12th month)

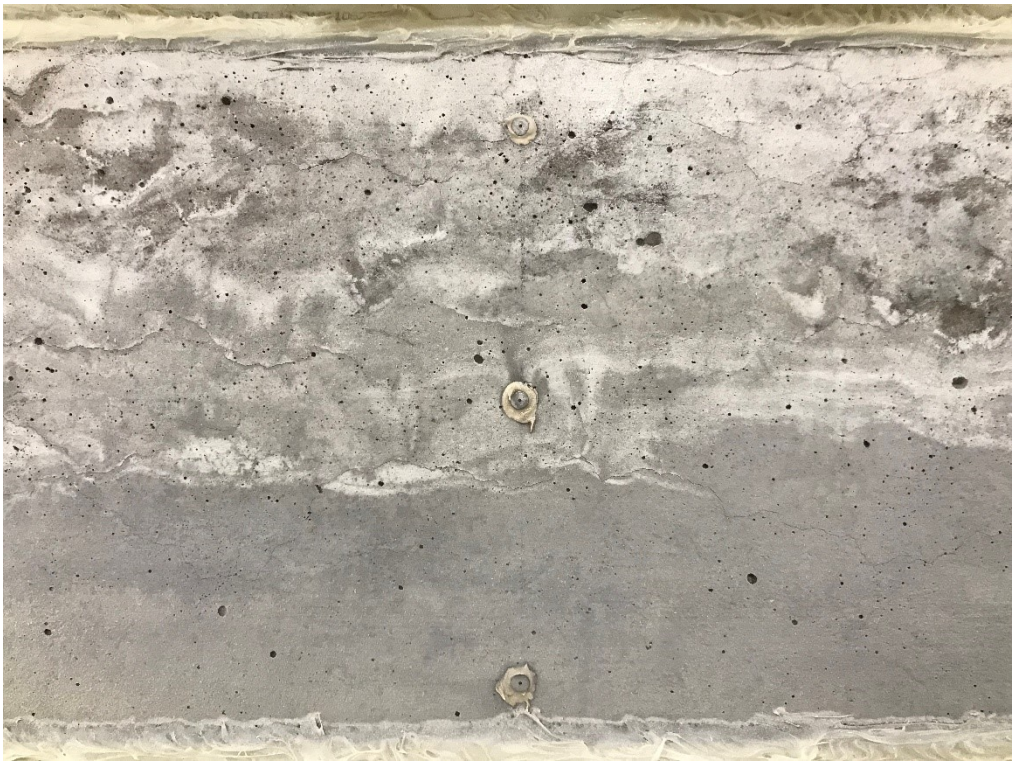

Figure 7. 30 Cracking on R1 beam surface
(photo taken on 31/03/2020, 12th month)

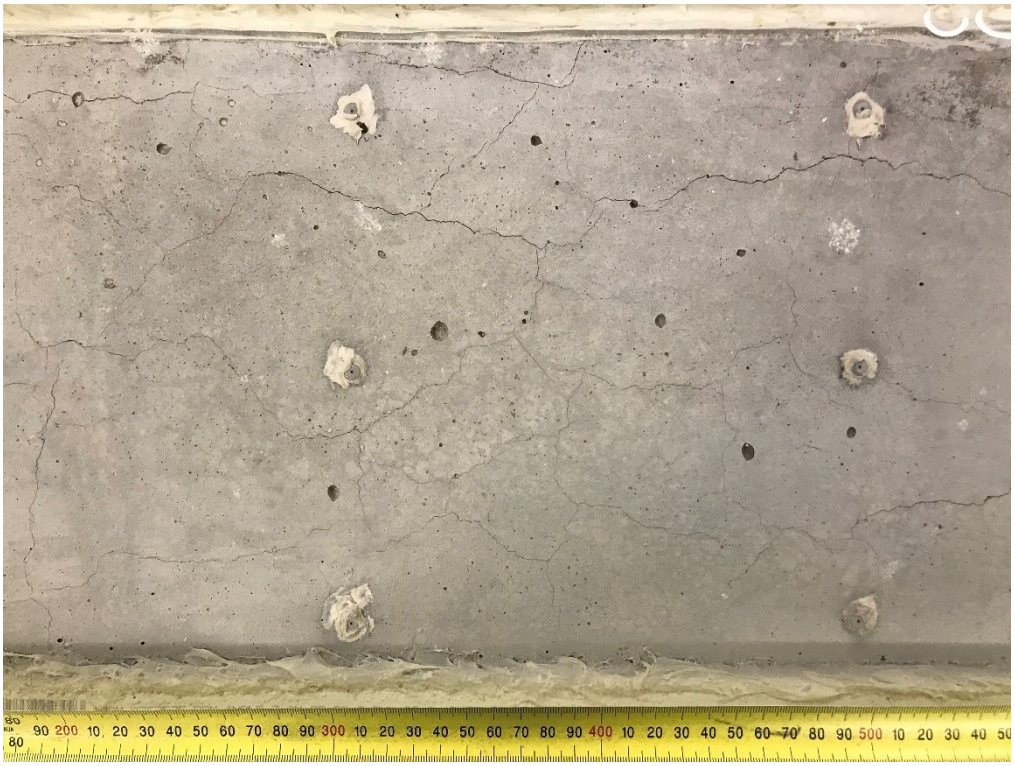

Figure 7. 31 Map cracking on R1 beam surface
(photo taken on 10/08/2020, 500 days)

Figure 7. 32 Cracking on R1 beam surface
(photo taken on 10/08/2020, 500 days)

The cracking pattern of reinforced concrete beams with reactive aggregates is different to that of the plain concrete beam. Crack pattern of the R2 and R3 reactive reinforced concrete beams are shown in Figure 7.33 to Figure 7.36. Cracking on the wetting surface of the reactive reinforced concrete beams were first noticed at the age of six to seven months. Typical longitudinal cracking aligned with the direction of the longitudinal reinforcement eventually developed on the wetting surface of the beam after the beams were stored in the 38 °C climate chamber and supplied with enough water.

Figure 7. 33 Longitudinal cracking on R2 beam surface
(photos taken on 31/03/2020, 12th month)

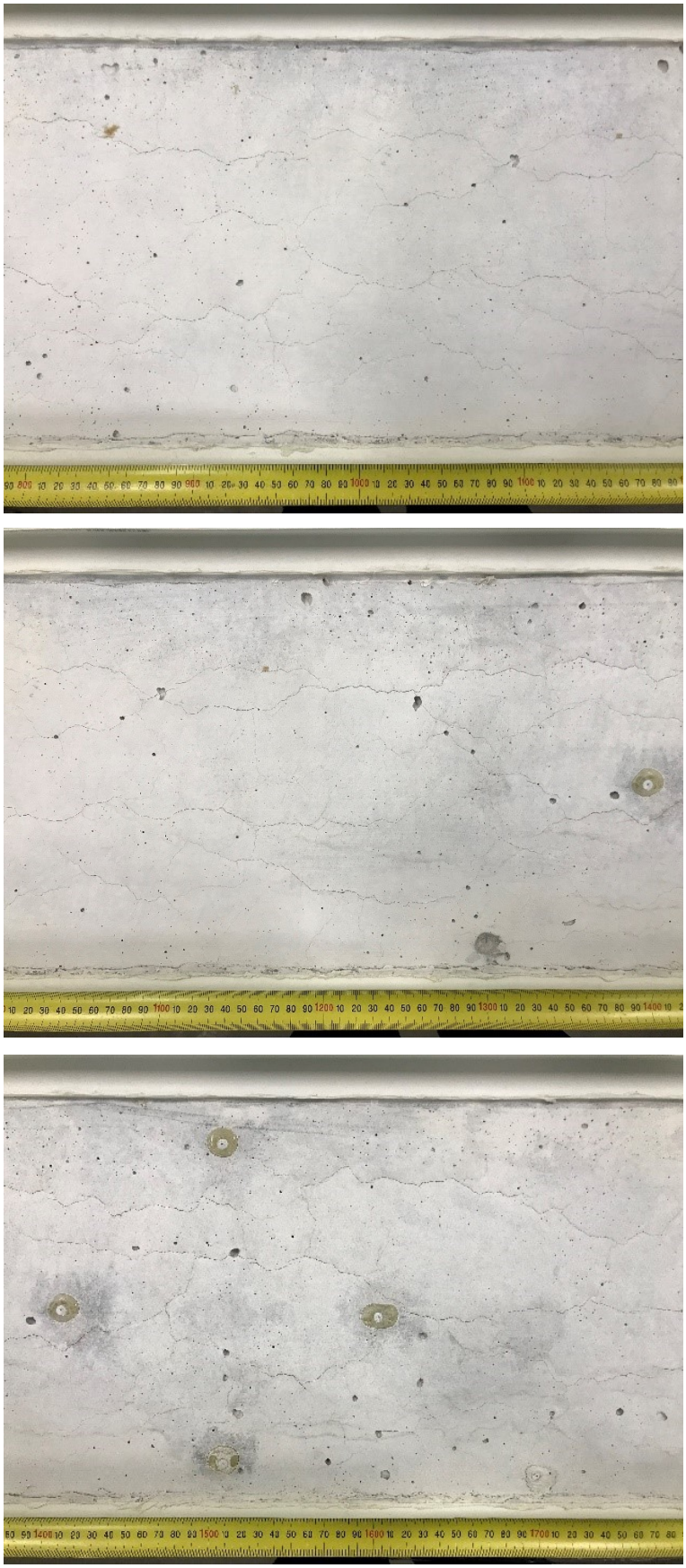

Figure 7. 34 Longitudinal cracking on R2 beam surface
(photos taken on 17/08/2020, 500 days)

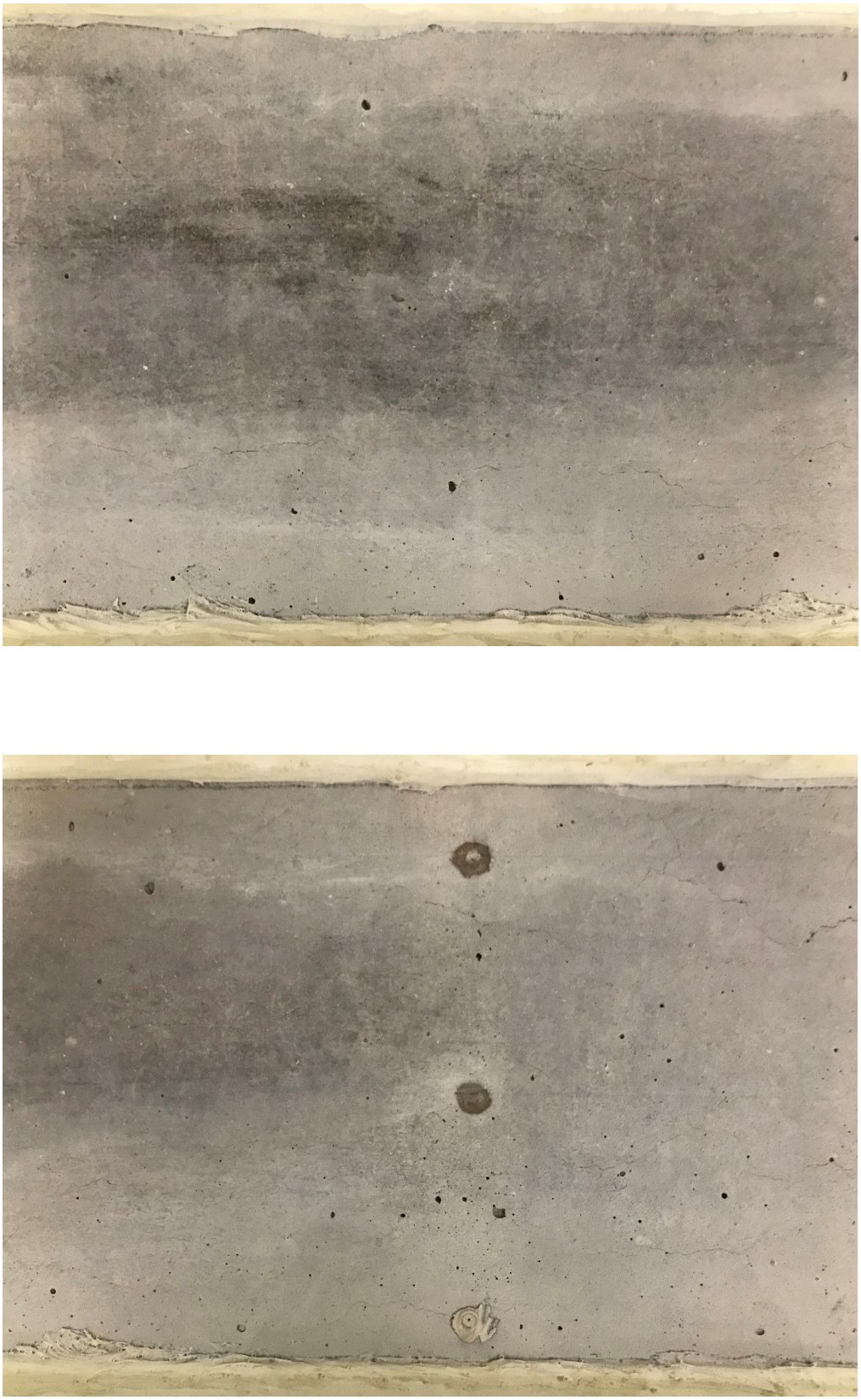

Figure 7. 35 Longitudinal cracking on R3 beam surface
(photos taken on 10/04/2020, 12th month)

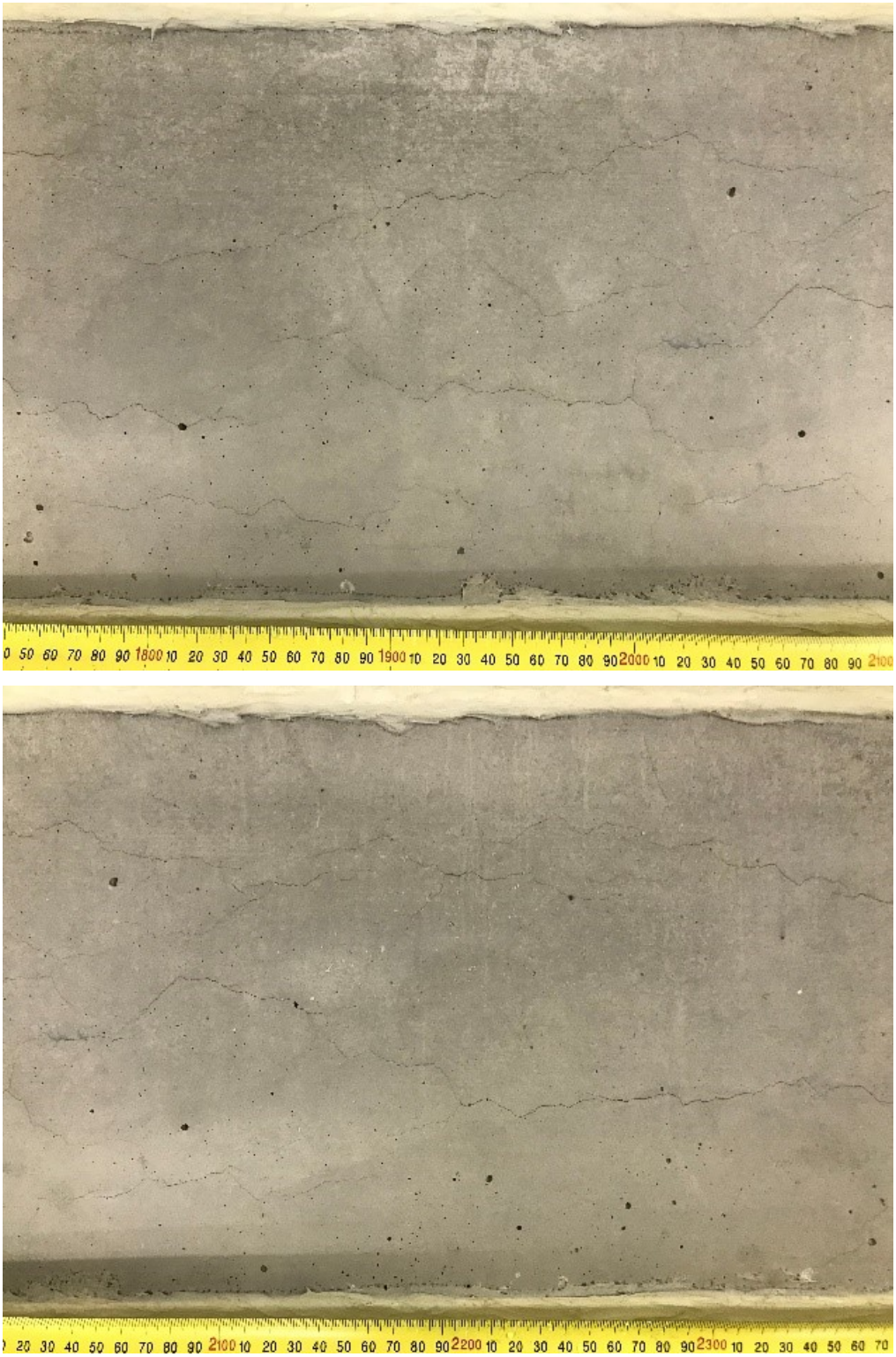

Figure 7. 36 Longitudinal cracking on R3 beam surface
(photos taken on 24/08/2020, 500 days)

7.4.3 Convex Curvature of Reinforced Concrete Beam Caused by ASR

During the conditioning period, displacement of R2 beam was measured by a laser displacement transducer. Figure 7.37(a) shows the schematic set-up of the laser sensor placed beneath the beam at the mid-point of the span to measure the vertical displacement of the beam.

Figure 7.38 shows the upward displacement of R2 beam at the mid-span during the period of being stored in the 38 °C climate chamber and being supplied with water as shown in Figure 7.37(b). The convex displacement of R2 beam increased up to approximately 3.5 mm during the monitoring period of 360 days. Based on the observation of cracking propagation, crack pattern and the measured upward displacement of the beam, it can be concluded that ASR was accelerated by simply supplying water on one side surface of the beam while the other side surface was exposed to 20% RH atmosphere. Because in the current water supply method, the top surface is directly exposed to water thus it suffered higher ASR expansion than the bottom surface. Consequently, it results in an upward displacement of the beam due to the different level of ASR expansion between the top surface and the bottom surface. Apart from the influence of ASR expansion, other factors, such as bending of the beam due to self-weight and the weight of water ponding, differential shrinkage due to different moisture condition across depth of the beam, potential warping due to unsymmetrical arrangement of reinforcement, may also contribute to the displacement of the beam.

(a)

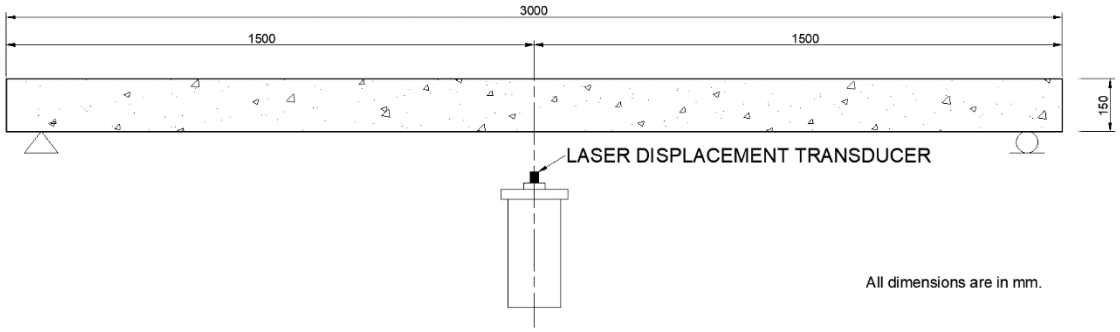

(b)

Figure 7. 37 (a) Schematic set-up of laser displacement sensor; (b) Deployment of laser sensor for R2 beam to measure the displacement of the beam

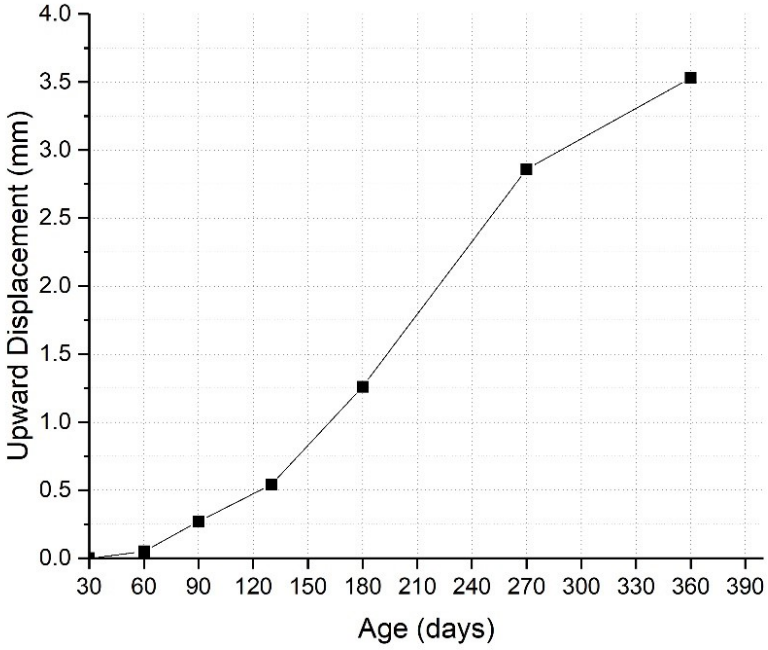

Figure 7. 38 Upward displacement of R2 beam

7.4.4 Expansions

7.4.4.1 Free expansion of cylinders and prisms

Figure 7.39 shows the average free expansion of the accompanying prisms with embedded stainless-steel studs at two ends of the prism and the accompanying cylinders with DEMEC points adhered on the surfaces. In the period of moist curing up to the age of 28 days at 23 ± 2.0 °C, a slight shrinkage of 0.019% to 0.020% was observed. After being stored in the 38 °C climate chamber with the 3 m long beams, at the age of one year, a total average free expansion of about 0.17% was recorded. At the age of one year and 500 days, the cylinders showed external macrocracks as demonstrated in Figure 7.21 and 7.22, while the cracking pattern of external macrocracks on prism specimen is displayed in Figure 7.25.

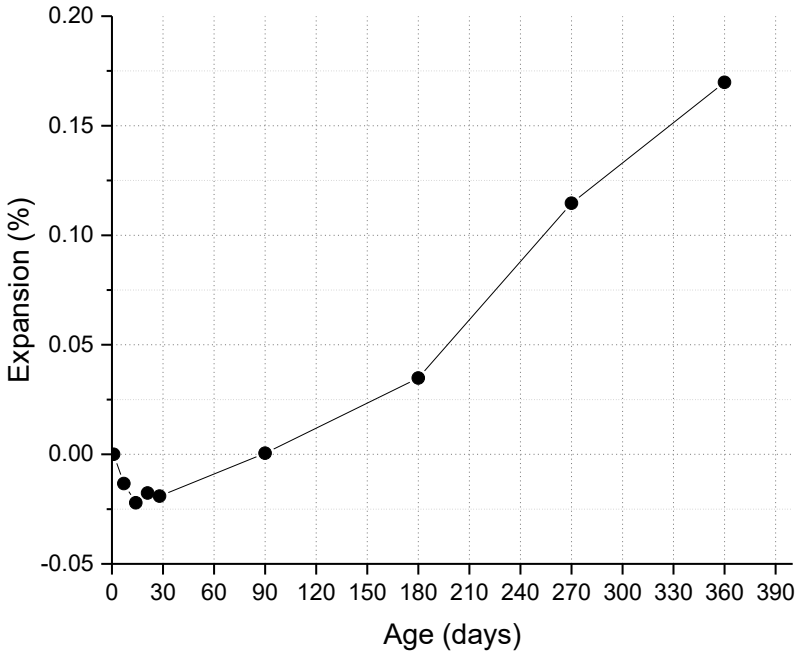

Figure 7. 39 Average free expansion of prisms and cylinders stored in 38 °C climate chamber with the 3 m long beams

7.4.4.2 Expansion of R1 plain concrete beam

The average longitudinal and lateral expansion measured on the DEMEC points adhered to the surface of R1 plain concrete beam is displayed in Figure 7.40. It should be noted that, water supplying to the shallow water tank build on the side surface of the beam started at the age of 120 days. As can be seen from Figure 7.40, before water was supplied to the side surface of the beam, a slight shrinkage measured on the beam surface was recorded after the beam was moved into the 38 °C climate chamber. Afterwards, the beam started to expand longitudinally and laterally. At the age of one year, an average longitudinal expansion of about 0.104%, and an average of lateral expansion of about 0.187% were recorded.

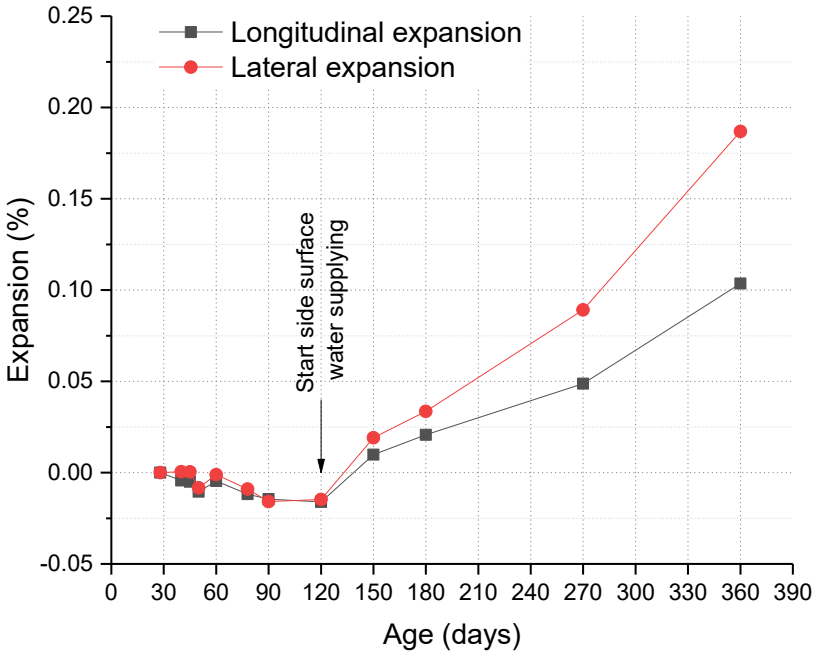

Figure 7. 40 Average longitudinal and lateral expansion of R1 plain concrete beam stored in 38 °C climate chamber

7.4.4.3 Expansion of R2 reinforced concrete beam

Figure 7.41 shows the average longitudinal and lateral expansion of R2 reinforced beam.

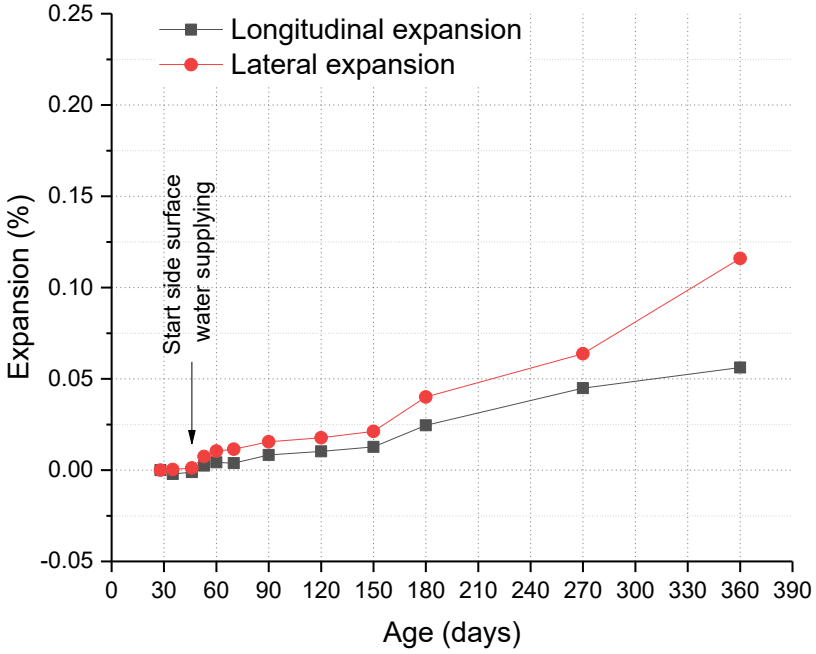

Figure 7. 41 Average longitudinal and lateral expansion of R2 reinforced concrete beam stored in 38 °C climate chamber

Water supplying to the side surface of the beam started at the age of 46 days. At the age of one year, an average longitudinal expansion of about 0.056%, and an average of lateral expansion of about 0.116% were recorded. Longitudinal cracking on the wetting surface of the beam are shown in Figure 7.33 and 7.34.

7.4.4.4 Expansion of R3 reinforced concrete beam

Figure 7.42 shows the average longitudinal and lateral expansion of R3 reinforced beam.

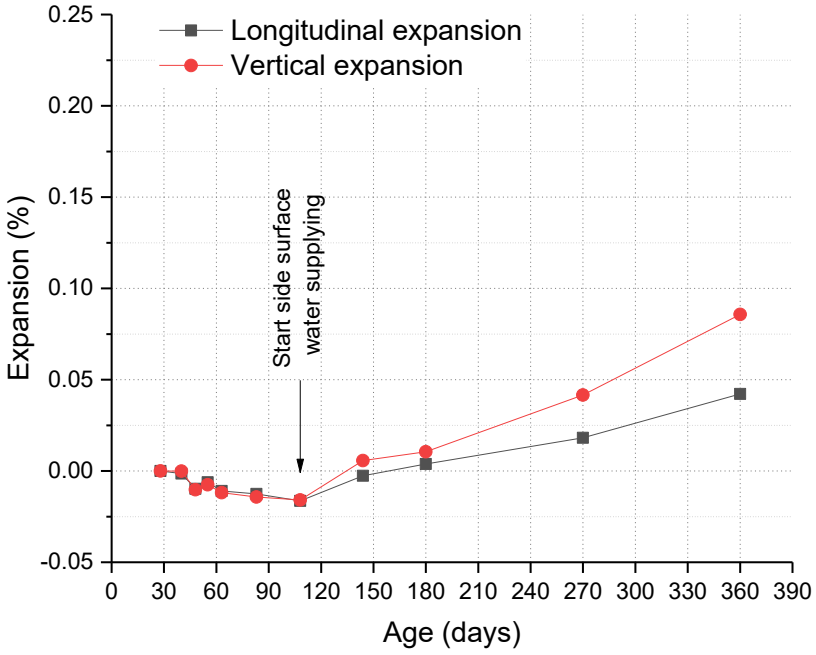

Figure 7. 42 Average longitudinal and lateral expansion of R3 reinforced concrete beam stored in 38 °C climate chamber

The beam was moved into the 38 °C climate chamber after 28 days of moist curing in the laboratory at 23 ± 2.0 °C environment. At the age of 108 days, before water was supplied to the side surface of the beam, a slight shrinkage of about 0.016% was recorded. The water supplying started at 108 days of age. At the age of one year, an average longitudinal expansion of about 0.042%, and an average of lateral expansion of about 0.086% were recorded. Longitudinal cracking on the wetting surface of the beam are shown in Figure 7.35 and 7.36.

7.5 Summary

Five full-scale 3 m long beams are fabricated for the purpose of assessing the long-term effect of ASR on the behaviour of the affected concrete structures. The full-scale 3 m long beams and their companion specimens are currently stored in 38 °C climate chamber to accelerate ASR. The alkali loading of the 3 m long beams and their companion specimens are 1.25% Na_2O_{eq} by mass of cement, which is in accordance with the recommendations of AS 1141.60.2 or ASTM C1293. In addition, to accelerate ASR, a side surface water supplying method for the plain and reinforced concrete beams is adopted in this study. Expansion of the beams and their companion specimens are measured up to one year. Furthermore, mechanical properties, including modulus of elasticity and compressive strength of the companion cylinders are measured up to one year to study the degradation caused by ASR. The main findings can be drawn as follows:

(1) For plain concrete beam (R1) containing Dacite aggregate with 1.25% alkali loading subjected to 38 °C environment, when one side surface is supplied with water and the other side surface is exposed to 20% RH atmosphere, an average longitudinal expansion of about 0.104% and an average lateral expansion of about 0.187% are recorded at the age of one year.

(2) At the age of one year, for the reactive reinforced concrete beam R2, an average longitudinal expansion of about 0.056% and an average lateral expansion of about 0.116% are recorded, while for the reactive reinforced concrete beam R3, an average longitudinal expansion of around 0.042% and an average lateral expansion of around 0.086% are recorded. The difference in expansion of the two beams at the age of one year is due to the different starting time of supplying water. Water supplying has crucial influence on the expansion of the beams.

(3) The beams exhibited an upward displacement due to differential expansion caused by ASR. After supplying water to one side surface of the beam, the wetting surface expands, while the opposite side surface provides constraints to the expansion as it is exposed to 20% RH atmosphere. In addition, cracking on wetting surface of the beams are observed, for the plain concrete beam, the cracking pattern is map cracking, while for the reinforced concrete beams, cracking develops longitudinally align with direction of the main reinforcement.

(4) Mechanical properties tests on companion cylinders show that, modulus of elasticity increases up to 90 days of age when the measured free expansion is around 0.0%. Afterwards, the modulus of elasticity starts to decrease with the increasing expansion. At the age of one year, when relevant free expansion is about 0.17%, the modulus of elasticity is decreased about 30% compared to the 90-day value. The compressive strength of cylinders is found increasing up to 6 months of age while the relevant free expansion is around 0.035%. thereafter, the compressive strength starts to decrease. However, up to free expansion level of around 0.17% at the age of one year, no dis-earnable changes are noticed compared with the 28-day compressive strength. The findings about the trends of the degradation in mechanical properties due to ASR are consistent with the findings from multi-cycle autoclave test performed at 80 °C. The difference in percentage of changing in the mechanical properties could be attributed to the different concrete mix proportion used, especially the alkali content in the mixes.

Due to the time constraints of this study, expansion measurements on the plain and reinforced concrete beams and their companion prisms are conducted up to 360 days. Similarly, the mechanical properties of the companion cylinders are measured up to one year. Currently, the full-scale 3 m long beams and the left companion specimens are

stored in the 38 °C climate chamber at UTS Tech Lab to further study the long-term behaviour of the ASR-affected concrete structures. Ultimately, load carrying capacity tests on the reactive and non-reactive reinforced concrete beams will be conducted, to provide a better understanding of the effect of ASR on the residual load capacity of the ASR affected reinforced concrete structures.

Chapter 8

Conclusions and Recommendations

8.1 Overview

As part of a wider project which is currently being conducted at the University of Technology Sydney and funded by Australian Research Council Hub for Nanoscience Based Construction Materials Manufacturing (ARC NanoComm Hub) with the support of the Cement, Concrete & Aggregates Australia (CCAA), this study investigated the residual load capacity and bond deterioration of ASR-affected reinforced concrete structures through laboratory accelerated tests. Based on previous research on accelerated autoclave test for ASR, a novel multi-cycle accelerated test, by adopting 80 °C steam warming, with 60-hour cycles and appropriate alkali loading is investigated. Furthermore, the multi-cycle accelerated test was applied to study the flexural and shear behaviour of small-scale reinforced concrete beams. In addition, bond behaviour between reinforcing steel bar and ASR affected concrete was studied by performing pull-out tests on specimens with and without autoclaving. This study also included full-scale 3 m long plain and reinforced concrete beams, and these were utilised to study the long-term behaviour of ASR-affected concrete structures. The beams are currently stored in the 38°C climate chamber at UTS Tech Lab to accelerate ASR.

The conclusions from this investigation, which have also been presented in the previous chapters, are summarised in Chapter 8.2. It is worth noting that, in comparison with the CPT test, although the multi-cycle accelerated autoclave test can accelerate ASR within a short period, the expansion achieved by 3 cycles of autoclaving is still at early ASR stage. Effects of high ASR expansion levels on structural behaviour needs further investigation. In addition, due to the time constraints of this study, further research on the

long-term behaviour of the ASR-affected full-scale 3 m long plain and reinforced concrete beams is needed. Ultimately, the load-carrying capacity of ASR-affected reinforced concrete beams will be obtained by laboratory testing, and these results would provide verification to assess the residual load capacity of ASR-affected reinforced concrete structures.

8.2 Conclusions

- The 130 °C autoclave test method appears to be suitable for screening potential alkali-silica reactivity of aggregates within a short period of time. Significant expansion is observed for concrete made with reactive aggregate and with alkali boosting. This test method can also cause damage to the ordinary Portland cement concrete made with reactive aggregate or non-reactive aggregate, resulting in reductions in concrete mechanical properties within a short period of time, which could be utilised to simulate long-term deterioration of concrete.
- The multi-cycle 130 °C autoclave test method appears to be able to simulate damage of concrete and to investigate the subsequent consequences on load capacity of the damaged reinforced concrete members. However, correlation between reduction of mechanical properties of concrete under multi-cycle 130 °C autoclave condition and deterioration of concrete caused by ASR expansion needs further investigation.
- The novel multi-cycle 80 °C accelerated autoclave test, with 60 hours per cycle, is suitable for preliminary tests to identify the potential reactivity of aggregate. For mortar bars containing dacite aggregate subjected to autoclaving cycles, the expansion was marginally affected by increasing alkali loading from 2.5% to 3.5% when the steam warming temperature was at 70 °C, and the maximum expansion was 0.23% at the end of three cycles. While at a steam warming temperature of 80 °C, the expansion was significantly increased by increasing the alkali content from 2.5% to

3.5%. A maximum expansion of 0.39% (a 70% increase over 0.23%) was achieved in three cycles. However, more tests on different aggregate types which include very highly reactive, highly reactive, moderately reactive and non-reactive aggregates need to be conducted. Correlation between the expansion obtained from the new accelerated autoclave test and the expansion of concrete in the field needs further investigation.

- The novel multi-cycle 80 °C accelerated autoclave test method appears to be suitable for investigating ASR deterioration of actual concrete mixes within a short period of time. For concrete prisms containing dacite aggregate with 2.5% alkali boosting, a maximum expansion of 0.18% was achieved after three cycles of autoclaving. The compressive strength showed an initial increase under low expansion (up to 0.13%) followed by a reduction under higher expansion, while the modulus of elasticity systemically decreased with the increasing expansion.
- Load capacity tests on small-scale reinforced concrete beams at the age of 28 days and after subjected to subsequent 1, 2 and 3 cycles of 80 °C autoclaving, with 60 hours per cycle, revealed that at early stage of ASR:
  (1) cracking load of the tested beams was increased,
  (2) although the modulus of elasticity of the concrete systematically decreased, the flexural stiffness of the beams subjected to 1, 2 and 3 cycles of 80 °C autoclaving did not show any measurable reduction due to the presence of reinforcement,
  (3) shear resistance of the tested beams was increased, and
  (4) flexural capacity of the tested beams was not significantly influenced.

Results suggest that at early stage of ASR, chemical prestressing induced by ASR expansion could have beneficial effects on strength and stiffness of the affected structure.

- Pull-out tests on specimens at the age of 28 days and specimens subjected to 1, 2 and 3 cycles of 80 °C autoclaving showed that, up to a free expansion level of about 0.18% at early stage of ASR, the bond strength between the deformed reinforcing steel bar and the ASR affected concrete is increased. Similarly, the bond stiffness is also augmented.
- Three cycles of 80 °C autoclaving is able to accelerate ASR. Expansion level and morphology of ASR products compared with field structure suggest that accelerated ASR under three cycles of 80 °C autoclaving is still at its early stage. Compared to the entire service life of the structure in the field, laboratory tests reveal only a short-term indication of load-carrying capacity of the structure. Long-term load-carrying capacity of ASR-affected reinforced concrete structures needs further investigation.

8.3 Recommendations for Future Work

As ASR is a long-term durability problem for concrete structures, to achieve high levels of expansion and damage within a short period of time which correlate to field structures damaged by ASR is a challenge. More extensive studies are needed to assess the residual load capacity of the ASR affected concrete structures and some of the future research areas are recommended.

Further investigation on laboratory accelerated ASR test by using an autoclave is needed.

Firstly, in the area of identifying potential reactivity of aggregates, more tests on different types of aggregate need to be conducted, including very highly reactive, highly reactive, moderately reactive and non-reactive aggregate.

Secondly, by applying more cycles, or combined cycles of autoclaving and then immersing in water for a period of time alternatively, it could be helpful to accelerate ASR expansion and damage in concrete within a short period. Correlation between laboratory accelerated tests and performance of field structures affected by ASR is also of interest.

Although full-scale 3 m long beams are currently tested in a controlled climate chamber, a large-scale autoclave which can accommodate full-scale structural members will facilitate rapid evaluation of the actual structural members affected by ASR. This will establish more realistic understanding of the structural behaviour of field structures affected by ASR.

It will also be meaningful to investigate the combined effect of ASR and other deterioration mechanisms such as reinforcement corrosion, on the performance of concrete structures. Likewise, it will also be important to study the combined effect of ASR and freeze-thawing by utilising an autoclave and other laboratory facilities in order to simulate the performance in cold climates.

Supplementary Cementitious Materials (SCMs), such as fly ash, slags or silica fume is often used with field placed concrete mixes. The addition of SCMs will generally mitigate ASR expansion and damage. To study these effects, usually it takes much longer testing time (e.g., two years of test duration or more). Using the accelerated autoclave test method developed, these effects can be studied within a much short period. These tests are recommended in future investigations.

References

Ahmed, T., Burley, E. & Ridgen, S. 1999, 'Effect of alkali-silica reaction on tensile bond strength of reinforcement in concrete tested under static and fatigue loading', *Materials Journal*, vol. 96, no. 4, pp. 419-28.

Ahmed, T., Burley, E. & Rigden, S. 1998, 'The static and fatigue strength of reinforced concrete beams affected by alkali-silica reaction', *Materials Journal*, vol. 95, no. 4, pp. 376-88.

Ahmed, T., Burley, E., Rigden, S. & Abu-Tair, A.I. 2003, 'The effect of alkali reactivity on the mechanical properties of concrete', *Construction and Building Materials*, vol. 17, no. 2, pp. 123-44.

Allard, A., Bilodeau, S., Pissot, F., Fourinier, B., Bastien, J. & Bissonnette, B. 2016, 'Performance evaluation of thick concrete slabs affected by alkali-silica reaction (ASR)–Part I: Material aspects', *Proceedings of 15th International Conference on Alkali-Aggregate Reaction in Concrete*, Sao Paulo, Brazil.

Allard, A., Bilodeau, S., Pissot, F., Fournier, B., Bastien, J. & Bissonnette, B. 2018, 'Expansive behaviour of thick concrete slabs affected by alkali-silica reaction (ASR)', *Construction and Building Materials*, vol. 171, pp. 421-36.

Alnaggar, M., Di Luzio, G. & Cusatis, G. 2017, 'Modeling time-dependent behaviour of concrete affected by alkali silica reaction in variable environmental conditions', *Materials*, vol. 10, no. 5, p. 471.

AS 1012.2, Methods of testing concrete, Method 2: Preparing concrete mixes in the laboratory, Standards Australia Ltd, Sydney, Australia, 2014.

AS 1012.9, Methods of testing concrete, Method 9: Compressive strength tests - Concrete, mortar and grout specimens, Standards Astralia Ltd, Sydney, Australia, 2014.

AS 1012.17, Methods of testing concrete, Method 17: Determination of the static shord modulus of elasticity and Poisson's ratio of concrete specimens, Standards Astralia Ltd, Sydney, Australia, 2014.

AS 1141.60.1, Methods for Sampling and Testing Aggregates Part 60.1: Potential alkali-silica reactivity - Accelerated mortar bar method, Standards Astralia Ltd, Sydney, Australia, 2014.

AS 1141.60.2, Methods for Sampling and Testing Aggregates Part 60.2: Potential alkali-silica reactivity - Concrete prism method, Standards Australia Ltd, Sydney, Australia, 2014.

Aslani, F. & Nejadi, S. 2012, 'Bond behavior of reinforcement in conventional and self-compacting concrete', *Advances in Structural Engineering*, vol. 15, no. 12, pp. 2033-51.

ASTM C78, Standard test method for flexural strength of concrete (using simple beam with third-point loading), ASTM International, West Conshohocken, USA, 2016.

ASTM C1260, Standard test method for potential alkali reactivity of aggregates (mortar–bar method), ASTM International, West Conshohocken, USA, 2014.

ASTM C1293, Standard test method for determination of length change of concrete due to alkali–silica reaction, ASTM International, West Conshohocken, USA, 2015.

ASTM C1778-20, Standard guide for reducing the risk of deleterious alkali-aggregate reaction in concrete, ASTM International, West Conshohocken, USA, 2020.

Bach, F., Thorsen, T.S. & Nielsen, M. 1993, 'Load-carrying capacity of structural members subjected to alkali-silica reactions', *Construction and Building Materials*, vol. 7, no. 2, pp. 109-15.

Barbosa, R.A., Hansen, S.G., Hansen, K.K., Hoang, L.C. & Grelk, B. 2018, 'Influence of alkali-silica reaction and crack orientation on the uniaxial compressive strength of concrete cores from slab bridges', *Construction and Building Materials*, vol. 176, pp. 440-51.

Barbosa, R.A., Hansen, S.G., Hoang, L.C. & Hansen, K.K. 2018, 'Residual shear strength of a severely ASR-damaged flat slab bridge', *Engineering Structures*, vol. 161, pp. 82-95.

Beglarigale, A. & Yazıcı, H. 2013, 'The effect of alkali–silica reaction on steel fiber–matrix bond characteristics of cement based mortars', *Construction and Building Materials*, vol. 47, pp. 845-60.

Ben Haha, M., Gallucci, E., Guidoum, A. & Scrivener, K.L. 2007, 'Relation of expansion due to alkali silica reaction to the degree of reaction measured by SEM image analysis', *Cement and Concrete Research*, vol. 37, no. 8, pp. 1206-14.

Berra, M., Faggiani, G., Mangialardi, T. & Paolini, A. 2010, 'Influence of stress restraint on the expansive behaviour of concrete affected by alkali-silica reaction', *Cement and Concrete Research*, vol. 40, no. 9, pp. 1403-9.

Bérubé, M.-A., Duchesne, J., Dorion, J. & Rivest, M. 2002, 'Laboratory assessment of alkali contribution by aggregates to concrete and application to concrete structures

affected by alkali–silica reactivity', *Cement and Concrete Research*, vol. 32, no. 8, pp. 1215-27.

Bérubé, M.-A. & Fournier, B. 1993, 'Canadian experience with testing for alkali-aggregate reactivity in concrete', *Cement and Concrete Composites*, vol. 15, no. 1-2, pp. 27-47.

Bérubé, M.-A. & Frenette, J. 1994, 'Testing concrete for AAR in NaOH and NaCl solutions at 38 C and 80 C', *Cement and Concrete Composites*, vol. 16, no. 3, pp. 189-98.

Bilodeau, S., Allard, A., Bastien, J., Pissot, F., Fourinier, B., Mitchell, D. & Bissonnette, B. 2016, 'Performance evaluation of thick concrete slabs affected by alkali-silica reaction (ASR)–Part II: Structural aspects', *Proceedings of 15th International Conference on Alkali-Aggregate reaction in Concrete*, Sao Paulo, Brazil.

Blight, G., Alexander, M., Ralph, T. & Lewis, B. 1989, 'Effect of alkali-aggregate reaction on the performance of a reinforced concrete structure over a six-year period', *Magazine of Concrete research*, vol. 41, no. 147, pp. 69-77.

Blight, G.E. & Alexander, M.G. 2011, *Alkali-aggregate reaction and structural damage to concrete: engineering assessment, repair and management*, CRC Press.

Capra, B. & Bournazel, J.P. 1998, 'Modeling of induced mechanical effects of alkali-aggregate reactions', *Cement and Concrete Research*, vol. 28, no. 2, pp. 251-60.

Carse, A. 1996, 'The asset management of a long bridge structure affected by alkali-silica reaction', *Proceedings of the 10th International Conference on Alkali-Aggregate Reaction in Concrete*, Melbourne, Australia, pp. 1025-32.

Castel, A. & Foster, S.J. 2015, 'Bond strength between blended slag and Class F fly ash geopolymer concrete with steel reinforcement', *Cement and Concrete Research*, vol. 72, pp. 48-53.

Castel, A., Khan, I., François, R. & Gilbert, R.I. 2016, 'Modeling steel concrete bond strength reduction due to corrosion', *ACI Structural Journal*, vol. 113, no. 5, p. 973.

CEB-FIP model code 1990: Design code, Comité Euro-International du Béton, Thomas Telford Publishing, 1993.

Chana, P. 1989, *Bond strength of reinforcement in concrete affected by Alkali Silica Reaction*, Contractor Report 141, Transport and Road Research Laboratory, Department of Transport, UK.

Clark, L. 1989, *Critical review of the structural implications of the alkali silica reaction in concrete*, Contractor Report 169, Transport and Road Research Laboratory.

Clark, L. 1990, 'Structural aspects of alkali-silica reaction', *Structural engineering review*, vol. 2, no. 2, pp. 81-7.

Clark, L. & Ng, K. 1989, 'The effect of alkali silica reaction on the punching shear strength of reinforced concrete slabs', *Proceedings of the 8th International Conference on Alkali-Aggregate Reaction in Concrete*, Kyoto, Japan, pp. 659-64.

Clayton, N., Currie, R. & Moss, R. 1990, 'Effects of alkali-silica reaction on the strength of prestressed concrete beams', *Structural Engineer*, vol. 68, pp. 287-92.

Comi, C., Fedele, R. & Perego, U. 2009, 'A chemo-thermo-damage model for the analysis of concrete dams affected by alkali-silica reaction', *Mechanics of Materials*, vol. 41, no. 3, pp. 210-30.

Cope, R. & Slade, L. 1992, 'Effect of AAR on shear capacity of beams, without shear reinforcement', *Proceedings of the 9th International Conference on Alkali-Aggregate Reaction in Concrete*, London, UK, pp. 184-91.

Çopuroğlu, O., Andiç-Çakir, Ö., Broekmans, M.A. & Kühnel, R. 2009, 'Mineralogy, geochemistry and expansion testing of an alkali-reactive basalt from western Anatolia, Turkey', *Materials Characterization*, vol. 60, no. 7, pp. 756-66.

Courtier, R. 1990, 'The assessment of ASR-affected structures', *Cement and Concrete composites*, vol. 12, no. 3, pp. 191-201.

Criaud, A., Defossé, C., Chabanis, B., Debray, L., Michel, B., Sorrentino, D., Gallias, M., Salomon, M., Guédon, S. & Le Roux, A. 1994, 'The French standard methods for evaluating the reactivity of aggregates with respect to AAR: Results of an inter-laboratory program', *Cement and Concrete Composites*, vol. 16, no. 3, pp. 199-206.

CSA A23.2-25A-14, Test Method for Detection of Alkali-silica Reactive Aggregate by Accelerated Expansion of Mortar Bars, Canadian Standards Association, Canada, 2014.

CSA A23.2-27A-14, Standard Practice to Identify Potential for Alkali-Reactivity of Aggregates and Measures to Avoid Deleterious Expansion in Concrete, Canadian Standards Association, Canada, 2014.

den Uijl, J.A. & Kaptijn, N. 2002, 'Structural consequences of ASR: An example on shear capacity', *Heron*, vol. 47, no. 2, pp. 125-39.

Dent Glasser, L.S. & Kataoka, N. 1981, 'The chemistry of 'alkali-aggregate' reaction', *Cement and Concrete Research*, vol. 11, no. 1, pp. 1-9.

Deschenes, D., Bayrak, O. & Folliard, K. 2009, 'Shear capacity of large-scale bridge bent specimens subject to alkali-silica reaction and delayed ettringite formation', pp. 1-9.

Deschenes Jr, R.A., Giannini, E.R., Drimalas, T., Fournier, B. & Hale, W.M. 2018, 'Effects of moisture, temperature, and freezing and thawing on alkali-silica reaction', *ACI Materials Journal*, vol. 115, no. 4.

Desnerck, P., Lees, J.M. & Morley, C.T. 2015, 'Bond behaviour of reinforcing bars in cracked concrete', *Construction and Building Materials*, vol. 94, pp. 126-36.

Dunant, C.F. & Scrivener, K.L. 2010, 'Micro-mechanical modelling of alkali-silica-reaction-induced degradation using the AMIE framework', *Cement and Concrete research*, vol. 40, no. 4, pp. 517-25.

Dunant, C.F. & Scrivener, K.L. 2012, 'Effects of aggregate size on alkali-silica-reaction induced expansion', *Cement and concrete research*, vol. 42, no. 6, pp. 745-51.

Esposito, R., Anaç, C., Hendriks, M.A. & Çopuroğlu, O. 2016, 'Influence of the alkali-silica reaction on the mechanical degradation of concrete', *Journal of Materials in Civil Engineering*, vol. 28, no. 6, p. 04016007.

Esposito, R. & Hendriks, M. 2016, 'A multiscale micromechanical approach to model the deteriorating impact of alkali-silica reaction on concrete', *Cement and Concrete Composites*, vol. 70, pp. 139-52.

Esposito, R. & Hendriks, M. 2017, 'Literature review of modelling approaches for ASR in concrete: A new perspective', *European Journal of Environmental and Civil Engineering*, pp. 1-21.

Fan, S. & Hanson, J.M. 1998, 'Effect of alkali silica reaction expansion and cracking on structural behaviour of reinforced concrete beams', *ACI Structural Journal*, vol. 95, pp. 498-505.

Ferguson, P.M. & Thompson, J.N. 1965, 'Development length for large high strength reinforcing bars', *ACI Journal Proceedings*, vol. 62, no. 1, pp. 71-94.

Fernandes, I. 2009, 'Composition of alkali–silica reaction products at different locations within concrete structures', *Materials Characterization*, vol. 60, no. 7, pp. 655-68.

Fernandes, I., Medeiros, S., Costa, I.R., Nunes, J.C. & Quinta-Ferreira, M. 2015, 'Petrographic and chemical characterization of concrete deterioration products',

International Multidisciplinary Scientific GeoConference: SGEM: Surveying Geology & mining Ecology Management, vol. 2, p. 511.

Fernandes, I., Noronha, F. & Teles, M. 2004, 'Microscopic analysis of alkali–aggregate reaction products in a 50-year-old concrete', *Materials Characterization*, vol. 53, no. 2-4, pp. 295-306.

Fournier, B. & Bérubé, M.-A. 2000, 'Alkali-aggregate reaction in concrete: A review of basic concepts and engineering implications', *Canadian Journal of Civil Engineering*, vol. 27, no. 2, pp. 167-91.

Fournier, B., Bérubé, M. & Bergeron, G. 1991, 'A rapid autoclave mortar bar method to determine the potential alkali-silica reactivity of St. Lawrence lowlands carbonate aggregates (Quebec, Canada)', *Cement, concrete and aggregates*, vol. 13, no. 1, pp. 58-71.

Fournier, B., Ideker, J.H., Folliard, K.J., Thomas, M.D., Nkinamubanzi, P.-C. & Chevrier, R. 2009, 'Effect of environmental conditions on expansion in concrete due to alkali–silica reaction (ASR)', *Materials Characterization*, vol. 60, no. 7, pp. 669-79.

Fu, X. & Chung, D. 1997, 'Effect of corrosion on the bond between concrete and steel rebar', *Cement and Concrete Research*, vol. 27, no. 12, pp. 1811-5.

Fujii, M., kabayashi, K., Kojima, T. & Maehara, H. 1986, 'The static and dynamic behaviour of reinforced concrete beams with cracking due to alkali-silica reaction', *Proceedings of the 7th International Conference on Alkali–Aggregate Reaction in Concrete*, Ottawa, Canada, pp. 126-30.

Garcia-Diaz, E., Riche, J., Bulteel, D. & Vernet, C. 2006, 'Mechanism of damage for the alkali–silica reaction', *Cement and Concrete Research*, vol. 36, no. 2, pp. 395-400.

Gardoni, P., Pagnotta, A., Huang, Q. & Trejo, D. 2012, *Evaluation of concrete structures affected by alkali-silica reaction and delayed ettringite formation-part 2*, Texas. Dept. of Transportation. Research and Technology Implementation Office.

Gautam, B.P. & Panesar, D.K. 2017, 'The effect of elevated conditioning temperature on the ASR expansion, cracking and properties of reactive Spratt aggregate concrete', *Construction and Building Materials*, vol. 140, pp. 310-20.

Gautam, B.P., Panesar, D.K., Sheikh, S.A. & Vecchio, F.J. 2017, 'Effect of coarse aggregate grading on the ASR expansion and damage of concrete', *Cement and Concrete Research*, vol. 95, pp. 75-83.

Gavrilenko, E., García del Amo, D., Calvo Pérez, B. & García García, E. 2007, 'Comparison of ASR-gels in concretes against accelerated mortar bar test samples', *Magazine of Concrete Research*, vol. 59, no. 7, pp. 483-94.

Giaccio, G., Zerbino, R., Ponce, J.M. & Batic, O.R. 2008, 'Mechanical behaviour of concretes damaged by alkali-silica reaction', *Cement and Concrete Research*, vol. 38, no. 7, pp. 993-1004.

Giannini, E. & Folliard, K. 2013, 'A rapid test to determine alkali-silica reactivity of aggregates using autoclaved concrete prisms', *SN3235, Portland Cement Association, Skokie, Illinois, USA*, vol. 21.

Giannini, E.R. 2012, 'Evaluation of concrete structures affected by alkali-silica reaction and delayed ettringite formation', PhD thesis, The University of Texas at Austin, TX, USA.

Godart, B., de Rooij, M.R. & Wood, J.G. 2013, *Guide to diagnosis and appraisal of AAR damage to concrete in structures*, Springer.

Grattan-Bellew, P.E. 1997, 'A critical review of ultra-accelerated tests for alkali-silica reactivity', *Cement and Concrete Composites*, vol. 19, no. 5, pp. 403-14.

Grimal, É., Sellier, A., Le Pape, Y. & Bourdarot, É. 2008, 'Creep, shrinkage, and anisotropic damage in alkali-aggregate reaction swelling mechanism - Part I: A constitutive model', *ACI Materials Journal*, vol. 105, no. 3, p. 227.

Grimal, E., Sellier, A., Multon, S., Le Pape, Y. & Bourdarot, E. 2010, 'Concrete modelling for expertise of structures affected by alkali aggregate reaction', *Cement and Concrete Research*, vol. 40, no. 4, pp. 502-7.

Ha, T.M., Fukada, S. & Torii, K. 2017, 'Effects of fly ash on mechanical properties of PC girder using reactive andesite aggregates', *Journal of Advanced Concrete Technology*, vol. 15, no. 10, pp. 579-94.

Haddad, R.H. & Numayr, K.S. 2007, 'Effect of alkali-silica reaction and freezing and thawing action on concrete–steel bond', *Construction and Building Materials*, vol. 21, no. 2, pp. 428-35.

Hamada, H., Otsuki, N. & Fukute, T. 1989, 'Properties of concrete specimens damaged by alkali-aggregate reaction, laumontite related reaction and chloride attack under

marine environments', *Proceedings of the 8th International Conference on AAR*, Kyoto, Japan, pp. 603-8.

Hansen, S.G., Barbosa, R.A. & Hoang, L.C. 2016, 'Prestressing of reinforcing bars in concrete slabs due to concrete expansion induced by Alkali-Silica Reaction', *Proceedings of fib Symposium 2016: Performance-based approaches for concrete structures*, Cape Town, South Africa.

Hansen, S.G., Barbosa, R.A., Hoang, L.C. & Hansen, K.K. 2016, 'Shear capacity of ASR damaged structures–In-depth analysis of some in-situ shear tests on bridge slabs', *Proceedings of 15th International Confrence on Alkali-Aggregate Reaction in Concrete*, Sao Paulo, Brazil.

Hobbs, D. & Gutteridge, W. 1979, 'Particle size of aggregate and its influence upon the expansion caused by the alkali–silica reaction', *Magazine of Concrete research*, vol. 31, no. 109, pp. 235-42.

Hobbs, D.W. 1988, *Alkali-silica reaction in concrete*, Thomas Telford Ltd, London.

Hooton, R. & Rogers, C. 1993, 'Development of the NBRI rapid mortar bar test leading to its use in North America', *Construction and Building Materials*, vol. 7, no. 3, pp. 145-8.

Hou, X., Kirkpatrick, R.J., Struble, L.J. & Monteiro, P.J. 2005, 'Structural investigations of alkali silicate gels', *Journal of the American Ceramic Society*, vol. 88, no. 4, pp. 943-9.

Hou, X., Struble, L.J. & Kirkpatrick, R.J. 2004, 'Formation of ASR gel and the roles of C-S-H and portlandite', *Cement and Concrete Research*, vol. 34, no. 9, pp. 1683-96.

Huang, Q., Gardoni, P., Trejo, D. & Pagnotta, A. 2014, 'Probabilistic model for steel – concrete bond behaviour in bridge columns affected by alkali silica reactions', *Engineering Structures*, vol. 71, pp. 1-11.

Idorn, G.M. 1989, 'Alkali-silica reactions in retrospect and prospect', *Proceedings of the 8th International Conference on Alkali–Aggregate Reaction in Concrete*, Kyoto, Japan, pp. 1-9.

Imai, H., Yamasaki, T., Maehara, H. & Miyagawa, T. 1987, 'The deterioration by alkali-silica reaction of hanshin expressway concrete structures - Investigation and repair', *Proceedings of the 7th International Conference on Alkali-Aggregate Reaction in Concrete, Ottawa, Canada*, pp. 131-5.

Inoue, S., Fujii, M., Kobayashi, K. & Nakano, K. 1989, 'Structural behaviors of reinforced concrete beams affected by alkali–silica reaction', *Proceedings of the 8th International Conference on Alkali–Aggregate Reaction in Concrete*, Kyoto, Japan, pp. 727-32.

ISE 1992, *Structural effects of alkali-silica reaction: Technical guidance on the appraisal of existing structures*, SETO Ltd, London, United Kingdom.

Islam, M.S., Alam, M.S., Ghafoori, N. & Sadiq, R. 2016, 'Role of solution concentration, cement alkali and test duration on expansion of accelerated mortar bar test (AMBT)', *Materials and Structures*, vol. 49, no. 5, pp. 1955-65.

Islam, M.S. & Ghafoori, N. 2013, 'Evaluation of alkali-silica reactivity using aggregate geology, expansion limits of mortar bars and concrete prisms, and kinetic model', *Journal of Materials Science Research*, vol. 2, no. 2, p. 103.

Johnston, D., Stokes, D. & Surdahl, R. 2000, 'A kinetic-based method for interpreting ASTM C 1260', *Cement, concrete and aggregates*, vol. 22, no. 2, pp. 142-9.

Jones, A. & Clark, L. 1996, 'The effects of restraint on ASR expansion of reinforced concrete', *Magazine of Concrete Research*, vol. 48, no. 174, pp. 1-13.

Kagimoto, H., Yasuda, Y. & Kawamura, M. 2014, 'ASR expansion, expansive pressure and cracking in concrete prisms under various degrees of restraint', *Cement and Concrete Research*, vol. 59, pp. 1-15.

Kankam, C.K. 1997, 'Relationship of bond stress, steel stress, and slip in reinforced concrete', *Journal of structural engineering*, vol. 123, no. 1, pp. 79-85.

Karthik, M.M., Mander, J.B. & Hurlebaus, S. 2016a, 'ASR/DEF related expansion in structural concrete: Model development and validation', *Construction and Building Materials*, vol. 128, pp. 238-47.

Karthik, M.M., Mander, J.B. & Hurlebaus, S. 2016b, 'Deterioration data of a large-scale reinforced concrete specimen with severe ASR/DEF deterioration', *Construction and Building Materials*, vol. 124, pp. 20-30.

Karthik, M.M., Mander, J.B. & Hurlebaus, S. 2018, 'Experimental behaviour of large reinforced concrete specimen with heavy ASR and DEF deterioration', *Journal of Structural Engineering*, vol. 144, no. 8, p. 04018110.

Kawabata, Y., Dunant, C., Yamada, K. & Scrivener, K. 2019, 'Impact of temperature on expansive behavior of concrete with a highly reactive andesite due to the alkali–silica reaction', *Cement and Concrete Research*, vol. 125, p. 105888.

Kawabata, Y., Seignol, J.-F., Martin, R.-P. & Toutlemonde, F. 2017, 'Macroscopic chemo-mechanical modeling of alkali-silica reaction of concrete under stresses', *Construction and Building Materials*, vol. 137, pp. 234-45.

Kawabata, Y., Yamada, K., Sagawa, Y. & Ogawa, S. 2018, 'Alkali-wrapped concrete prism test (AW-CPT) – New testing protocol toward a performance test against alkali-silica reaction', *Journal of Advanced Concrete Technology*, vol. 16, no. 9, pp. 441-60.

Kawamura, M., Takemoto, K. & Ichise, M. 1989, 'Influence of the alkal-silica reaction on the corrosion of steel reinforcement in concrete', *Proceedings of the 8th International Conference on Alkali-Aggregate Reaction in Concrete*, Kyoto, Japan, pp. 115-20.

Korkanç, M. & Tuğrul, A. 2005, 'Evaluation of selected basalts from the point of alkali–silica reactivity', *Cement and Concrete Research*, vol. 35, no. 3, pp. 505-12.

Koyangi, W., Rokugo, K. & Ishida, H. 1986, 'Failure behaviour of reinforced concrete beams deteriorated by alkali-silica reactions', *Proceedings of the 7th International Conference on Alkali–Aggregate Reaction in Concrete*, Ottawa, Canada, pp. 141-5.

Koyangi, W., Rokugo, K. & Uchida, Y. 1992, 'Mechanical properties of concrete deteriorated by alkali-aggregate reaction under various reinforcement ratios', *Proceedings of the 9th International Conference on Alkali-Aggregate Reaction*, London, UK, pp. 556-63.

Koyangi, W., Rokugo, K., Uchida, Y. & Iwase, H. 1996, 'Deformation behaviour of reinforced concrete beams deteriorated by ASR', *Proceedings of the 10th International Conference on Alkali-Aggregate Reaction in Concrete*, Melbourne, Australia, pp. 458-65.

Larive, C. 1998, 'Apports combinés de l'expérimentation et de la modélisation à la compréhension de l'alcali-réaction et de ses effets mécaniques', PhD thesis, Laboratoires des Ponts et Chausse´es, Paris, France.

Latifee, E.R. & Rangaraju, P.R. 2015, 'Miniature concrete prism test: rapid test method for evaluating alkali-silica reactivity of aggregates', *Journal of Materials in Civil Engineering*, vol. 27, no. 7, p. 04014215.

Lee, B. & Mulheron, M. 2015, 'Measurement of bar strain during pull-out tests: use of electrical resistance gauge methods under large displacement', *Magazine of Concrete Research*, vol. 67, no. 10, pp. 523-31.

Leemann, A., Le Saout, G., Winnefeld, F., Rentsch, D. & Lothenbach, B. 2011, 'Alkali–silica reaction: the influence of calcium on silica dissolution and the formation of reaction products', *Journal of the American Ceramic Society*, vol. 94, no. 4, pp. 1243-9.

Leonhardt, F. 1964, *Prestressed concrete: Design and construction*, W. Ernst.

Li, P., Tan, N., An, X., Maekawa, K. & Jiang, Z. 2020, 'Restraint effect of reinforcing bar on ASR expansion and deterioration characteristic of the bond behaviour', *Journal of Advanced Concrete Technology*, vol. 18, no. 4, pp. 192-210.

Lin, H. & Zhao, Y. 2016, 'Effects of confinements on the bond strength between concrete and corroded steel bars', *Construction and Building Materials*, vol. 118, pp. 127-38.

Lindgård, J., Thomas, M.D., Sellevold, E.J., Pedersen, B., Andiç-Çakır, Ö., Justnes, H. & Rønning, T.F. 2013, 'Alkali–silica reaction (ASR) – performance testing: Influence of specimen pre-treatment, exposure conditions and prism size on alkali leaching and prism expansion', *Cement and Concrete Research*, vol. 53, pp. 68-90.

Liu, S.-H., Bracci, J.M., Mander, J.B. & Hurlebaus, S. 2017, 'Performance of D-regions affected by alkali-silica reaction: Experimental and analytical study', *Journal of Structural Engineering*, vol. 143, no. 9, p. 04017109.

Lu, D., Fournier, B., Grattan-Bellew, P.E., Xu, Z. & Tang, M. 2008, 'Development of a universal accelerated test for alkali-silica and alkali-carbonate reactivity of concrete aggregates', *Materials and Structures*, vol. 41, no. 2, pp. 235-46.

Lundgren, K. 2005, 'Bond between ribbed bars and concrete. Part 1: Modified model', *Magazine of Concrete Research*, vol. 57, no. 7, pp. 371-82.

Lutz, L.A. & Gergely, P. 1967, 'Mechanics of bond and slip of deformed bars in concrete', *ACI Journal Proceedings*, vol. 64, no. 11, pp. 711-21.

Mahanama, D., De Silva, P., Kim, T., Castel, A. & Khan, M. 2019, 'Evaluating effect of GGBFS in alkali–silica reaction in geopolymer mortar with accelerated mortar bar test', *Journal of Materials in Civil Engineering*, vol. 31, no. 8, p. 04019167.

Majlesi, Y. 1994, 'A laboratory investigation into the structural performance and mechanical properties of plain and reinforced concrete elements affected by alkali silica reaction', PhD thesis, Queen Mary, University of London.

Marzouk, H. & Langdon, S. 2003, 'The effect of alkali-aggregate reactivity on the mechanical properties of high and normal strength concrete', *Cement and Concrete Composites*, vol. 25, no. 4, pp. 549-56.

Mather, B. 1999, 'How to make concrete that will not suffer deleterious alkali-silica reaction', *Cement and Concrete Research*, vol. 29, no. 8, pp. 1277-80.

Menzel, C.A. 1939, 'Some factors influencing results of pull-out bond tests', *ACI Journal Proceedings*, vol. 35, no. 6, pp. 517-42.

Miyagawa, T. 2013, 'Fracture of reinforcing steels in concrete damaged by ASR', *Construction and Building Materials*, vol. 39, pp. 105-12.

Miyagawa, T., Seto, K., Sasaki, K., Mikata, Y., Kuzume, K. & Minami, T. 2006, 'Fracture of reinforcing steels in concrete structures damaged by alkali-silica reaction', *Journal of Advanced Concrete Technology*, vol. 4, no. 3, pp. 339-55.

Mohammed, T.U., Hamada, H. & Yamaji, T. 2003a, 'Alkali-silica reaction-induced strains over concrete surface and steel bars in concrete', *Materials Journal*, vol. 100, no. 2, pp. 133-42.

Mohammed, T.U., Hamada, H. & Yamaji, T. 2003b, 'Relation between strain on surface and strain over embedded steel bars in ASR affected concrete members', *Journal of Advanced Concrete Technology*, vol. 1, no. 1, pp. 76-88.

Monette, L.J., Gardner, N.J. & Grattan-Bellew, P.E. 2002, 'Residual strength of reinforced concrete beams damaged by alkali-silica reaction - Examination of damage rating index method', *ACI Materials Journal*, vol. 99, no. 1, pp. 42-50.

Morenon, P., Multon, S., Sellier, A., Grimal, E., Hamon, F. & Bourdarot, E. 2017, 'Impact of stresses and restraints on ASR expansion', *Construction and Building Materials*, vol. 140, pp. 58-74.

Morenon, P., Multon, S., Sellier, A., Grimal, E., Hamon, F. & Kolmayer, P. 2019, 'Flexural performance of reinforced concrete beams damaged by alkali-silica reaction', *Cement and Concrete Composites*, vol. 104, p. 103412.

Multon, S., Cyr, M., Sellier, A., Diederich, P. & Petit, L. 2010, 'Effects of aggregate size and alkali content on ASR expansion', *Cement and Concrete Research*, vol. 40, no. 4, pp. 508-16.

Multon, S., Seignol, J.-F. & Toutlemonde, F. 2005, 'Structural behaviour of concrete beams affected by alkali-silica reaction', *Materials Journal*, vol. 102, no. 2, pp. 67-76.

Multon, S. & Sellier, A. 2016, 'Multi-scale analysis of alkali–silica reaction (ASR): Impact of alkali leaching on scale effects affecting expansion tests', *Cement and Concrete Research*, vol. 81, pp. 122-33.

Multon, S. & Toutlemonde, F. 2006, 'Effect of applied stresses on alkali–silica reaction-induced expansions', *Cement and Concrete Research*, vol. 36, no. 5, pp. 912-20.

Multon, S. & Toutlemonde, F. 2010, 'Effect of moisture conditions and transfers on alkali silica reaction damaged structures', *Cement and Concrete Research*, vol. 40, no. 6, pp. 924-34.

Nishibayashi, S., Kuroda, T., Inoue, S. & Okawa, Y. 1996, 'Expansion characteristics of AAR in concrete by autoclave method', *Proceedings of the 10th International Conference on Alkali-Aggregate Reaction in Concrete*, Melbourne, Australia, pp. 370-6.

Nishibayashi, S., Yamura, K. & Matsushita, H. 1987, 'A rapid method of determining the alkali-aggregate reaction in concrete by autoclave', *Proceedings of the 7th International Conference on Alkali-Aggregate Reaction in Concrete*, Ottawa, Canada.

Page, C. & Treadaway, K. 1982, 'Aspects of the electrochemistry of steel in concrete', *Nature*, vol. 297, no. 5862, p. 109.

Pan, J.W., Feng, Y.T., Wang, J.T., Sun, Q.C., Zhang, C.H. & Owen, D.R. 2012, 'Modeling of alkali-silica reaction in concrete: A review', *Frontiers of Structural and Civil Engineering*, vol. 6, no. 1, pp. 1-18.

Park, R. & Paulay, T. 1975, *Reinforced concrete structures*, John Wiley & Sons.

Powers, T. & Steinour, H. 1955, 'An interpretation of some published researches on the alkali-aggregate reaction Part 2 - A hypothesis concerning safe and unsafe reactions with reactive silica in concrete', vol. 51, pp. 785-812.

Poyet, S., Sellier, A., Capra, B., Thèvenin-Foray, G., Torrenti, J.-M., Tournier-Cognon, H. & Bourdarot, E. 2006, 'Influence of water on alkali-silica reaction: Experimental study and numerical simulations', *Journal of Materials in civil Engineering*, vol. 18, no. 4, pp. 588-96.

Rajabipour, F., Giannini, E., Dunant, C., Ideker, J.H. & Thomas, M.D. 2015, 'Alkali–silica reaction: Current understanding of the reaction mechanisms and the knowledge gaps', *Cement and Concrete Research*, vol. 76, pp. 130-46.

Regourd, M. & Hornain, H. 1987, 'Microstructure of reaction products, concrete alkali-aggregate reactions', *Proceedings of the 7th International Conference on Alkali-Aggregate Reaction in Concrete*, Ottawa, Canada, pp. 375-80.

RILEM Recommended Test Method AAR-2, Detection of potential alkali-reactivity - Accelerated mortar-bar test mothod for aggregates, RILEM Technical Committee 219-ACS, 2016.

RILEM Recommended Test Method AAR-3, Detection of potential alkali-reactivity - 38°C Test method for aggregate combinations using concrete prisms, RILEM Technical Committee 219-ACS, 2016.

RILEM Recommended Test Method AAR-4.1, Detection of potential alkali-reactivity - 60°C Test method for aggregate combinations using concrete prisms, RILEM Technical Committee 219-ACS, 2016.

RMS T363, Test method T363: Accelerated mortar bar test for the assessment of alkali-reactivity of aggregate, Roads & Maritime Services, NSW, Australia, 2012.

RMS T364, Test method T364: Concrete prism test for AAR assessment, Roads & Maritime Services, NSW, Australia, 2012.

Sanchez, L., Drimalas, T., Fournier, B., Mitchell, D. & Bastien, J. 2018, 'Comprehensive damage assessment in concrete affected by different internal swelling reaction (ISR) mechanisms', *Cement and Concrete Research*, vol. 107, pp. 284-303.

Sanchez, L., Fournier, B., Jolin, M. & Duchesne, J. 2015, 'Reliable quantification of AAR damage through assessment of the damage rating index (DRI)', *Cement and Concrete Research*, vol. 67, pp. 74-92.

Sanchez, L., Fournier, B., Jolin, M., Mitchell, D. & Bastien, J. 2017, 'Overall assessment of alkali-aggregate reaction (AAR) in concretes presenting different strengths and incorporating a wide range of reactive aggregate types and natures', *Cement and Concrete Research*, vol. 93, pp. 17-31.

Sanchez, L., Fournier, B., Mitchell, D. & Bastien, J. 2020, 'Condition assessment of an ASR-affected overpass after nearly 50 years in service', *Construction and Building Materials*, vol. 236, p. 117554.

Saouma, V. 2014, *Numerical modeling of AAR*, CRC press.

Saouma, V., Perotti, L. & Shimpo, T. 2007, 'Stress analysis of concrete structures subjected to alkali-aggregate reactions', *ACI structural journal*, vol. 104, no. 5, p. 532.

Saouma, V.E. & Hariri-Ardebili, M.A. 2020, 'Integrative experimental and numerical study of ASR affected nuclear concrete containments', *Materials and Structures*, vol. 53, no. 1, p. 3.

Sargolzahi, M., Kodjo, S.A., Rivard, P. & Rhazi, J. 2010, 'Effectiveness of nondestructive testing for the evaluation of alkali–silica reaction in concrete', *Construction and Building Materials*, vol. 24, no. 8, pp. 1398-403.

Schmidt, J.W., Hansen, S.G., Barbosa, R.A. & Henriksen, A. 2014, 'Novel shear capacity testing of ASR damaged full scale concrete bridge', *Engineering Structures*, vol. 79, pp. 365-74.

Shayan, A., Ivanusec, I. & Diggins, R. 1994, 'Suitability of two rapid test methods for determining the alkali reactivity of sands', *Cement and Concrete Composites*, vol. 16, no. 3, pp. 177-88.

Sirivivatnanon, V., Mohammadi, J. & South, W. 2016, 'Reliability of new Australian test methods in predicting alkali silica reaction of field concrete', *Construction and Building Materials*, vol. 126, pp. 868-74.

Smaoui, N., Bérubé, M., Fournier, B., Bissonnette, B. & Durand, B. 2005, 'Effects of alkali addition on the mechanical properties and durability of concrete', *Cement and Concrete Research*, vol. 35, no. 2, pp. 203-12.

Smaoui, N., Bissonnette, B., Bérubé, M.-A., Fournier, B. & Durand, B. 2006, 'Mechanical properties of ASR-affected concrete containing fine or coarse reactive aggregates', *Journal of ASTM International*, vol. 3, no. 3, pp. 1-16.

Stanton, T.E. 1940, 'Expansion of concrete through reaction between cement and aggregate', *Publications of the American Society of Civil Engineers*, vol. 66, no. 10, pp. 1781-811.

Strack, C.M., Barnes, E., Ramsey, M.A., Williams, R.K., Klaus, K.L. & Moser, R.D. 2020, 'Impact of aggregate mineralogy and exposure solution on alkali-silica reaction product composition and structure within accelerated test conditions', *Construction and Building Materials*, vol. 240, p. 117929.

Swamy, R. 1997, 'Assessment and rehabilitation of AAR-affected structures', *Cement and Concrete Composites*, vol. 19, no. 5-6, pp. 427-40.

Swamy, R.N. 1992, *The alkali-silica reaction in concrete*, CRC Press.

Swamy, R.N. & Al-Asali, M. 1988, 'Engineering properties of concrete affected by alkali-silica reaction', *ACI Materials Journal*, vol. 85, no. 5, pp. 367-74.

Swamy, R.N. & Al-Asali, M. 1989, 'Effect of alkali-silica reaction on the structural behavior of reinforced concrete beams', *ACI Structural Journal*, vol. 86, no. 4, pp. 451-9.

Tamura, H. 1987, 'A test method on rapid identification of alkali reactivity aggregate (GBRC rapid method)', *Proceedings of the 7th International Conference on Alkali-Aggregate Reaction in Concrete*, Ottawa, Canada, pp. 304-8.

Tang, M., Han, S. & Zhen, S. 1983, 'A rapid method for identification of alkali reactivity of aggregate', *Cement and Concrete Research*, vol. 13, no. 3, pp. 417-22.

Tapas, M.J. 2020, 'Role of supplementary cementitious materials in mitigating alkali-silica reaction', PhD thesis, University of Technology Sydney, Sydney, Australia.

Tepfers, R. 1979, 'Cracking of concrete cover along anchored deformed reinforcing bars', *Magazine of concrete research*, vol. 31, no. 106, pp. 3-12.

Thaulow, N., Jakobsen, U.H. & Clark, B. 1996, 'Composition of alkali silica gel and ettringite in concrete railroad ties: SEM-EDX and X-ray diffraction analyses', *Cement and Concrete Research*, vol. 26, no. 2, pp. 309-18.

Thomas, M. 1998, 'The role of calcium in alkali-silica reaction', *Materials Science of Concrete - The Sidney Diamond Symposium*, pp. 325-37.

Thomas, M. 2001, 'The role of calcium hydroxide in alkali recycling in concrete', in J.P. Skalny, J. Gebauer & I. Odler (eds), *Materials Science of Concrete Special Volume: Calcium Hydroxide in Concrete*, American Ceramic Society, pp. 225-36.

Thomas, M. 2011, 'The effect of supplementary cementing materials on alkali-silica reaction: A review', *Cement and concrete research*, vol. 41, no. 12, pp. 1224-31.

Thomas, M. 2018, 'Alkali-silica reaction: Eighty years on', *Proceedings of the 5th International fib Congress*, Melbourne, Australia, pp. 27-41.

Thomas, M., Folliard, K., Fournier, B., Rivard, P., Drimalas, T. & Garber, S. 2013, *Methods for Evaluating and Treating ASR-Affected Structures: Results of Field Application and Demonstration Projects–Volume II: Details of Field Applications and Analysis*, FHWA-HIF-14-0003, Office of Pavement Technology, Federal Highway Administration, United States.

Thomas, M., Fournier, B. & Folliard, K. 2013, *Alkali-aggregate reactivity (AAR) facts book*, FHWA-HIF-13-019, Office of Pavement Technology, Federal Highway Administration, United States.

Thomas, M., Fournier, B., Folliard, K., Ideker, J. & Shehata, M. 2006, 'Test methods for evaluating preventive measures for controlling expansion due to alkali–silica reaction in concrete', *Cement and Concrete Research*, vol. 36, no. 10, pp. 1842-56.

Tondolo, F. 2015, 'Bond behaviour with reinforcement corrosion', *Construction and Building Materials*, vol. 93, pp. 926-32.

Tordoff, M. 1990, 'Assessment of pre-stressed concrete bridges suffering from alkali-silica reaction', *Cement and Concrete Composites*, vol. 12, no. 3, pp. 203-10.

Torii, K., Yamato, H., Andrade, O. & Tarui, T. 2008, 'Mechanisms of fracture of steel bars in ASR-affected bridge piers', *Proceedings of the 8th International Conference on Creep, Shrinkage and Durability of Concrete and Concrete Structures*, vol. 2, Ise-Shima, Japan, pp. 1139-45.

Ulm, F.-J., Coussy, O., Li, K. & Larive, C. 2000, 'Thermo-chemo-mechanics of ASR expansion in concrete structures', *Journal of Engineering Mechanics*, vol. 126, no. 3, p. 233.

Wald, D., Martinez, G.A. & Bayrak, O. 2017, 'Expansion behaviour of a biaxially reinforced concrete member affected by alkali ‐ silica reaction', *Structural Concrete*, vol. 18, no. 4, pp. 550-60.

Wang, H. & Gillott, J.E. 1991, 'Mechanism of alkali-silica reaction and the significance of calcium hydroxide', *Cement and Concrete Research*, vol. 21, no. 4, pp. 647-54.

Wood, S.G., Giannini, E.R., Bentivegna, A.F., Rashidian-Dezfouli, H., Rangaraju, P.R., Drimalas, T., Ramsey, M.A., Johnson, T.R. & Moser, R.D. 2017, 'Five-hour autoclave test for determining potential alkali-silica reactivity of concrete aggregates: A multi-laboratory study', *Advances in Civil Engineering Materials*, vol. 6, no. 1, pp. 550-63.

Wood, S.G., Giannini, E.R., Ramsey, M.A. & Moser, R.D. 2018, 'Autoclave test parameters for determining alkali-silica reactivity of concrete aggregates', *Construction and Building Materials*, vol. 168, pp. 683-91.

Yalciner, H., Eren, O. & Sensoy, S. 2012, 'An experimental study on the bond strength between reinforcement bars and concrete as a function of concrete cover, strength and corrosion level', *Cement and Concrete Research*, vol. 42, no. 5, pp. 643-55.

Yamada, K., Karasuda, S., Ogawa, S., Sagawa, Y., Osako, M., Hamada, H. & Isneini, M. 2014, 'CPT as an evaluation method of concrete mixture for ASR expansion', *Construction and Building Materials*, vol. 64, pp. 184-91.

Appendices

Appendix A. Morphology of ASR Products

Appendix A.1. ASR Products Observed from a 25-year-old Bridge

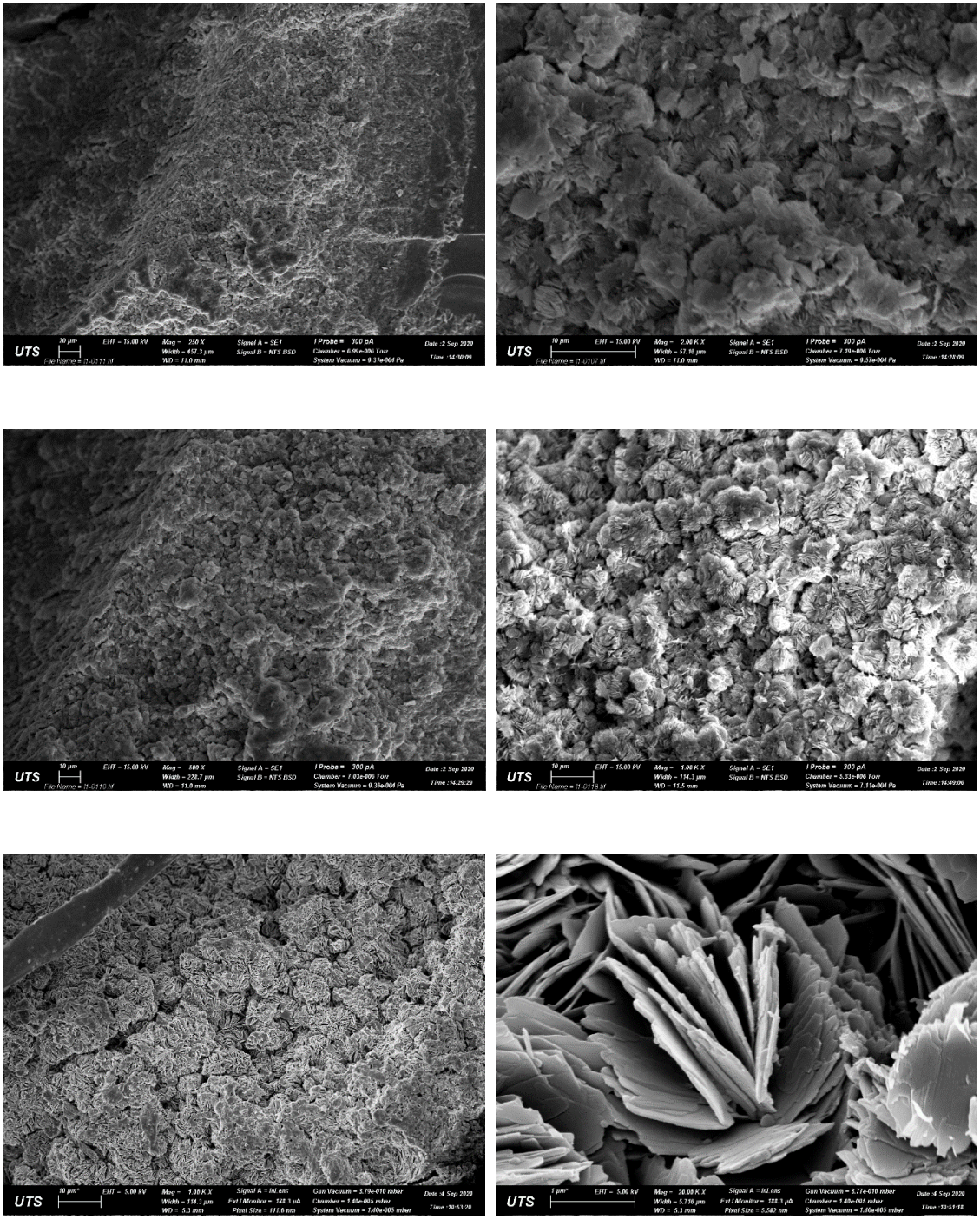

Figure A. 1 SEM images showing ASR products with rosette-type morphology (sample from a 25-year-old bridge)

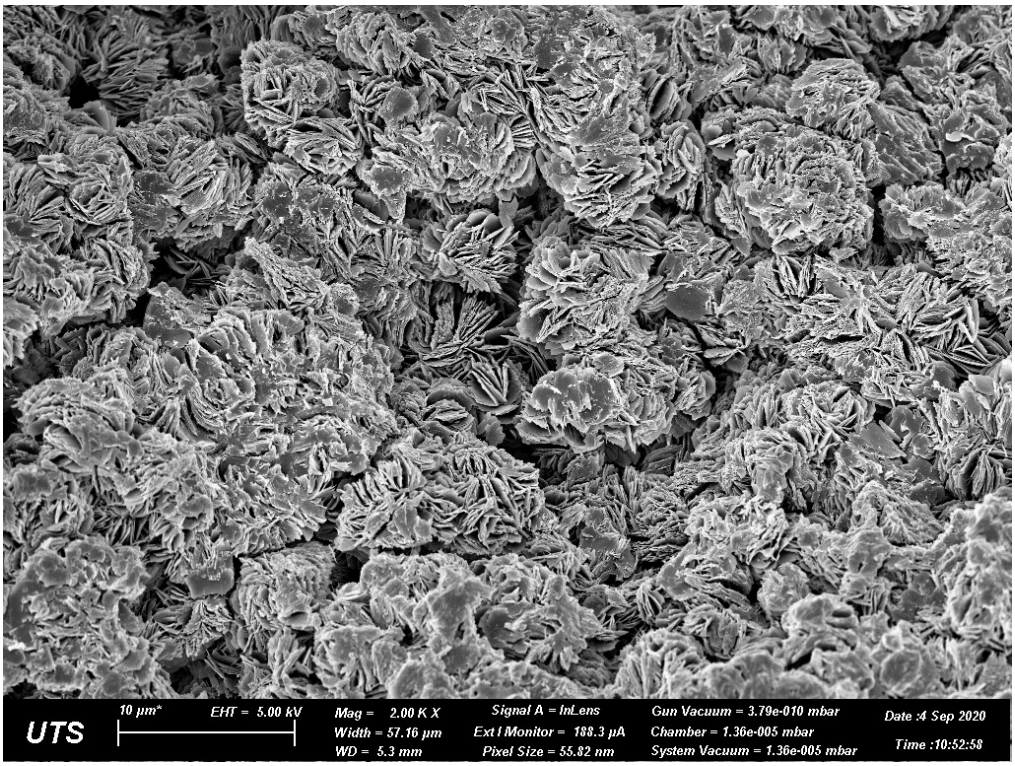

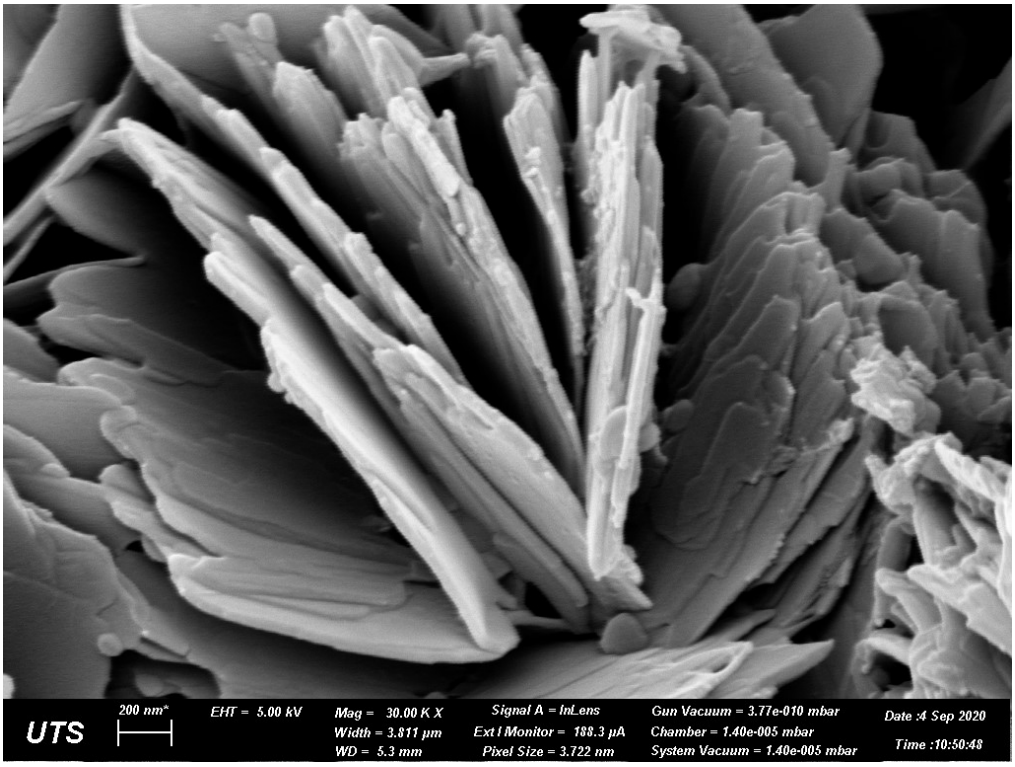

Figure A. 2 SEM images showing ASR products with rosette-type morphology (sample from a 25-year-old bridge)

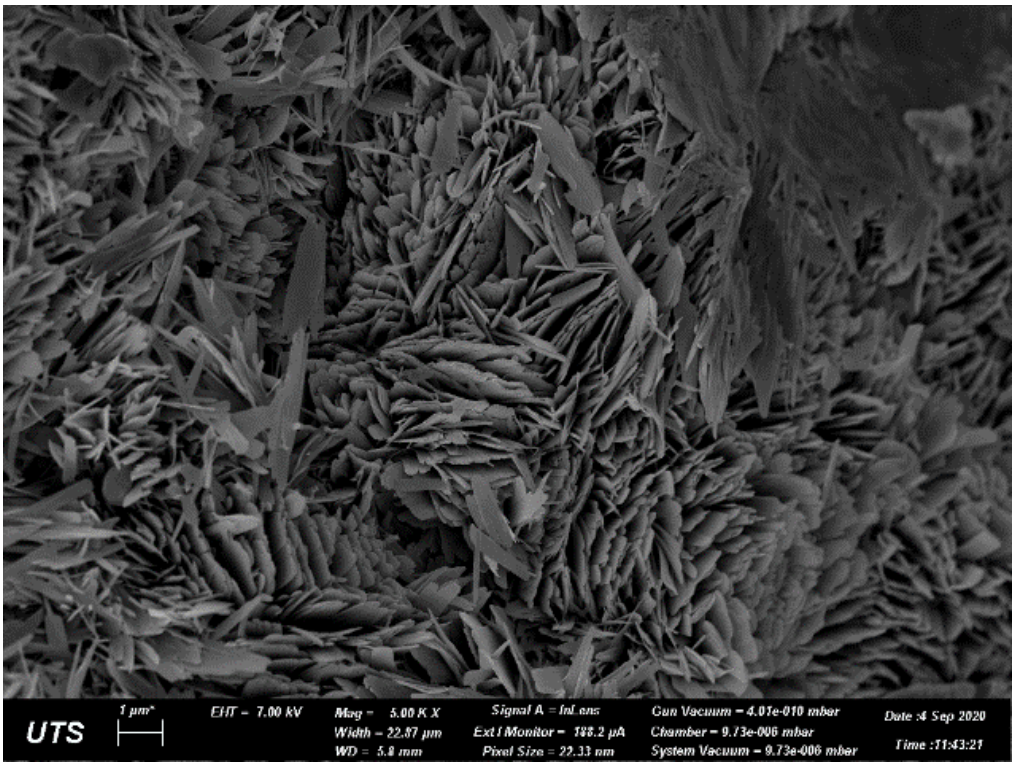

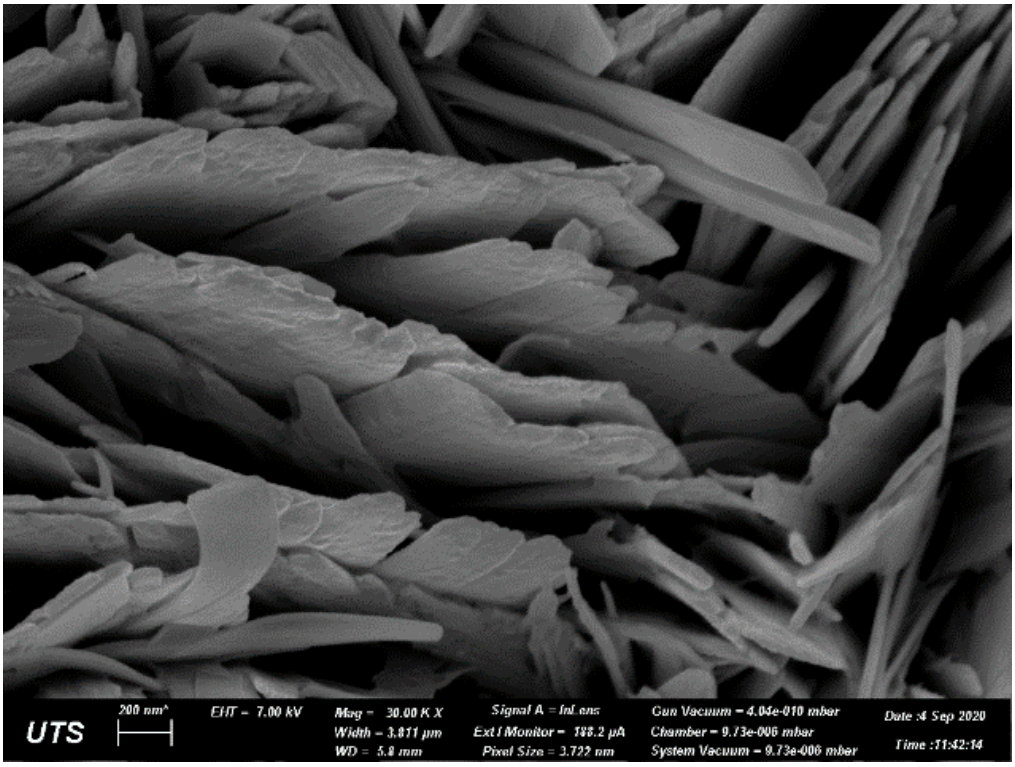

Figure A. 3 SEM images showing ASR products with crystalline morphology (sample from a 25-year-old bridge)

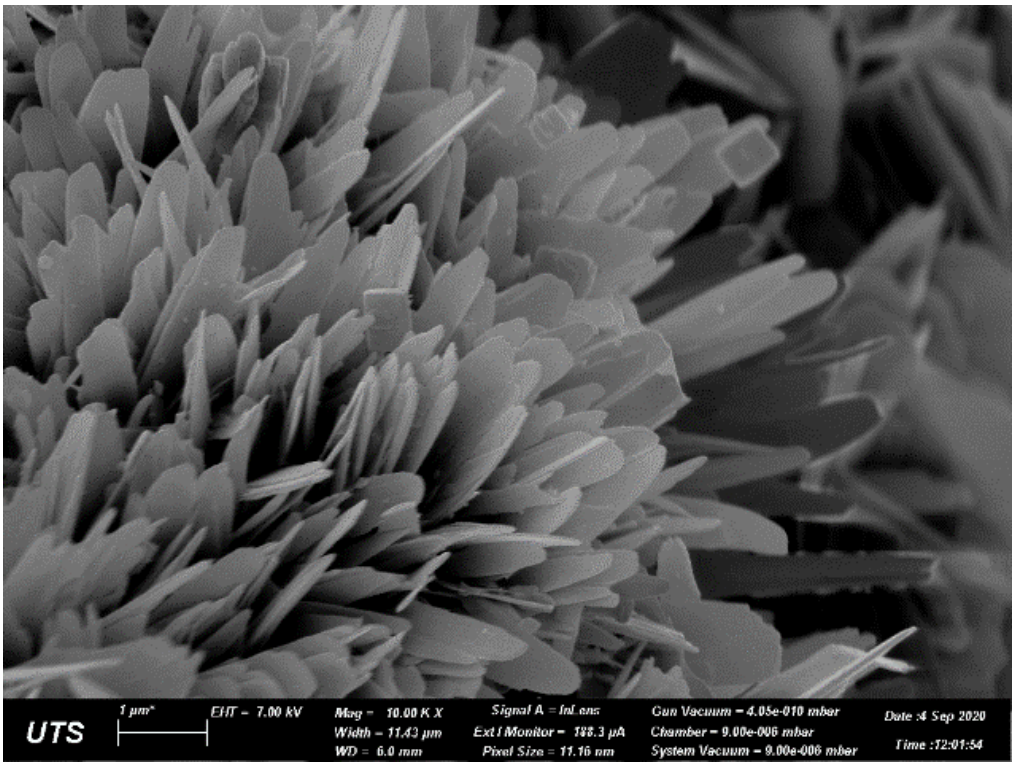

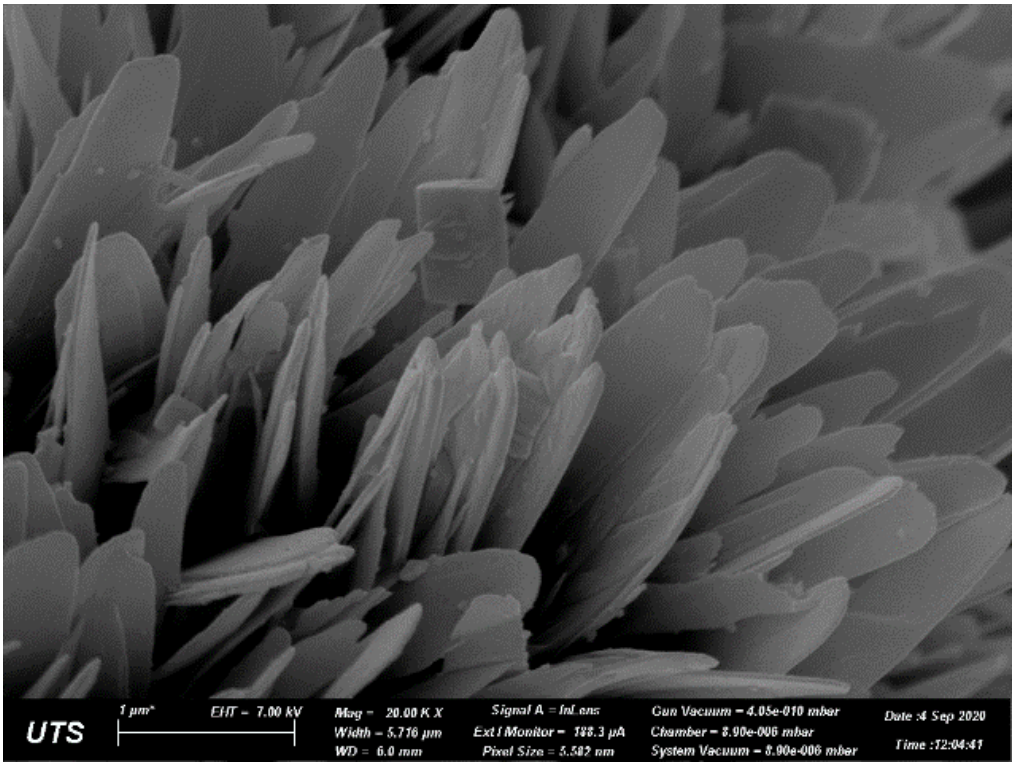

Figure A. 4 SEM images showing ASR products with crystalline morphology (sample from a 25-year-old bridge)

Appendix A.2. ASR Products Formed under 80°C Accelerated Autoclave Test

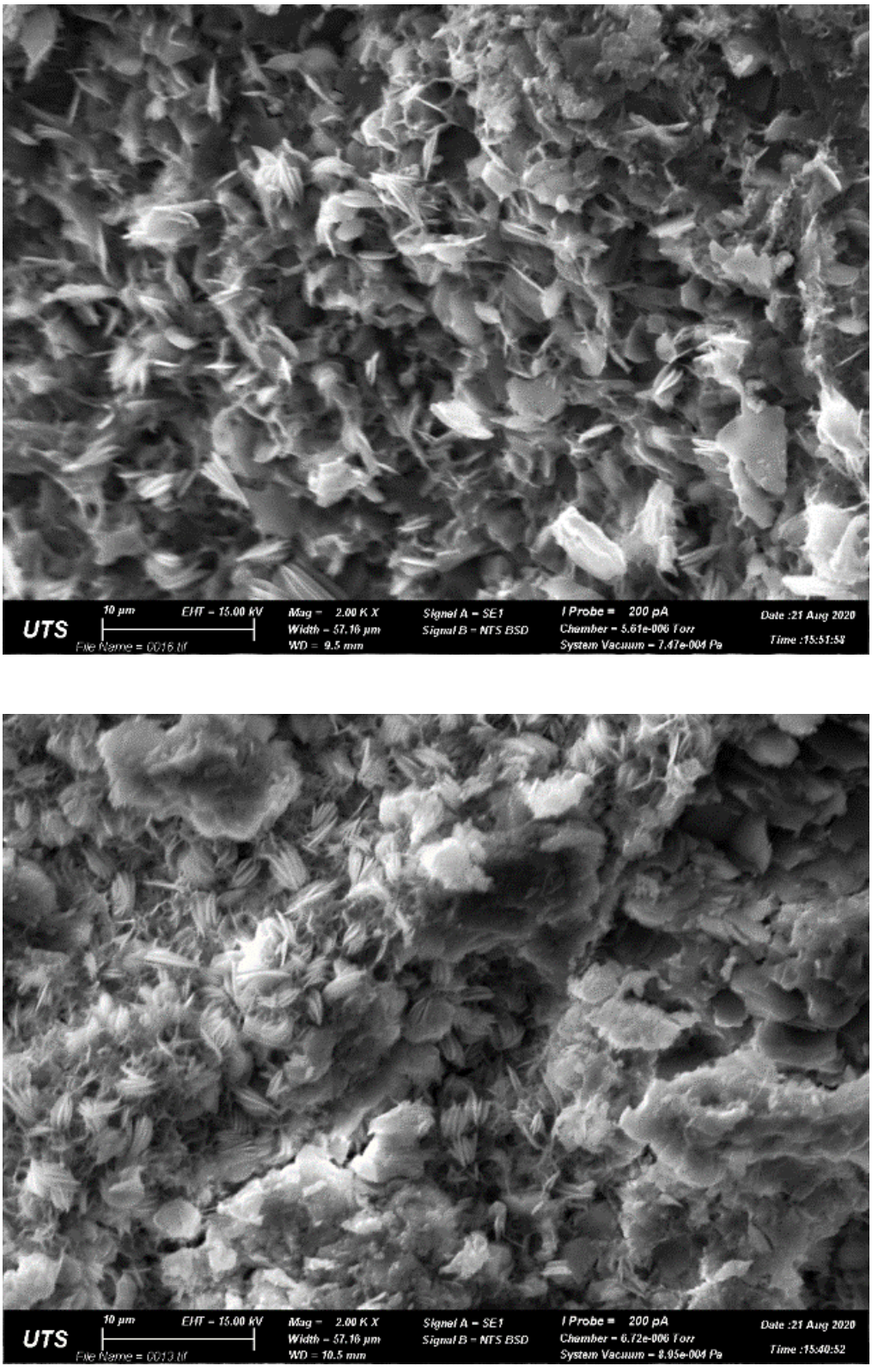

Figure A. 5 SEM images showing ASR products with rosette-type morphology (sample from 80°C accelerated autoclave test)

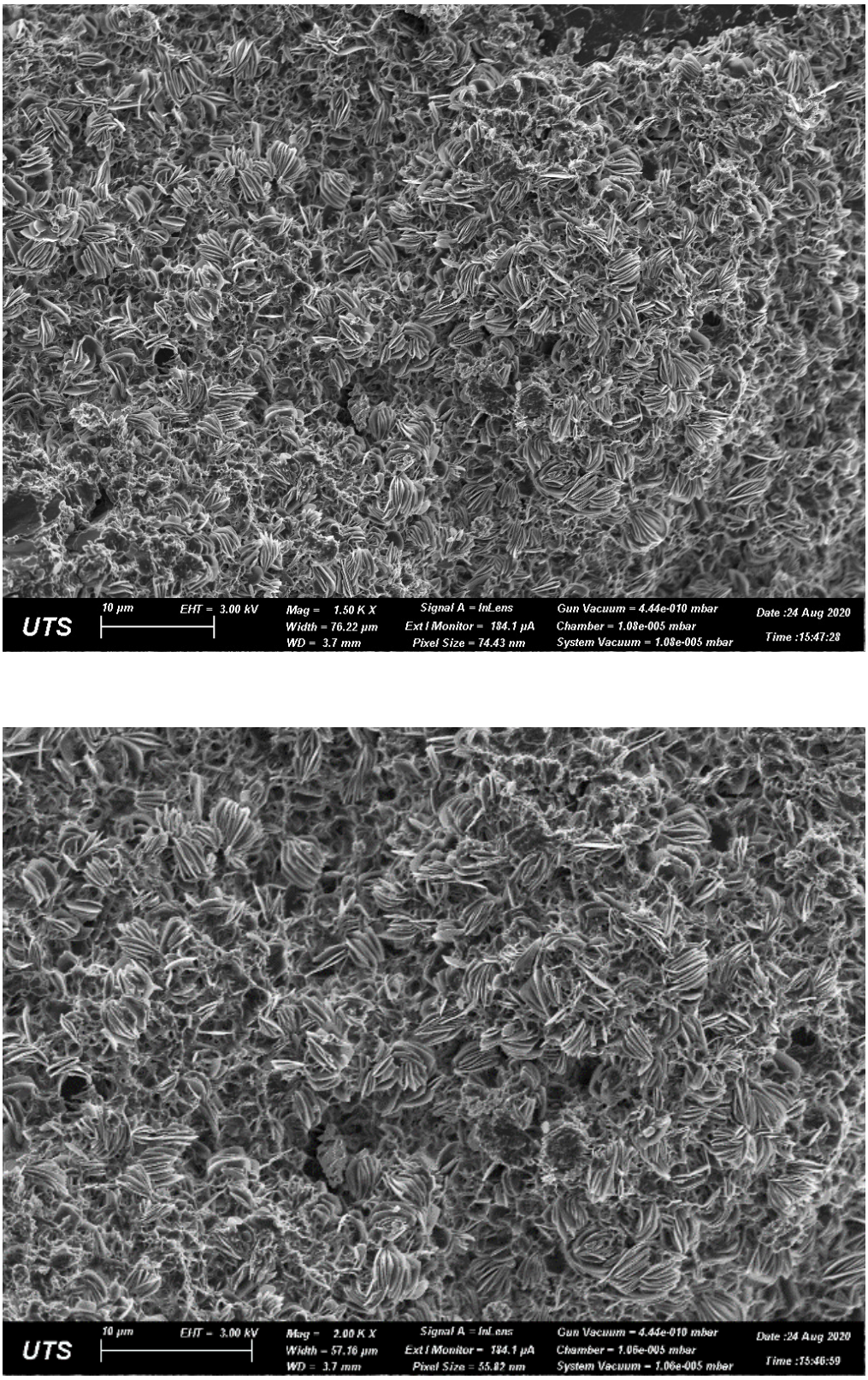

Figure A. 6 SEM images showing ASR products with rosette-type morphology (sample from 80°C accelerated autoclave test)

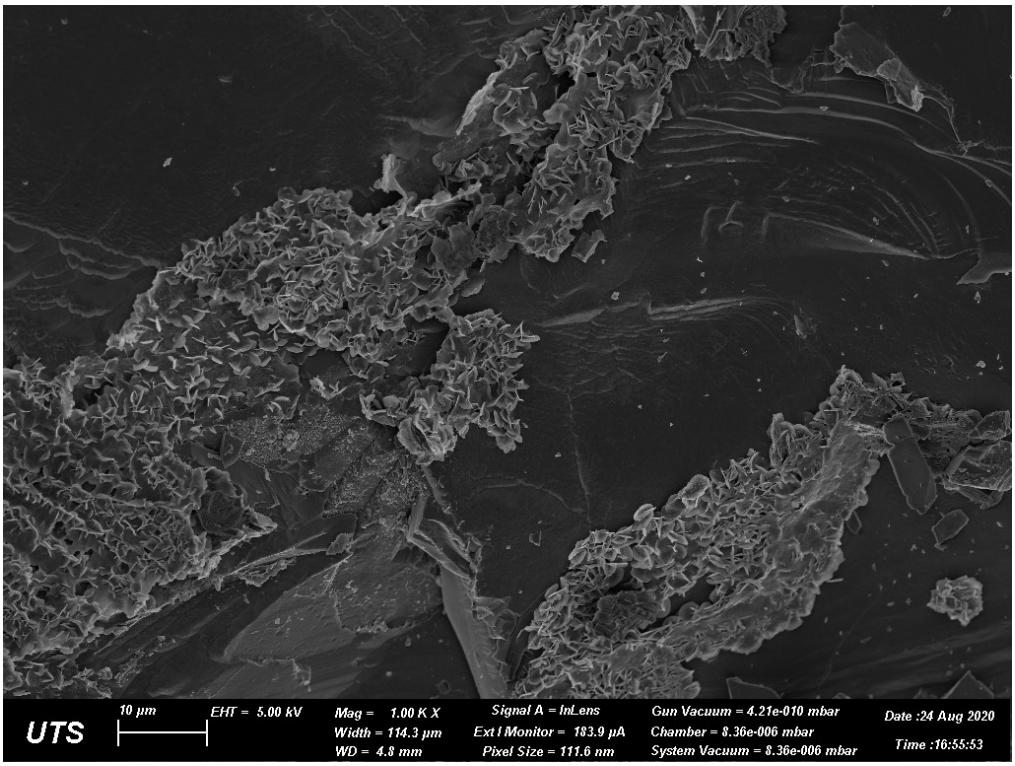

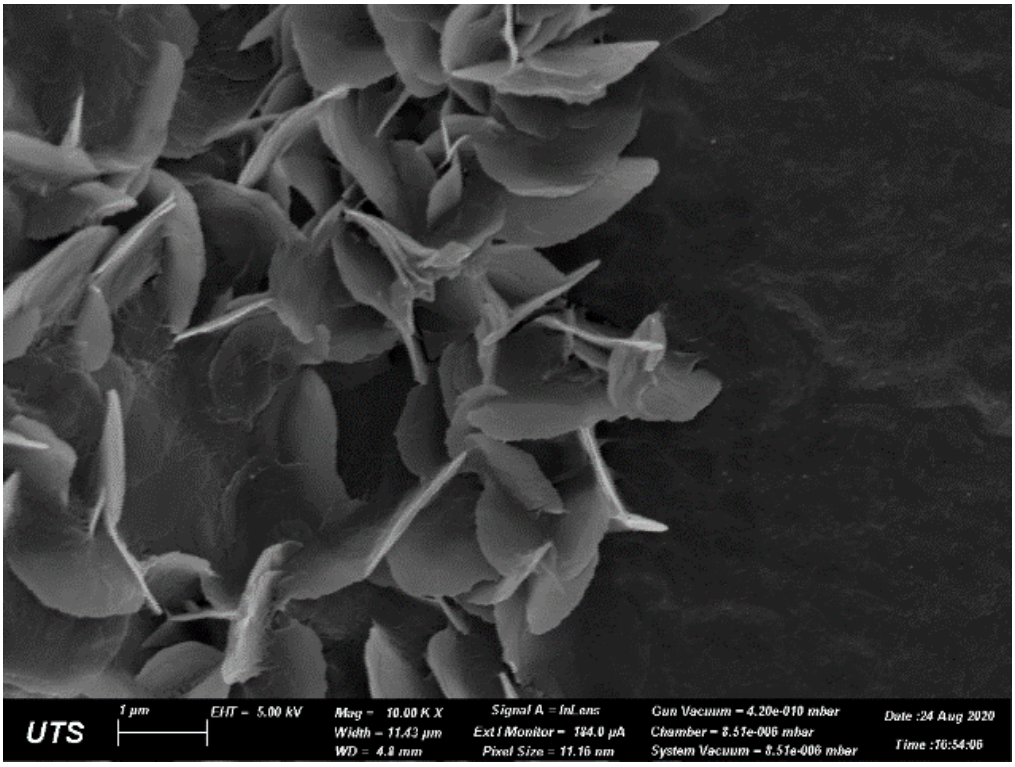

Figure A. 7 SEM images showing ASR products with crystalline morphology (sample from 80°C accelerated autoclave test)

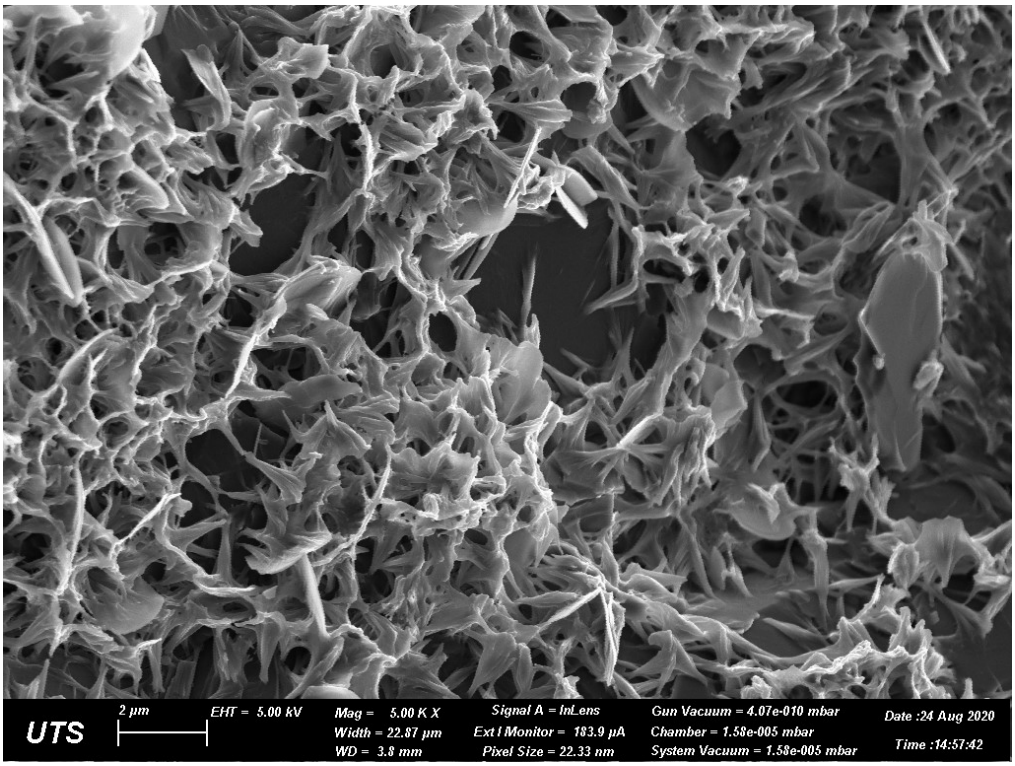

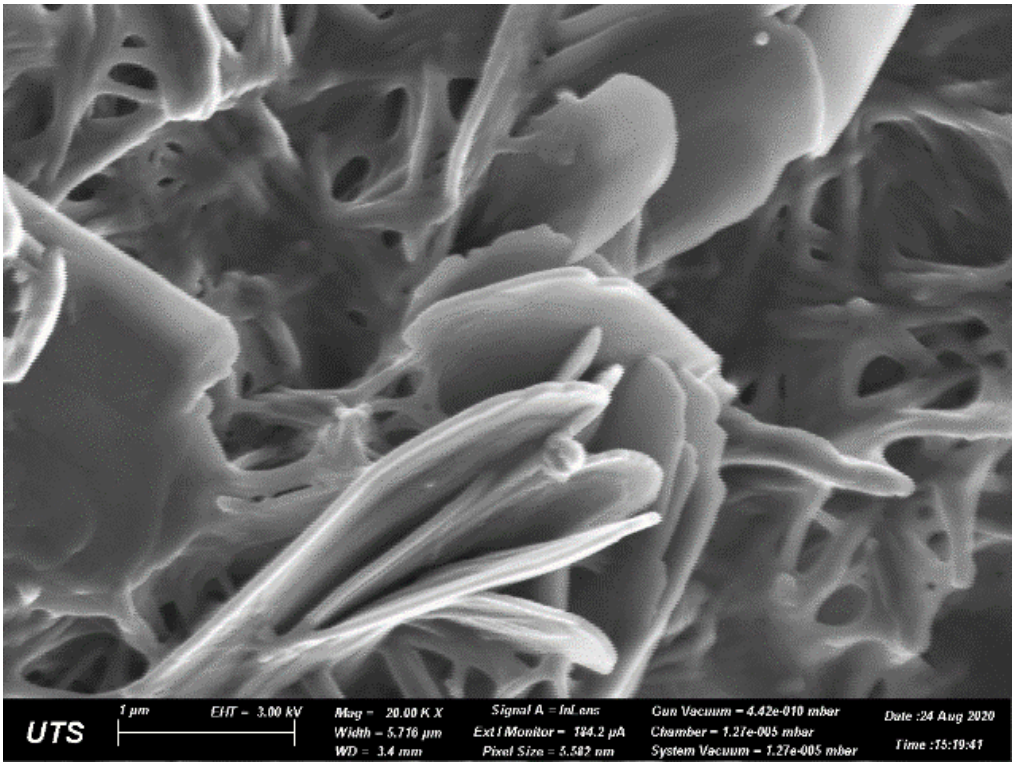

Figure A. 8 SEM images showing ASR products with network and plate-like morphology (sample from 80°C accelerated autoclave test)

Appendix A.3. ASR Products Observed from 38°C CPT Specimens

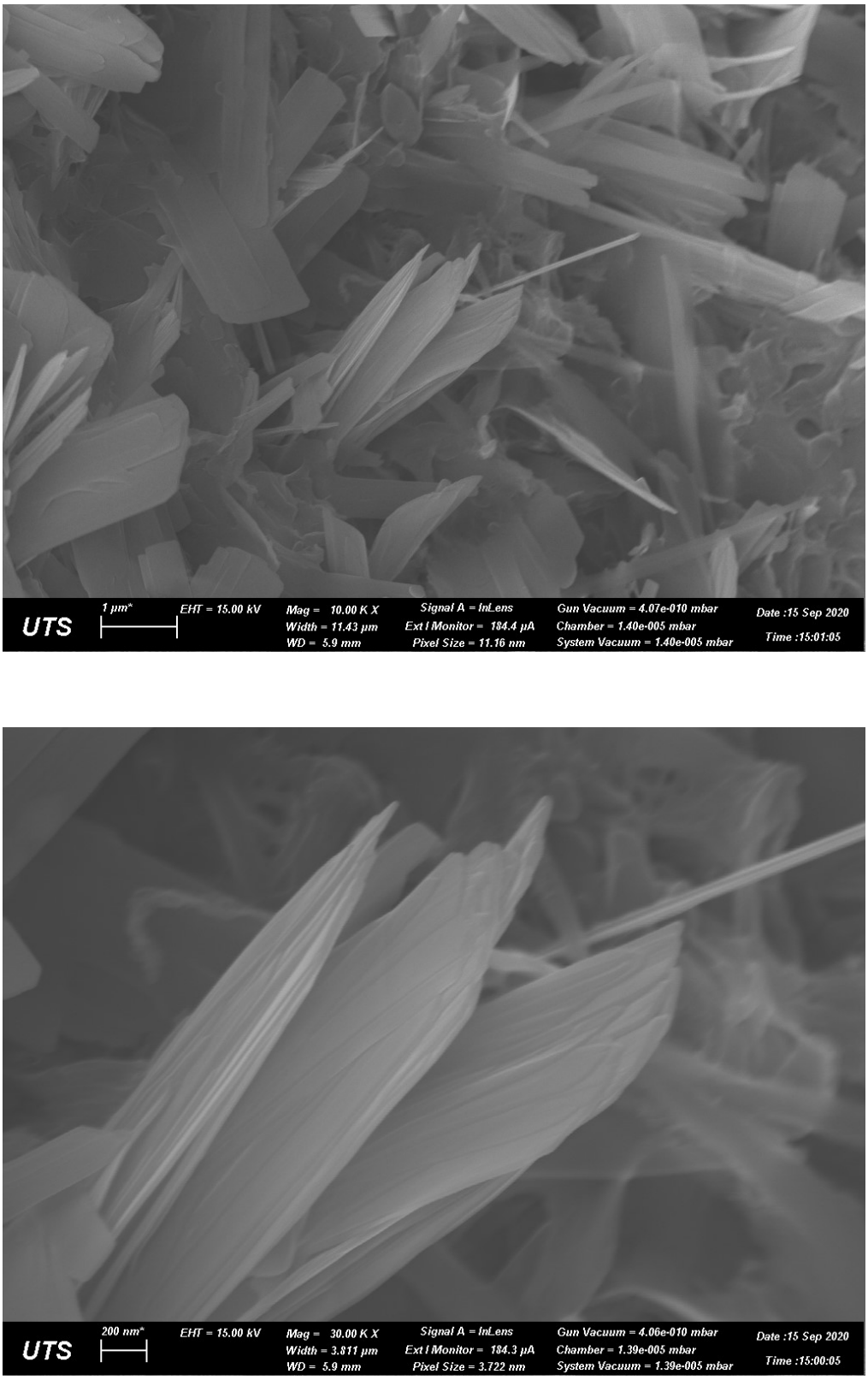

Figure A. 9 SEM images showing ASR products with plate-like morphology (observed from 38°C CPT test sample)

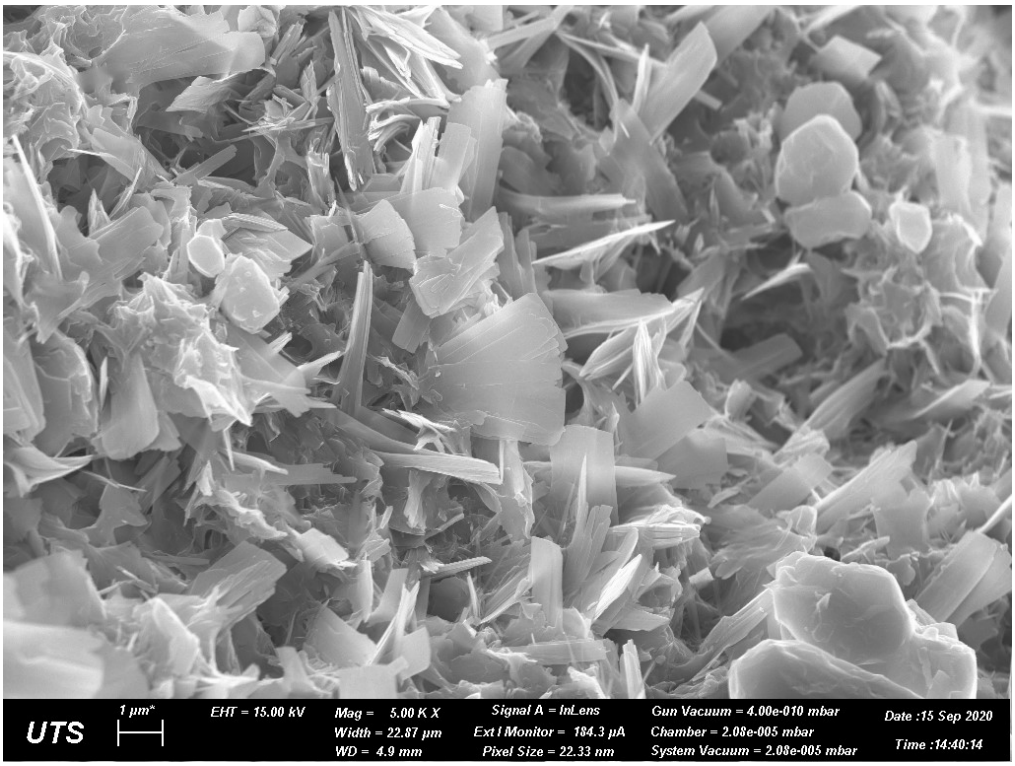

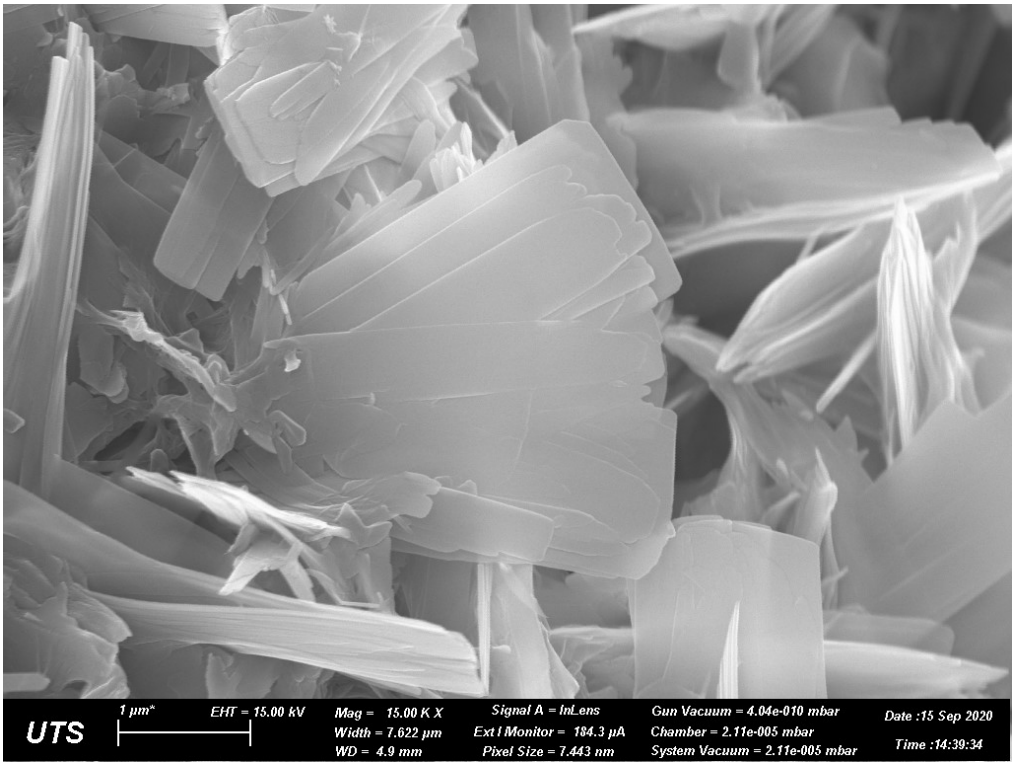

Figure A. 10 SEM images showing ASR products with plate-like morphology (observed from 38°C CPT test sample)

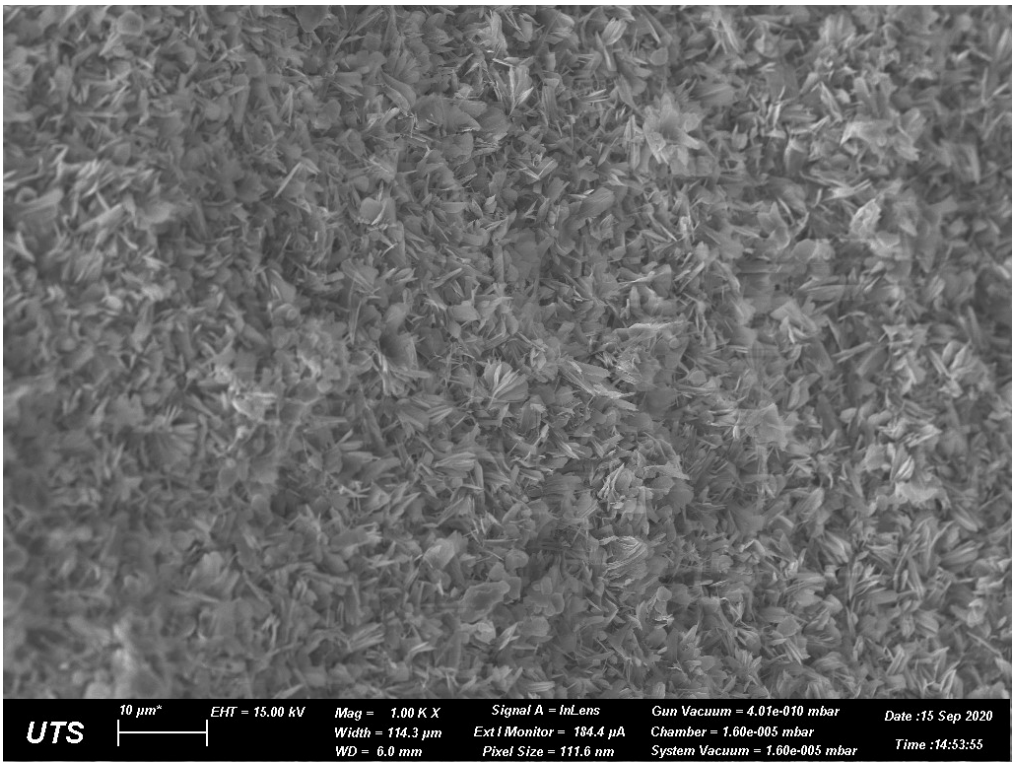

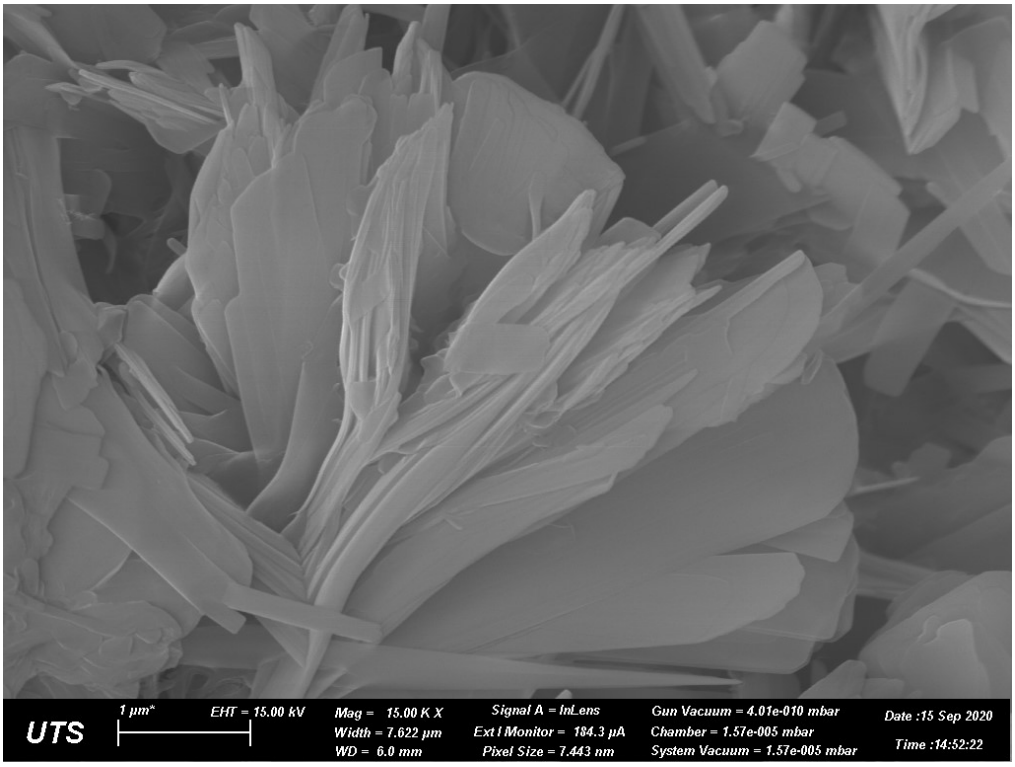

Figure A. 11 SEM images showing ASR products with crystalline and rosette-type morphology (observed from 38°C CPT test sample)

Appendix B. Mechanical Property Test Results (2.5% Na_2O_{eq} boosting)

Appendix B.1 Modulus of Elasticity

Table B. 1 Modulus of elasticity test results

Testing time	Cylinder name	Modulus of elasticity (GPa)	Reduction (%)
28-day (without autoclaving)	D1-1 (28-day)	37.04	
	D1-2 (28-day)	35.69	
	D1-3 (28-day)	37.43	
	Average	36.7	--
31-day (after 1 cycle 80°C Autoclaving)	D1-4 (1 cycle)	29.02	
	D1-5 (1 cycle)	27.12	
	D1-6 (1 cycle)	26.81	
	Average	27.7	24.5%
34-day (after 2 cycles 80°C Autoclaving)	D1-7 (2 cycles)	23.27	
	D1-8 (2 cycles)	22.56	
	D1-9 (2 cycles)	22.47	
	Average	22.8	37.9%
37-day (after 3 cycles 80°C Autoclaving)	D1-10 (3 cycles)	23.07	
	D1-11 (3 cycles)	21.69	
	D1-12 (3 cycles)	22.46	
	Average	22.4	39.0%

(a)

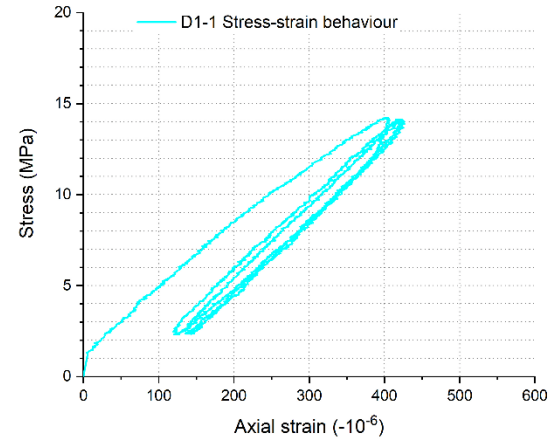

(b)

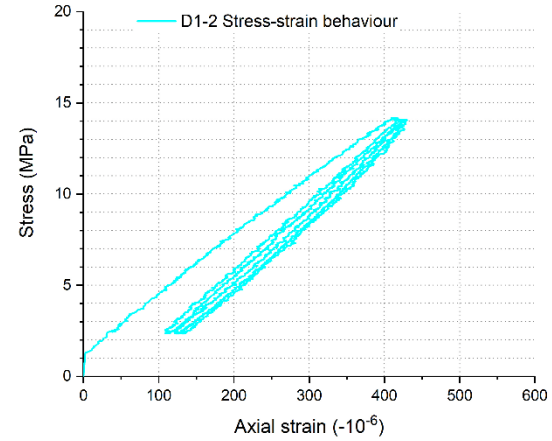

(c)

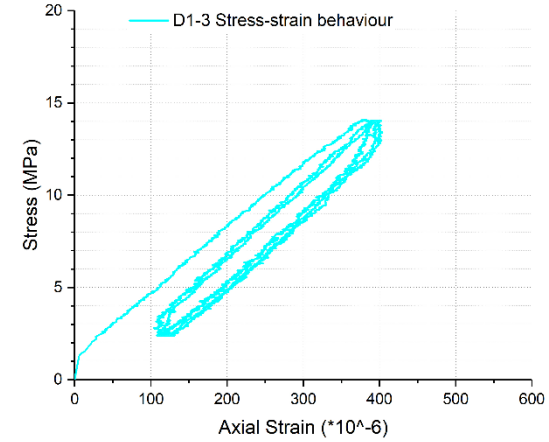

Figure B. 1 MOE test results (28-day)

(a)

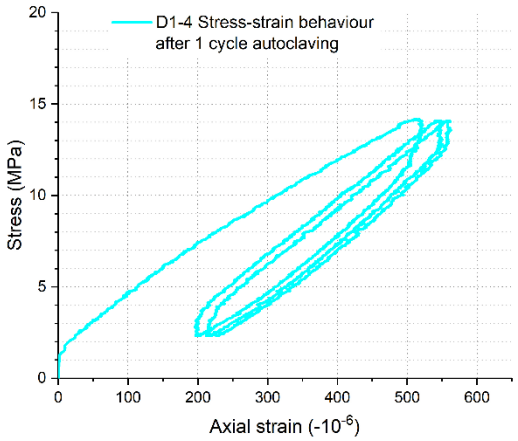

(b)

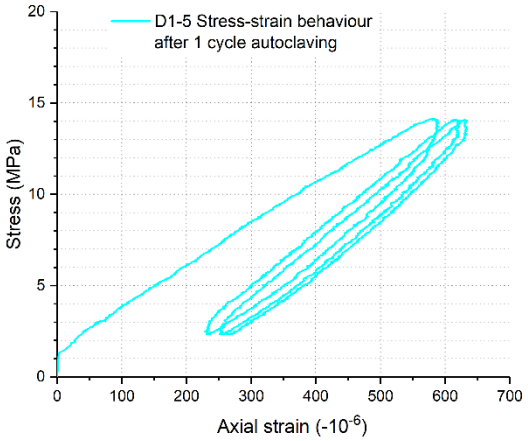

(c)

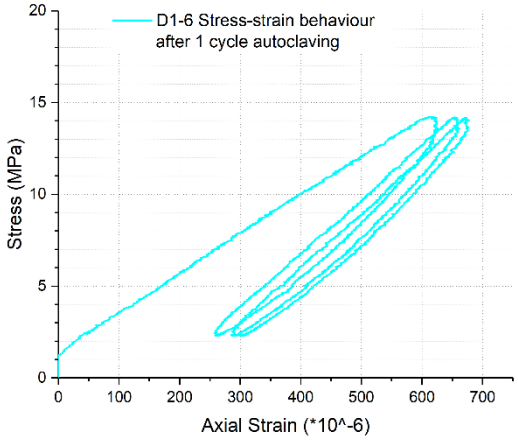

Figure B. 2 MOE test results (after 1 cycle of 80 °C autoclaving)

(a)

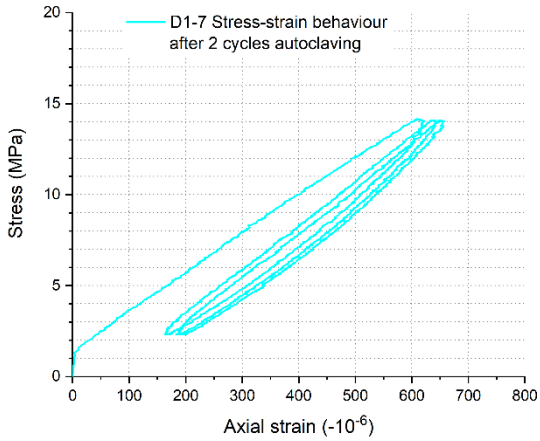

(b)

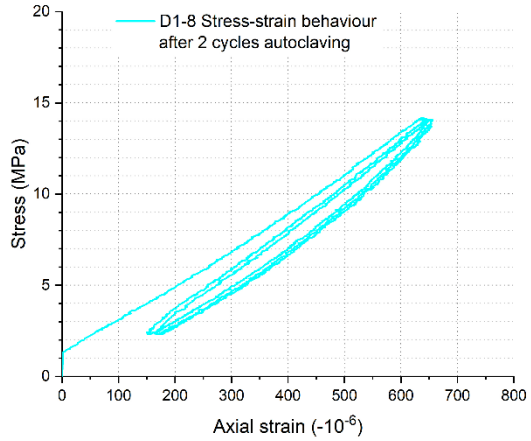

(c)

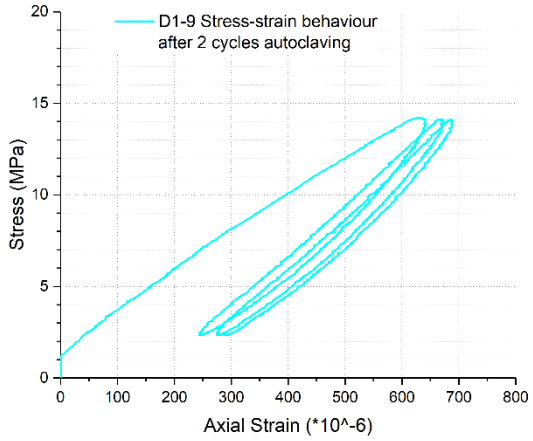

Figure B. 3 MOE test results (after 2 cycles of 80 °C autoclaving)

(a)

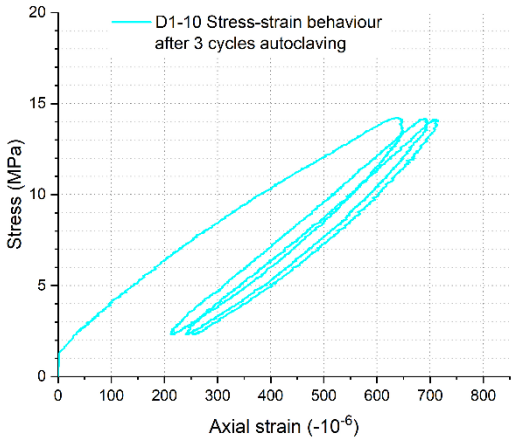

(b)

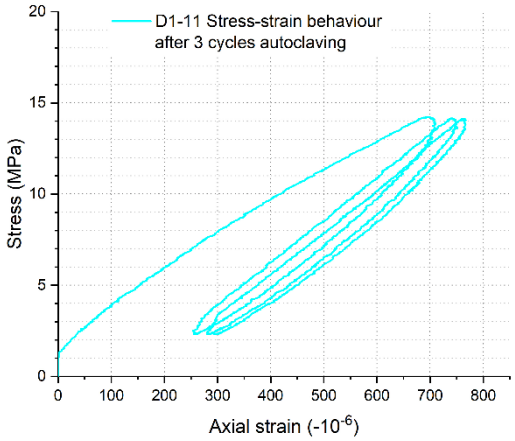

(c)

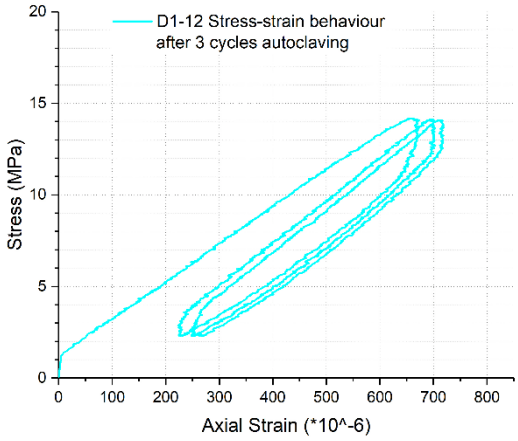

Figure B. 4 MOE test results (after 3 cycles of 80 °C autoclaving)

Appendix B.2 Compressive Strength

Table B. 2 Compressive strength test results

Testing time	Cylinder name	Compressive strength (MPa)
28-day (without autoclaving)	D1-1 (28-day)	34.15
	D1-2 (28-day)	37.24
	D1-3 (28-day)	37.14
	Average	36.0
31-day (after 1 cycle 80°C Autoclaving)	D1-4 (1 cycle)	41.46
	D1-5 (1 cycle)	40.99
	D1-6 (1 cycle)	42.98
	Average	41.5
34-day (after 2 cycles 80°C Autoclaving)	D1-7 (2 cycles)	42.73
	D1-8 (2 cycles)	46.17
	D1-9 (2 cycles)	44.49
	Average	44.5
37-day (after 3 cycles 80°C Autoclaving)	D1-10 (3 cycles)	43.51
	D1-11 (3 cycles)	42.55
	D1-12 (3 cycles)	40.04
	Average	42.0

Appendix B.3 Splitting Tensile Strength

Table B. 3 Splitting tensile strength test results

Testing time	Cylinder Name	Splitting Tensile Strength (MPa)
28-day (without autoclaving)	D4-1 (28-day)	3.06
	D4-2 (28-day)	3.74
	D4-3 (28-day)	3.71
	Average	3.50
31-day (after 1 cycle 80°C Autoclaving)	D4-4 (1 cycle)	3.85
	D4-5 (1 cycle)	3.32
	D4-6 (1 cycle)	4.03
	Average	3.73
34-day (after 2 cycles 80°C Autoclaving)	D4-7 (2 cycles)	3.90
	D4-8 (2 cycles)	3.88
	D4-9 (2 cycles)	3.76
	Average	3.85
37-day (after 3 cycles 80°C Autoclaving)	D4-10 (3 cycles)	3.57
	D4-11 (3 cycles)	3.79
	D4-12 (3 cycles)	3.81
	Average	3.72